This book was bound by

Badminton Press
18 Half Croft, Syston, Leicester, LE7 8LD
Telephone: Leicester (0533) 602918.

A NEW REAL-TIME HIGH SPEED ULTRASONIC IMAGING SYSTEM

BY

G.P.P. GUNARATHNE, B.Sc., M.Sc.

A Doctoral Thesis
Submitted in partial fulfilment of the requirements
for the award of
The Degree of Doctor of Philosophy of the
Loughborough University of Technology

August 1986

Supervisor: Dr. J. Szilard.

ACKNOWLEDGEMENTS

I wish to express my sincere gratitude and indebtness to my supervisor, Dr. J. Szilard for his valuable guidance, supervision and encouragement throughout the course of this research. Also, I am grateful to professor I.R. Smith, Head of the Department of Electronic and Electrical engineering for his kind help and advice over the years.

My thanks are due to the United Kingdom Atomic Energy Authority for sponsoring this project and specially to Dr. Paul Highmore, the project supervisor at the Risley Nuclear Power Development Laboratories for his continual support and encouragement.

The technical staff of this department are warmly thanked and the very special assistance given to me by Mr. Phil Atkinson, Mr. John Rippon, Mr. Andrew Coaton, Mr. Peter Barrington and Mr. Keith Allen are gratefully acknowledged.

Also, I wish to thank Mr. Roger Tomlinson for his whole hearted support and carrying out all the constructional work concerning the thick film circuits.

I am also very grateful to Mr. Peter LeGood of the Department of Mechanical Engineering for drawing all the diagrams.

Thanks are due to my colleague Mr. Peter Senior for all his help and my friend Dr. Chris Ofuya for his valuable comments.

Finally, the support and the moral encouragement given to me by my wife, Kanthi and my son, Tharaka are gratefully acknowledged.

--- // ---

To my wife

and

my little son

LIST OF SYMBOLS

CHAPTER 1.

c	=	Velocity of sound
d	=	Axial resolution
Δt	=	Pulse duration
D	=	Depth
λ	=	Wave length
A	=	Aperture
f	=	Repetition frequency
dB	=	Decibel

CHAPTER 2.

N	=	Number of echo lines
d	=	Depth
F	=	Repetition frequency

CHAPTER 3.

v	=	Image distance
f	=	Focal length
u	=	Object distance
M_A	=	Axial magnification
Δu	=	Change in object distance
Δv	=	Change in image distance
DUVD	=	Direct Ultrasonic Visualization of Defects

CHAPTER 4.

p.d.	=	Path difference
ϕ	=	Phase angle

Chapter 5.

exp	=	Exponential function
rect	=	rect operator
L	=	Aperture
Si	=	sine integral
DI	=	Directivity Index
comb	=	comb operator
$P_{(x,y)}$	=	Acoustic pressure at point (x, y)
k	=	Wave number
$\delta\theta$	=	Angular resolution
w	=	Width of the array element

g	=	Gap between array elements

Chapter 6

N	=	Near field
v	=	Velocity of sound
ω	=	Angular frequency
$v_{i(t)}$	=	Time domain input signal
*	=	Convolution
T	=	Period
t_p	=	Pulse length

Chapter 7

V	=	Threshold output voltage
G	=	Voltage gain
f_H	=	High frequency cutoff
BW	=	Bandwidth
ADR	=	Actual Dynamic Range of Amplifiers
ESR	=	Effective input signal range
EDR	=	Effective Dynamic signal range
TVG	=	Time Varying Gain
α	=	Attenuation coefficient
R_{DAMP}	=	Damping resistance
Q	=	Quality factor
V_Q	=	Quiescent voltage
I_Q	=	Quiescent collector current
η	=	Efficiency
t_s	=	Settling time

Chapter 8

sgn	=	Signum function
n	=	refractive index
$\mathcal{F}$	=	Fourier transform
λ	=	Optical wavelength
Λ	=	Ultrasonic wavelength
M	=	Figure of merit

Chapter 9

q	=	Electronic charge
K	=	Boltzman constant
B	=	Apparent brightness

mcd = microcandella

LED = Light emitting diode

Chapter 10

Z = Impedance

C_o = Static capacitance of the transducer

K = Cross-coupling factor

Chapter 11.

G^* = G star

$r_{ds(on)}$ = Drain-source on resistance

FET = Field effect transistor

G.O. = Gated oscillator

KS = Key switch

CRT = Cathode ray tube

--- // ---

SYNOPSIS

An ultrasonic imaging technique was to be developed for sizing and characterization of defects in thick sections of steel. The problems generally found with the existing techniques in such applications are low speed, inadequate image quality, large size and high cost.

This work is a development of a new ultrasonic imaging system. It is based on an extension of the technique called DUVD [Direct Ultrasonic Visualization of Defects] by P. D. Hanstead (1973). The main problem with the DUVD being a 'passive' system is its low sensitivity. Introducing electronic amplification using transducer arrays, the concept of the DUVD is changed from passive to 'active', solving the problem of low sensitivity, while preserving its ideal characteristics by a new sonoptical design. A complete image field is formed with a single pulse, practically within its time of flight, hence the ultimate speed possible in imaging has been reached.

The work involved studies in a variety of disciplines relating to the formulation, analysis and identification of system parameters, evaluation of conceptual validity and the design and construction of the instrument. Parameters such as array element spacing, aperture required were theoretically assessed while signal amplification required investigations into areas involving gain, bandwidth, terminal impedance, dynamic range etc.. The process of re-transmission needed investigations into the new sonoptics as a whole, leading to a design capable of producing high resolution focused B-scan type images of the whole object field.

A number of areas have also been developed as part of this work including a compact wide aperture compact schlieren system, a new sub-miniature stroboscope using a light emitting diode, high performance miniature wideband amplifiers, high quality transducer arrays with backings etc..

After completing a feasibility study the first prototype for NDT applications was built and its performance demonstrated. Future prospects of development are also presented.

- Patent pending -

CONTENTS

CHAPTER - 3

HANSTEAD'S DUVD SYSTEM AND ITS PROSPECTIVE LINES OF DEVELOPMENT

CHAPTER - 4

THE NEW CONCEPT

CHAPTER - 5

SIGNAL INTERCEPTION

CHAPTER - 6

PULSED OPERATION

CHAPTER - 7

SIGNAL INTERCEPTION

CHAPTER - 8

RE-TRANSMISSION AND VISUALIZATION

CHAPTER - 9

DEVELOPMENT OF A NEW STROBOSCOPE

CHAPTER - 10

DESIGN AND CONSTRUCTION OF TRANSDUCER ARRAYS

CHAPTER - 11

DESIGN AND CONSTRUCTION OF ELECTRONIC CIRCUITS

CHAPTER - 12

THE ASSEMBLED NEW IMAGING SYSTEM

CHAPTER - 13

RESULTS AND CONCLUSIONS

APPENDICES

--- // ---

- CHAPTER 1 -

IMPORTANT FACTORS RELATING TO ULTRASONIC IMAGING

This chapter deals with general treatment of problems relating to the subject of ultrasonic imaging. The potential of ultrasonic testing and in particular the relative importance of 'imaging' are outlined. Imaging techniques are broadly classified into two categories. The fundamental limits and various important factors concerning all imaging systems such as accuracy, resolution, sensitivity and dynamic range etc. are briefly defined and analysed.

1.1 INTRODUCTION

The tendency to demand higher performance from fabricated structures and plant places an ever-increasing onus on Non Destructive Testing (NDT) methods to determine accurately the degree of integrity of such structures. Application of fracture mechanics depends on specific, detailed knowledge of the nature of all defects and discontinuities in the structures and it is the uncertainty of the available NDT methods to meet this demand that is a major cause for concern.[1]

Of the available methods for quantifying defects in structures or in routine quality control work, ultrasonic testing has the potential to size defects with sufficient accuracy in a wide range of applications. Similarly in medical diagnostics, ultrasonic techniques are being widely used in a number of important applications,[2,3] making this area a very demanding field of technology.

1.1.1 Imaging versus conventional techniques

Conventional techniques, for example the well known A-scan[4] may provide accurate results, but the amount of information is limited. In general,

with conventional testing, a large number of uncertainties are involved and the necessary degree of operator skill and experience is difficult to define. This is where ultrasonic imaging plays an important role in providing a great deal of additional information about critical defect features such as size, shape and orientation.

The potential of ultrasonic imaging in NDT, sonar and medical applications has led to the development of a variety of ultrasonic instrumentation systems.[4,5] Although the complexity and sophistication of these systems have been growing over the years, the degree of improvements achieved in this field considering the effort and apparent investment seems rather low.

1.1.2 Orthographic and co-axial imaging systems

The term imaging in a classical sense may be defined as a process by which an image of an object is formed with the object-to-image spatial relationship correctly maintained. The early attempts of ultrasonic pictorial displays such as Pohlman cell[4] were so crude and fraught with difficulties that the idea of imaging in the classical sense was seen only as an ideal academic goal. Later other techniques were gradually evolved such as B-scan[1] and C-scan[2], which may be broadly classified as (1). othographic and (2). coaxial systems.[4]

(1) Othographic : i.e. displaying an object plane perpendicular to the ultrasonic beam axis

(2) Co-axial : i.e. displaying a plane containing the axis of the beam

The results obtained with the simple B-scan and the C-scan systems are too crude to be considerd as imaging without the adoption of special techniques to enhance the image quality. They are therefore simply referred to as B-scan and C-scan displays, respectively.

In spite of the drawbacks, the majority of the imaging systems today

make use of some form of B-scan display using manual, mechanical or electronic scanning together with signal processing techniques to enhance image quality.

Another category of imaging may be called 'focused B-scan' displays. It does not necessarily use focused probes or an actual scan, but other methods such as the use of ultrasonic lenses and dynamic focusing to form a focused image of an ultrasonic object field similar to a B-scan display format. Hanstead's Direct Ultrasonic Visualization of Defects[6] [DUVD] system is one such example. Although it is not implemented in practice, DUVD has the potential of producing three-dimensional focused ultrasonic image of a complete object volume, even though the actual display is usually restricted to two dimensions.

Some other pictorial techniques, although not widely used, are ultrasonic tomography - a pictorial representation technique utilizing through-transmission time of flight information of a given object field containing acoustic inhomogeneities and ultrasonic holography, a three dimensional pictorial representation using coherent ultrasonic irradiation. The important areas with regard to image quality and interpretation are :

1. Accuracy
2. Resolution
3. Sensitivity
4. Dynamic range
5. Repeatability

1.2 Accuracy and resolution

In conventional flaw detection techniques, the accuracy of measurement is usually stated. However, in imaging applications, what is more relevent is the accuracy of maintaining linear spatial relationships between the object and the image fields.

Resolution in the case of an imaging system may be loosely defined as a measure of its ability to display structural details in its images.

Structural details in imaging terms not only apply to linear dimensions, but extend to other important and more complicated areas such as movement and contrast as well. Various aspects of resolution relating to image definition may be listed as follows.

1. Axial resolution
2. Lateral resolution
3. Amplitude or reflectivity resolution
4. Temporal resolution

1.2.1 Axial resolution

Axial resolution is the ability of the instrument to produce separate echoes from structures lying one behind the other along the sonic beam. Assuming that the theoretical limit of the axial resolution is only a function of the pulse length, a simple expression may be derived, as follows. (Fig. 1.1).

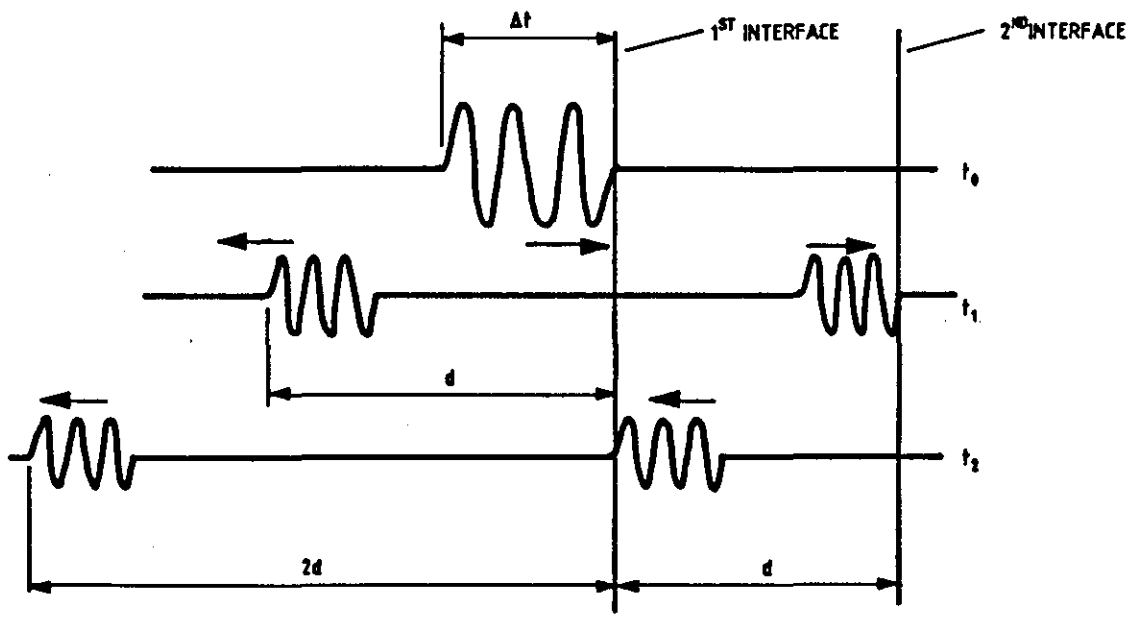

FIG. 1.1. AXIAL RESOLUTION CONCEPTS.

If c = velocity of sound in the medium
d = axial separation of targets

Δt = pulse duration

In order to resolve,

$$2d \geq c \Delta t$$

since Δt = Pulse length in the medium / c

$$d \geq \frac{\text{Pulse length}}{2} \quad . \quad . \qquad (1.1)$$

i.e. the theoretical limit of axial resolution in the pulse echo mode is one half of the pulse length in the medium.

1.2.2 Lateral resolution

Lateral resolution may be defined as the ability of the instrument to display separate echoes from structures that are lying side by side across the ultrasonic beam. As might be expected it depends on the effective width of the ultrasound beam and the depth at which the measurement is carried out.

In practice, the lateral resolution of a system may be examined by imaging a series of small targets or small drilled holes of various spacings in a suitable test object medium. Although complications such as near field problems could arise, this method can give a fair idea of the lateral resolution achieved as a function of depth.

In theoretical terms the lateral resolution may be defined with reference to the point where the transverse pressure profiles of two point targets cross each other at a specified db down. For example 3 dB correspond to half power points as illustrated in Fig. 1.2. It may be estimated as a function of the aperture A, wavelength λ, and the depth D using the formula[7]

$$x = \frac{1.22 \lambda D}{A} \quad . \quad . \quad . \qquad (1.2)$$

where x is the minimum lateral separation resolved

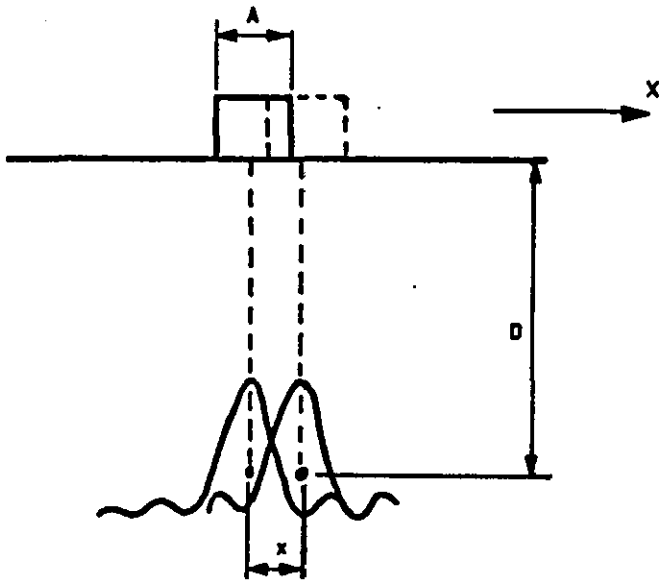

FIG. 1. 2. LATERAL RESOLUTION CONCEPTS.

1.2.3 Amplitude or reflectivity resolution

The details of an image depends also on the power of the system to identify the differences in the reflectivity of targets. An assessment of this would be particularly useful in medical applications where a wide range of reflectivity difference exists between tissues. However, in NDT work the reflectivity of acoustic discontinuities is nearly perfect, except in rare occurrence such as a thin crack filled with a liquid. This knowledge of the reflectivity of defects in NDT applications therefore eliminates the necessity of having to specify this parameter.

1.2.4 Temporal resolution

Temporal resolution is a measure of the power of the instrument to separate two events closely spaced in time. Because of its critical significance in real time imaging, the factors governing temporal resolution have to be considered more carefully.

There are two important factors concerning the absolute real time capabilities of an ultrasonic imaging system. They are :

1. Maximum single frame speed
2. Maximum repetition rate

In order to estimate the fundamental limits, consider a test object whose depth is D, and the sound velocity c. Assuming the imaging is done in the pulse echo mode, and neglecting the pulse length in comparison to depth, the approximate minimum time, Δt required for gathering data will be

$$\Delta t \simeq 2D / c \quad . \quad . \quad . \quad (1.3)$$

If insonification is repeated within a time less than that given by the above equation, the resulting image field may be confusing. Hence the maximum repetition frequency f_{rep} permissible is $c / 2 D$.

1.3 SENSITIVITY

This defines the ability of the instrument to display weak targets. However, unlike in the case of most standard equipment it is not possible to give an absolute specification for sensitivity in this case. The common practice is to specify the weakest target (in terms of its geometry and depth) which could be imaged with a given system.

1.4 DYNAMIC RANGE

Dynamic range is a measure of the range in signal amplitudes that are generated by or can be handled by the portion of the system under study. It applies to quite unrelated topics, for example transducers, displays, reflecting targets etc.

In the case of medical imaging, higher dynamic range gives a greater number of grey levels corresponding to different tissue reflectivities. However, in NDT imaging this does not apply in the same way, but what

would be of interest is the dynamic range determined by the actual signal levels present which can be very large. However, it is the dynamic range of the display, the recording medium or our ability to appreciate grey levels, that usually reduce the overall dynamic range to about 24 dB in most cases.

Some examples of typical dynamic range values encountered in practical imaging situations[2] are :

Transducer	:	40 dB
TV monitor	:	20 dB
Scan converter storage memory	:	30 dB
Grey scale response	:	30 dB
Biological tissue reflectivities	:	36 dB
Instrumentation amplifier	:	60 dB

When faced with dynamic range limitations, techniques such as dynamic compression or dynamic range control may be used, if the resulting signal distortion can be tolerated.

1.5 REPEATABILITY

Lack of repeatability is often seen in ultrasonic inspection systems, more than in many other fields of instrumentation. This can be mainly due to the critical nature of ultrasonic inspection techniques, transducer behaviour and in some cases due to the difficulty of meeting proper operational standards.

1.6 OTHER CONSIDERATIONS

In addition to the academic concepts discussed above, two other important factors regarding the commercial success of a new system are the compactness and cost. Some imaging equipment are so bulky and expensive that their use in practice is limited to special localized applications only. However, the present trend of miniaturization and cost reduction of the instruments entering into the competitive market

is rapidly advancing and therefore must be taken into account at all times in the development of any new system or process.

1.7 CONCLUSIONS

The study and the comparison of existing ultrasonic inspection systems against the factors outlined in this chapter will be used in identifying the potential areas of new development.

--- // ---

- CHAPTER 2 -

BRIEF DESCRIPTION AND ANALYSIS OF EXISTING TECHNIQUES

In this chapter, basic techniques of some existing ultrasonic inspection systems are briefly examined in order to identify the areas of potential development. Particular emphasis will be placed on the B-scan type real time imaging systems and the use of linear arrays because of their relative importance.

2.1 THE ULTRASONIC PULSE-ECHO FLAW DETECTOR - (A-SCAN)

The ultrasonic flaw detector is the most conventional, general purpose, real time ultrasonic inspection system in the widest use. The principle is called the A-scan and the essential elements are shown[4] in Fig. 2.1.

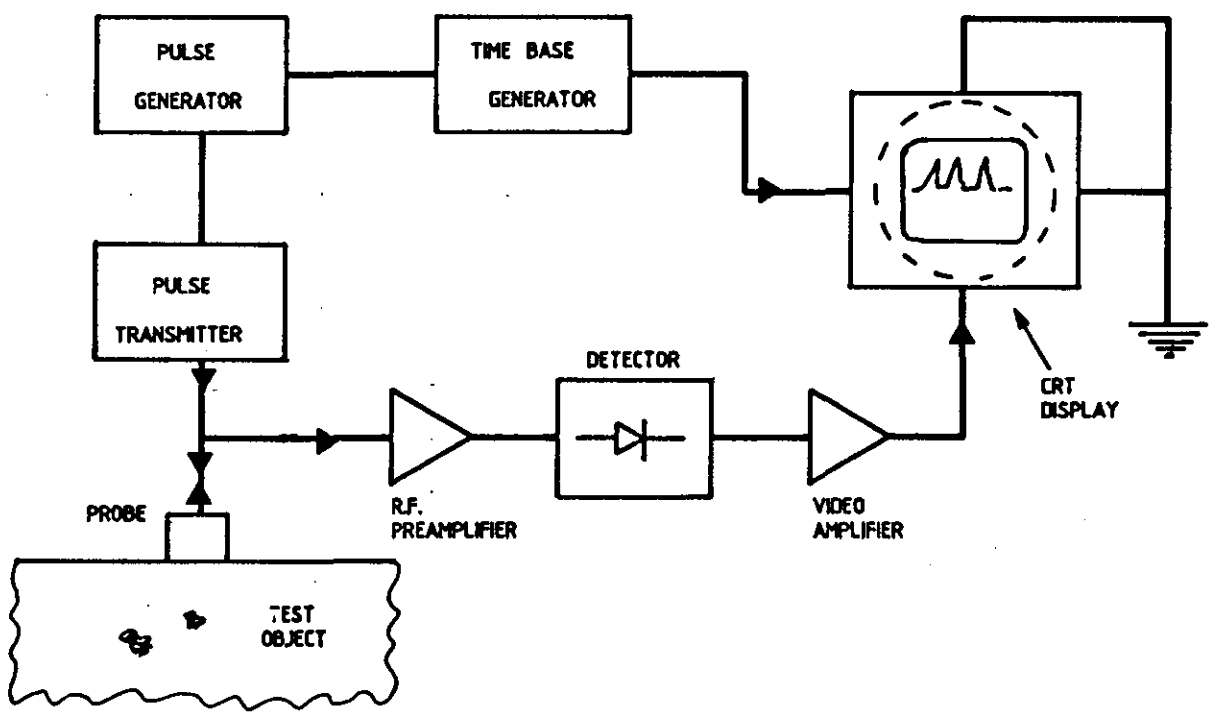

FIG. 2.1. PRINCIPLE OF A-SCAN DISPLAY.

The basic operation is as follows. A high voltage electrical spike

presented to the transducer generates an ultrasonic pulse which interacts with the targets in the test object medium. The echo signals are then picked up by the same transducer or by a separate one and are presented to a receiving amplifier. These signals are then rectified and further amplified before applying to the Y - deflection plates of a CRT whose time base is synchronized to the transmitter pulse in a suitable manner. The resulting arrangement therefore presents depth-amplitude information about the targets in the test object medium and is commonly known as the A-scan display. Its typical performance capabilities are such that :

1. Accuracy of range measurement[4] : $\pm$ 2 to 3 %
2. Resolution
   - (a) Axial : Approaches the limits shown in chapter 1
   - (b) Lateral : " " "
   - (c) Amplitude : Very good (far better than other techniques)
   - (d) Temporal : Only repetition frequency is applicable which can approach the limit shown in chapter 1
3. Sensitivity : Very good
4. repeatability : satisfactory

From the above, it is evident that apart from its use as an inspection tool, the A-scan flaw detector is most useful in calibration work and also as a real time monitoring device in other ultrasonic inspection systems. The main drawback however, is the difficulty of interpretation of results in characterizing defects due to the limited amount of information presented.

2.2 B-SCAN INSTRUMENTS

There are various forms of B-scan systems.[2,8] The simplest B-scan system uses a series of A-scan signals obtained from a single transducer which is mechanically moved along the test surface to produce a two dimensional pictorial representation of the corresponding target plane on a CRT. The display format may be understood with reference to Fig.2.2[4]

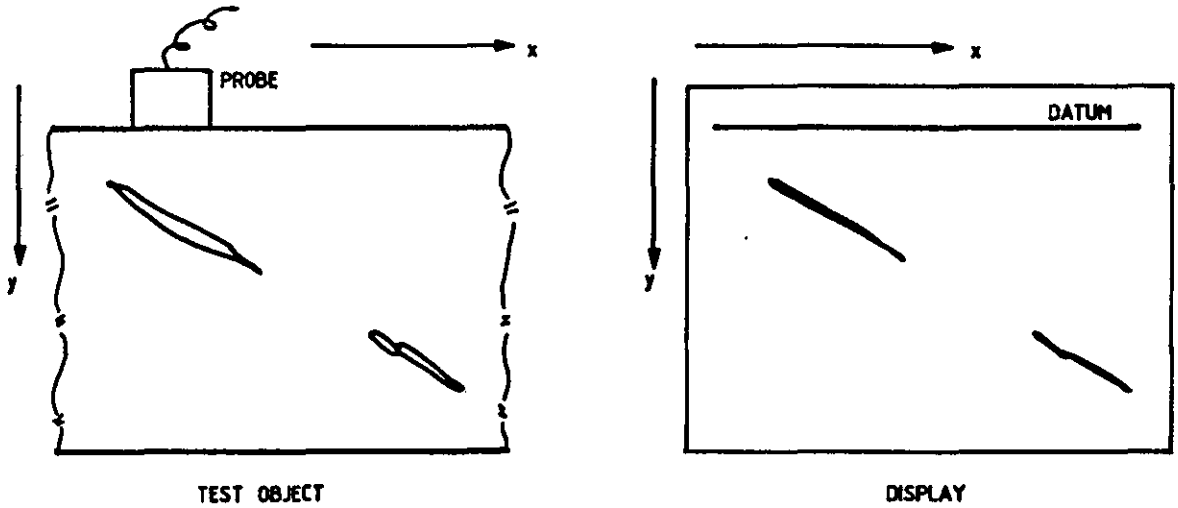

FIG. 2.2. B-SCAN DISPLAY FORMAT.

The mechanical movement of the transducer is sensed by a potentiometer and the corresponding electrical signal is used to move the CRT spot linearly in the x - direction. The time of flight information is electronically translated as depth and is used to deflect the spot in the y - direction, while the amplitude of the signals are used to modulate the brightness. Some form of storage is usually employed such as a digital frame store.

Several modifications and refinements have been made to improve the image quality of the basic B-scan technique over the years, some of which are :

1. Improved co-ordinate sensing systems to track the movement of the transducer along non-planar surface profiles
2. Use of linear arrays and electronic switching to simulate a fast repetitive mechanical scan, thus approaching real time performance
3. Improvements in lateral resolution, using,
   (a) Focused probes
   (b) Phased arrays
   (c) Dynamic focusing
4. Sector scanning, using,
   (a) Phased arrays and electronic beam steering[5,9] techniques
   (b) Single oscillating transducer
5. Synthetic aperture and computer re-construction techniques

Schematic diagram of the basic elements in a typical mechanical B-Scanner is shown in Fig.2.3.

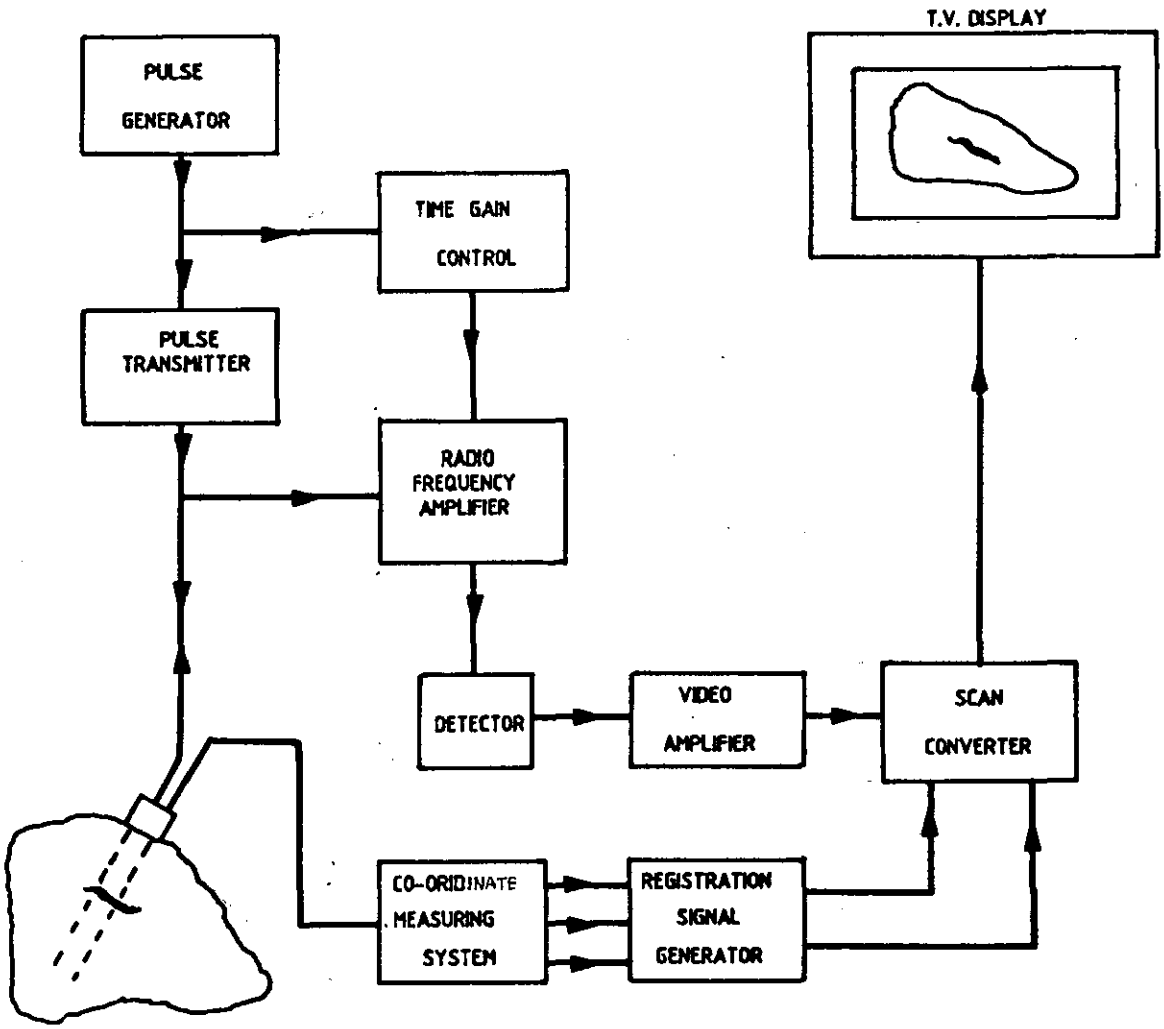

FIG. 2.3 BASIC ELEMENTS OF A MECHANICAL SCANNER.

The images are built up by a series of echo lines. If the mechanical scan is performed in a time t, and the depth of the object field is d, then the maximum number of scan echo lines in the image field is N, then

$$N = \left(\frac{c}{2d} \right) \times t \quad . \quad . \quad . \qquad (2.1)$$

However, the actual number of lines in the field may be much less as it is necessary to allow time in between the scan lines for the multiple reflections to settle down.

2.2.1 Use of linear arrays in B-scan imaging

B-scan imaging with a single probe as described above has many drawbacks. Firstly, the lateral resolution achieved is limited by the

relatively wider beamwidth of the transducer. Secondly, the signal-to-noise ratio can be relatively poor. Thirdly, the scanning speed is low. In many instances, the use of linear arrays could provide satisfactory solutions to these problems. It enhances the detectability, resolution and directional measurement of targets. Furthermore, the freedom to operate in many different modes as outlined above, makes the linear arrays rather versatile in the field of ultrasonic imaging.

However, one of the main practical problems is to ensure proper coupling of the entire length of the array to the test surface, which could be much more difficult compared to a single transducer of smaller size. Proper coupling is vital in achieving good results with arrays, not only because of sensitivity problems, but also the success of achieving good lateral resolution depends largely on the trueness of the beam characteristics in the test object medium.

In the case of a linear array B-scanner, the beam is rapidly switched through a succession of parallel directions by altering the particular group of elements fired in some sequence, for example, 1 to 5, 2 to 6, ... By repeating the sequence in succession, a certain degree of real time performance is achieved. If the frame rate is F per second and the number of lines in the field is N, then,

$$N = \left(\frac{c}{2d}\right) \times \frac{1}{F} \quad . \quad . \qquad (2.2)$$

Some factors concerning B-scan techniques can be observed at this stage.

1. From the above equation it is clear that the frame rate cannot be increased without a corresponding reduction of line density.
2. Comparison of equation 2.1 and 2.2 reveals that the image definition in the case of a real time B-scan image is inferior to that presented by a single frame B-scan image due to the reduction of line density, because in practice $t \gg 1/F$
3. None of the B-scan techniques can approach the fundamental limits

of temporal resolution discussed in chapter 1, as all B-scan techniques require a large number of discrete echo lines to form just one frame.

4. The resolution is usually determined by the size of the transducer or the group of elements fired(in the case of an array) and hence the full aperture does not directly contribute to image resolution.

In order to improve the lateral resolution, focused probes are sometimes used. However, this has the serious disadvantage of degrading the image quality outside the focal region much more rapidly than in the case of non-focused transducers, due to the divergence of the beam. In this respect one of the advantages of using arrays is the ability to manoeuvre the focus or the beam direction by electronic means. If the focusing is done in both the transmitter and the receiver mode, then much better side-lobe rejection can be achieved in addition to the improvement in sensitivity. It is also possible to manipulate the delays such that the focus follows the transmitted pulse. This is found in some sophisticated B-scanners and is known as dynamic focusing[4], which improves the lateral resolution throughout the image field. However, these techniques generally suffer from bandwidth limitations and therefore may be used only in applications where signal distortion is less critical.

Another popular technique is to use frequency multiplexing, where the beam sweep is effected by connecting each channel with a local oscillator whose frequency varies by constant increments along the array. However, one of the difficult practical problems with this technique is to generate phase locked signals of different frequencies for all the channels.

2.2.2 Sector scanning systems

These techniques are mainly used in medical imaging systems[2,3] where access to some organs such as the heart is limited. The scanning sectors are formed by the mechanical movement of the transducer or a group of identical transducers in rapid succession.

Although the single point entry provided by these techniques is very beneficial, the image quality can be inferior compared to other methods, mainly due to the smallness of the transducer generating a wider beam.

2.3 C-SCAN SYSTEMS

C-scan is an orthogonal imaging technique[4] and is used in situations where the depth of defects is irrelevant, but their distribution parallel to the test surface is an important feature. The image has to be built up in a similar fashion to B-scan and the principle may be understood with reference to Fig. 2.4.

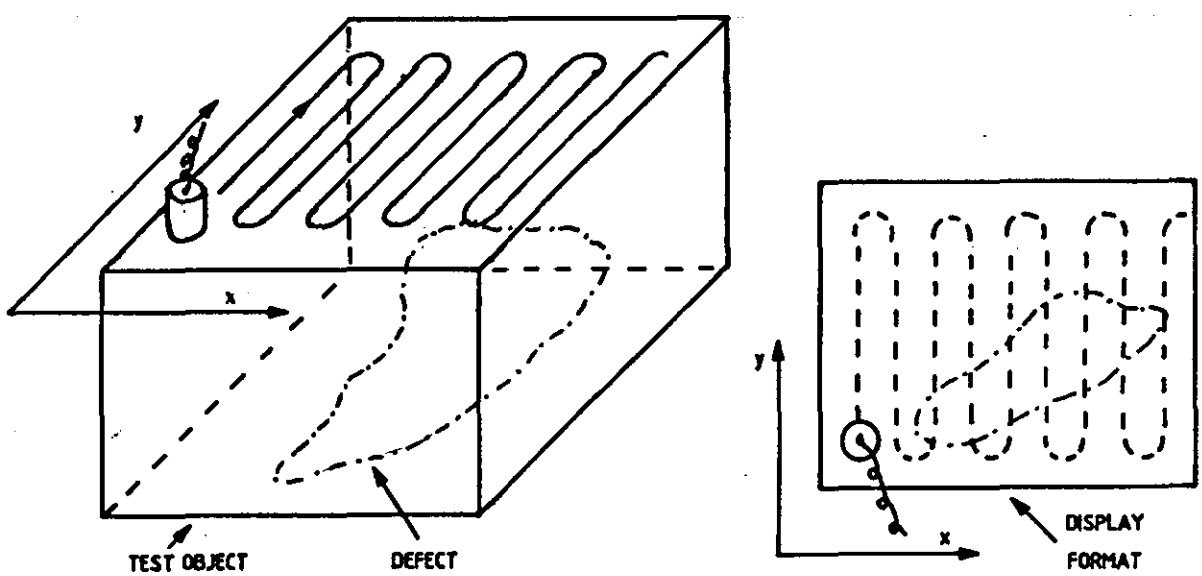

FIG. 2.4 THE PRINCIPLES OF C-SCANNING.

An advantage with C-scan technique is that a required plane (usually a thin layer of the test object) may be effectively selected by electronic range gating. The lateral resolution can also be improved using focused probes in this case as the focusing could be held fixed at a particular depth of interest.

However, the use of C-scan technique is particularly limited to special applications like bond line testing. Some problems that limit its use are the lack of speed, difficulties in direct interpretation and the uncertainties involved with the finite thickness of the layers selected.

2.4 ULTRASONIC HOLOGRAPHY

In contrast to pulse echo imaging techniques described above, ultrasonic holography is based on a conceptually more advanced approach of using phase-amplitude and time of flight information to reconstruct acoustic wavefronts.[8] Holographic systems may be broadly classified into two groups. The first contains those systems which are approximately analogous to optical holography, while the second contains those systems which are analogous to synthetic aperture radar in which a scanning technique is used. Fig. 2.5 shows an elementary form of optically analogous ultrasonic holography using a liquid surface levitation technique.[4]

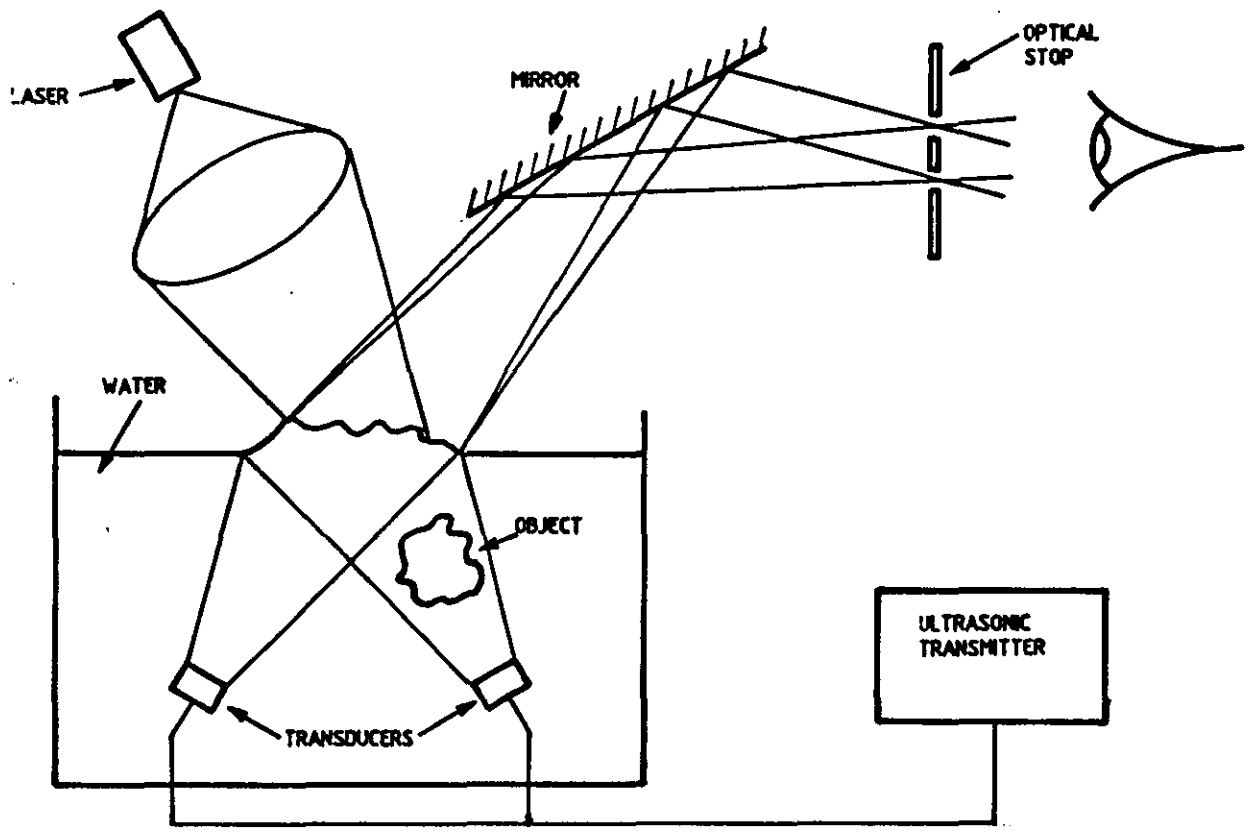

FIG. 2.5 ULTRASONIC HOLOGRAPHY (OPTICAL ANOLOGY).

In the above arrangement, two transducers driven from the same generator are placed in a water tank such that they overlap at the liquid surface. The ripple pattern formed on the surface in the absence of any disturbance in the sonic paths are modified accordingly when an object is placed in the path of one of the beams. The resultant static displacement is the ultrasonic hologram and the images are viewed by means of coherent light reflected from the surface which is focused on to an optical stop to remove all but the first order diffraction patterns. The detailed theory is given by Hilderland and Brendon.[10]

In the scanning systems, the wavefronts from the object is sampled on point by point basis over the receiving aperture as illustrated in Fig. 2.6. After multiplying the received signal with a reference to obtain a holographic coding, it is laid down on the recording medium by a scan similar and synchronous to that of the receiving aperture. The recorded hologram is converted into a photographic transparency and the image is viewed optically. Alternatively the holographic coding may be recorded in a computer store and re-construct the image using digital techniques.[8]

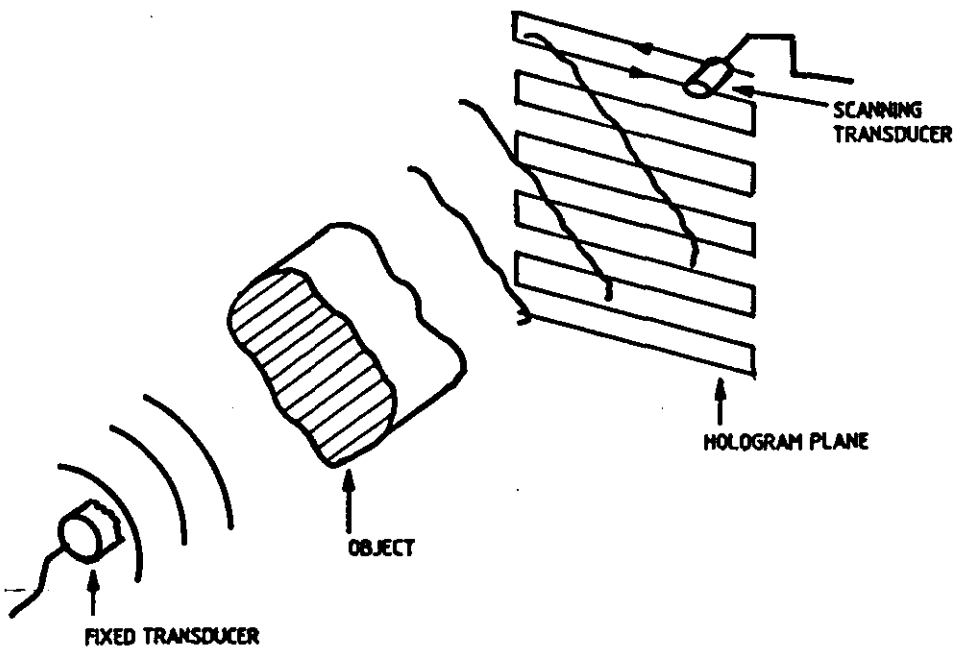

FIG. 2.6. ACOUSTIC HOLOGRAPHY (synthetic aperture analogy).

The main advantage of holography seems to be its ability to give good resolution to large depths. However, holography has not found wide acceptance in NDT, mainly due to the instrumental complexity, economics

and difficulties of using it.

2.5 DIRECT ULTRASONIC VISUALIZATION OF DEFECTS, [DUVD] SYSTEM

In 1973, Hanstead demonstrated a new imaging system called Direct Ultrasonic Visualization of Defects,[6,11] [DUVD]. It is comparable to ultrasonic holography in achieving a three dimensional image, but unlike other pictorial methods, DUVD operates without the need for mechanical or electronic scanning. Furthermore it does not require coherent light and it operates in real time. Fig.2.7 shows one form of DUVD using plastic lenses in water.[12,13]

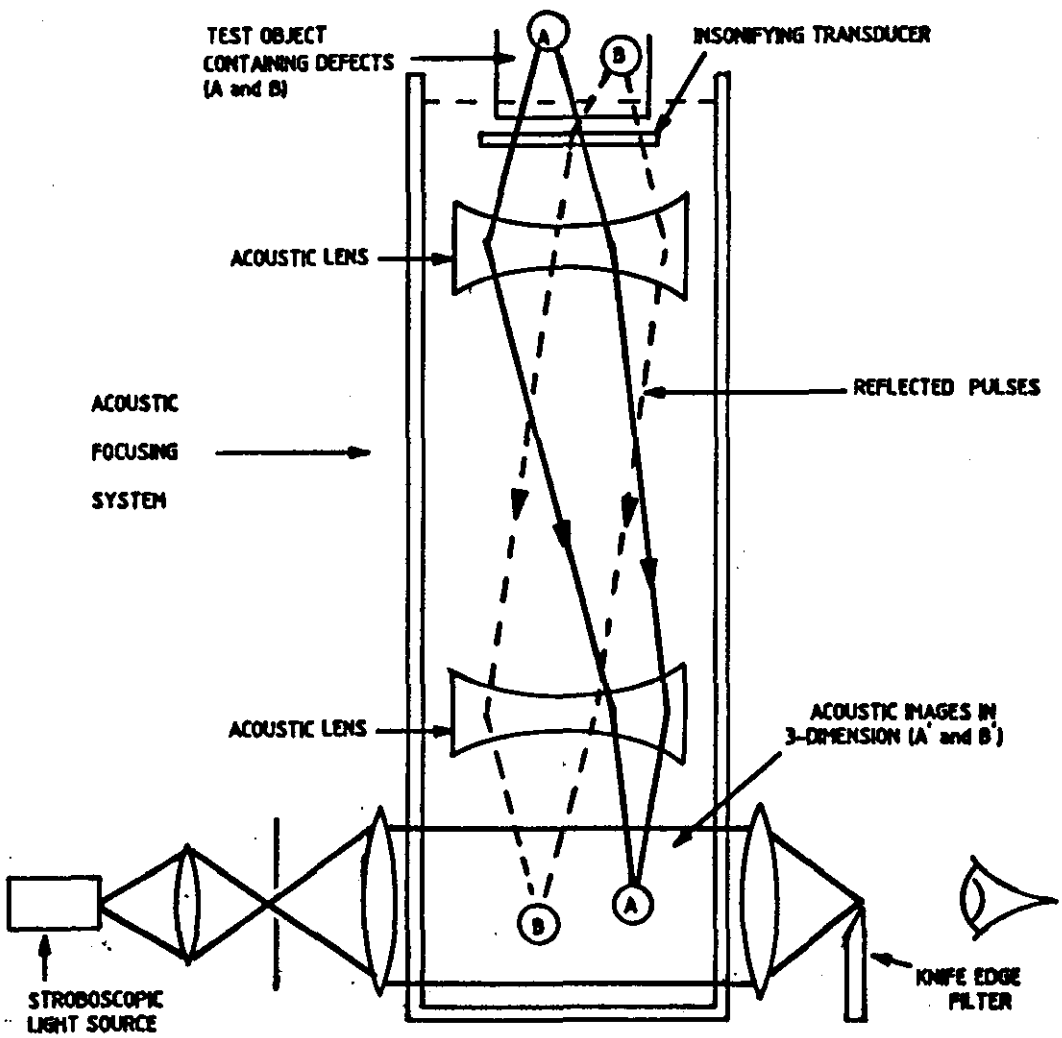

FIG. 2.7 DUVD USING PLASTIC LENSES IN WATER.

DUVD essentially consists of a pair of acoustic lenses arranged in such

a way to produce a three dimensional image with two other special properties called linearity and isochronicity. The term 'linearity' here refers to its ability to maintain a constant object-to-image spatial relationship, while 'isochronicity' means that when the test object is insonified with a short pulse, all the echoes from different targets [defects], irrespective of their distances, arrive simultaneously at their respective image points, thus giving the system its ability to display the whole image focused at once.

The acoustic images formed are made visible in a suitable transparent medium either by photoelastic technique[14,15] or by the schlieren technique[16,17] of visualization using stroboscopic flashes of light.

Although DUVD has very remarkable features, as mentioned above, the fundamental problem is its low sensitivity. This is mainly so as the system is 'passive' in that it only utilizes the insonifying energy for acoustic image formation and heavy energy losses are involved. Further work on this technique has also been reported by Hayman[12] and by Bar-Cohen et.al.[18,19] Even so, at its best the sensitivity of DUVD falls far short of that required for practical implementation. The other drawbacks are the difficulties in coupling and manipulation.

2.6 OTHER PICTORIAL METHODS

There are several other pictorial methods for ultrasonic examination, such as Bragg diffraction imaging, and various forms of ultrasonic cameras.[4,5] They too have many problems and drawbacks which limit their use in practice. Two recent developments have been an American system by the brand name SIGMA SDL 1000, based on computer reconstructed holographic technique with mechanically scanned aperture and the Zipscan developed at the AERE Harwell. The latter uses diffraction based time of flight measurements to locate and size defects. Although they have many attractive capabilities, the instrumental complexity, low speed, size and particularly the price being around £200,000 and £80,000 respectively are the major set backs.

2.7 CONCLUSIONS

It is evident from the above that most of the existing systems fall far short of the features that could be considered as ideal for imaging applications. It is also noted that in many cases the fundamental limitations of the particular techniques do not permit much room for significant improvement.

However, it is interesting to note that the DUVD system has many features which are very close to the 'ideal', except for its main problem of low sensitivity. Therefore, it seems reasonable to examine this technique in details and the ways and means by which further developments could be made.

--- // ---

- CHAPTER 3 -

HANSTEAD'S DUVD SYSTEM AND ITS PROSPECTIVE LINES OF DEVELOPMENT

In this chapter, DUVD technique is examined in detail to study its remarkable features and the root causes of the drawbacks, as an important step towards identifying prospective lines of development.

3.1 DUVD DESIGN FEATURES

The basic concept of the DUVD is formulated to satisfy the requirements that, an ultrasonic focusing system should ideally have two essential properties called linearity and isochronicity as defined in the previous chapter. This is achieved in the DUVD using a special design of pair of acoustic lenses as shown below.

3.1.1 Conditions relating to linearity

Hanstead used calculations based on ray optics[11] to derive the necessary conditions. The sign conventions and the symbols used are as shown in Fig. 3.1 below.

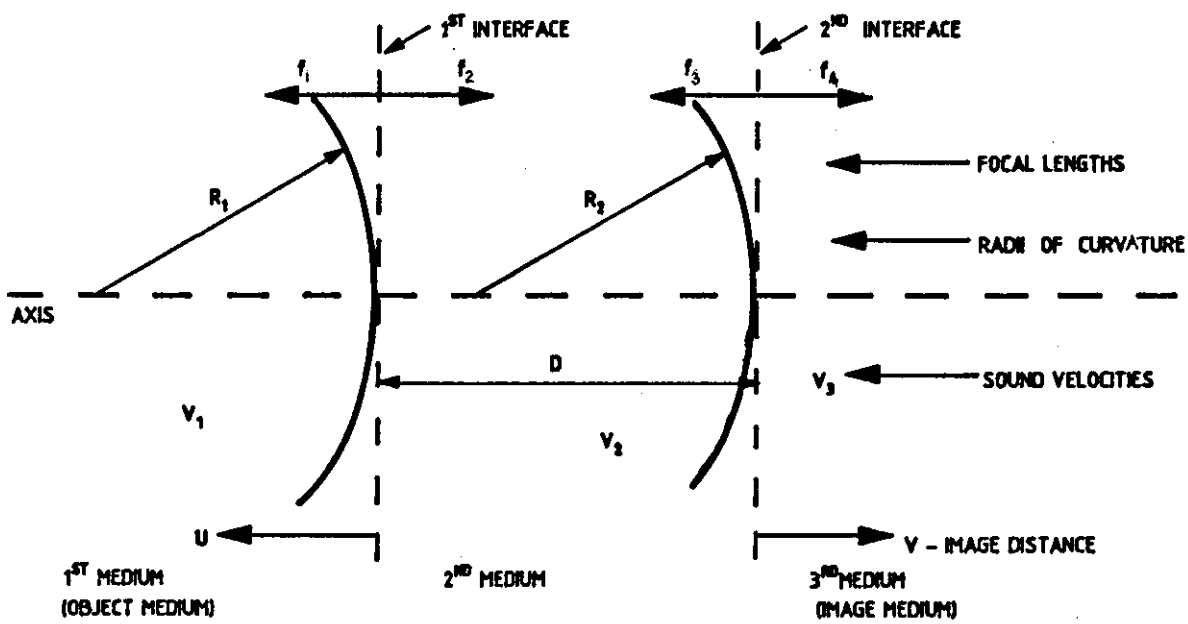

FIG. 3. 1. TWO-LENS DUVD PARAXIAL ANALYSIS : CONVENTIONS AND SYMBOLS.

The object distance to image distance relationship for a combination of lenses as above may be written as :

$$v = \frac{f_3 f_4}{D-\left[f_1 f_2 /(u-f_1)\right]-f_2-f_3} + f_4 \quad \ldots (3.1)$$

This relationship can be made linear by incorporating the condition

$$D = f_2 + f_3 \quad \ldots (3.2)$$

which makes the focal points coincident. Then,

$$v = -\frac{f_3 f_4}{f_1 f_2}(u-f_1) + f_4 \quad \ldots (3.3)$$

This is linear in v and u and therefore the arrangement gives axial linearity. Also, the axial magnification M_A may be written as,

$$M_A = -f_3 f_4 / f_1 f_2 \quad \ldots (3.4)$$

The linearity in the lateral direction may be seen from the ray diagram as in Fig. 3.2.

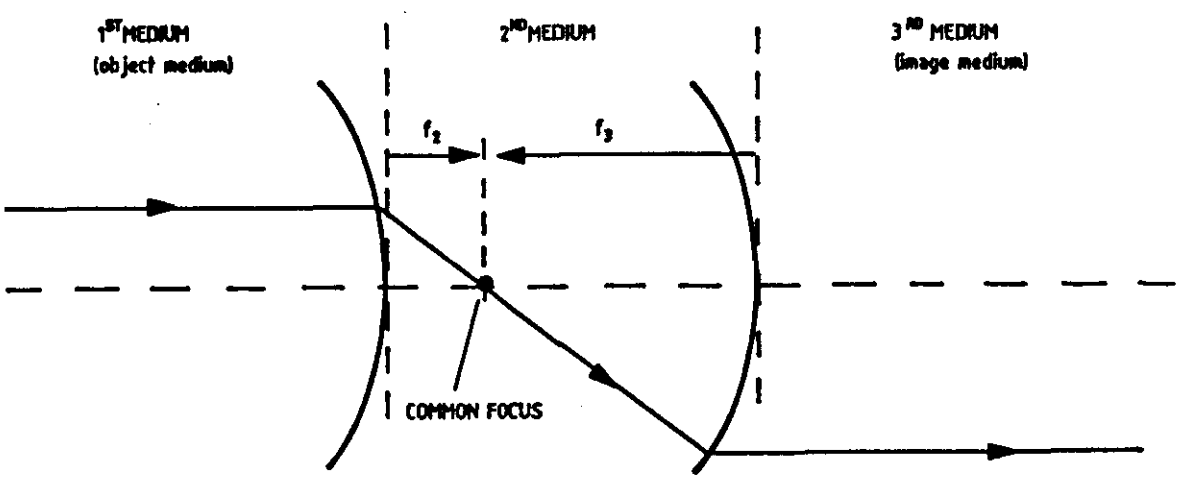

FIG. 3. 2. TRANSVERSE LINEARITY

From the above paraxial ray diagram it is seen that the lateral magnification M_L can be written as :

$$M_L = - f_3 / f_2 \quad . \quad . \quad . \quad . \qquad (3.5)$$

Therefore it follows that taking the focal points coincident is the only necessary constraint to produce the overall property called 'linearity'. It is also noted that the two magnifications are not necessarily equal, except in the case where f_2 and f_3 are equal.

The maximum usable object and image distances are found by substituting zero for v and u, respectively, in equation 3.3, giving,

$$u_{max} = (f_1 \, f_2 / f_3) + f_1 \quad . \quad . \qquad (3.6)$$

and

$$v_{max} = (f_3 \, f_4 / f_2) + f_4 \quad . \quad . \qquad (3.7)$$

3.1.2 conditions relating to isochronicity

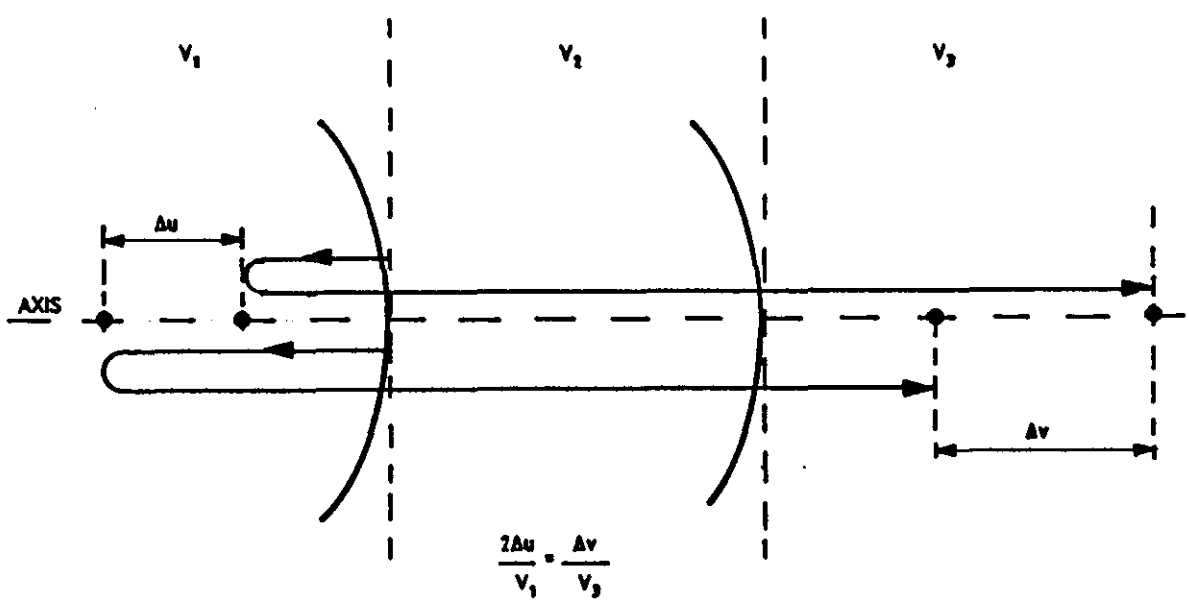

FIG. 3. 3. REQUIREMENTS FOR ISOCHRONICITY

Referring to Fig. 3.3, if an axial displacement of Δu in the object

medium results in a corresponding displacement of Δv in the image medium, then the necessary conditions for isochronicity would be :

$$\frac{2\Delta u}{v_1} = \frac{\Delta v}{v_3} \quad . \quad . \quad . \quad . \qquad (3.8)$$

Hence from equations (3.4) and (3.8), the axial magnification M_A can be written as

$$M_A = -\frac{2v_3}{v_1} \quad . \quad . \quad . \quad . \qquad (3.9)$$

since $f_1 / f_2 = v_2 / v_1$ and $f_3 / f_4 = v_3 / v_2$,and using equations (3.4) and (3.9) it can be shown that the necessary condition for isochronicity is obtained when

$$f_1/f_4 = 1/\sqrt{2} \quad . \quad . \quad . \quad . \qquad (3.10)$$

Thus the necessary and sufficient conditions for linearity and isochronicity are :

1. The internal focal points must be coincident
2. The external focal lengths must be related by : $f_4 = \sqrt{2}\ f_1$

It also follows from equations (3.4), (3.5) and (3.10) that

$$M_A = \sqrt{2}\ M_L \quad . \quad . \quad . \quad . \qquad (3.11)$$

which is the relationship between axial and lateral magnifications.

Because of its direct relevance in the present work, the following table[11] gives a set of parameters for the design of a DUVD system, where v_1 , v_2 , v_3 and f_1 are regarded as independent variables.

Item No.	Symbol	Definition	Value in terms of independent variables
1	V_1	Sonic velocity in 1st medium	Independent Variables
2	V_2	" " " 2nd "	
3	V_3	" " " 3rd "	
4	f_1	1st focal length of 1st lens	
5	f_2	2nd focal length of 1st lens	$\frac{V_1}{V_2} f_1$
6	f_3	1st " " " 2nd "	$\sqrt{2} \frac{V_3}{V_2} f_1$
7	f_4	2nd " " " " "	$\sqrt{2}\ f_1$
8	R_1^*	Radius of curvature of 1st interface	$\left(1 - \frac{V_1}{V_2}\right) f_1$
9	R_2^*	" " " " 2nd "	$\sqrt{2}\left(\frac{V_3}{V_2} - 1\right) f_1$
10	D	Distance between lenses	$\left(\frac{V_1}{V_2} + \sqrt{2}\ \frac{V_3}{V_2}\right) f_1$
11	u_{MAX}	Maximum object distance	$\left(1 + \frac{1}{\sqrt{2}}\ \frac{V_1}{V_3}\right) f_1$
12	v_{MAX}	" image "	$\left(\sqrt{2} + 2\ \frac{V_3}{V_1}\right) f_1$
13	M_L	Longitudinal magnification	$2 \frac{V_3}{V_1}$
14	M_T	Transverse "	$-\sqrt{2} \frac{V_3}{V_1}$

Table 3.1 DUVD design parameters - (after Hanstead)

One of the problems with the original DUVD system is that the object medium acts virtually as a part of the system, severely limiting its use in practice. This is because the curved interface between the two media represents the first acoustic lens. Also the design is not feasible as the velocity of the second medium approches the first. Hence another configuration utilizing two thin lenses and a coupling medium has been deviced by Hanstead and the appropriate design equations are given in several references.[6,11,13]

Figs. 3.5 and 3.6 show some results achieved with the Hanstead's DUVD system. The first shows an image of some holes drilled in a steel specimen to which the insonifying transducer was bonded, while the latter shows an image of some steel pins immeresed in water.

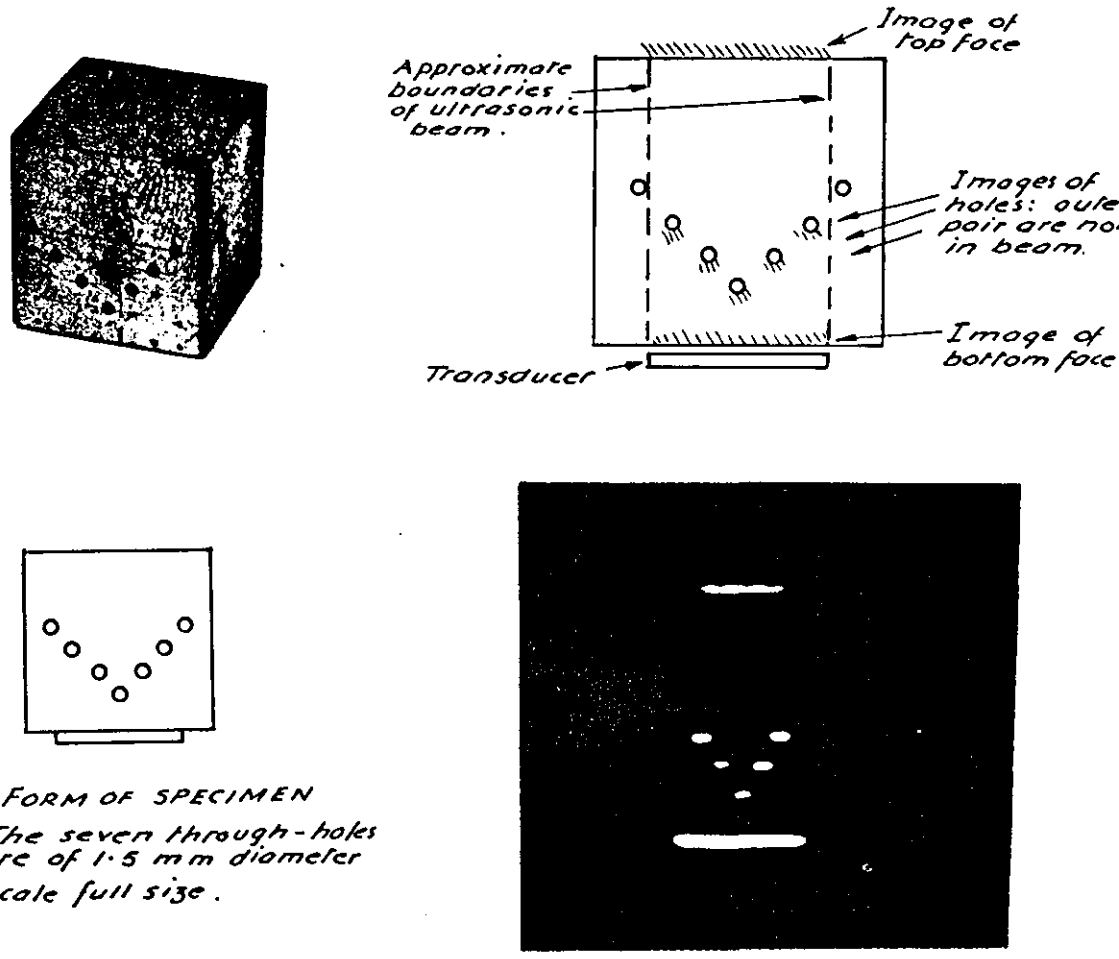

Fig. 3.5 DUVD image of some holes drilled in a steel specimen (after Hanstead)

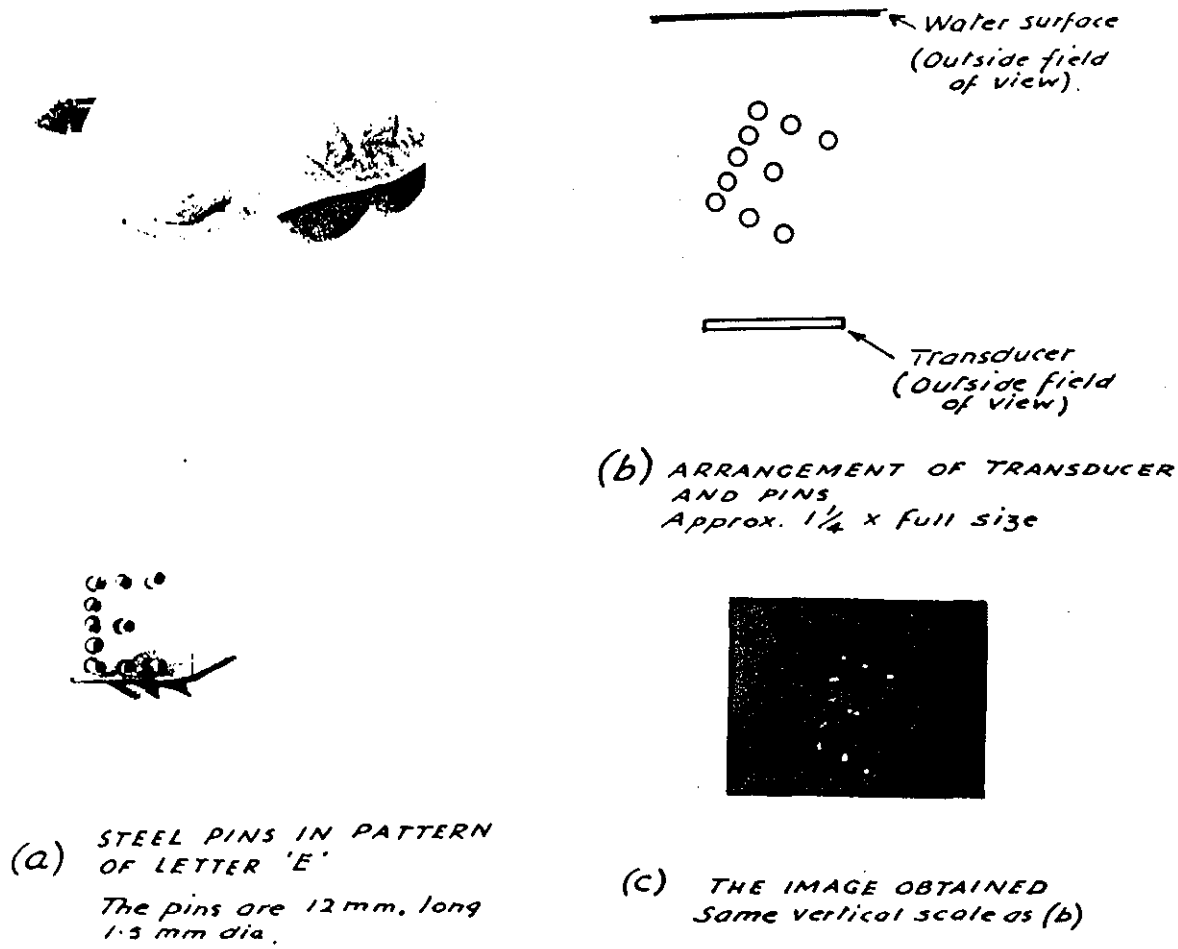

Fig. 3.6 DUVD image of some steel pins immersed in water (after Hanstead)

3.1.3 Practical limitations of the DUVD

Although the DUVD technique has many features which are close to the characteristics of an ideal imaging system, it has not been implemented in practice due to a series of drawbacks. The most serious problem is its very low sensitivity, about 50 dB less than other conventional techniques. Most of the other limitations like small field of view, necessity to bond transducers to the test material in some cases, the need to have a high insonifying power, are linked with this problem. It also lacks manouverability as the test object is virtually a part of the system forming the first refracting interface. If the images are to be viewed in three dimensions, stereoscopic visualization is required which makes the system even more difficult to handle. On the other hand, viewing a 3-D acoustic image in 2-D could be very confusing depending on the nature and the extent of defects present in the object medium.

Further work on this technique mainly concerning the ways of improving its sensitivity has also been reported by Hayman[12], and Bar-Cohen et. al.[18] In this respect Hayman investigated the following.

(1) Use of more sensitive visualizing media instead of water
(2) Improvements of optics in the schlieren system
(3) Reduction of optical scatter
(4) Increased insonifying power
(5) Optimum choice of materials
(6) Astigmatic defocusing

From these studies Hayman ruled out the general application of DUVD in NDT and in medical diagnostics, mainly on the ground of low sensitivity.

Bar-Cohen et. al used a different sonoptical geometry consisting of a single lens and a reflecting concave mirror as shown in Fig. 3.7.[18]

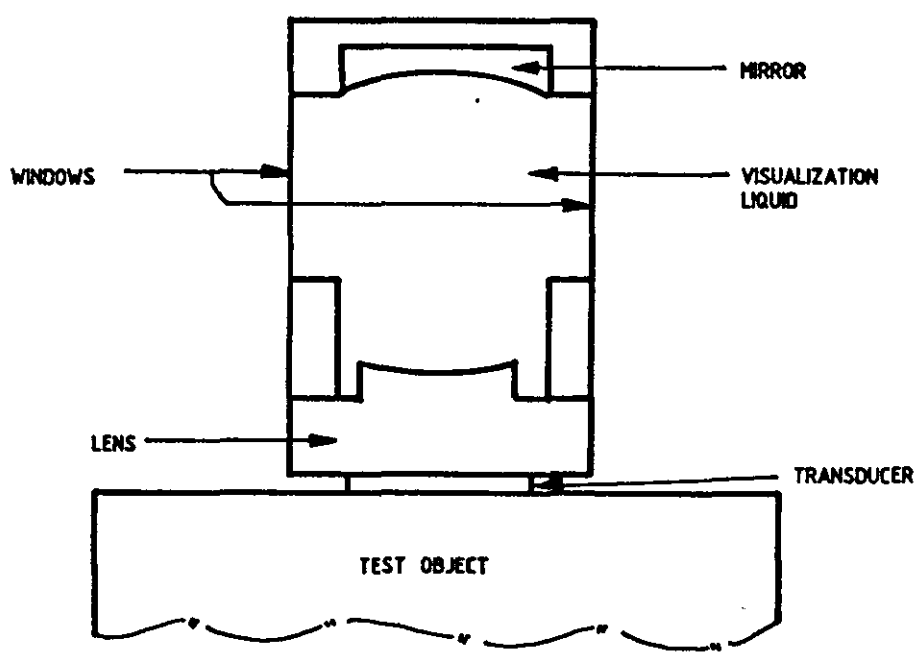

FIG. 3.7 DUVD USING A LENS AND A MIRROR ARRANGEMENT
(BAR-COHEN ET. AL)

This arrangement gave some improvements in sensitivity, partly due to the less attenuation of the system. Another useful finding was when testing materials with rather different sound velocities with the same

arrangement, the degradation of image quality due to the loss of isochronicity can be tolerated if slight alterations are made to the delay between the insonifying pulse and the stroboscopic flash.

In spite of all these efforts however, the sensitivity of the DUVD was still far below that required for practical implementation.

3.2 PROSPECTIVE LINES OF DEVELOPMENT OF THE DUVD

From the above, it is clear that conventional approach to enhance the performance of DUVD is not adequate to promote its use as a practical inspection tool. Its main problem of low sensitivity therefore has to be solved in a different way. For example by introducing electronic amplification. One natural option is to consider the use of ultrasonic arrays with which amplification may be introduced. However, the technique will then no longer be a direct ultrasonic visualization of defects in that sense, but one which is essentially an active, sampling and re-construction technique to which the ideal features of the DUVD are introduced. Such a new concept would obviously involve a great deal of investigations to identify the parameters and to study the feasibility. It would also be inevitable that a great deal of hardware development would be involved. However, because no other system presents the ideal characteristics of the DUVD, it appears to be well worth pursuing along this new approach.

--- // ---

- CHAPTER 4 -

THE NEW CONCEPT

This chapter deals with the formulation of a new concept for developing an ultrasonic imaging system that has the ideal characteristics of the DUVD principle by adopting a new sonoptical geometry, while eliminating its major drawbacks by means of transducer arrays and electronic amplification.

4.1 OBJECTIVES OF THE NEW CONCEPT

As seen from the previous chapter, the most attractive features that are found in the DUVD and that are to be preserved in the development of a new system are :

(1) Linearity
(2) Isochronicity
(3) Real time operation

At the same time the main problems to be solved are :

(1) Low sensitivity
(2) Lack of manouverability
(3) Imaging a selected axial plane, rather than producing a 3-D image which is viewed in 2-D

4.2 CONCEPTUAL FORMULATION

In order to examine various possibilities of achieving the above objectives, consider the basic block diagram of the original DUVD as shown in Fig. 4.1. The blocks are placed adjacent to each other to appreciate the fact that the original DUVD is an integral design.

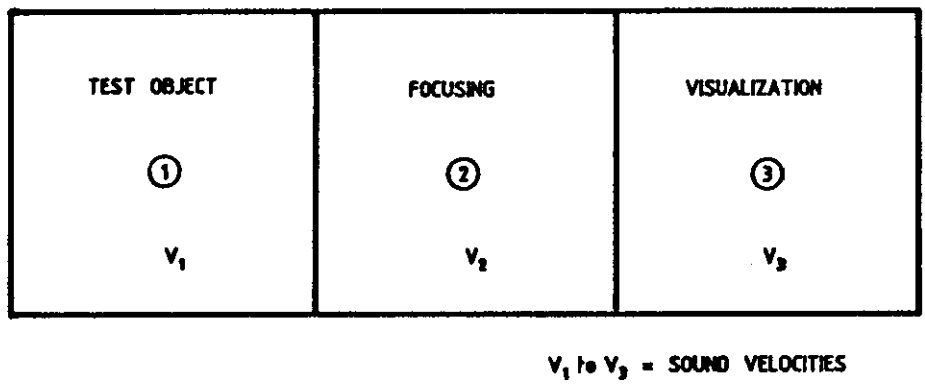

FIG. 4. 1. BASIC BLOCK DIAGRAM OF THE DUVD

Supposing the interface between 1 and 2 is separated and replaced with a set of transducer arrays having a large number of elements between which amplification is introduced in parallel channels, all the factors listed under 4.1 may be achieved. In acoustic terms, this is equivalent to introducing a 4th medium between blocks 1 and 2, whose sound velocity is infinitely high, causing no change in the acoustic focusing properties of the original system. Therefore the same design equations are valid and hence linearity, isochronicity and real-time operation are preserved. This new concept is schematically shown in Fig. 4.2 which is also briefly summarized as follows.

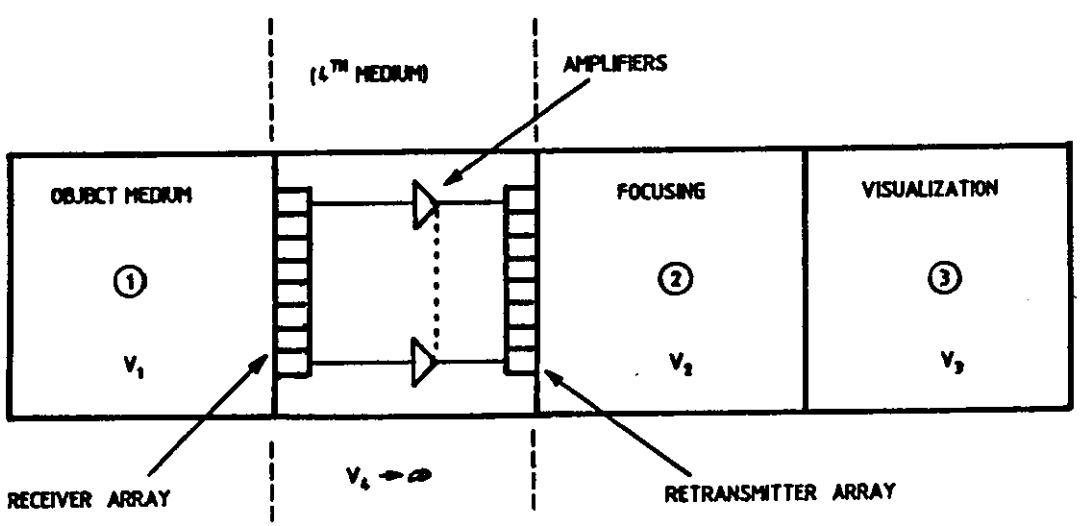

FIG. 4. 2. A NEW CONCEPT OF ULTRASONIC IMAGING

(1) Echo signal reception by means of a linear array of transducers

(2) Electronic amplification of received signals in parallel channels

(3) Re-transmission of amplified echo signals into a visualizing medium using a second array of transducers forming a part of an acoustic focusing system, capable of forming focused B-scan type images.

In Fig. 4.2, the block containing the receiver/re-transmitter arrays together with the amplifiers is considered as the 4th transmission medium whose sound velocity is infinite. It illustrates the fact that this will not alter the characteristics of the DUVD principle.

Since amplification is now employed, the problem of low sensitivity can be eliminated. The lack of manoeuverability is also solved as the test object can now be separated from the rest of the system. In order to achieve co-axial imaging, the focusing system may be re-designed with cylindrical surfaces instead of spherical surfaces used in the original DUVD, so that targets in a selected plane may be displayed as focus B-scan type images.

4.3 DIFFERENT POSSIBLE WAYS OF IMPLEMENTING THE NEW CONCEPT.

For the following discussion, the validity of the new concept is assumed which will be proved later. The arrays are considered as of one dimensional strip element construction and the refractive interfaces are designed to be cylindrical, so that focused B-scan type images are formed.

4.3.1 Implementing the new concept using the two-lens DUVD

One straight forward method of implementing the new concept is illustrated in Fig. 4.4. Here, the two lens DUVD configuration as the one showed in Fig. 2.7 is used and amplification is virtually introduced within the coupling medium.

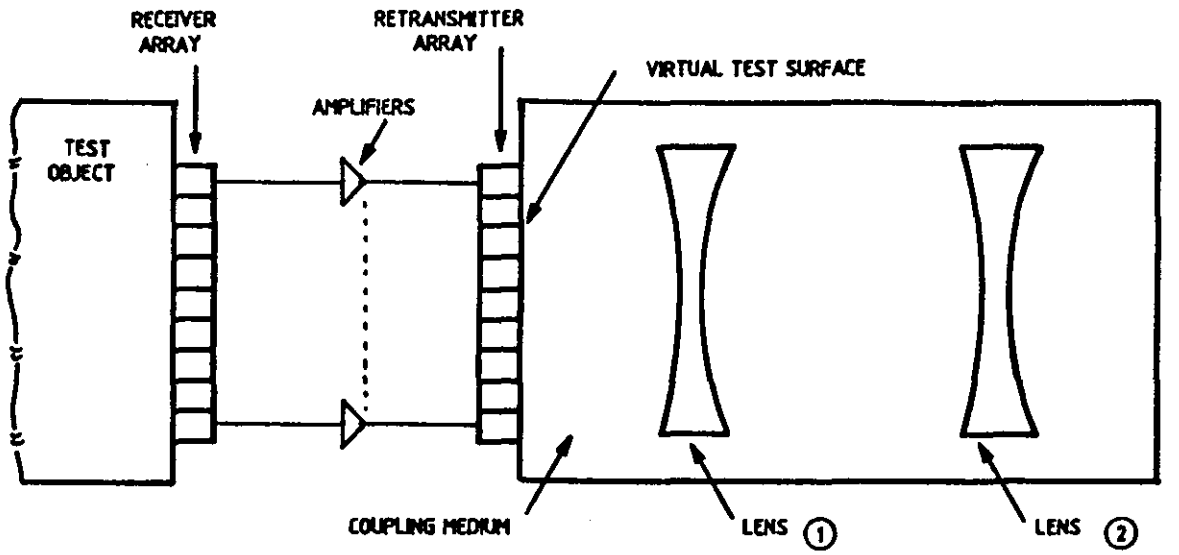

FIG. 4. 4. IMPLEMENTING THE NEW CONCEPT USING THE TWO LENS DUVD

The advantage of this approach is the simplicity, as no other major changes to the DUVD technique are necessary. The surface of the re-transmitting array becomes a virtual test surface where the re-transmitted wave fronts are much more strong than those received at the true test object surface. However, the drawbacks are the low efficiency due to acoustic mismatch, excessive multiple reflections and attenuation etc.

Transducer arrays could also be manipulated to simulate the action of a lens in addition to their use as receivers, transmitters and various other applications. Such techniques are well established in sonar and medical applications and therefore it is worth investigating these possibilities as well in the present case, as elimination of any lens or a refracting interface would naturally enhance the sensitivity even more and simplify the system further.

4.3.2 Use of electronically phased arrays

As mentioned earlier, electronic focusing by means of introducing phase delays[5,20] is commonly used with arrays and therefore to examine the applicability of this approach for the present purpose, the following analysis is presented. Fig. 4.5 shows an illustration of a possible arrangement where electronic phase delays are introduced to the received electrical signals to simulate the action of the first refracting interface of the DUVD which is designed with the single refracting

interfaces at both the lens positions.

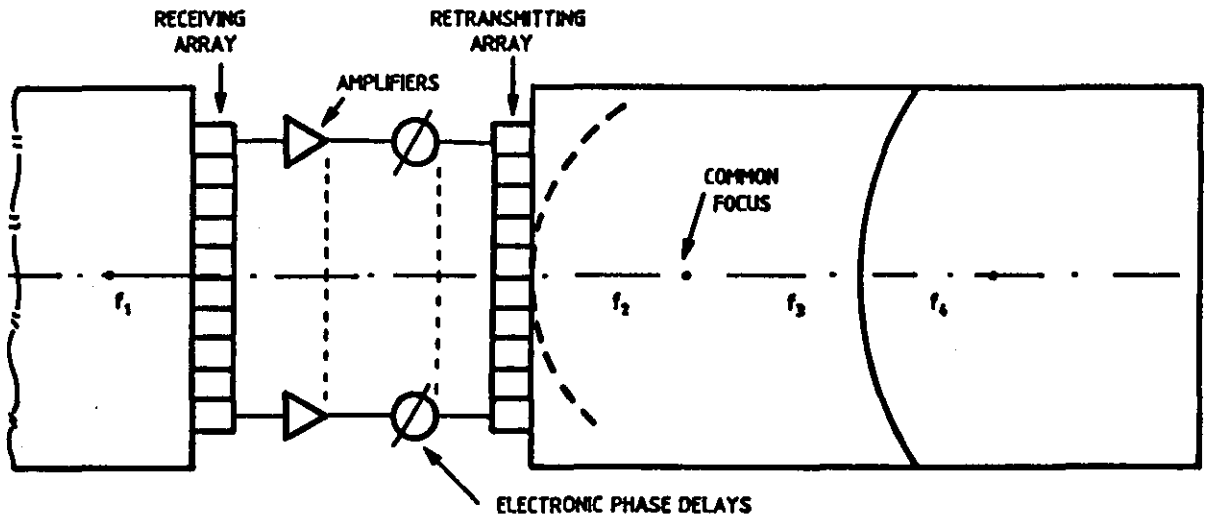

FIG. 4. 5. IMPLEMENTING THE NEW CONCEPT WITH THE DUVD, HAVING SINGLE REFRACTIVE INTERFACES AT BOTH THE LENS POSITIONS.

An attractive feature of this technique is the ability to manipulate the second focus, and hence the focal length f_2 , by electronic means which gives greater flexibility in the sono-geometrical design. With reference to fig. 4.6 below, the necessary amount of phase delays to be applied to the elements of the array with respect to the middle element may be calculated as follows.

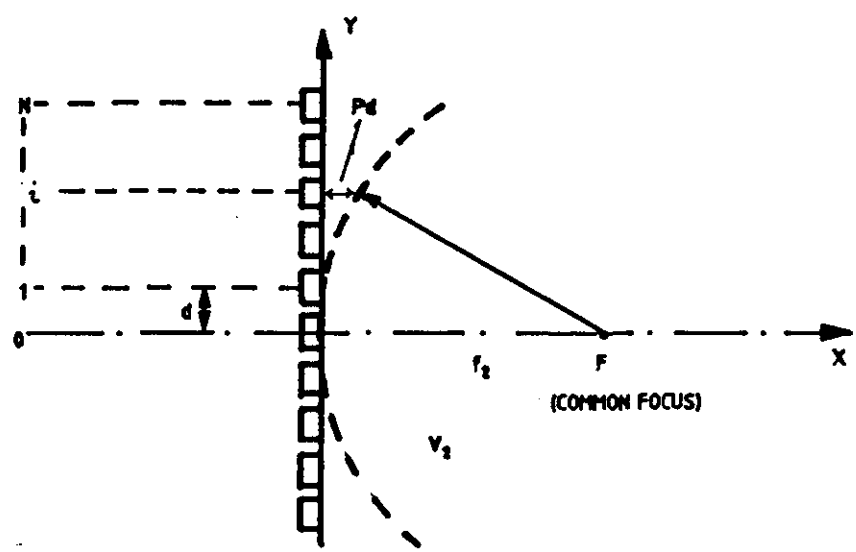

FIG. 4. 6. PHASE DELAY REQUIREMENTS TO SIMULATE THE ACTION OF THE FIRST REFRACTING INTERFACE.

i	=	i th element	p.d	=	path difference
d	=	element spacing	v_2	=	sound velocity in the second medium
2N	=	number of elements	v_1	=	sound velocity in the first medium
f_2	=	second focal length			

y co-ordinate of the ith element is

$$y_i = i\,d$$

$$\therefore \text{ p.d.} = (f_2^2 - i^2 d^2)^{\frac{1}{2}} \quad . \quad . \quad . \qquad (4.1)$$

$$f_2 = \left(\frac{v_2}{v_1}\right) f_1$$

$$\therefore \text{ p.d.} = \left(\frac{v_2}{v_1}\right) f_1 - \left[\left(\frac{v_2}{v_1} f_1\right)^2 - i_1^2 d^2\right]$$

$$\phi_i = \left[\left(\frac{v_2}{v_1}\right) f_1 - \left[\left(\frac{v_2}{v_1} f_1\right)^2 - i_1^2 d^2\right]\right] \times \frac{2\pi}{\lambda}$$

where ϕ_i is the necessary phase to be introduced into the i th element relative to the middle element in order to define the focal length f_2 .

Phase delays can be introduced by means of active analogue delay circuits or by passive lump parameter delay lines. However, these methods can cause problems. Firstly, these are essentially narrow band techniques leading to signal distortion problems particularly if dealing with short pulses and therefore the full potential of the new concept cannot be realised. As an attempt to overcome signal distortion problems, non dispersive broad band time delay lines such as co-axial cables may be used, but the shear length of the cables required is unacceptable for a multichannel transmission system. The second problem

is caused by the non ideal behaviour of the array elements. In practice, array elements do not possess omni-directional response and hence the response fades away off their axes leading to amplitude shading with the increase in the array aperture.

Since both the amplitude and phase information have much greater significance in the image formation compared to many other techniques, the use of electronic focusing methods do not seem to be a good choice for the present purpose. Therefore it is worth investigating other possible methods of using arrays where focusing is achieved by mechanical means.

4.3.3 Use of a curved re-transmitting array

One of the interesting possibilities of applying phase delays to simulate the action of the first refracting interface is shown in Fig. 4.6. Here, a curved re-transmitting array is used whose focal length f_2, is made equal to that required by the equation (3.2), $D = f_2 + f_3$, where symbols are as defined previously.

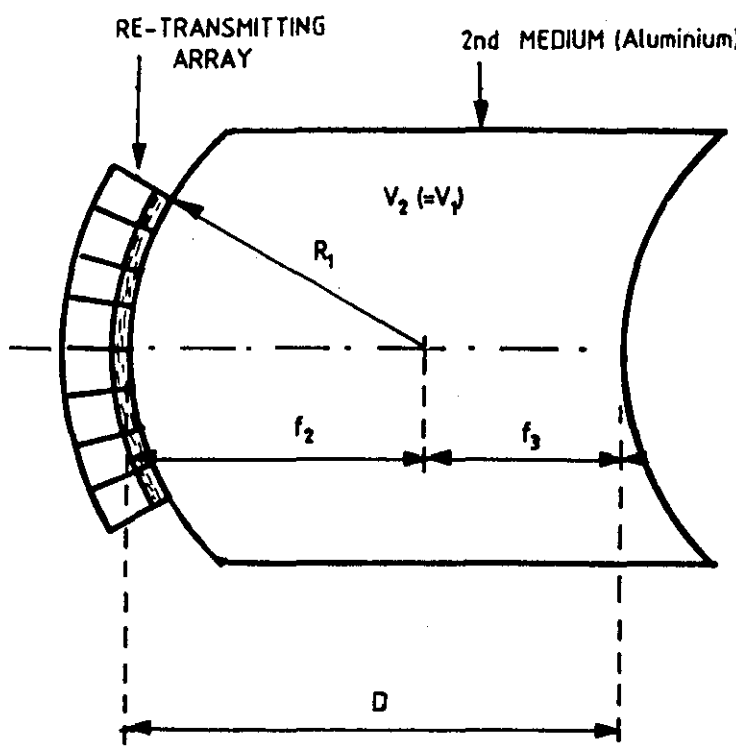

FIG. 4.6 USE OF A CURVED RE-TRANSMITTING ARRAY

Apart from eliminating the first refracting interface which lowers the acoustic signal losses, the other main advantages of this arrangement are the simplicity, compactness and less amplitude shading.

As mentioned in chapter 3, the sound velocities in the test object medium and the second medium in the original DUVD must differ significantly in order to be able to design a two-lens DUVD system. However with the above approach this restriction is also removed because focusing is done by the re-transmitter array itself, irrespective of refractive index differences of the two media. This gives the freedom to use a 2nd medium having a high sound velocity, such as aluminium which eases the construction of the of the re-transmitting array.

One problem can arise due to the curvature of the array, as the effective element spacings along the aperture are not exactly equal. However, if care is taken to avoid the use of a very large aperture and a small radius of curvature, this problem will not be significant.

4.4 *CONCLUSIONS*

Of the methods discussed above to implement the new concept, it is clear that the design of a sonoptical geometry consisting of a curved array and a cylindrical lens is far more promising than the other methods. However, in order to be able to design a complete system, the requirements concerning the new concept in the areas, namely, signal interception, amplification and re-transmission using transducer arrays must now be considered in sufficient detail in order to identify the design parameters and to study the feasibility of the new system.

--- // ---

- CHAPTER 5 -

SIGNAL INTERCEPTION

This chapter deals with the theoretical concepts concerning the requirements of signal interception using transducer arrays for the proposed new imaging system. Some features of linear arrays are examined in comparison to that of a continuous line aperture in order to study limits of transducer performance. The necessary design parameters of the transducer arrays are then estimated by a preliminary computer simulation

5.1 USING TRANSDUCER ARRAYS

In a DUVD system the wavefronts are received with a continuous aperture which are then focused by the sonoptical focusing system. In the proposed new concept, however, it is not possible to have a continuous aperture of the same kind, but the wave fronts are discretely sampled and re-transmitted by the corresponding elements of the two arrays.

The continuous aperture can be thought of as having an infinite number of sampling elements representing an absolute upper limit. However, in the case of a linear array, the choice of parameters such as the number of elements, element spacing are dependent on many factors including cost and complexity. In this regard it is useful to examine the features of the discrete line aperture in comparison to that of the continuous aperture to estimate some limits of transducer array performance.

5.2 ONE DIMENSIONAL SPATIAL FILTERS

5.2.1 Continuous line aperture

The one dimensional line aperture as shown in Fig. 5.1 satisfies the

basic requirements of a spatial filter. If a plane wave is incident at an angle to the line transducer producing a signal s(t) at the origin, then the signal at any other point along the x axis may be written as [21]:

$$S(t,x) = S\left(t + \frac{x\sin\phi}{c}\right) \quad . \quad . \quad . \qquad (5.1)$$

where c is the speed of sound in the medium.

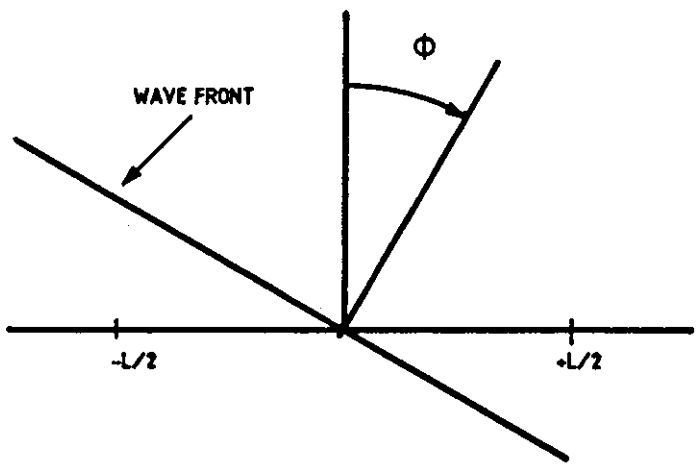

FIG. 5. 1. LINE TRANSDUCER AS A SPATIAL FILTER

If g(x)dx is the response to a unit signal at x, the total output of the line transducer may be expressed in the form

$$S_o(t,\phi) = \int_{-\infty}^{\infty} g(x)\, S\left(t + \frac{x\sin\phi}{c}\right) dx \qquad (5.2)$$

where g(x) is the aperture function.

If s(f) is the frequency domain Fourier transform of s(t),

$$S\left(t + \frac{x\sin\phi}{c}\right) \longleftrightarrow S(f) \exp\left(\frac{j2\pi f x\sin\phi}{c}\right)$$

Then the output $s(t,\phi)$ can be expressed in the frequency domain as,

$$s_o(t,\phi) = \int_{-\infty}^{\infty} \left[\int_{-\infty}^{\infty} S(f) \exp\left(j2\pi f x \frac{\sin\phi}{c} + j2\pi f t\right) df \right] g(x)\, dx$$

$$s_o(t,\phi) = \int_{-\infty}^{\infty} S(f) \left[\int_{-\infty}^{\infty} g(x) \exp\left(\frac{j2\pi f x \sin\phi}{c}\right) dx \right] \exp(j2\pi f t)\, df \quad \ldots \quad (5.3)$$

where the inner integral is the Fourier transform of the aperture function $g(x)$ in a domain represented by the variable $u = (\sin\phi)/\lambda$. This transform $G(u) = G(f,\phi) = \int_{-\infty}^{\infty} g(x) \exp(j 2 \pi x u)\, dx$ is the pattern function of the line aperture.

If $g(x)$ is constant over the length of the aperture and zero elsewhere, then $g(x)$ is a rectangular aperture function as shown in Fig. 5.2 and may be represented in the normalised form as

$$g(x) = \frac{1}{L} \text{ rect } \left(\frac{x}{L}\right) \quad . \quad . \quad . \quad (5.4)$$

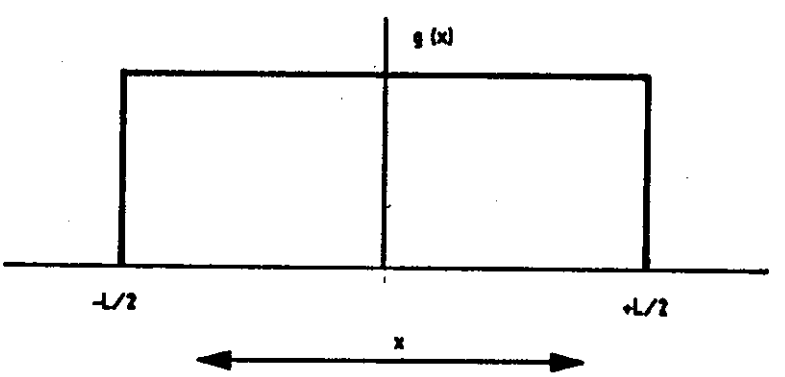

FIG. 5. 2. RECTANGULAR APERTURE FUNCTION

The corresponding pattern function is therefore,

$$G(U) = \frac{1}{L} \int_{-\infty}^{\infty} \text{rect } \left(\frac{x}{L}\right) \exp(j2\pi x u)\, dx \quad . \quad . \quad . \quad (5.5)$$

which is shown in Fig. 5.3 in both cartesian and polar forms.

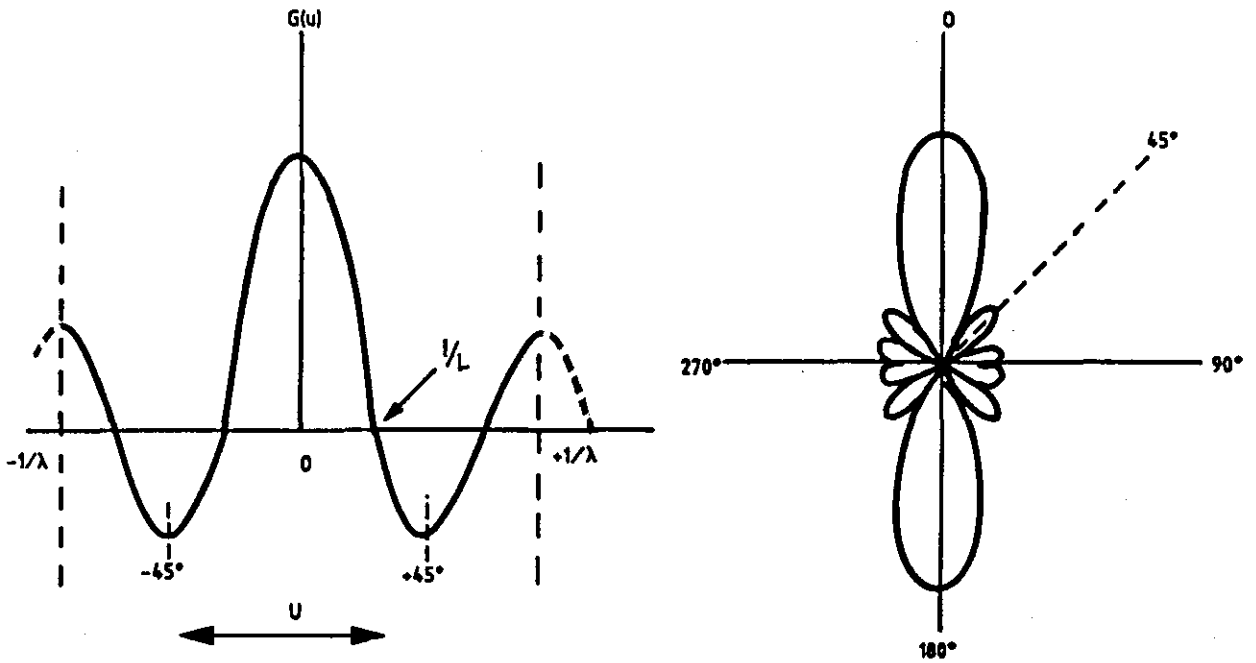

FIG. 5.3. PATTERN FUNCTION OF THE RECTANGULAR APERTURE

From the above, the angular width of the main lobe is obtained as,

$$\phi_B = \sin^{-1}\left(\frac{\lambda}{L}\right) \text{ rad} \quad . \quad . \quad . \quad . \qquad (5.6)$$

$$\approx \frac{\lambda}{L}, \quad \text{if } L >> \lambda$$

The 3 dB beam width in degrees is approximately equal to

$$\phi_{3dB} = 50\,\frac{\lambda}{L} \quad \text{deg.}$$

The Directivity Index may also be obtained as[21]

$$DI = 10\,\text{Log}\left(\frac{2L}{\lambda}\left\{\frac{2}{\pi}Si\left(\frac{2\pi L}{\lambda}\right) + \left[\cos\frac{2\pi L}{\lambda} - 1\right]\right\}^{-1}\right)$$

where $Si\left(\frac{2\pi L}{\lambda}\right) = \int_0^{\frac{2\pi L}{\lambda}} \left(\frac{\sin x}{x}\right) dx$ (sine integral function)

For $L \gg \lambda$

$$DI = 10 \log\left(\frac{2L}{\lambda}\right) \quad . \quad . \quad . \quad . \qquad (5.7)$$

5.2.2 Discrete spatial arrays

The characteristics of a line array aperture with constant element spacing d, will now be examined by extending the results obtained for the continuous line aperture. In this case, the aperture function may be thought of as a sampled version of the corresponding rectangular aperture function with the samples consisting of spatial impulse functions as shown in Fig. 5.4.

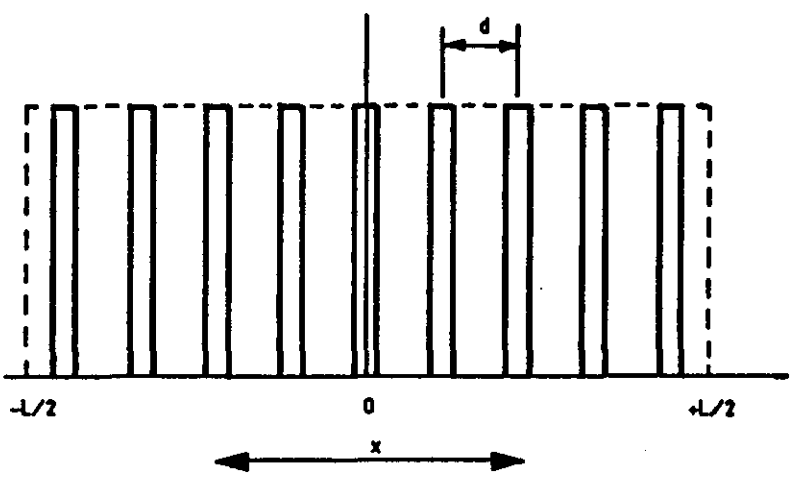

FIG. 5. 4. DISCRETE RECTANGULAR APERTURE.

Since d is constant, the discrete form of the rectangular aperture function can be obtained by using the comb sample function, such that,

$$g(x) = d\,\mathrm{comb}_d\left[\frac{1}{L}\,\mathrm{rect}\left(\frac{x}{L}\right)\right] \quad . \quad . \quad . \qquad (5.8)$$

$$= \frac{d}{L}\sum_{n=-\infty}^{\infty} \delta\,(x-nd)\,\mathrm{rect}\left(\frac{x}{L}\right)$$

where, $L = Nd$ and $N = 2m + 1$, giving m equally spaced elements

on each side of the origin with one element at the origin itself. The corresponding pattern function, which is the Fourier transform of g(x) is

$$\text{dcomb}_d \left[\frac{1}{L} \text{rect}\left(\frac{x}{L}\right) \right] \longleftrightarrow \left[\text{rep}_{1/d} \ \text{sinc}\ (Lu) \right]$$

$$\therefore \quad G(U) = \left[\text{rep}_{1/d} \ \text{sinc}\ (Lu) \right] = \frac{1}{N} \left[\frac{\sin \pi N d u}{\sin \pi d u} \right] \quad \ldots \quad (5.9)$$

i.e. sampling the rectangular aperture function results in a repetitive sinc pattern function as shown in Fig. 5.5.

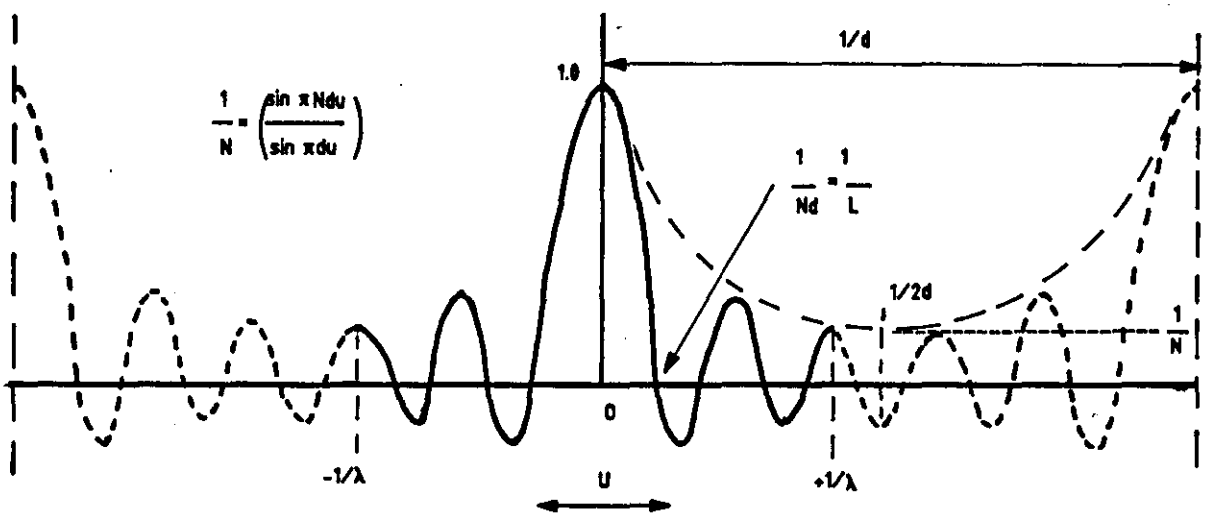

FIG. 5. 5. DISCRETE APERTURE PATTERN FUNCTION

The following observations are made at this stage.

(1) The width of the main lobe as measured at the first zero crossing is the same as for the continuous aperture, and hence the beam width is $\phi_{3dB} = \sin^{-1}\left(\frac{\lambda}{Nd}\right)$ rad.

(2) If $d < \lambda/2$, then the real pattern function is confined to a region where $u < 1/\lambda$ and hence the minimum side-lobe level exceeds 1 / N. Fig. 5.6(a).

(3) If $d = \lambda / 2$, the minimum side-lobe energy level is $1 / N$ and occurs at $\phi = \pm \pi/2$. Fig. 5.6(b).

(4) If $\lambda / 2 < d < \lambda$, the minimum side-lobe level occurs prior to $\phi = \pm \pi/2$ and exceeds $1/N$ at $\phi = \pm \pi / 2$. Fig. 5.6(c).

(5) If $d = \lambda$, the first repeated main lobe at $u = 1 / d$ occurs at $1 / \lambda$ resulting in full amplitude lobes being located at $\phi = \pm \pi/2$ in addition to that at $\phi = 0$ and π. Fig. 5.6(d).

(6) If the element spacing is increased further, more and more grating lobes would move into the real pattern, thus seriously degrading the performance of the array as a spatial filter.

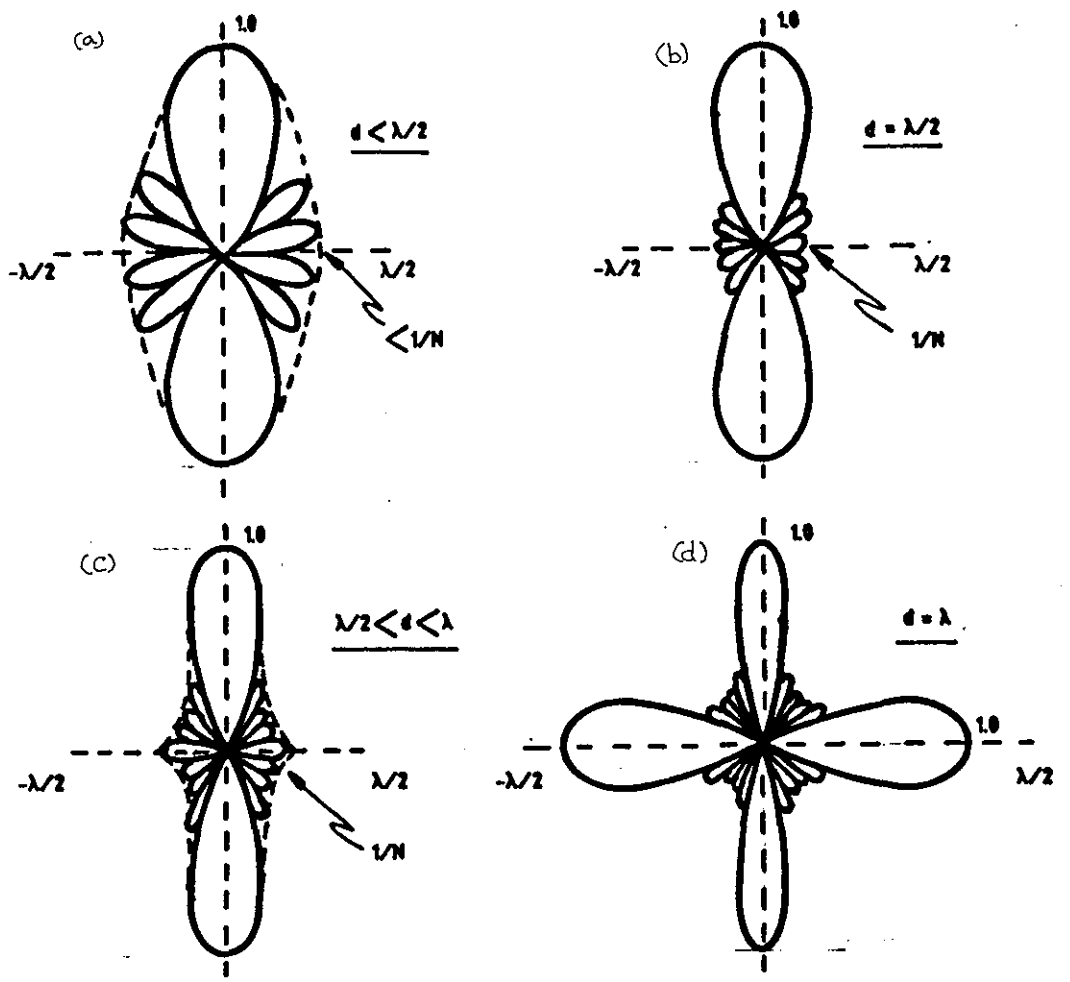

FIG. 5. 6. DISCRETE LINE ARRAY PATTERN FUNCTIONS (POLAR FORM).

In practice the need often arises to use the maximum permissible element spacing due to construction difficulties and cost. However, as seen from the above, the optimum spacing d for a discrete line array aperture would be equal to $\lambda/2$. Although useful performance may still be obtained at slightly wider spacings, the performance will be seriously degraded if d exceeded $\lambda/2$ by a significant amount (Fig. 5.6 d).

5.3 SYSTEM MODELLING FOR COMPUTER ANALYSIS

The main object of modelling at this stage is to obtain the design parameters of the arrays for the present application. Since the new concept represents a combination of different techniques it is useful to categorise them broadly as:

(1) Those involving sampling, amplification and re-transmission,
(2) Those involving passive sonoptical focusing,
(3) Those involving optical visualization.

For the purpose of modelling, the subject of optical visualization can be left out at this stage as it simply deals with the way in which the acoustic images are optically mapped.

The design dealing with the sonoptical focusing geometry has a common basis of operation with the DUVD, at least in a limited sense, and may be best examined by ray tracing techniques. This can also be omitted here from the present analysis, as the image spread is largely dominated by the diffraction effects of the system rather than by geometrical relations.

The subject dealing with sampling, amplification and re-transmission using transducer arrays and amplifiers, covers a wide area of activities and may be modelled in a way to represent the principal process of operation as close as possible.

For simplicity, the following basic assumptions are made:

1. Continuous wave operation - (Although the system is pulse operated, considerable knowledge may be gained with continuous waves regarding the use of arrays for the present purpose)

2. Array elements giving identical, point source, omni-directional behaviour

Considering Fig. 5.7, in a theoretical sense, diffraction limited acoustic images of targets in an object plane may be produced with two linear arrays[20] if appropriate phase delays are introduced into the channels to make the combination act as an acoustic lens.

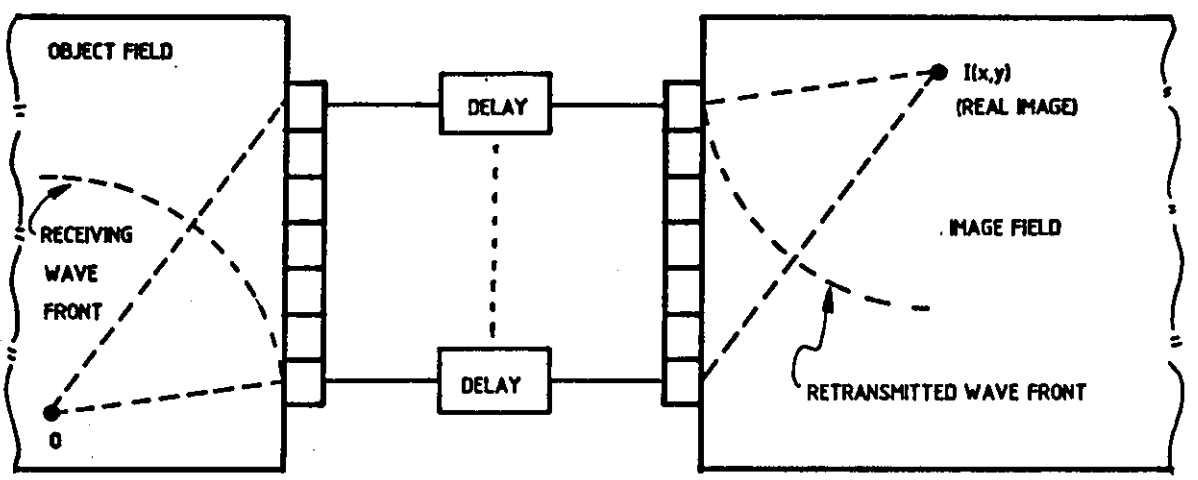

FIG. 5.7. MODELLING WITH TWO LINEAR ARRAYS.

Acoustic images are formed at corresponding image points where all the wave fronts originating from the transducer elements arrive in phase. This is what basically takes place in the new system where the necessary delays for constructive interference are taken care of by the sonoptical focusing system. As mentioned above, the image quality is largely determined by the diffraction effects of the array and not by the sonoptics, it is usually possible to design the focusing system to give sufficiently good performance so that there is no significant image deterioration occuring due to the focusing system itself. Hence, the image quality is primarily determined by the performance of the arrays.

As far as the basic parameters of the arrays are concerned, the situation may be further simplified by considering the symmetrical or reversible nature of the arrangement shown in Fig. 5.6. For the present purpose, it is therefore sufficient to consider only one array, e.g. the re-transmitting array to which the appropriate phase delays are introduced to achieve focusing at any given point in the image space, as shown in Fig. 5.8.

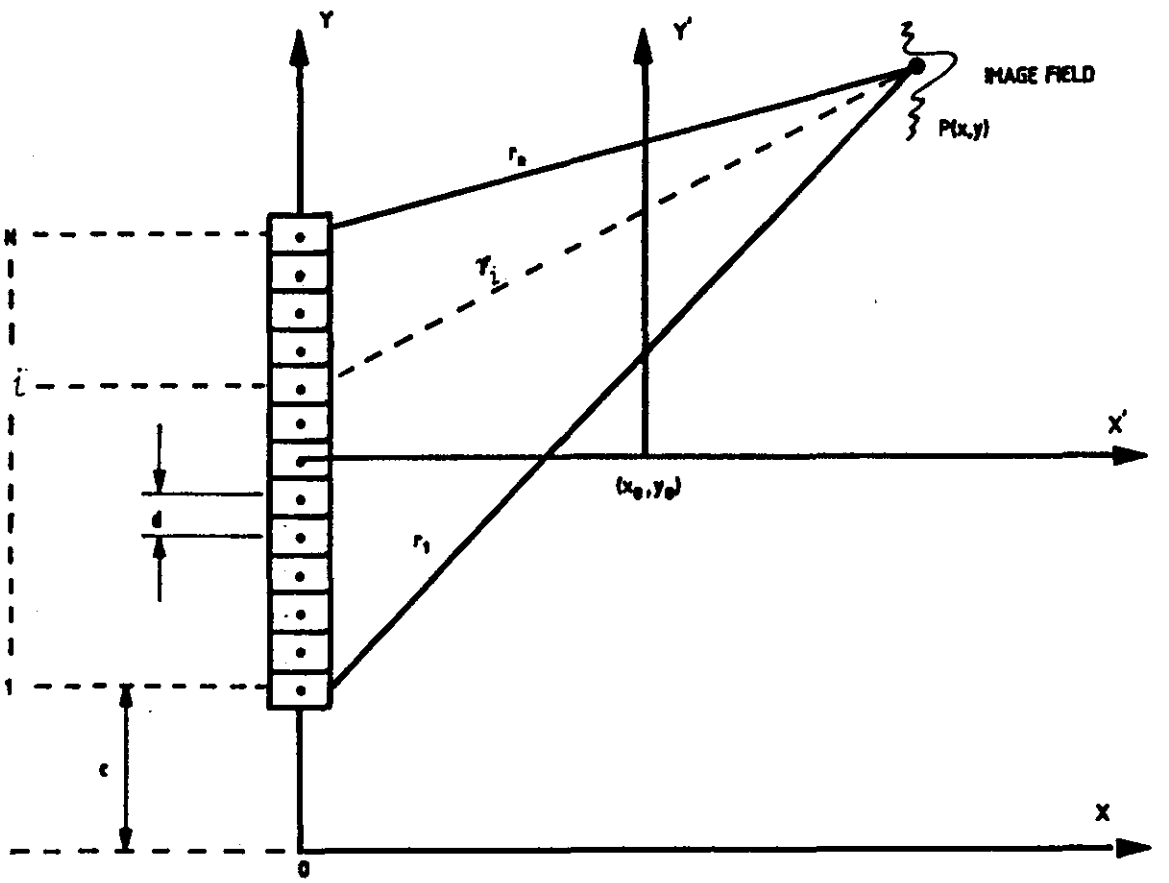

FIG. 5.8. REPRESENTING THE BASIC OPERATION OF THE SYSTEM WITH A SINGLE ARRAY. (A SIMPLIFIED APPROACH).

The necessary phase delays for each point of interest may be calculated as a function of the x,y co-ordinates in the image space. This approach has the advantage of being able to represent a focused image field which is functionally closer to that of the real system. Using this model, it is possible to observe the acoustic pressure distribution on and around a given point in the image space as a function of the array

parameters, such as λ , N , d , L, etc. In this regard, the necessary equations for computer analysis will now be developed with the help of Fig. 5.8.

The acoustic pressure $P_{(x,y)}$ at a point (x,y) in the image space may be written in the normalised form,

$$P_{(x,y)} = \sum_{i=1}^{N} \frac{\exp^{-j(kr_i + \phi_i)}}{r_i} \quad . \quad . \quad . \quad (5.10)$$

where, k = $2\pi / \lambda$ (wave number)

r_i = the distance from the ith element to the point (x,y)

ϕ_i = phase function

In order to deal with a phase function of one polarity, the origin is chosen to be below the first element of the array. Also to utilize the symmetry about the axis of the array and to avoid the ambiguity of zero axial distance, the axes are linearly transformed to a point of reference x_o, y_o, as shown in Fig. 5.8 and the computations can still be done without loss of generality. The relationships for r_i and ϕ_i may be written as follows.

$$r_i = [X^2 + (Y - Y_i)^2]^{1/2}$$

$$y_i = c + (i - 1) d \quad ; \quad (i = 1, 2, ...N)$$

$$\phi_i = \phi_o - k (r_i - r_1)$$

where c = y co-ordinate of the first element

d = transducer element spacing

Applying linear transform to x,y co-ordinates and making c = 0

$$X = x_0 + J \quad ; \quad J = 0, 1, 2, ... P$$

$$Y = y_0 + K \quad ; \quad K = 0, 1, 2, ... Q$$

J and K are considered as integer variables for simplicity although they can assume any fractional value. $P_{(x,y)}$ in equation 5.10 defines an image space matrix of dimension (P x Q), whose elements represent the peak acoustical pressure at the corresponding points. In order to examine the lateral resolution and the degree of artefacts formed, the pressure distribution may be examined by varying the y co-ordinate around the point where the conditions for constructive interference, i.e. effective focusing is maintained. This is equivalent to examining a focused image space on a point-by-point basis with which a preliminary estimation of various parameters of the arrays could be made. One of the programmes initially developed to compute the acoustic pressure distribution in the image space is given below. (Page 51). The results achieved with this preliminary simulation were sufficient to proceed with the feasibility study.

5.3.1 Choosing the number of elements N and element spacing d

It was then necessary to select suitable ranges for the random variables used in equation 5.10 on some criteria to reduce the amount of computations. This was done with the help of the observations made under section 5.2.2 above, where it was noted that the element spacing of the array d must be in the range $\lambda/2 < d < \lambda$. Hence examination could be limited to this range.

Also it is noted that the angular resolution of the main lobe can be written as $\delta\theta = \lambda/Nd$. Using this relationship, the on axis lateral resolution in terms of wavelengths may be written as

$$\frac{\lambda}{Nd} \leq \frac{m\lambda}{x}$$

where m is the lateral resolution as a multiple of wavelengths and x is the x co-ordinate at which the lateral resolution is measured. Using the above relationship, some practical limits could be imposed on the size of the aperture required. Hence if the range of aperture values to be

PROGRAMME LISTING

```
      REAL M,M2
      COMPLEX SUM,VALUE,SM,VALU
      DIMENSION X(161),Y(161)
      PI = 3.14159
      SCALE = (2*PI)/0.1
      PRINT 10
10    FORMAT('J,K,L,N')
      READ(1,*)J,K,L,N
      SM = CMPLX(0.0,0.0)
      DO 60 I = 1,N
      Z1 = (5.0+J)**2
      Z2 = (N+1.0-2*I)*L/(2*N)
      R = SQRT(Z1+(Z2+K)**2)
      IF(I.EQ.1)R1 = R
      X2 = -1.0*SCALE*(2.0*R-R1)
      Y3 = COS(X2)/R
      Y4 = SIN(X2)/R
      VALU = CMPLX(Y3,Y4)
      SM = SM+VALU
60    CONTINUE
      TRU = REAL(SM)
      ARGU = AIMAG(SM)
      AN = ARGU/TRU
      PHASE1 = ATAN(AN)
      DO 100 M1 = 1,161
      M2 = M1-81
      M = FLOAT(M2)/4.0
      SUM = CMPLX(0.0,0.0)
      DO 90 I = 1,N
      Z1 = (5.0+J)**2
      Z2 = (N+1.0-2*I)*L/(2*N)
      R = SQRT(Z1+(Z2+K)**2)
      IF(I.EQ.1)R1 = R
      RD = SQRT(Z1+(Z2+K+M)**2)
      X1 = -1.0*SCALE*(R+RD-R1)
      Y1 = COS(X1)/RD
      Y2 = SIN(X1)/RD
      VALUE = CMPLX(Y1,Y2)
      SUM = SUM+VALUE
90    CONTINUE
      TRUE = REAL(SUM)
      ARGUE = AIMAG(SUM)
      ANG = ARGUE/TRUE
      PHASE = ATAN(ANG)
      IF(M.EQ.0.0)PHASE1 = PHASE
      RPHASE = ABS(PHASE1-PHASE)
      ABSUM = CABS(SUM)
      SPEC = ABSUM*COS(RPHASE)
      X(M1) = M
      Y(M1) = SPEC
      WRITE(1,70)SUM,ABSUM,PHASE,RPHASE,SPEC
70    FORMAT(6(F9.5,2X))
      WRITE(5,80)X(M1),Y(M1)
80    FORMAT(2(F10.5,5X))
100   CONTINUE
      CALL EXIT
      END
```

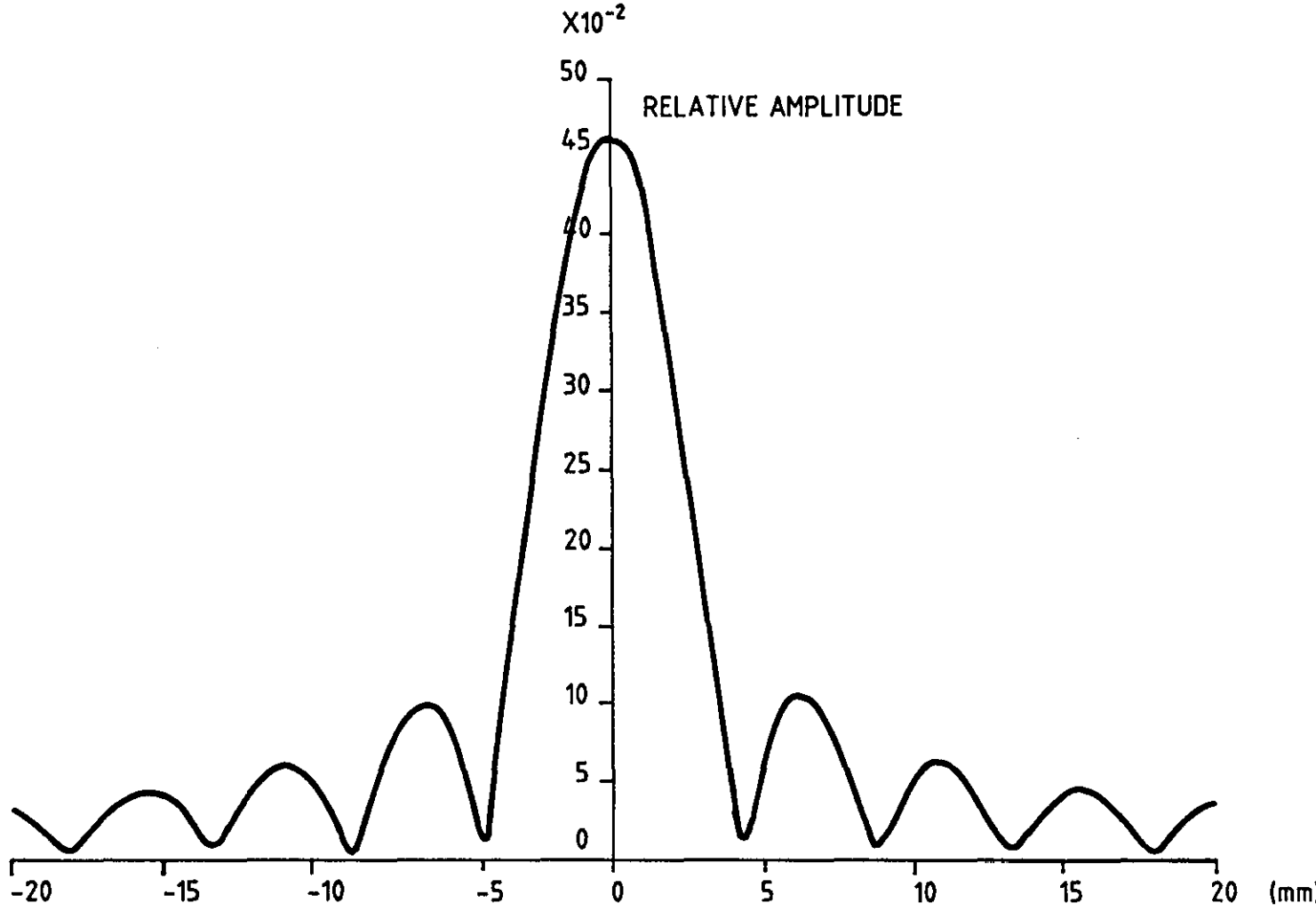

J = 65λ , K = 0 , L = 15λ , N= 30 .

FIG. 5.9 (a) SAMPLE PRESSURE AMPLITUDE PLOTS (on axis)

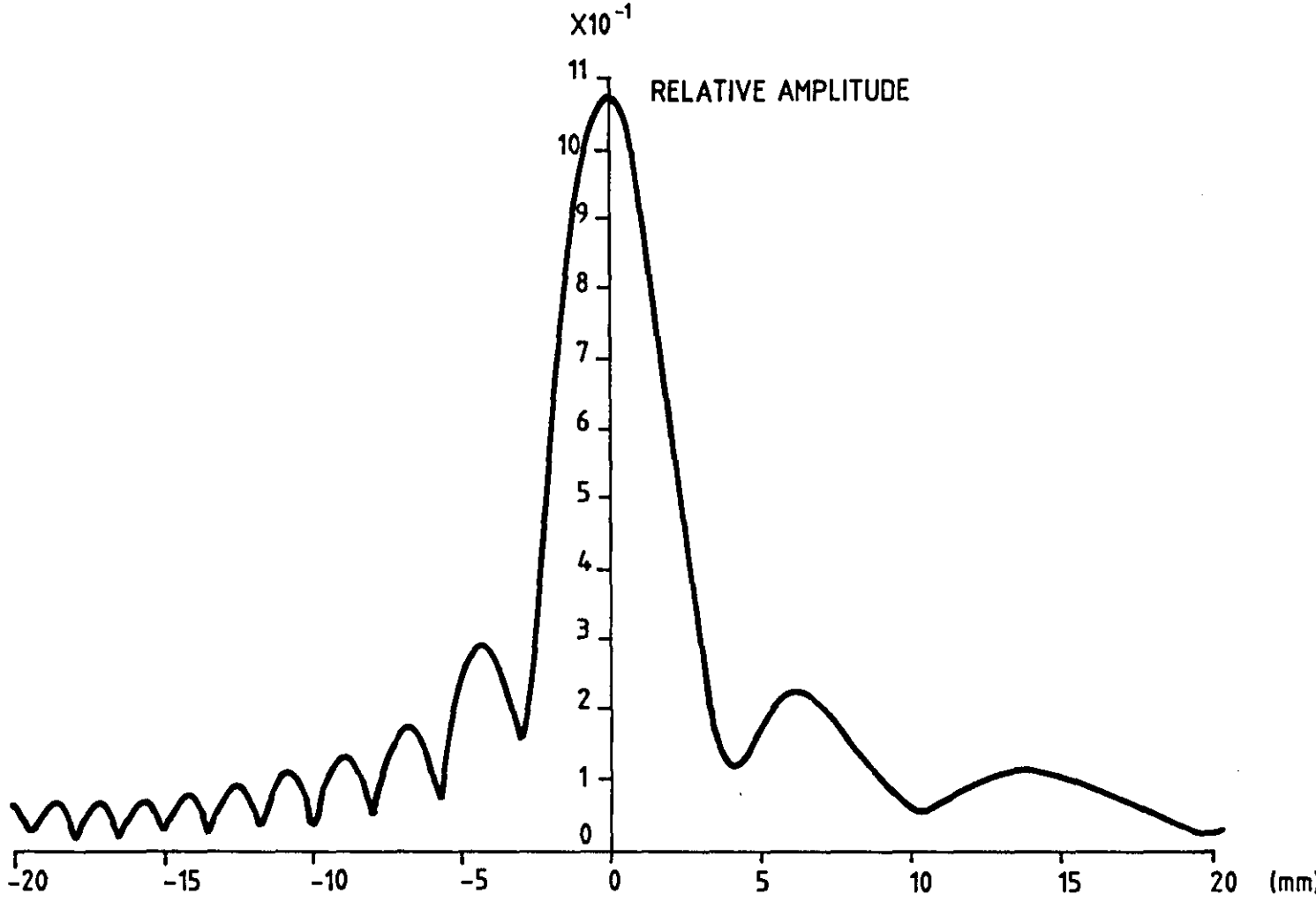

FIG. 5.9 (b) SAMPLE PRESSURE AMPLITUDE PLOTS (off axis)

examined are limited between 2 cm to 8 cm say, a fairly practical range of interest concerning the present application can be covered as seen from table 5.1 below.

APERTURE SIZE (Nd) cm	MAXIMUM AXIAL DISTANCE (cm) FOR A RESOLUTION OF			
	~ λ	~2λ	~3λ	~4λ
2	2	4	6	8
3	3	6	9	12
4	4	8	12	16
5	5	10	15	20
6	6	12	18	24
7	7	14	21	28
8	8	16	24	32

Table 5.1 Approximate aperture-resolution values for given axial distances

Within the above range of values for the element spacings and the aperture, a large number of acoustic pressure profiles were plotted such as that shown in Fig. 5.9(a) and(b), in order to examine lateral resolution and the level of artefacts found in the image field as a function of the aperture, element spacing and the wavelength. From this exercise, the number of elements N and the element spacing d were chosen as 30 and 0.7λ respectively as a satisfactory compromise to proceed with the feasibility study.

5.4 SELECTION OF CENTRE FREQUENCY (f_c) AND WIDTH-TO-GAP RATIO (w/g)

So far the analyses were carried out on the assumption that the array elements behave as point sources. However, the transducer elements in practice are not point sources in a physical sense nor give omni-directional response. Among others, two important aspects relating to the finite size of the transducer elements, namely the width (w), and the element-to-element gap (g), are briefly examined below.

Recalling equation 5.7, the Directivity Index for a line transducer of width w can be written as:

$$DI = 10 \log \left(\frac{2L}{\lambda}\right) \quad . \quad . \quad . \quad . \qquad (5.7)$$

From the above equation it can be seen that a transducer element approaches omni-directional response only when L / λ approaches zero. Obviously L cannot be made smaller than certain limits due to :

(1) Construction difficulties

(2) Reduction of sensitivity below usefulness

(3) Complications due to lateral modes of vibrations

Lack of omni-directional response modifies the transducer array performance and it has some adverse effects as shown below.

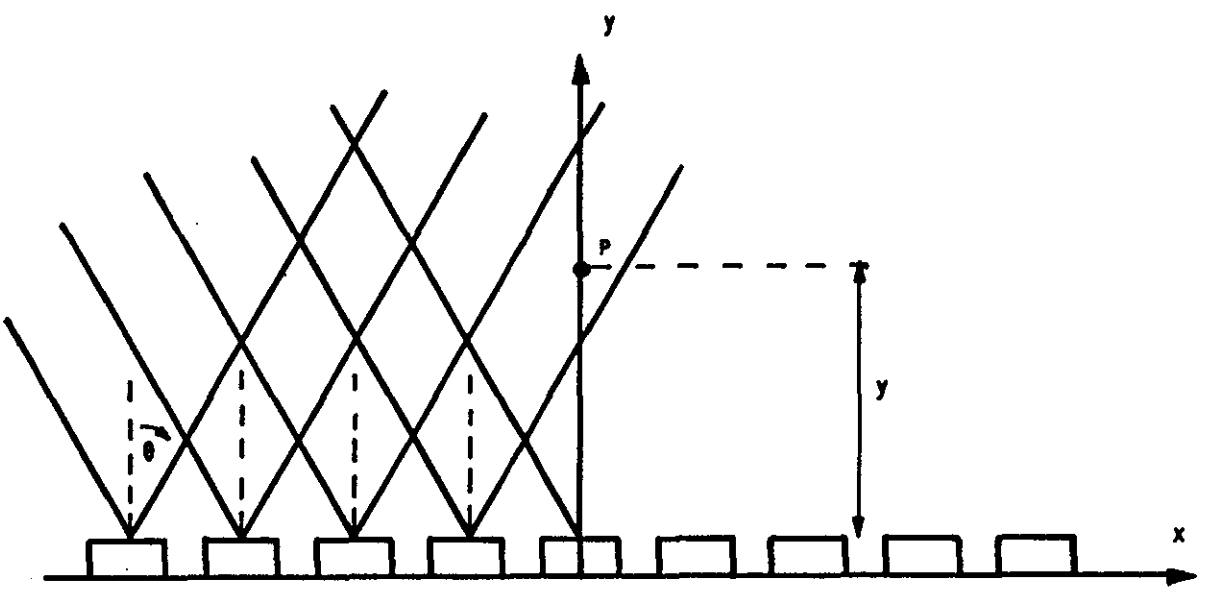

FIG. 5.10. EFFECT OF FINITE BEAMWIDTH OF ARRAY ELEMENTS ON THE TARGETS CLOSE TO THE ARRAY.

As can be seen from the above diagram, the contribution from the outer elements gradually decreases as a target or an image point is moved close to the array. This progressively reduces the ability of the array to function as a spatial filter at small axial distances. If θ is the half angle of the beam width of an element and x is the x co-ordinate of the element with respect to the centre, the contribution from that element ceases at an axial distance of

$$y = x \cot \theta \quad . \quad . \quad . \quad . \quad (5.12)$$

Hence achieving beam width as wide as possible from individual elements of the array is important.

When the elements are small, the lateral clamped conditions for the transducer elements are not strictly valid and hence lateral modes of vibrations begin to appear. As the thickness mode of vibration is selected in the present case, the width of the elements must therefore be reasonably greater than the thickness to reduce the influence of width expander mode of vibration. According to literature and the experiments carried out, a width to thickness ratio (w/t) in the range of 1.5 to 2 seems adequate.

Directivity Index on the other hand requires w to be small for omnidirectional response which is contradictory to the above. At the same time, the resolution offered by the array according to equation 5.6

$$\phi_{3dB} = \sin^{-1} \frac{\lambda}{Nd} \quad . \quad . \quad . \quad . \quad (5.6)$$

which becomes progressively worse as λ increases. Smaller λ favours higher resolution, but acts against omni-directional response. Hence a compromise between the conditions set out for λ by equations (5.6), (5.7) and (w/t) ratio is necessary for choosing a suitable wavelength.

Since the aim of the project is mainly to develop an NDT imaging system for inspection of thick sections of steel, an operational frequency in the range of about 1.5 MHz to 5 MHz may be adequate. If a frequency of 2 MHz is chosen as the centre frequency for a feasibility study, then the wavelength λ in steel would be approximately 3 mm. Since N and d are already chosen as 30 and 0.7λ, the theoretical resolution achievable according to table 5.1 would be close to a wavelength around a depth of about 6 cm. This seems satisfactory for the present purpose.

The question of width-to-gap ratio is now considered. In practice the width of the element (w) is finite and also it is important to maintain

a certain gap (g) between the elements to avoid significant cross-coupling. If the (w/g) ratio is excessive, it can seriously degrade the performance of the array, even though the element spacing as determined previously is correctly maintained. The following diagrams obtained from the literature[3] show the effect of w/g ratio in the far field with the aperture size and the wavelength are kept constant. These are used here to estimate a reasonable w/g ratio for the present application.

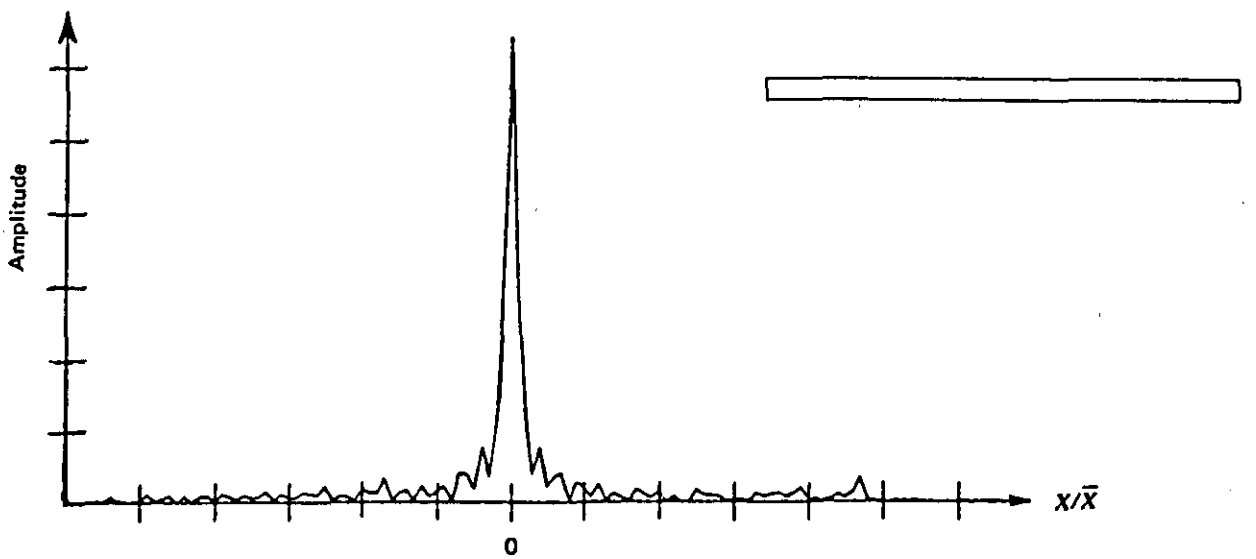

Fig. 5.11(a) SAMPLE PLOT - FAR FIELD LATERAL PRESSURE PROFILE (w/g =∞)

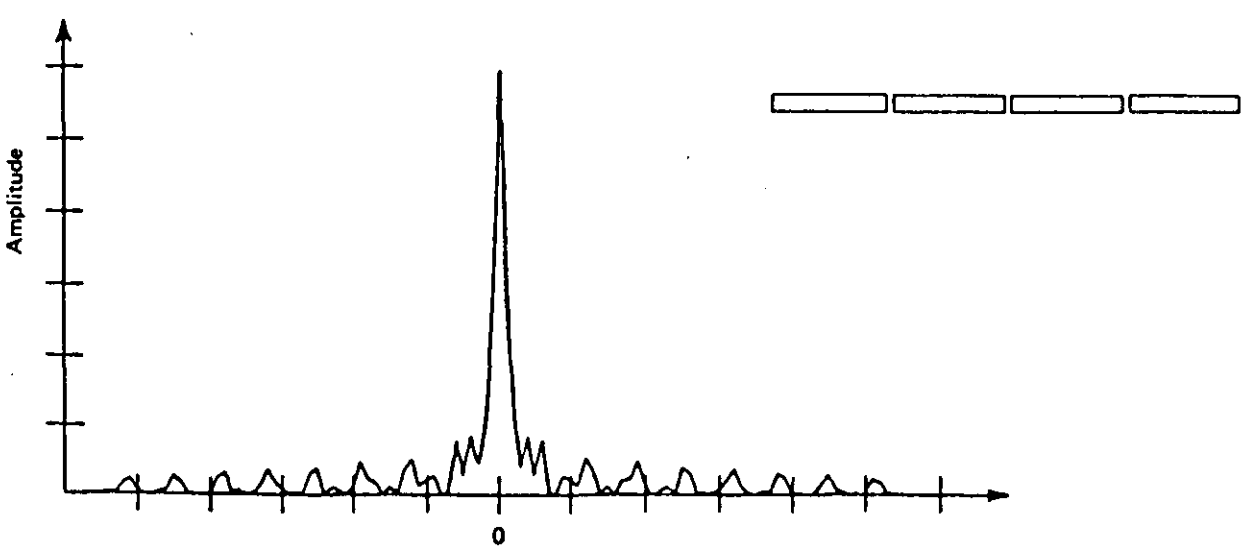

Fig. 5.11(b) w/g ratio - 15

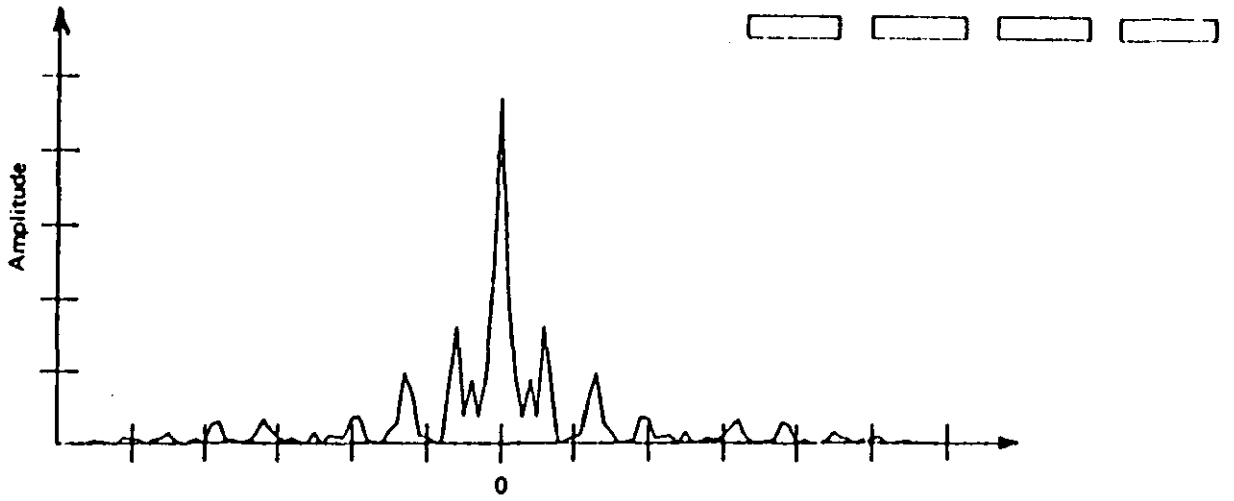

Fig. 5.11(c) w/g RATIO - 3

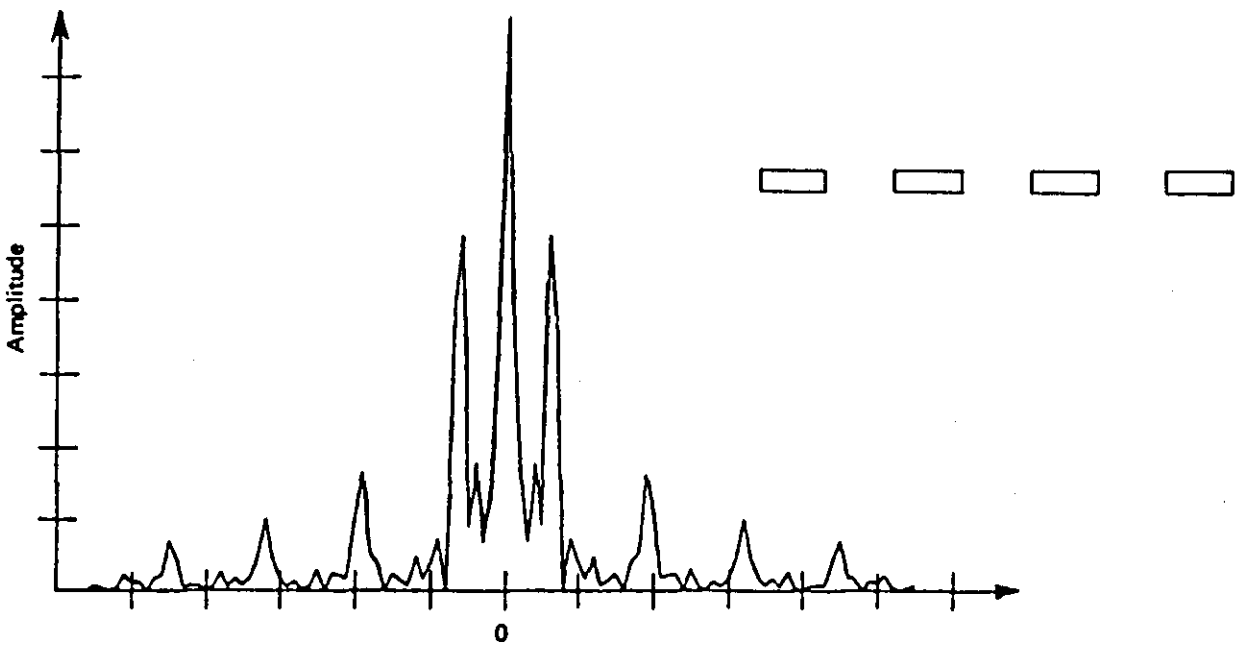

Fig. 5.11(d) w/g RATIO - 1

From the above it can be seen that a w/g ratio below 3 is very unsatisfactory. Using these results, a w/g ratio in the range of 5 to 10 seems to be adequate.

Now the actual values for w and g may be obtained as follows.

From the above results, let w/g = 9 . . . (5.13)

From previous analysis, $d = 0.7\lambda$

$$\therefore \quad w + g \simeq 2 \text{ mm} \qquad (5.14)$$

From eq. (5.13) and (5.14), $w = 1.8$ mm

$g = 0.2$ mm

5.5 SELECTION OF ELEMENT LENGTH (1)

One more parameter that needs to be estimated is the length of the array elements. This was not considered so far due to it having less important influence on the imaging system as a whole. However, in the proposed new system the 3D feature of the original DUVD is changed to 2D, so that focused B-scan type images can be obtained. In this respect, the thickness of a selected object plane must be as small as possible which in this case is primarily determined by the length of the array elements in the y-direction as marked on the Fig.5.12 below.

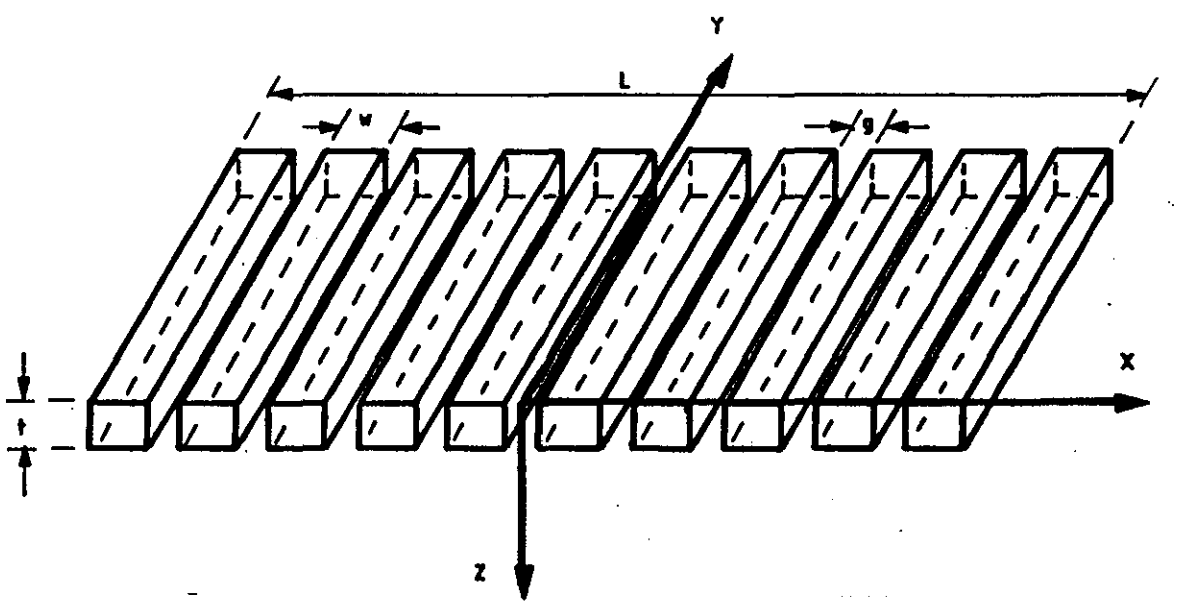

FIG. 5.12. PHYSICAL DIMENSIONS OF THE ARRAY

The thickness of the imaging section is obtained by the beam-width in the y-z plane and according to equation (5.6), for $L \gg \lambda$

$$\phi_B \simeq \frac{\lambda}{L}$$

Obviously the beam is diverging and hence the section thickness gradually increases with depth. For the feasibility study, if a section thickness of about 2 cm is accepted around 10 cm below the test surface, then

$$\lambda / L = 20 / 100$$

$$\therefore \quad L \simeq 15 \text{ mm}$$

5.6 *CONCLUSIONS.*

Parameters concerning the use of arrays for the proposed new concept have been estimated by theoretical analysis, system modelling and numerical computations, and also using existing data. For the feasibility study in the case of steel being the object medium, a centre frequency of 2 MHz was chosen with element spacing of 2mm and 30 elements together with an element width of 1.8 mm, gap size of 0.2 mm and an element length of about 15 mm.

f	=	2 MHz
d	=	2 mm
N	=	30
w	=	1.8 mm
g	=	0.2 mm
L	=	15 mm

---- // ----

- CHAPTER 6 -

PULSED OPERATION

In the previous chapter, the parameters of the arrays concerning signal reception was estimated on the basis of continuous waves, although the real system is pulse operated. This was simpler and adequate for the parameters already evaluated, but there are further important aspects to be examined when the pulsed operation of the real system is considered. Analysis and identification of these factors are the subject of this chapter.

6.1 NEED OF PULSE OPERATION

The DUVD principle is essentially based on pulse operation. Apart from the aspect of axial resolution, the need of time resolution to achieve the property called isochronicity, requires pulses as short as possible. However, generation and processing of short ultrasonic pulses is one of the most challenging subjects in ultrasonic engineering. This has been dealt with in considerable depth in the course of this project with good results. Apart from the aspects mentioned above, some other important benefits of using short pulses for the present application are now examined.

6.2 NEAR FIELD CONSIDERATIONS

The near field distance of a transducer in the CW operation is defined as the point on the axis of the transducer separating a region of intensity fluctuations from a region of a smooth intensity decay[22] as shown in Fig. 6.1.

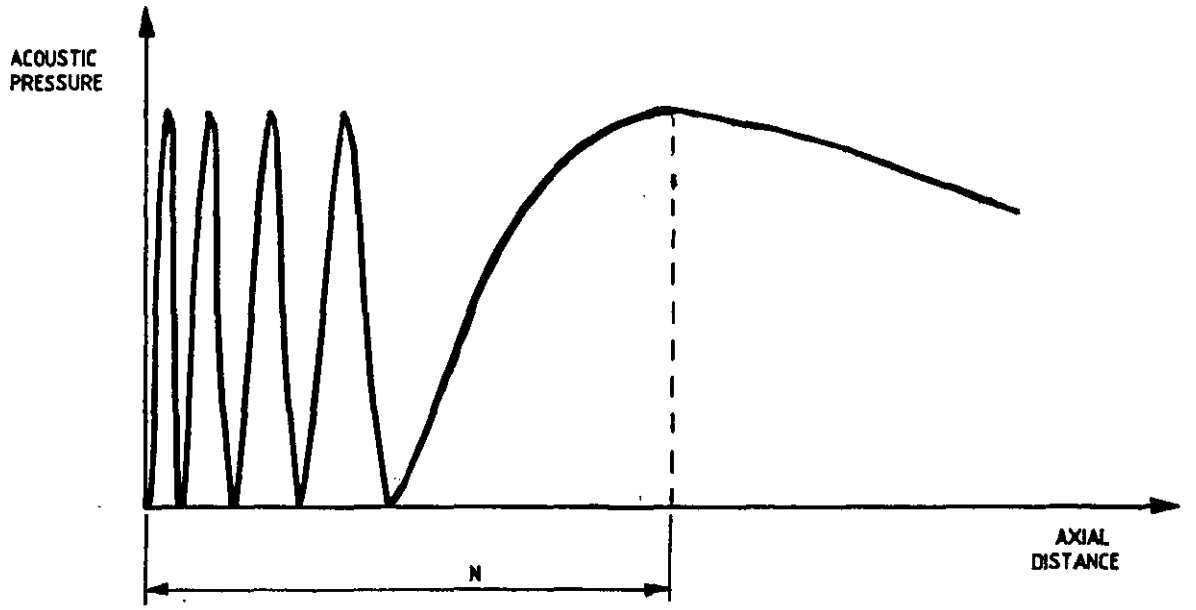

FIG. 6. 1. TYPICAL AXIAL PRESSURE PROFILE.

In quantitative terms for example in the case of a disc transducer, the near field N may be shown to be equal to

$$N \simeq \frac{D^2}{4\lambda} = \frac{D^2 f}{\lambda} = \frac{D^2 f}{4v}$$

where, f is the centre frequency of the transducer and v is the sound velocity of the medium in which the acoustic waves are travelling and D is the diameter of the transducer. The end of the near field may also be shown approximately at the point of intersection of the projection of the transducer diameter on the angle of beam divergence as shown in Fig. 6.2.[5]

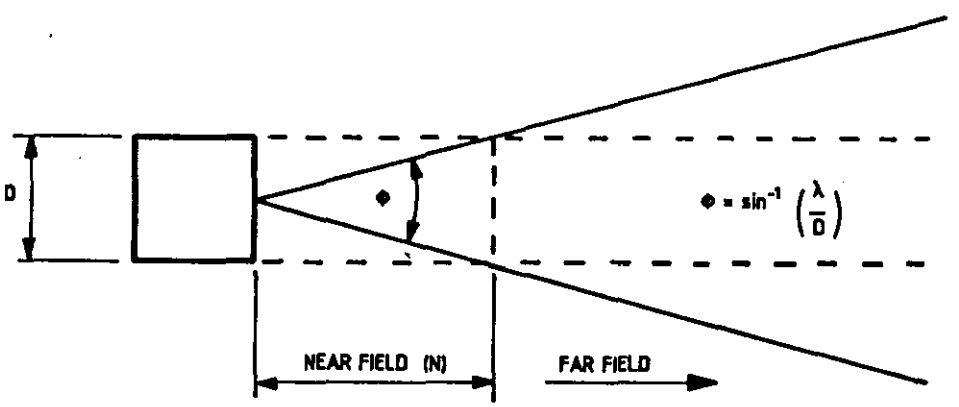

FIG. 6. 2. NEAR AND FAR FIELD

The large intensity variations in the near field are the result of

constructive and destructive interference and the situation becomes increasingly prominent with the decrease of the wavelength. This behaviour is obviously undesirable in practical situations but the effect could be significantly reduced by adopting short ultrasonic pulses as illustrated in the following diagrams.[3]

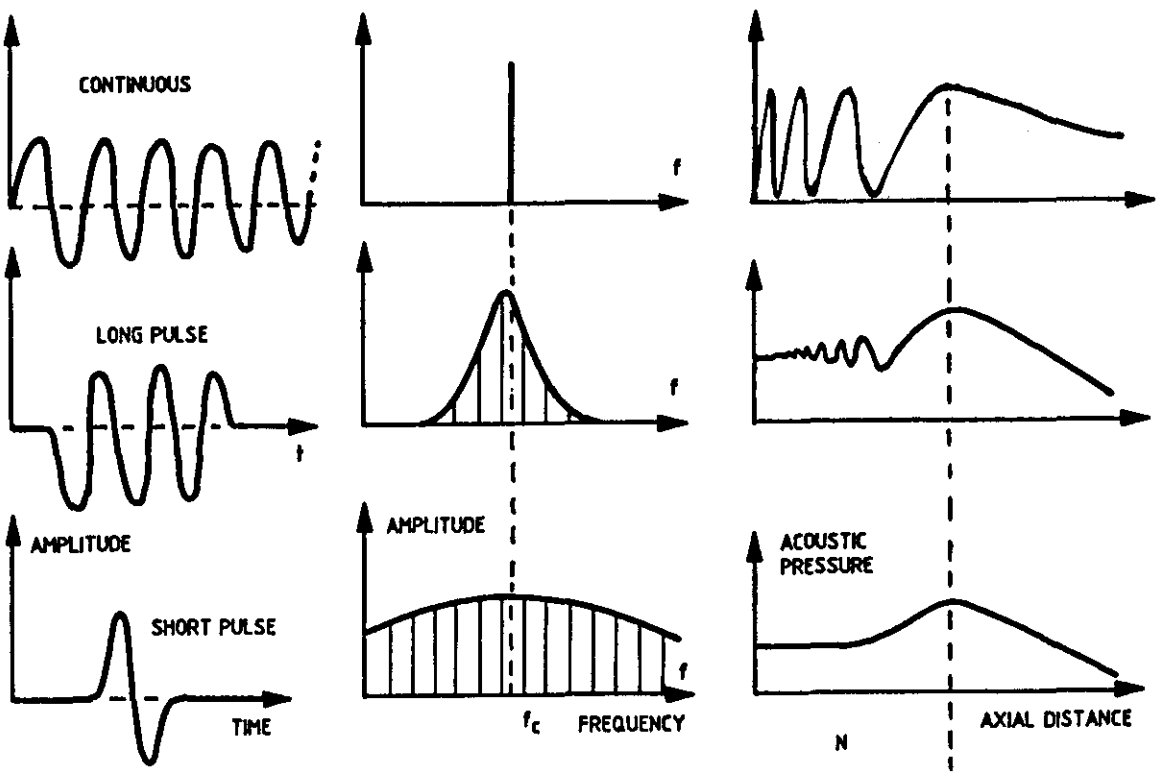

(a) PULSE SHAPE (b) FREQUENCY SPECTRUM (c) AXIAL PRESSURE

FIG. 6. 3.

It is seen that, although the near field length remains unaltered, a distinct smoothing effect occurs in the near field as the input pulse becomes increasingly broad band. This effect can be understood on the basis of wave superposition and the resulting constructive and destructive interference phenomena for the different finite frequency components as they propagate in the medium. The transverse pressure profile is also modified in a similar fashion.

At the same time the directional pattern also changes giving a much smoother response[3] as shown in Fig. 6.4. This is also an advantage in

achieving omnidirectional response from the elements of the array, which is a much needed aspect as mentioned in section 5.4.

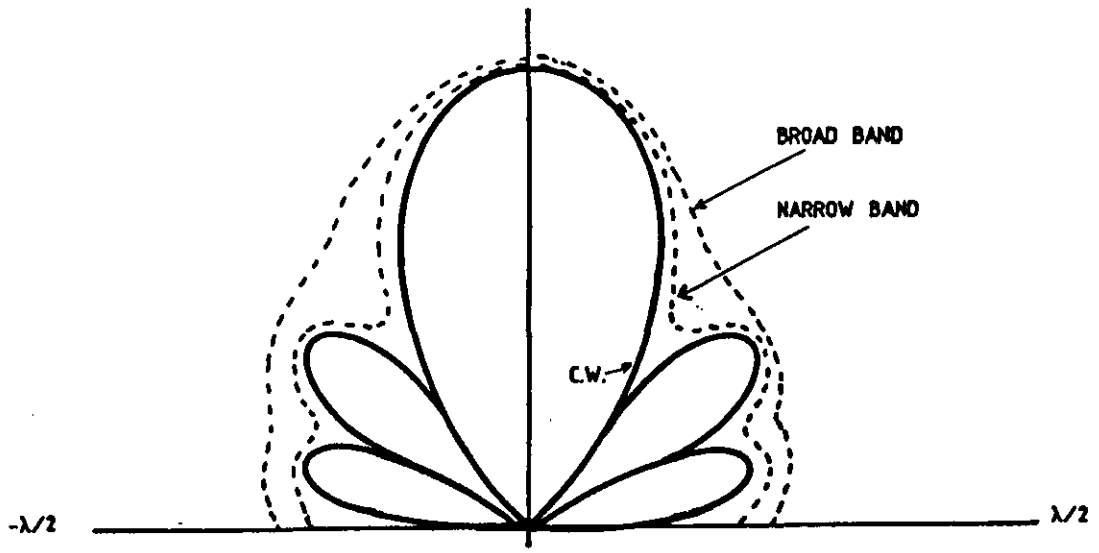

FIG. 6. 4. EFFECT OF PULSE LENGTH ON DIRECTIONAL RESPONSE

The beam angle of divergence is therefore not exactly the same as in the case of CW and may be examined by computer analysis using wave superposition of individual ultrasonic fields generated by individual frequency components of the pulse. In practice, it may be estimated using a test probe in the through-transmission mode as shown in Fig.6.3.

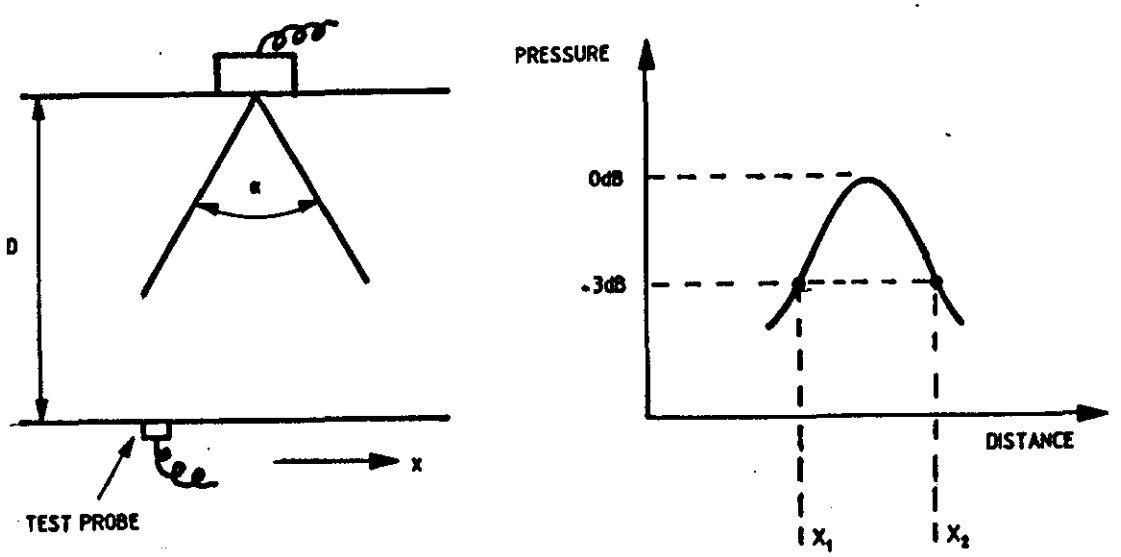

FIG. 6. 5. MEASUREMENT OF ANGLE OF BEAM DIVERGENCE

The 3 dB beam width may then be written as

$$\alpha = 2 \tan^{-1} \left[\frac{x_2 - x_1}{2D} \right]$$

6.3 FURTHER DIFFERENCES

It is also worth noting that the actual ultrasonic pulse shape in the medium is changing as it propagates in the material. This is because the spectral composition of the pulse is changing as the different frequencies have different pressure profiles. Also, the shape of the received pulse echoes depends on the nature of the targets and the attenuation characteristics of the medium. Attenuation distortion of broad band pulses is the result of preferential absorption of high frequency components from the incident pulse. In contact testing, the pulse shape also depends on the state of the coupling of the transducer to the medium. All these mean in the case of a multichannel system using arrays whose elements are operating in parallel, the received waveforms are very complex and tend to be critical with respect to many variables.

6.4 FREQUENCY CONTENT OF DRIVING PULSES

It is now useful to examine the frequency spectrum of some driving pulses in order to choose an appropriate method of energizing the transducers. The driving electrical pulses may either be

(1) Sharp high voltage spikes of appropriate shape and duration - (Shock excitation)
(2) Truncated sinusoidal excitation.

The usual approximation of the bandwidth of a pulse expressed as the inverse of its duration is not adequate here because the characteristics of the driving pulses have critical influence on the ultrasonic pulses generated.

6.4.1 Shock excitation

The shortest shock pulse is a time domain unit impulse of negligible duration (delta function), as shown in Fig. 6.6.

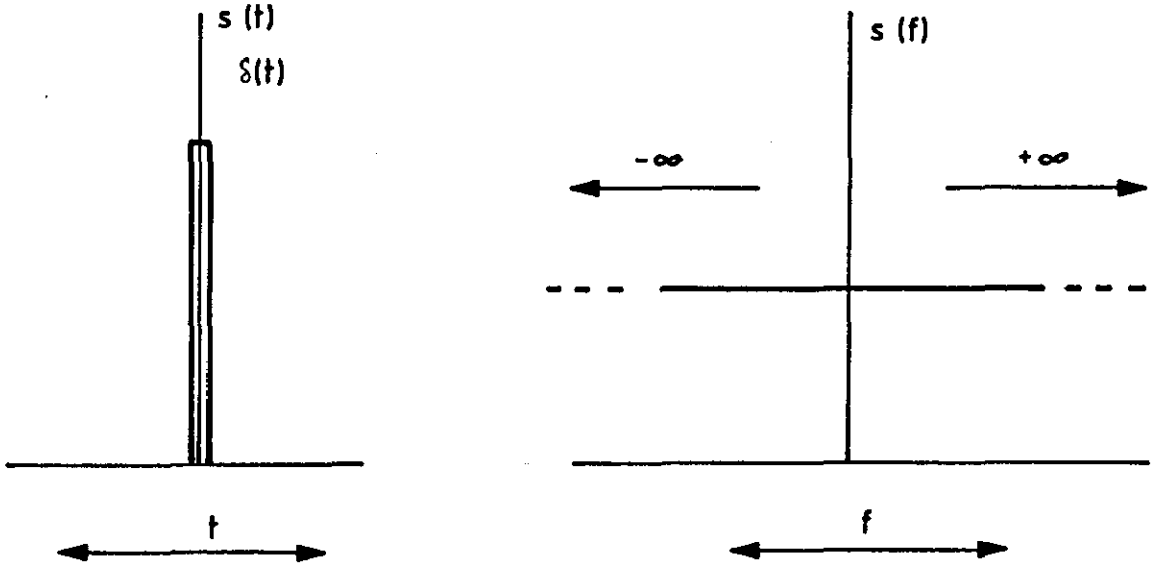

FIG. 6.6. DELTA FUNCTION AND ITS FREQUENCY DISTRIBUTION.

Although infinitely broad banded, such a pulse is of little or no use in driving a transducer, mainly because the spectral energy is widely distributed outside the bandwidth of the transducer making the excitation ineffective. On the other hand, if the duration of the pulse is large, the equivalent frequency spectrum which is a sinc function in the frequency domain has a large zero and near zero frequency components as seen from Fig. 6.7 and again is of little use.

It therefore follows that between these limits, a shock pulse of appropriate shape and duration must be found which has a large spectral energy density in and around the resonance frequency of the transducer.

In practice shock pulses are produced in a rather uncontrolled manner for example by discharging a high voltage capacitor through a thyristor or to a lesser extent by using a high voltage transistor in the avalanche mode.[23] Controlling the pulse shape is therefore difficult although the required duration may be achieved.

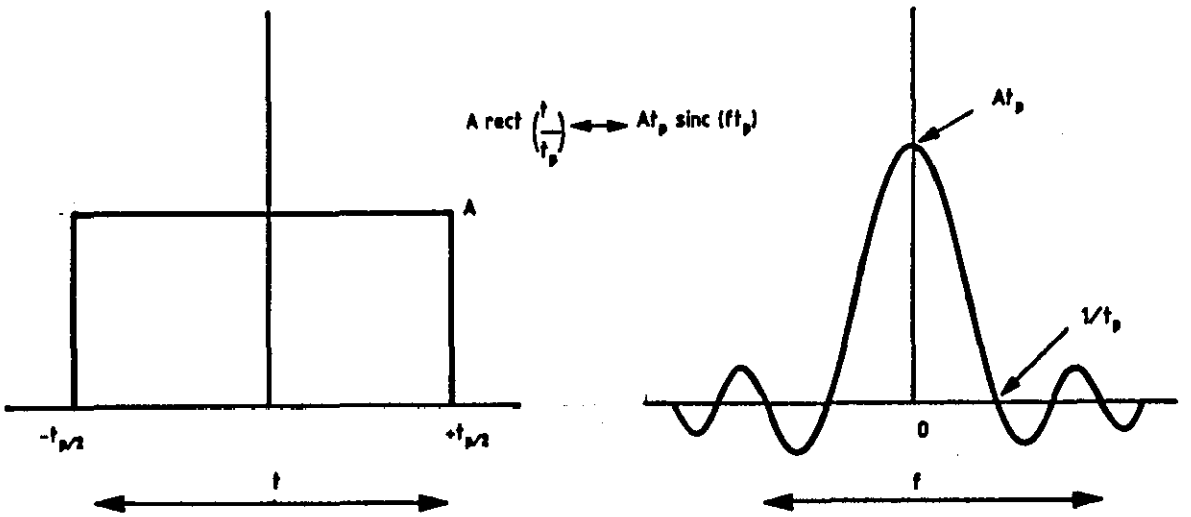

FIG. 6. 7. RECTANGULAR PULSE AND ITS FREQUENCY DISTRIBUTION

Fig. 6.8 shows a typical shock pulse on an exaggerated time axis.

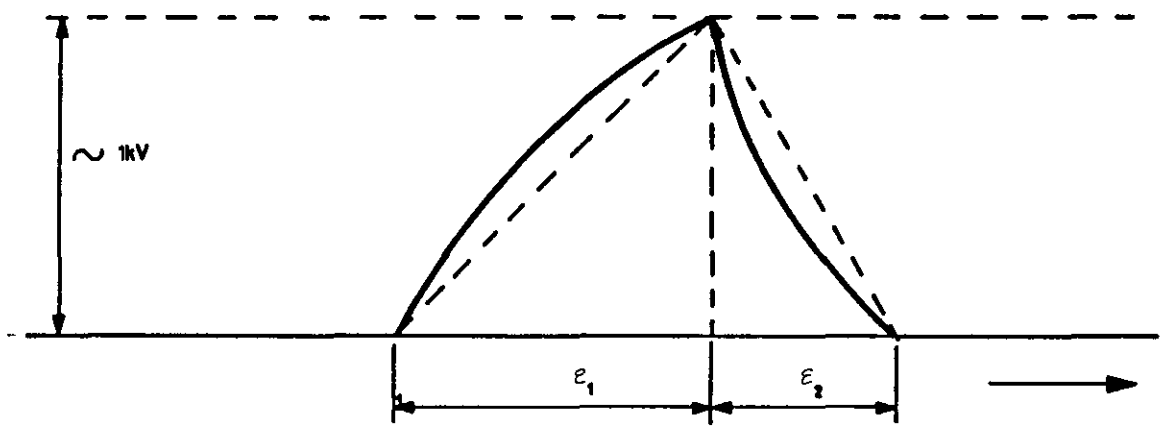

FIG. 6. 8. A TYPICAL SHOCK PULSE (exaggerated)

Assuming the frequency response of the transducer $H(\omega)$ to be linear and if $F(\omega)$ is the frequency spectrum of the applied voltage waveform $v_i(t)$, then the frequency spectrum $F_o(\omega)$ of the emitted ultrasonic pulse may be written as

$$F_0(\omega) = H(\omega) \cdot F(\omega) \quad . \quad . \quad . \quad . \quad (6.1)$$

The spectral energy density of the applied waveform $v_i(t)$ is propotional to $[F_0(\omega)]^2$ at any ω. Assuming linear transition of voltage, $v_i(t)$ may be written as

$$V_i(t) = 0 \quad , \quad t < 0$$

$$= t/\varepsilon_1 \quad , \quad 0 < t < \varepsilon_1$$

$$= t/\varepsilon_2 \quad , \quad \varepsilon_1 < t < \varepsilon_2$$

$$= -1 \quad , \quad \varepsilon_2 < t$$

In order to examine the effect of transition time, it is sufficient to consider only one edge of the pulse waveform, e.g. the falling edge and the Fourier transform $F(\omega)$ may be expressed in the form

$$F(\omega) = \int_{-\infty}^{\infty} f(t) \exp^{-j\omega t} dt$$

$$= \int_{-\infty}^{\infty} \frac{t}{\varepsilon_2} \exp^{-j\omega t} dt$$

$$= -\frac{1}{\varepsilon_2} \left[\frac{1}{\omega} (\exp^{-j\omega t} - 1) \right]$$

The spectral energy density is therefore

$$|F(\omega)|^2 = \frac{2}{\varepsilon_2^2 \omega^4} (1 - \cos \omega\varepsilon_2)$$

which is a maximum when $\omega\varepsilon_2 = \pi/2$ or $\varepsilon_2 = T/4$

where $T = 1/f$

f = Centre frequency of the transducer

This implies that in order to effectively shock excite a transducer, the transition time of the shock voltage waveform must be in the order of a

quarter period of the cycle. Hence it follows that for optimum results in the shock excitation mode the rise and fall times of the pulse must ideally be equal to T/4, giving a total pulse length of T/2. This is rarely achieved in practice and only one edge of the waveform is normally utilized.

One other problem with shock-excitation is that it is not always easy to obtain the required waveform or to make adjustments (trimming) to optimize performance. Furthermore, the shortness of duration of the driving pulse compared to the resultant ultrasonic pulse it generates in practice means that the total input energy available for shock exciting a transducer is rather small. As such, the only variable to compensate for the low input energy is the peak discharge voltage. This accounts for the need of very high voltages to operate transducers in the shock excitation mode.

6.4.2 Truncated sinusoidal excitation

Truncated sinusoidal excitation is sometimes used as an alternative form of driving a transducer in the pulsed mode. Although producing such pulses requires much more elaborate and complex circuits, it is useful to investigate the extent of their relative merits for the present application.

Two forms of truncated sinusoidal excitation may be used, each varying to some extent in character and in the complexity involved in generating them. They are:

(1) Phase coherent high frequency pulse train
(2) Periodic high frequency pulse train

A phase coherent high frequency pulse train as shown in Fig. 6.9 may be expressed as a product of a periodic rectangular pulse train and a continuous sinusoidal carrier. The resultant time domain pulse s(t) may then be written in the form[21]

$$S(t) = \left[\text{rep}_T \ (t/t_p) \right] \cos 2\pi f_o t \quad . \quad . \quad . \qquad (6.2)$$

The corresponding frequency domain transform, which is the convolution of the two functions in the frequency domain, is

$$S(f) = \frac{t_p}{2} F \ \text{comb}_F \ \text{sinc} \ (ft_p) * \left[\delta(f-f_o) + \delta(f+f_o) \right] \quad . \quad . \qquad (6.3)$$

where $F = 1/T$

This resultant frequency spectrum is shown in Fig. 6.9.

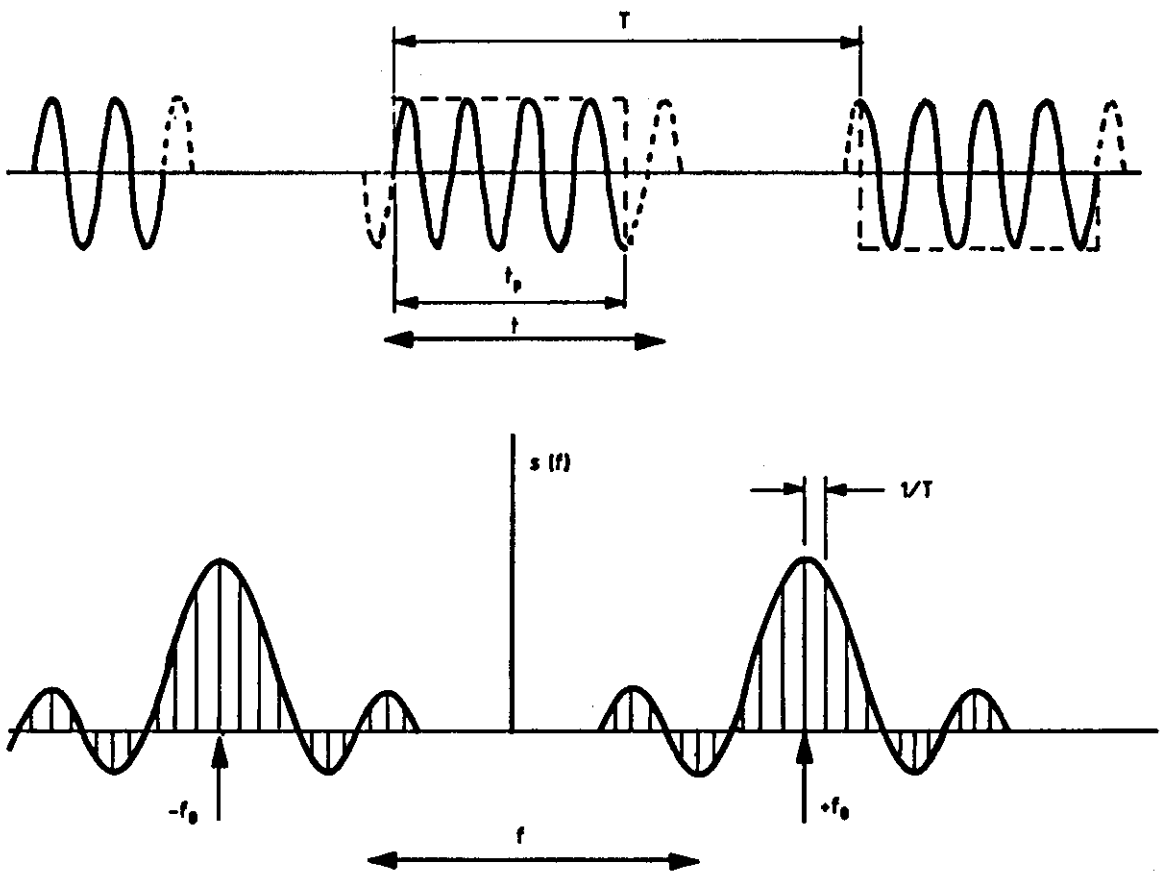

FIG. 6. 9. PHASE COHERENT PULSE TRAIN AND ITS FOURIER TRANSFORM

It is seen in this case that a line of maximum amplitude exists at f_o in the frequency spectrum. Also there is a large spectral density centred around f_o and therefore this form of excitation is highly efficient. However in this case, the phase of the carrier in each pulse according to the equation 6.2 is determined by the phase of the continuous sinusoid. This is undesirable as the separate picture frames produced by each pulse will have some spreading effect due to phase jitter in the absence of a reference phase.

For the above reason, it is therefore useful to examine the features of a truly periodic high frequency pulse train, although this would be rather more involved in generating them in practice. In here, the start of the gating pulse must be synchronized to the carrier itself. A high frequency pulse train as shown in Fig. 6.10 may be obtained by repeating a single high frequency rectangular pulse of the form[A1]

$$s'(t) = \text{rect}\left(\frac{t}{t_p}\right) \cos 2\pi f_o t) \quad . \quad . \quad . \quad . \quad (6.4)$$

Then the time domain periodic waveform would be

$$S(t) = \text{rep}_T \left[\text{rect}\left(\frac{t}{t_p}\right) \cos(2\pi f_o t) \right] \quad . \quad . \quad . \quad . \quad (6.5)$$

where $T \gg t$ is the repetition period

The corresponding frequency domain transform in this case is

$$S'(f) = \frac{t_p}{2} \text{Fcomb}_F \left[\text{sinc}(f-f_o)t_p + \text{sinc}(f+f_o)t_p \right] \quad . \quad . \quad (6.6)$$

This spectrum is shown in Fig. 6.10

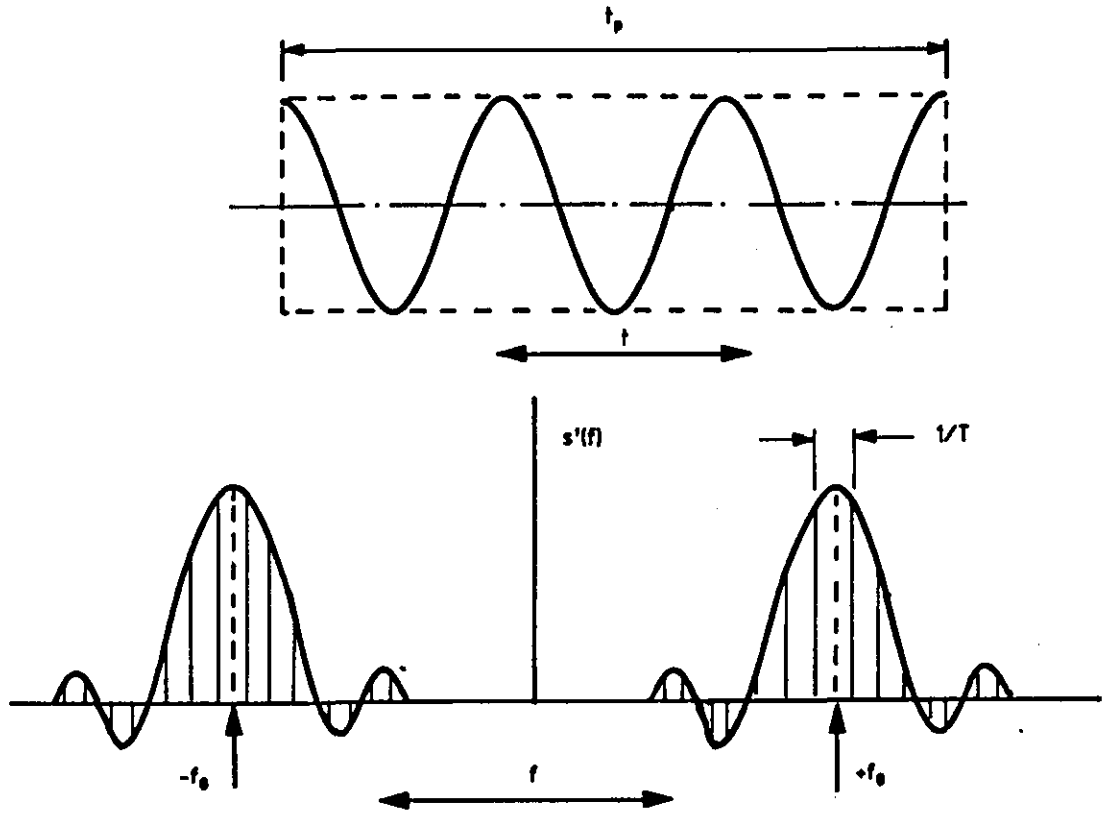

FIG. 6. 10. HIGH FREQUENCY PERIODIC PULSE TRAIN AND ITS FREQUENCY SPECTRUM.

Here there is no phase jitter but the repetition period may only be adjusted in steps of the period of the carrier. However, this is of no practical importance in the present imaging process. It is also seen that in this case a line at f_o does not necessarily exist unless f_0 is harmonically related to 1/T. This is not a great disadvantage since $T \gg t$, the spectrum is nearly continuous around f_0 and therefore the spectral energy density remains virtually unchanged. Hence this form of excitation is preferable.

Because the spectral energy is concentrated around the resonance frequency, the truncated sinusoidal pulses in general are much more effective and for this reason much lower voltages may be used. (e.g. 100 V compared to 1 kV). The other immediate advantages of this approach, as can be seen from above are, the freedom to vary the carrier frequency (trimming) if required, the pulse length and hence the bandwidth of the pulse and also the peak voltage level. All these features are very useful in optimizing the performance of the transducers. It is also interesting to note that in the limit of $t_p \longrightarrow 1/f$, the optimum duration of the pulse (section 6.4.1) agrees with that predicted by the

previous analysis on shock excitation.

6.5 *CONCLUSIONS*

For the present application the ultrasonic pulses must be as short as possible in order to overcome problems of near field, directional response of array elements and to achieve good resolution and to utilize the isochronicity aspect of the system to its full potential. Three forms of excitation of the transducers have been analysed, namely shock excitation, phase-coherent truncated cosinusoidal pulse train and the periodic truncated cosinusoidal pulse train. From this analysis the latter form of excitation is selected for the present application on the grounds of efficiency, controllability and phase stability.

--- // ---

- CHAPTER 7 -

SIGNAL AMPLIFICATION

This chapter deals with the theoretical investigations and experimental estimations of parameters concerning signal amplification. It is noted that the requirements of the proposed imaging system with regard to signal amplification is very high causing difficulties in the design of the amplifiers. The ways of overcoming these difficulties and the possibility of developing a new category of amplifiers for this type of application is outlined.

7.1 INTRODUCTION

The power of the received signals has to be raised to a level sufficient for the particular acousto-optic technique of visualization used. In order to achieve good resolution and image quality the received and the re-transmitted pulses must be as short as possible requiring faithful amplification over a broad band of frequencies. These together with the electrical damping requirements of the transducers to achieve wideband response places heavy demands on the amplifiers. In this respect, various areas have been investigated as listed below from which the amplifier design specifications have been formulated.

1. Typical and worst case input signal levels
2. Output signal levels
3. Phase distortion and bandwidth considerations
4. Dynamic range
5. Input and output impedances
6. Damping characteristics
7. Noise level
8. Power consumption

9. Size
10. Cost

As can be seen, most of these factors are related to one another and for a feasibility study it seems appropriate to begin by estimating the output requirements as this determines to a large extent the feasibility of the proposed new system.

7.2 OUTPUT SIGNAL LEVEL

The required output signal level is considered as that needed to produce a satisfactory visual effect in the schlieren medium. It may be estimated here on a practical basis using an appropriate model simulating the conditions of the proposed system. For reasons described in chapter 8, the schlieren technique was adopted. In this case the amplifiers must deliver sufficient pulse power to equal or exceed the threshold requirements of the particular schlieren medium used, in order to produce visualization.

Different liquids have different sensitivities in terms of threshold acoustic power.[12] However, working on the basis of absolute threshold power requirements for a given medium is of little use in this case, because the true power required for image formation will not only depend on the absolute sensitivity of the liquid but on many other factors related to the transmission efficiency of the sonoptics. Heavy energy losses are involved which may be as high as 90%. Secondly, although specifying power requirements is a common method of specifying sensitivity of schlieren media, it is far easier to work on the basis of the peak voltage requirement in this particular case.

Having made a re-transmitting array according to the specifications of Chapter 5, although the total number of channels were half the number planned, the output signal requirements were estimated using a practical arrangement as shown in Fig. 7.1. The transducer material was PZT 5H and when the array was made, the elements gave an impedance of about 500 ohm at 2 MHz. External electrical damping was also used to improve the

pulse performance and this was in the order of 75 ohm.

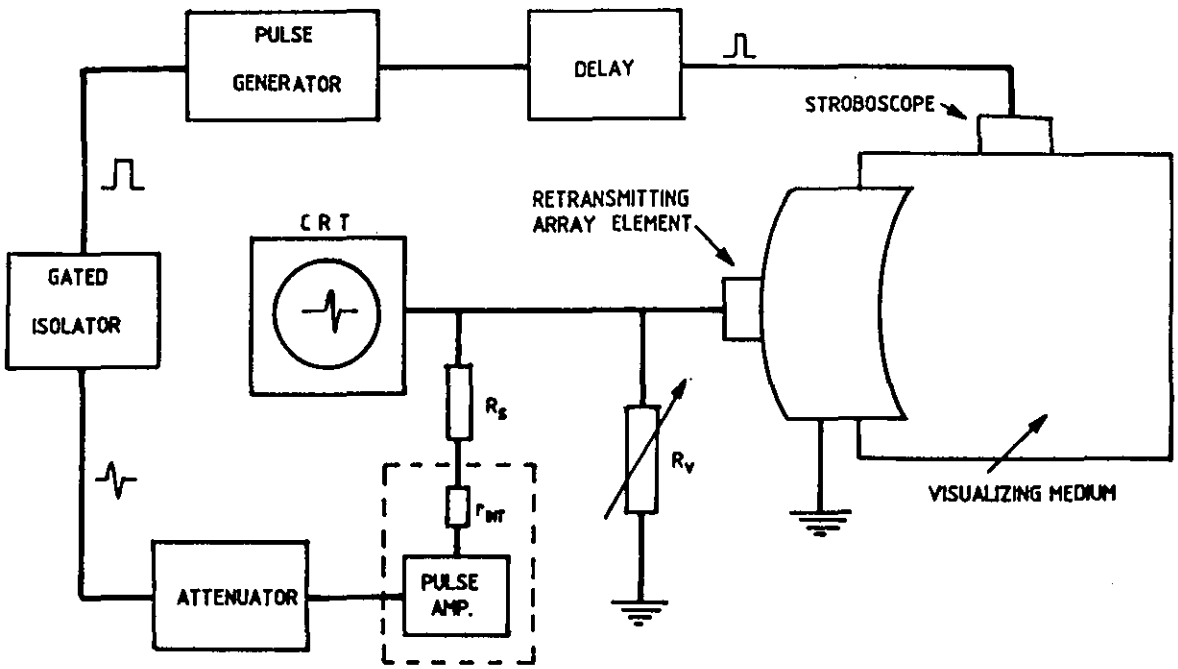

FIG. 7. 1. ESTIMATION OF OUTPUT SIGNAL REQUIREMENTS.

The frequency of the carrier and the pulse length of the gated burst was adjusted to give a suitable ultrasonic pulse and the amplitude of the excitation was then adjusted using the variable attenuator until the threshold level was found.

The above experimental approach is useful in two ways. Firstly, to determine the output voltage requirements for a given visualizing medium, and secondly to compare the merits of different media. A large number of liquids was compared and out of these a flourinated organic liquid with the brand name FC 75 was found to be the most promising . In the case of water as the schlieren medium, the required output voltage was in the order of 50 V, while for FC 75, this was only 15 V peak to peak at the time of original measurements which has later been further reduced by improving the optics.

Under the particular conditions, this measurement holds practically true whether it is a short pulse or a long train of waves and hence can

be treated as one of the independent specifications describing the required threshold output voltage of the amplifiers. The maximum permissible output voltage determined by the saturation of the schlieren medium could also be estimated using the same arrangement, but this was not regarded as crucial at this stage.

7.3 TYPICAL AND WORST CASE INPUT SIGNAL LEVELS

The signals received by a transducer from various targets within a test object can be of a very wide range. The theoretical lower limit is zero while the upper limit under given conditions depends on the insonifying energy and the target strength. The minimum detectable signal is, however, limited in this case either by the noise level or the maximum gain that could be meaningfully assigned to the amplifiers to boost the signals above the required output threshold. The input signal level was experimentally estimated using the arrangement shown in Fig. 7.2 below.

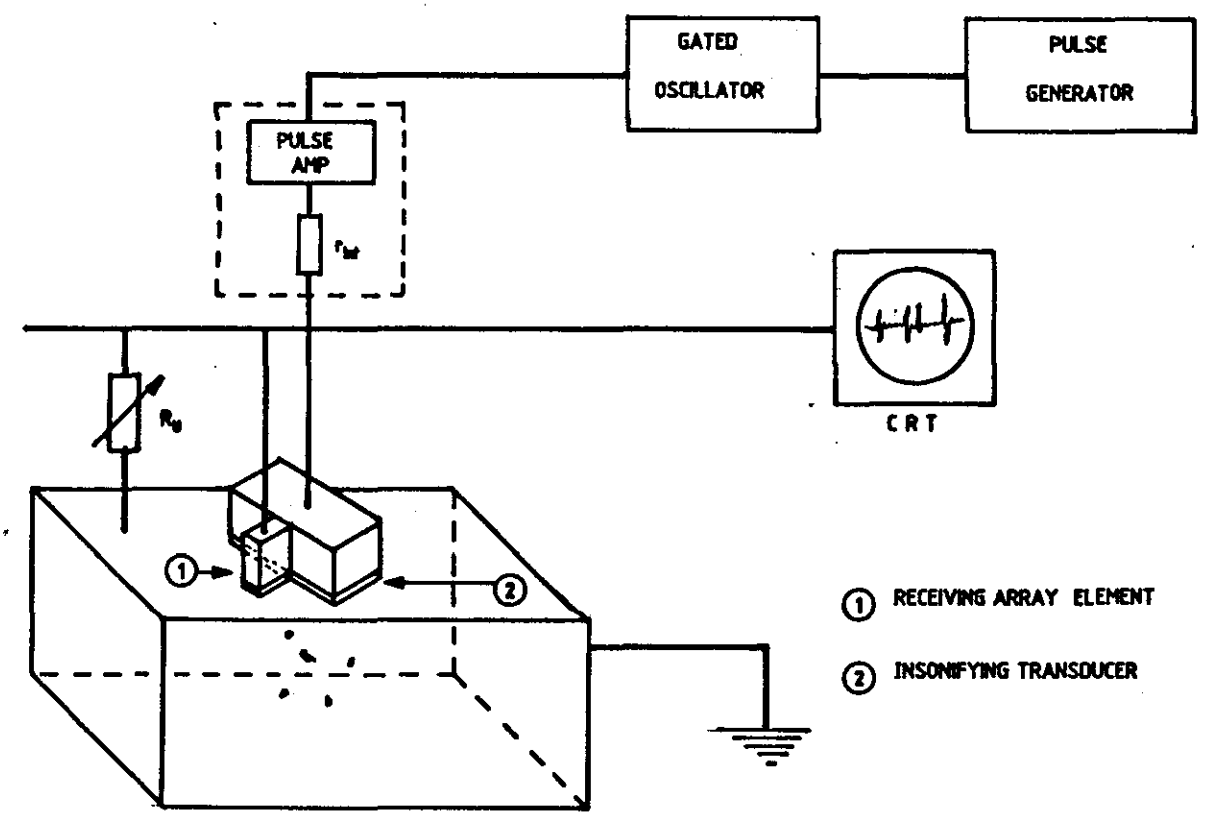

FIG. 7. 2. ESTIMATION OF MINIMUM AND TYPICAL INPUT SIGNAL LEVEL.

The gated oscillator produces a truncated sinusoidal excitation of appropriate frequency and duration. A separate transducer of similar dimensions and frequency is used for insonifying the test object which contained a range of defects of different sizes at various depths, the minimum size being 0.7 mm drilled hole which was 10 cm below the surface of the test object. The insonifying pulse amplitude is varied between 10 V and 200 V pp. Echo signals are picked up by the individual elements of the receiving array and were found to be between 75 to 500 mV approximately. Obviously these estimates have no general significance other than for the present feasibility study.

The above experimental approach served two main purposes. Firstly it gave an idea of what input signals to expect. Secondly, it made it possible to compare the uniformity of performance of the elements in the array in a controlled manner by placing them at a fixed location, one at a time, and observing the signal amplitudes and pulse lengths.

7.3.1 Gain specification

An estimation for amplifier gain could now be made. In order to produce visualization, the input signals must be boosted up such that

$$V_{i(min)} \times G \geqslant V_{th} \quad . \quad . \quad (7.1)$$

where $V_{i(min)}$ = Input signal generated by the receiving element
G = voltage gain of the amplifier
V_{th} = Threshold output voltage to produce visualization

Aaccording to the previous assessment of V_{th} being equal to 15 V and $V_{i(min}$ of 75 mV, the numerical gain required of the amplifiers would be

$$G > 15 / 75 \times 10^3$$

$$= 200$$

The maximum signal corresponding to 500 mV will also be raised according

to the same gain setting which would theoretically mean an output voltage of 100 V. This is obviously very difficult to achieve at the same time with many other constraints and requirements and therefore the use of variable gain control must be considerd in the design of the final system. However, for the present feasibility study a fixed gain setting of 200 may be used while the output voltage swing capabilities of the amplifiers must be made as large as possible.

7.4 SIGNAL DISTORTION AND BANDWIDTH CONSIDERATIONS

Three main types of signal distortion that can be present and that should be minimized are[24]

1. Phase distortion
2. Amplitude distortion
3. Harmonic distortion

The problem now is to know what limits are to be imposed. Firstly, it is possible to assign some arbitrary limits and proceed, but this has the serious drawback in the present case since the final results may not be conclusive. It will also be difficult to know exactly what areas are to be improved.

The second approach is to make a comprehensive investigation by theoretical analysis. However, in the absence of any previous work reported in this area, such an attempt will be extremely involved and time consuming. Besides, the approximations that may have to be used could in practice, largely devalue its relevance.

The third route is to take an experimental approach through hardware construction and deliberate introduction of errors to assess the limits of acceptance. Although such an approach would be closely related to the final arrangement, hardware construction and experimentation on an iterative basis would not be easy; the cost and the time required would be unacceptable.

The fourth approach is to first investigate what limits could be

practically achieved and impose those restrictions as tightly as possible on the design of the system making use of experimental estimations where ever possible. The advantage of this technique is that the results would closely represent the potential of the proposed new system. It is relatively easy to identify the limits of acceptance by relaxing the specifications one at a time or by deliberate introduction of errors. For these reasons, the latter strategy was chosen in the following discussions.

7.4.1 Phase distortion and differential phase delay

If the channel is dispersive, then phase distortion occurs in pulsed waveforms as a result of differences in the velocities at which the signals of different frequencies are travelling. The extent of phase distortion that can be tolerated in a given system depends on the particular technique used. For example in a conventional switched array B-scan system, the relative phase performance of the individual elements of the array are not very critical. However, in the present technique it is not difficult to appreciate the extreme importance of good phase performance when examining the imaging process as a whole. Here, the phase angle $\not{\emptyset}$ appears in a complex exponential form in the equation governing the acoustic radiation pressure which is responsible for forming the acoustic images in the schlieren medium.

$$P_{(x,y)} = \sum_{i=1}^{N} \frac{\exp^{-j(kr_i+\emptyset_i)}}{r_i} \qquad \cdots \qquad (5.10)$$

Because of this, it is necessary to investigate the factors relating to phase shifts. Furthermore, because of the difficulty of quantifying the effect of phase errors on image quality at this stage, it is advisable to excercise the tightest possible control over this parameter.

There are two distinctly different phase shift problems involved here. They are

1. Phase distortion present in a given transmission channel

2. Differential phase shifts between the channels

The first is an individual channel requirement while the second factor deals with a collective performance of all the channels. Fig. 7.3(a) shows schematic diagram of a transmission channel as a whole, including the receiver and re-transmitter transducers.

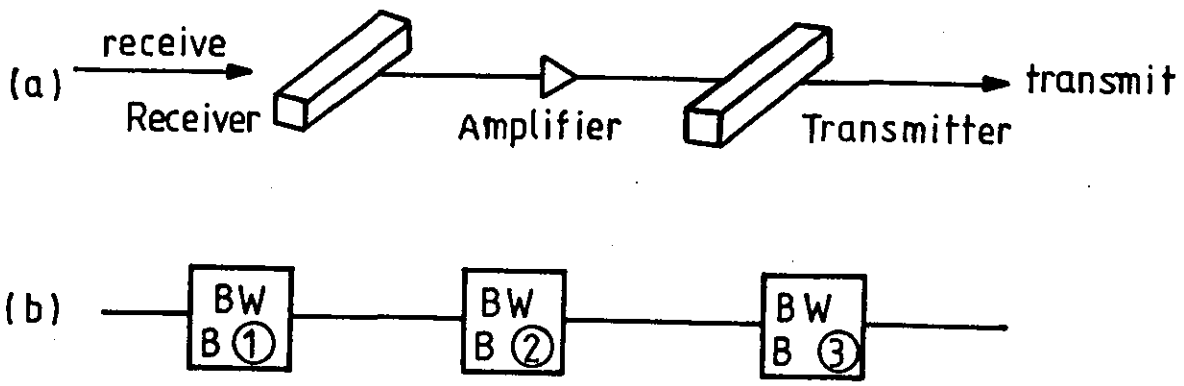

FIG.7.3 SCHEMATIC DIAGRAM OF A SINGLE TRANSMISSION CHANNEL

If t is the time delay experienced by a signal of frequency f passing through this channel, the phase shift ϕ may be written as

$$\phi = 2\pi f t \text{ rad} \quad . \quad . \quad . \quad . \qquad (7.2)$$

The extent of the phase error may be examined by partial differentiation of phase shift with respect to time delay and frequency using equation 7.2 giving

$$\delta\phi = 2\pi \left[\frac{\partial\phi}{\partial f}\Big|_t \delta f + \frac{\partial\phi}{\partial t}\Big|_f \delta t \right] .$$

$$\therefore \quad \delta\phi = 2\pi \left[t\delta f + f\delta t \right] \quad . \quad . \quad . \quad . \qquad (7.3)$$

The second term $f\,\delta t$ in equation 7.3 determines the degree of phase error experienced by two signals separated in frequency by an amount δf. The larger the δt, the greater the phase distortion. In order to

reproduce a received pulse faithfully, all the frequency components must arrive at the output of the channel simultaneously. If this is ensured, then δt in equation 7.2 becomes a constant and the phase shift is a linear function of the frequency such that

$$\phi = \text{const. } f \times 360 \text{ deg.}$$

where f is any frequency within the band of signal frequencies.

Under this condition the signals pass through without phase distortion and the form of the input signal will be retained.

7.4.1.1 Differential phase shift

Even if the phase distortion experienced by the signals passing through the channels are small, the adjacent channels may have a varying degree of phase shifts due to a number of reasons. This is the most severe form of phase shift problem that may appear in the present case as the quality of the images formed depends not only on the individual phase performance of the channels but also on the collective performance of all the channels operating in parallel.

For two channels having slightly different time delays t_1 and t_2 ,the phase delays ϕ_1 and ϕ_2 may be written as

$$\phi_1 = 360 \times t_1 \times f \text{ deg.}$$

$$\phi_2 = 360 \times t_2 \times f \text{ deg}$$

$$\therefore (\phi_2 - \phi_1) = (t_2 - t_1) f \times 360 \text{ deg} \quad . \quad . \qquad (7.4)$$

i.e. Differential phase shift = Differential delay x frequency

It is this differential phase shift that could seriously degrade the image quality. Here again quantifying the effect of random differential phase shifts on the image quality is extremely difficult at this stage

and minimizing this problem with tight control of parameters seems to be the most relevant approach. For example, if a differential phase shift of 1% is allowed for component tolerances, construction etc, i.e. 3.6 degrees at 2 MHz, then the equivalent differential delay would be

$$(t_2 - t_1) = \frac{3.6 \times 10^{-6}}{360 \times 2} \quad s$$

$$= 5 \text{ ns}$$

This can be ensured for all worst case conditions if the phase shift of the individual channels is not greater than approximately 4° at 2 MHz. In order to estimate what bandwidths are involved, if the channel response is assumed to be similar to that of a low pass filter, eg. a 3rd order Butterworth filter, the bandwidth requirements would be as high as 30 MHz. This is practically impossible to achieve when the transmission channel as a whole consisting of 2 MHz PZT transducers is considered, although the amplifiers alone may be designed to comply with such standards. Fortunately, the differential phase shifts can be made much smaller in practice than the individual phase shifts. If care is taken to ensure sufficiently identical behaviour of the transmitting channels and efforts are made to produce wide band transducers, then the phase shift problems may be significantly reduced. As will be shown later the transducers need to be damped heavily in order to obtain satisfactory performance but this would inevitably result in reduction of sensitivity which has to be compensated by increasing the gain of the amplifiers. At the same time the bandwidth of the amplifiers must be wide enough so that its presence does not significantly reduce the overall bandwith of the channel. Considering the limitations of the transducers, amplifier bandwidth of about 15 MHz seems to be adequate for the present purpose.

7.4.1.2 Influence of phase performance in system design

As discussed earlier, the present technique of acoustic image reconstruction places heavy demands on the phase performance of the system. This is one of the main reasons for not adopting the original

approach of introducing electronic phase delays with the two lens DUVD arrangement because electronic phase shifters are prone to phase distortion, However, this, method is popular in some other techniques where the phase performance is not a very critical feature. Based on the previous calculations, various other forms of introducing necessary phase delays by mechanical means were therefore considered which finally led to the design of the curved array and a cylindrical lens which simplified and improved the whole sonoptics further as discussed in chapter 4. There is however, a spatial error introduced by the distribution of the re-transmitting array elements along a curvature. This was also minimized in the design of the sonoptics by way of using small curvatures and adopting large F numbers, although the error is likely to have caused only a second order effect.

7.4.2 Amplitude distortion

Amplitude distortion is the result of non-uniform response of the channel to all the frequency components of the input waveform. If the insonifying electrical pulse is of the order of one cycle at 2 MHz, then the approximate frequency content would be in the order of 2 MHz centred around 2MHz. Ideally, the pass band of the channel must be adequate to accommodate this frequency spectrum if amplitude distortion is to be avoided. However, in general this is far from being the case with resonant PZT transducers due to their comparatively large Q factors which severely limit the overall bandwidth of the transmission channel. The result is therefore amplitude and phase distortion, elongation of pulse length, and ringing, as would be expected in the case of a bandpass filter impulse response.

7.4.2.1 Channel bandwidth

The upper cut off frequency of cascaded stages may be approximately evaluated from[28]

$$\frac{1}{f_H} = 1.1 \left[\frac{1}{f_1^2} + \frac{1}{f_2^2} + \ldots + \frac{1}{f_n^2} \right] \quad . \quad . \quad . \quad (7.5)$$

Referring to Fig. 7.3(b), This may be expressed for the channel as

$$\frac{1}{f_H} = 1.1 \left(\frac{1}{f_R^2} + \frac{1}{f_A^2} + \frac{1}{f_T^2}\right) \quad . \quad . \quad . \quad . \qquad (7.6)$$

where, f_R , f_A , f_T are the upper cut off frequencies of the receiving transducer, amplifier and the re-transmitting transducer respectively.

It therefore follows that as the bandwidth of the overall system is limited by the PZT transducers, if the amplifiers are designed with a bandwidth as large as possible such that $B_A \gg B_T$, where B_A = bandwidth of amplifiers and B_T = bandwidth of transducers, then the overall bandwidth of the channel (BW) is not further influenced by the presence of the amplifiers. Since the bandwidth of the receiving and the re-transmitting transducers can be considered as identical, the overall bandwidth of the channel may be derived in this case by assuming a cascade of two similar non-interactive stages in the form[26]

$$BW = B \left(2^{1/2} - 1\right)^{1/2}$$

If the bandwidth of a typical 2 MHz transducer is for example 200 kHz, then the overall channel bandwidth would be approximately 83 kHz which is obviously a very low value compared to the frequency content of the input pulses. It must therefore be emphasized that every attempt must be made to improve the bandwidth performance of the transducer for this particular application.

In the previous discussion a bandwidth of 15 MHz was estimated for the design of the amplifiers to avoid phase distortion problems. Since the dominant frequency content presented to the amplifiers is well below this value due to the much smaller bandwidth of the transducers, it also satisfies the requirements, to avoid amplitude distortion within the amplifiers at the same time.

7.5 DYNAMIC RANGE

This is another area needing much attention. With respect to the

dynamic range, the following terms applicable to the system under development are briefly described below.

1. Dynamic range of amplifiers
2. Input signal range and effective input signal range
3. Effective dynamic signal range
4. Dynamic range of the visualizing medium
5. Dynamic range of optional display tubes if used

7.5.1 Dynamic range of amplifiers

This is usually defined as a power ratio in dB, such that,

$$\text{Actual dynamic range ADR} = 20 \text{ Log } \left(\frac{V_{max}}{V_{min}}\right) \text{ dB} \quad . \quad . \quad . \qquad (7.7)$$

where V_{max} is the maximum undistorted output and V_{min} is the noise limited minimum output signal. Usually in ultrasonic imaging systems, the dynamic range of amplifiers is less of a problem compared to that of the actual display techniques. For example, a good instrumentation amplifier may have a dynamic range in the order of 60 dB, while that of a CRT display is only in the range of 20 dB. It will become clear later that for the present application also, the actual dynamic range of the amplifiers is not a limiting factor.

7.5.2 Input signal range and effective input signal range

According to the previous experimental estimation the maximum input signal is in the order of 500 mV and because the theoretical minimum is anything above zero, the available input signal range (ASR) may be defined as 0 to 500 mV peak to peak. If G is the gain setting of the amplifiers, then the range of the effective input signals (ESR) that may be visualized is

$$ESR = \frac{V_{max} - V_{min}}{G} \quad . \quad . \quad . \quad . \qquad (7.8)$$

The significance of the ESR is that it defines the portion of the input

signals that will be accomodated by the amplifiers for the particular gain setting which is a useful parameter when dealing with variable gain and time varying gain functions. Achieving a high voltage swing capability simultaneously with all the other requirements described above is practically difficult. Therefore if a reasonable value for V_{max} is assigned for the feasibility study at this stage for example 30 V pp, the range of the signals that will be examined according to equation 7.8 with preset gain of 200 will be 75 mV - 150 mV, defining an ESR of 75 mV

7.5.3 Effective Dynamic Signal Range (EDR)

Although the actual dynamic range of the amplifiers can be considerable,

the effective dynamic range (EDR) applicable to the transmission channel in the present application is very much smaller due to the threshold voltage requirement V_{th} for visualization. EDR can be represented as:

$$EDR = 20 \text{ Log } \left(\frac{V_{max}}{V_{th}} \right) \text{ dB} \quad . \quad . \quad . \qquad (7.9)$$

If typical values for V_{max} and V_{th} obtained previously are substituted in the above equation

$$EDR = 20 \text{ Log } \left(\frac{30}{15}\right)$$

$$= 6 \text{ dB}$$

From this it can be seen that as the effective dynamic range EDR of the system is very low compared to the actual signal ranges present, every attempt has to be made to improve this aspect by increasing V_{max} and/or decreasing V_{th}.

However, raising V_{max} at a low impedance of the order of 75 ohm in a multi channel system while preserving properties like wide bandwith, size, power consumption, cost etc. is a very challenging engineering problem. On the other, hand lowering V_{th} calls for

sensitive re-transmitting transducers which is usually contradictory to the requirements of improving their bandwidth. Also efficient coupling must be ensured while optimizing the sonoptics. In fact at the time of assembly of the first prototype, the effective dynamic range of the system was considerably increased by improvements to the optics to about 15 dB. It must be emphasized that EDR has to be further improved as far as possible to accommodate a greater proportion of the input signal range when the design of a final instrument is considered.

Because of the low effective dynamic range of the system, the amplifiers could often reach saturation. Although not a complete solution to this problem, the use of remote gain controls built into the amplifiers could be suggested here. In this way, weaker echoes may be examined at a higher gain while the stronger targets which normally drive the amplifiers into saturation could be examined at a much lower gain.

Dynamic compression (companding) is sometimes employed in various instruments, but in the present application the possibility of excessive amplitude and phase distortion may not permit this approach and hence will not be examined in details at this stage.

7.6 TIME VARYING GAIN (TVG)

Echo signals received from targets deep down the test object progressively become weaker due to two main reasons.

1. Attenuation losses
2. Beam divergence

These two causes of losses follow distinctly different distance laws. The first is due to sound absorption and scattering characteristics of the medium, leading to an exponential decay of the signal amplitude with depth, while the latter depends on spherical beam spreading at large depths where the wavefronts can no longer be considered plane. The combined effect of these two factors upon the acoustic pressure P at a distance d from the probe in the far field can be expressed as:[22]

$$P = P_o \pi \frac{N}{d} \exp^{-\alpha d} \quad . \quad . \quad . \quad . \qquad (7.10)$$

$$d \gg N$$

where
- P = Initial acoustic pressure at a given point
- N = Near field distance of the radiating probe
- α = Attenuation coefficient

If these losses are significant at the depth ranges of interest, then additional amplification may have to be employed according to a pre-determined depth/amplification weighting function, most appropriate for the particular loss pattern. The required amplification functions can be rather complicated, especially if the medium is not strictly homogeneous, e.g. biological tissues or even some alloys.

It is now necessary to investigate with the help of equation 7.10 whether or not TVG is essential for the present application. Here the insonifying transducer could either be the receiver array or a separate transducer. Since the array aperture is previously estimated to be 6 cm x 1.5 cm, the beam profile in the far field would approximate to a cylindrical wavefront where the acoustic pressure associated with the wavefront is now proportional to $1/\sqrt{d}$ and not to $1/d$ as would be the case with a spherical wavefront. Since the wave length at 2 MHz in steel is 3 mm and the array width is 15 mm, the corresponding near field would be approximately 18 mm. Also a typical value for the attenuation coefficient in steel at 2 MHz would be 5×10^{-3} dB/mm. Since the maximum object distance required for the present application is 25 cm, the total path length involved in the pulse echo mode would be 50 cm. Substituting all these values in to equation 7.10, the gross reduction in pressure amplitude may be estimated as:

$$\frac{P}{P_o} = \pi \frac{1.8}{\sqrt{50}} \times e^{-5\times10^{-2}\times50}$$

$$\simeq 0.06$$

It can now be seen that as the above value for P/P_0 is very low,

some form of TVG is needed. If P_0 is arbitarily specified as 100% at a given point, then the echo amplitude from a plane reflector at 25 cm below would only be about 6%. Hence a gain ratio of about 16 : 1 is needed just to compensate the echo amplitude at these depths. If the originally chosen gain of 200 is regarded as the lowest gain setting, then the numerical gain range required would be 200 - 3200, which is very difficult to achieve at the present time due to many other constraints. It can also be seen that the situation would be far worse still if a separate transducer of smaller size is used for insonification, e.g a commercial probe, as the far field radiation pattern would then take the form of a spherical wave front in which case p / p_0 would be equal to only 0.01, requiring a gain range of 100 : 1 as opposed to 16 : 1 in the previous case. Therefore it follows that if a separate insonifying probe is used, the probe dimensions must be such that it does not lead to a far field spherical wavefront in the far field within the depth range of interest.

7.6.1 Synthesis of an ideal TVG function for the present application.

A suitable TVG function may now be evaluated for the present application with the help of equation 7.10 for increasing values of d starting from a suitable distance of say, 5 cm from the test surface. The gain required at any other depth would then be calculated as in table 7.1. The resulting function represents the required gain pattern as shown in Fig. 7.7.

Depth cm	d cm	P/P_o	Gain Factor
5	10	1	1
10	20	0.46	2.17
15	30	0.23	4.35
20	40	0.12	8.33
25	50	0.06	16.7

TABLE 7.1

FIG. 7.7 A SUITABLE TVG FUNCTION

$$G_F = \frac{P_o}{P} = \frac{\sqrt{d}\ \exp^{0.05}}{1.8 \times \pi}$$

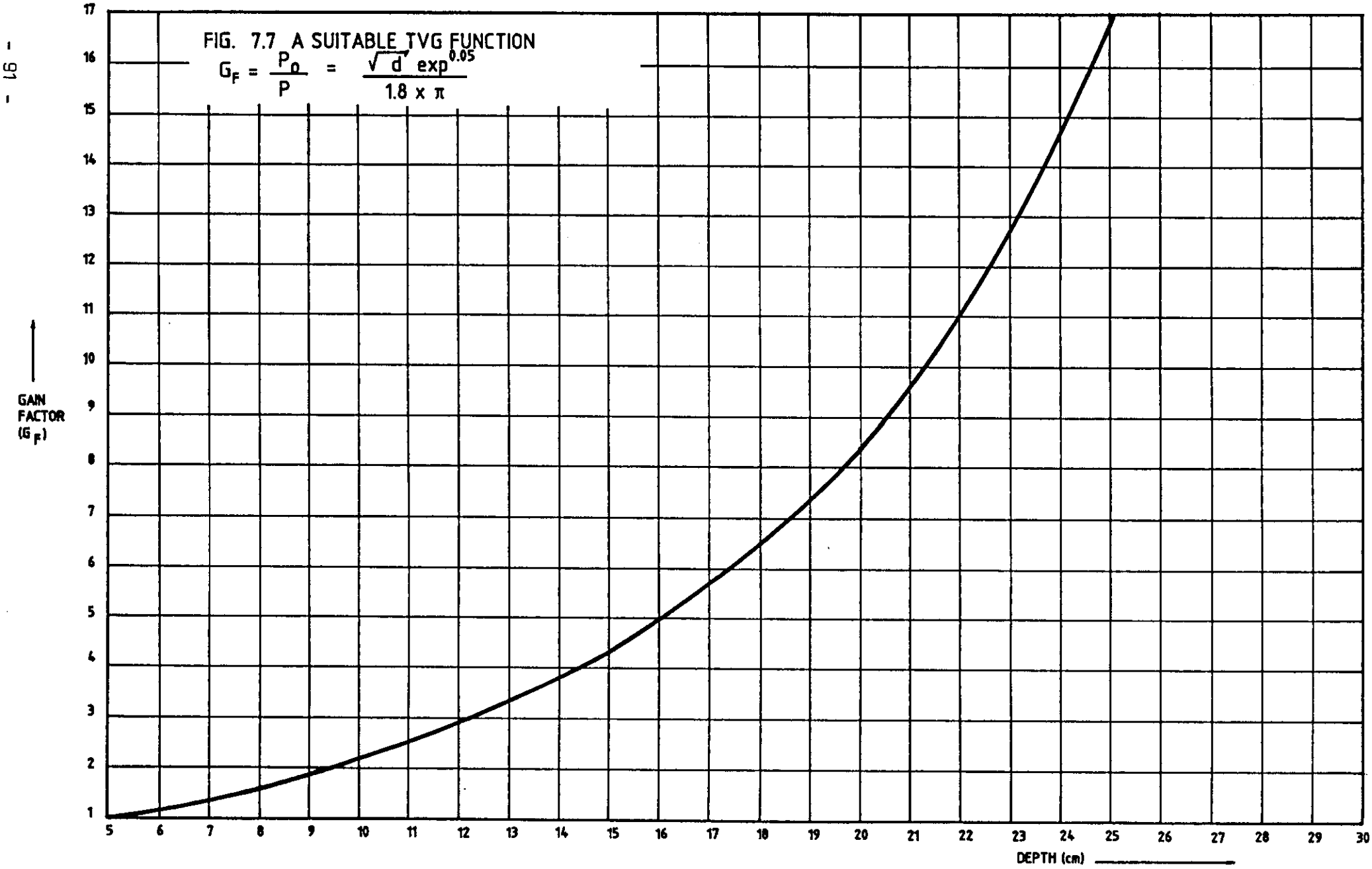

Although not immediately apparent, there are some hidden disadvantages with TVG in the present application. Firstly, TVG cannot discriminate target strength differences at various depth levels and as the gain is increased with the distance the ESR according to equation 7.8 also decreases such that

$$ESR = \frac{V_{max} - V_{th}}{G_1}$$

Hence the proportion of the target information that is accomodated by the amplifiers decreases with increasing depths, thus progressively reducing the ability of the system to display structural details of defects. It also elevates the problem of saturation. Secondly, increasing the gain has the effect of reducing the bandwidth of the amplifiers as normally the gain bandwidth product of an amplifier is a constant. Therefore if the bandwidth is fallen too low as the result of swept gain, then it may lead to phase distortion problems at elevated gain levels unless the amplifiers are designed with a much larger gain bandwidth product which is even more of a problem for reasons already discussed. The third problem is that the requirements for TVG in practice vary with the particular testing situation and therefore generation and control of TVG functions may become rather difficult.

The result of all these is that when TVG is considered in the design of the final system, a compromise has to be found between all the related parameters based more on practical estimations and not only the loss patterns, before assigning suitable TVG functions. This is an elaborate procedure and as such, at least for the feasibility study, TVG may be temporarily omitted at this stage as one would be dealing mainly with establishing the fundamental conceptual validity of the proposed system. However, according to the above investigations it is apparent that TVG has to be considered in the design of a final system.

7.7 ASSESSMENT OF TERMINAL IMPEDANCE AND DAMPING CHARACTERISTICS

The choice of right input and output impedance is extremely important in

the present case for good bandwidth performance and to prevent excessive loss of sensitivity. Due to the very complex and unpredictable behaviour of the transducer elements it is very difficult to provide an ideal match between the amplifiers and the transducers which would give maximum power transfer and at the same time, good bandwidth performance. For reasons discussed later, the terminal impedances have to be resistive and must be maintained at a low value to obtain wideband performance from the transducer elements. The inevitable reduction of the sensitivity has then to be compensated by raising the gain of the amplifiers and therefore the need of a high gain bandwidth product for the amplifiers can again be emphasized.

In a multi channel system, the need of low output impedance with high voltage requirements causes a rapid increase in the total power consumption, hence the size, cost and various other complications. Also the transducer impedance is not purely or dominantly resistive, but is complex and also frequency dependent causing great difficulties in broadband matching. Experiments show that the situation is even worse when narrow array elements are made out of PZT material, for their behaviour is quite different in many ways from that of the crystals from which they were cut. For example, attempts to assess the impedance characteristics of these elements by the usual impedance circle plotting technique was not very successful and showed the existence of many minor resonances and a great sensitivity to the environment, reducing the predictability of their characteristics.

For the above reasons, a more practical approach was taken by observing the improvement to the bandwidth of the transducer elements in response to the changes of terminal impedance in a manner simulating the conditions of the actual operation as shown in Fig 7.8(a) and (b).

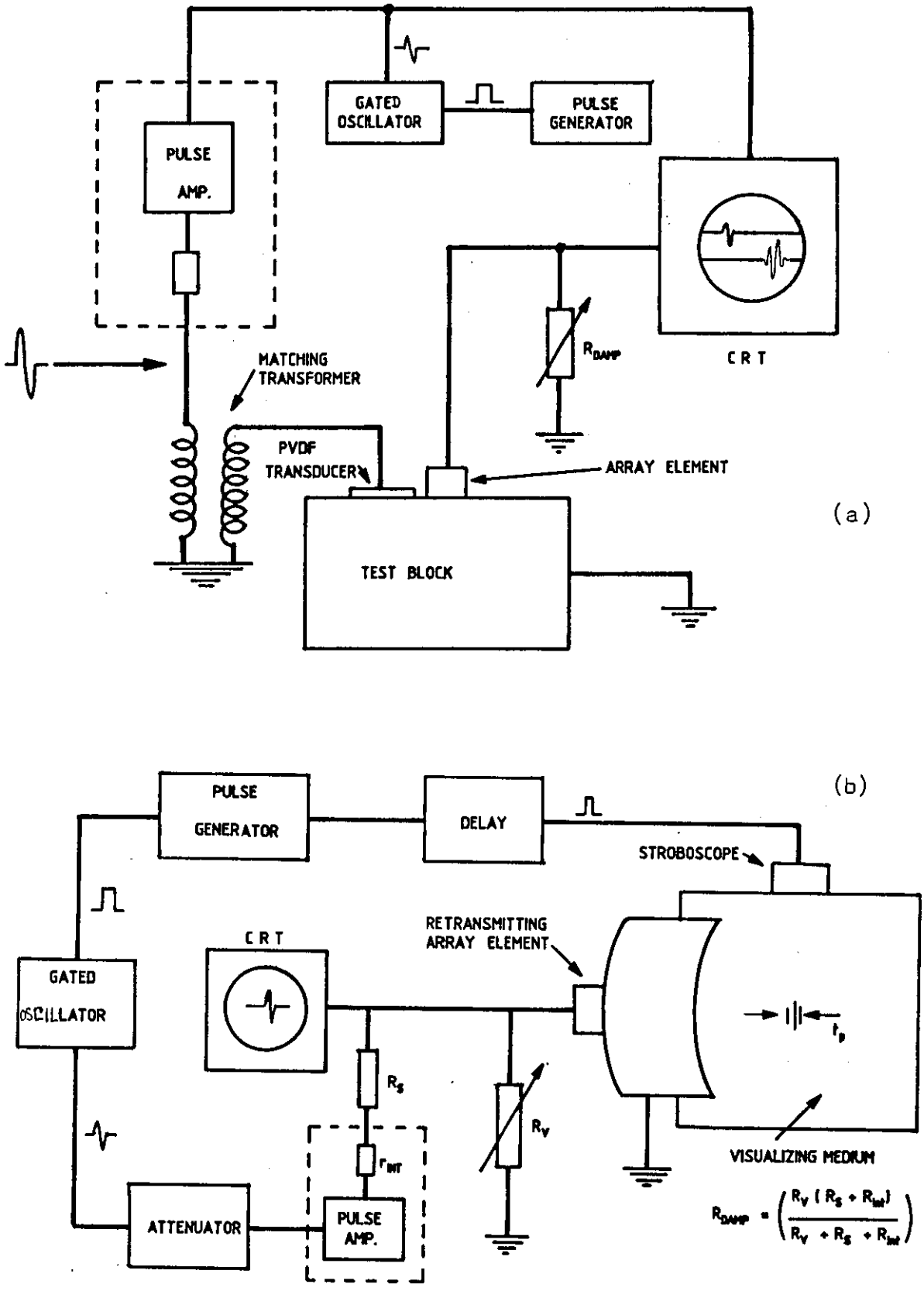

FIG. 7.8 ASSESSMENT OF TRANSDUCER DAMPING REQUIREMENTS

It must be mentioned here that the transducer elements were also mechanically damped with tungsten araldite backing. They were in fact the same elements used for sensitivity assessment described before. The pulse length was examined firstly using an A-scan display and secondly and more appropriately by forming an actual schlieren picture as in Fig. 7.8(b). The effect of varying the damping was carefully observed and as the damping resistance was gradually reduced while keeping the transmitted amplitude constant by increasing the amplifier gain, the pulse length was also reduced to some extent as expected, indicating an improvement on the bandwidth up to a point. Further reduction in the damping resistance gave no further improvement in the bandwidth and the only result was the continual reduction of the sensitivity. The value of the variable resistance at this point was noted and the equivalent damping resistance was calculated from

$$R_{damp} = \frac{R' \times R_V}{R' + R_V} \quad . \quad . \quad . \quad . \qquad (7.11)$$

where R_{damp} = Damping resistance required

R' = Internal resistance of the power amplifier + series resistance

R_V = External variable resistor.

Using this method the required damping resistance giving optimum performance was found to be in the order of 75 ohm and therefore can be regarded as the appropriate input and output impedance required of the amplifiers. Using the same experimental approach, the most suitable frequency of operation was also estimated. Although the original PZT crystal had a centre frequency of 2 MHz, the apparent centre frequency of operation of the small transducer elements according to the above assessment was found to be about 1.8 MHz.

It is now useful to examine the validity of the above observations using an equivalent circuit model. For this purpose, the one dimensional equivalent circuit[27] shown in Fig.7.9(a) and (b) was chosen mainly for its simplicity, although the behaviour of the array elements cannot be fully

represented by this model. However, adequate knowledge may still be gained with respect to the above experimental observations at least in a limited qualitative sense.

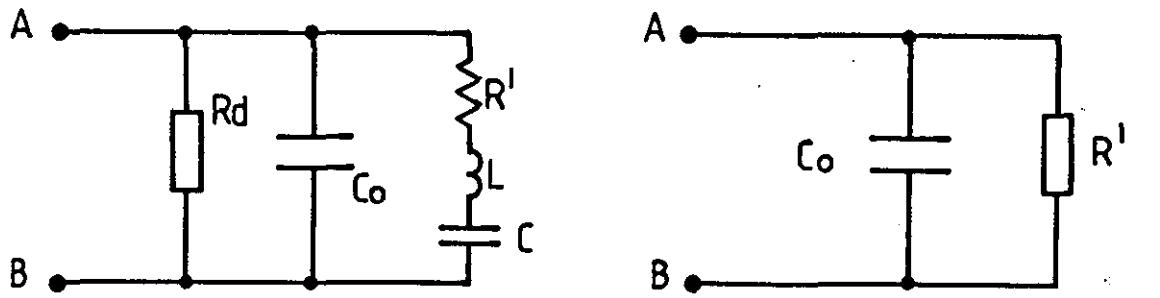

(a) Equivalent cct. of a PZT transducer near resonance frequency

(b) Simplified equivalent cct. at and near resonance

FIG. 7.9

C_o = Static capacitance of the transducer

R_d = Dielectric loss in C_o

R' = Radiation resistance and internal loss resistance

L = Equivalent mass of the transducer

C = Equivalent compliance of the transducer

Measurements showed that a moderately damped PZT transducer of 1.8 mm x 12 mm with a nominal centre frequency of 2 MHz used in this work (together with the connecting cables) had the typical values of C_0 $\simeq$ 250 pF and $R' \simeq$ 500 ohm, respectively. The loading effect of this parallel capacitance can be seen when the reactance, X_{C_o} at the centre frequency (2MHz) is considered.

$$X_{C_o} = \frac{10^{-6}}{2\pi x 250 x 500} \simeq 300\ \Omega$$

This means that more than 60% of the signal current at the resonant frequency is by-passed by the parallel capacitance C_0. In the present case, this capacitance was found to be frequency dependent and according to preliminary measurements on small strip elements, it varied from approximately 160 pF to 290 pF for frequencies between 2.1 MHz to 1.74 MHz, in a nonlinear fashion.

If C_o is absent and the source impedance is low, then the bandwidth of the ultrasonic pulse is solely determined by the appropriate component values of the LCR' branch. The effect of C_o may be thought of as reducing the electrical bandwidth when the source impedance is considerable and consequently the bandwith of the ultrasonic pulse in the way of forming a low pass RC network. To illustrate this, if C_o is assumed to be a fixed value at about 250 pF, and if the terminal impedance of the driving source is, say, 500 ohm, then the cutoff frequency of an equivalent RC network would be

$$f = \frac{10^{12}}{2\pi x 250 x 500} \simeq 1.2 \text{ MHz}$$

At this value of the source impedance, the static capacitance C_o clearly influences the bandwidth of the ultrasonic pulse emitted. If the source impedance is now reduced to about 75 ohm say, the cutoff frequency of the equivalent RC network is pushed up to about 8 MHz. Hence there is little or no influence of C_o on the bandwidth of the ultrasonic pulse.

Analytically, it can be shown that the mechanical loading on the transducer reduces the mechanical Q factor Q_m while raising the electrical Q factor. The bandwith of the ultrasonic pulse emitted depends on the combined effect of the mechanical and electrical Q factors of the circuit. The electrical Q factor Q_e of the circuit in this case where the transducer is damped by an external resistance with reference to Fig. 7.10 may be written as :

$$Q_e = \frac{Q}{1 + Q/2\pi f C R_{DAMP}} \quad . \quad . \quad . \quad . \qquad (7.12)$$

where Q is the electrical Q factor of the circuit without an external damping resistor. Hence according to equation 7.12, Q_e could be adjusted to match Q_m to optimize the bandwidth performance of the transducer. However, this does not necessarily optimize the sensitivity as any lowering of R_{damp} would invariably mean loss of sensitivity

due to the signal being developed across it as in Fig.7.10. Therefore a compromise has to be found to avoid having to demand higher gain from the amplifiers and unwanted escalation of power dissipation.

An alternative approach often used to nullify the effect of static capacitance C_0 is to use an inductor to resonate with C_0 at or near the centre frequency of the transducer thereby allowing the full signal current to be transfered to R' and hence maximizing the efficiency of the transducer at that particular frequency. However, one cannot expect better bandwidth performance compared to the approach described above which totally eliminates the influence of C_0 by way of deliberate mismatch and increase of electrical bandwidth provided by the low source resistance. Also, tuning a multichannel receiver probe with inductors possibly of different values is very difficult, considering the dimensions and space available in the construction of arrays. Therefore this method is not considered as appropriate here.

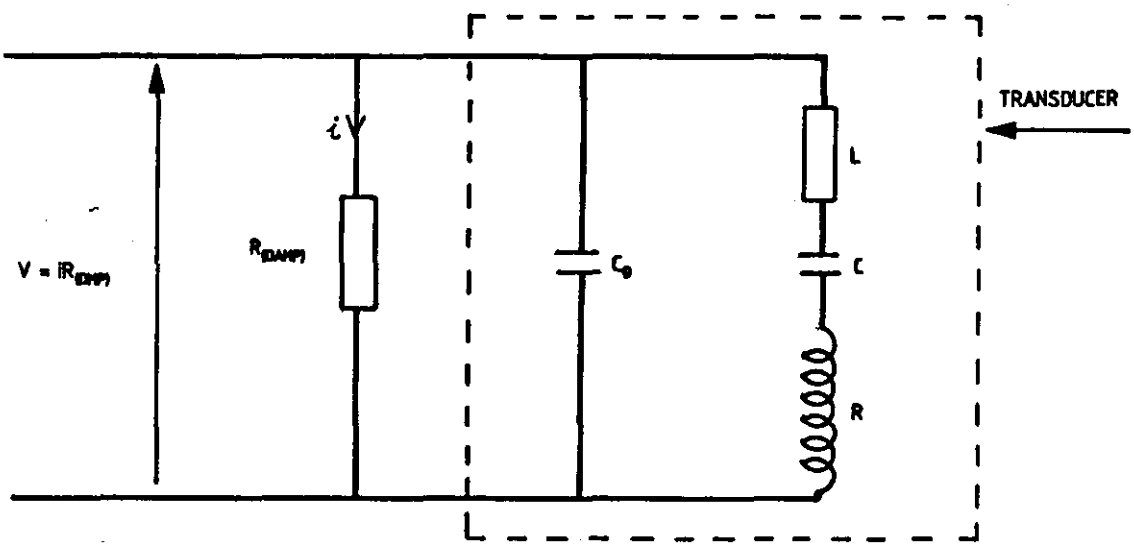

FIG. 7.10. USING EXTERNAL ELECTRICAL DAMPING

So far considerations have been primarily made for the transducers in the transmission mode. The same principles are valid in the case of receiving transducers as far as the bandwidth and efficiency are concerned, and the network topology can be altered accordingly with a voltage source in series with the LCR' branch as shown in Fig. 7.11(a) and (b).

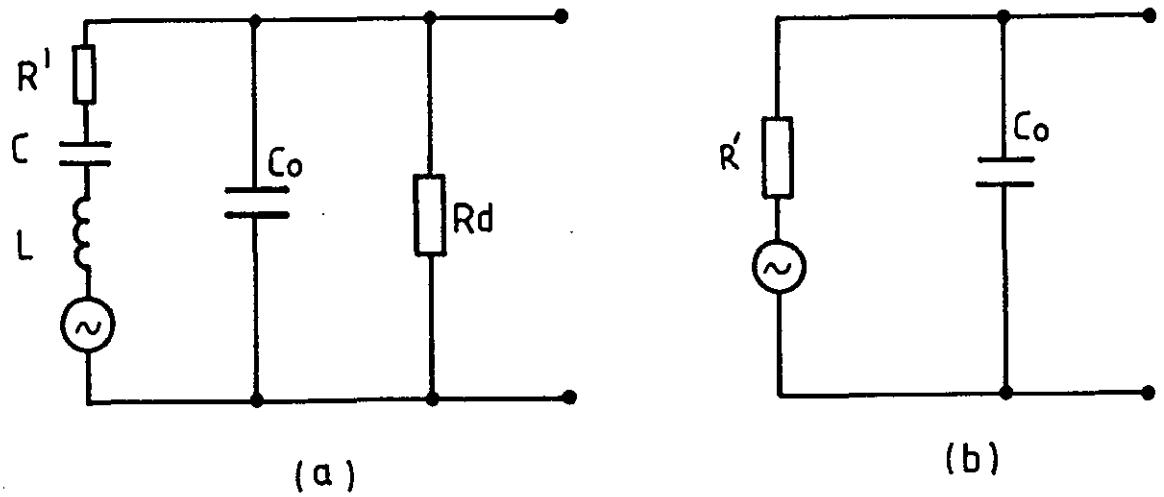

FIG.7.11 AN EQUIVALANT CIRCUIT REPRESENTATION OF THE TRANSDUCER IN THE RECEIVING MODE

Although the above approach will be useful as a guidance for initial experimentation, the above circuit models cannot be conveniently used to derive sufficient quantitative information with regard to the design of the transducers. More appropriate modelling has to be therefore considered at a later stage.

7.8 NOISE CONSIDERATIONS

Noise is one of the major concerns in most signal processing systems especially if signal to noise ratios are low. In some ultrasonic instrumentation systems, acoustically generated electrical noise[21] may also be present in addition to the electronic noise of the processing equipment. Acoustic noise will be present when there is random time varying acoustical interactions within the medium, e.g. in underwater acoustics or if testing some machineries or plants which are in operation, in which case, care has to be taken to avoid the possibility of correlated noise degrading the system performance.

However, in the present case, there is no acoustic noise involved as the echo signals are time invarient. Also the electrical noise of the

amplifiers will not significantly influence the image quality as the signal to noise ratios observed for the desired echoes are high and also because of the signal coherence and noise incoherence in the image field.

However, in this respect, if much weaker targets are to be imaged, it is far better to increase the insonifying energy as far as possible to maintain an acceptable S/N ratio than increasing the gain of the amplifiers excessively.

7.9 CHOICE OF THE CLASS OF AMPLIFIERS AND A CONCEPT FOR THE DEVELOPMENT OF A NEW CATEGORY OF AMPLIFIERS - (G* AMPLIFIERS)

Although there are several classes of amplifiers[28,29] the requirement of a wide bandwidth accompanied by low distortion naturally leads to the choice of class A amplifiers for the present work. However, the main problem with class A is its very low efficiency leading to high power consumption and cost, particularly when low output impedances and large voltage swings are required as in the present work.

In a class A amplifier, the maximum AC output power obtainable for sinusoidal signal amplification would be

$$P = 0.707\ V_Q \times 0.707\ I_Q$$

$$= 0.5\ V_Q I_Q$$

where V_Q and I_Q are the supply voltage and the quiescent collector current, respectively.

Since the DC input power is equal to $V_c \times I_Q$, the maximum efficiency for sinusoidal amplification would be

$$\eta_{max} = \frac{0.5 V_Q I_Q}{2 V_Q I_Q} = \frac{P_{out}}{P_{in}} = 0.25 \text{ or } 25\%$$

The total power consumption remains constant irrespective of whether

signals are presented to the amplifiers or not. Since the maximum object distance required in the present case is 25 cm, the maximum period t_{max} during which the amplifiers actually receive signals will be

$$t_{max} = 500/6 = 83\ \mu s$$

If the repetition rate is 100 Hz say, and assuming that the amplifiers deliver maximum signal output during the above period, then the average power delivered in one repetition cycle with reference to Fig. 7.12 would be $0.25 \times V_c \quad I_Q \times 83 / 10{,}000$.

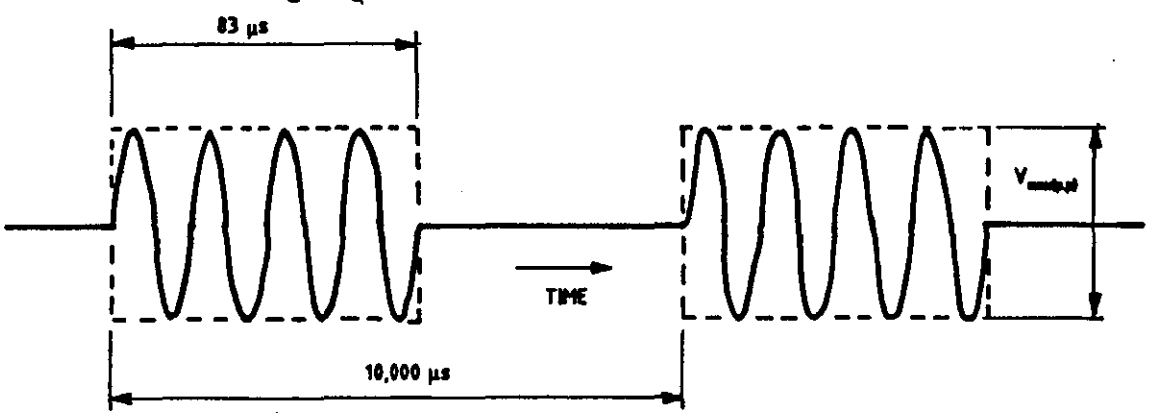

FIG. 7. 12. ASSESSMENT OF POWER CONVERSION EFFICIENCY OF CLASS A AMPLIFIERS IN THE PRESENT APPLICATION. (rep. rate = 100 Hz)

Since the total power consumption remains the same at $V_c \times I_Q$, the maximum efficiency would be

$$\eta = \frac{0.25 \times 83 \times 100}{10{,}000}$$

$$= 0.2\ \%$$

The actual efficency in practice would be even less as the echoes do not continuously occupy the whole 83 μs period, nor will mean full amplitude output signal swings all the time as can be seen from a typical A-scan display. Hence the whole power consumed is practically dissipated as heat within the amplifiers all the time causing even more complications of heat extraction and size, due to the large number of amplifiers involved. Therefore this form of amplification is

extremely inefficient, cost ineffective and cumbersome, although the ideal characteristics of class A in the present application cannot be overlooked.

7.9.1 A novel concept for signal amplification.

An ideal approach to preserve the characteristics of class A while solving the problem of low efficiency and high power consumption in the present and similar applications is now discussed. Supposing if a class A amplifier could be designed with additional circuits to enable it to switch on and off with sufficient speed to establish its quiescent conditions just before the insonifying pulse and switched off just after the 83 μs period with a low settling time, then the average power consumed over one cycle of the repetition frequency would be

$$P = V_C \times I_Q \times (83/10{,}000)$$

Hence the efficiency $$\eta = \frac{0.25 \times V_C \times I_Q \times 83 \times 10{,}000 \times 100}{10{,}000 \times V_C \times I_Q \times 83}$$

$$= 25\%$$

This means that if a fast switching scheme is provided to operate the amplifiers in synchronism with the pulse repetition frequency as described above, the efficiency of the amplifier can be theoretically restored to its original value. In the frequency domain the above act is equivalent to introducing an additional frequency spectrum of the rectangular aperture function, which is a sinc spectrum occupying a bandwidth of $\simeq 1 / 83 \times 10^{-6} \simeq 12$ kHz sampled by a comb sample function with spacing equal to $1 / 10{,}000 \times 10^{-6} = 100$ Hz. Clearly at these values there is no interference with the output signals transmitted except the possiblity of the high frequency switching on and off transients faintly breaking through to the image field, marking the beginning and the end of the ultrasonic field. This is only an advantage.

Apart from the improvement of efficiency, what would be even more

important is the saving of average power consumption which reduces a great deal of complications including heat dissipation problems, cost and size of the required power supply and the amplifiers. This is made clear by comparing the power consumption of the two cases.

For class A, the power consumed is $P_1 = V_C \times I_Q$

For the new amplifiers, the average power consumed is

$$P_2 = V_C \times I_Q \times t/T$$

$$\therefore \quad P_2/P_1 = \frac{V_C \times I_Q \times t}{V_C \times I_Q \times T}$$

$$P_2/P_1 = t \times F \quad . \quad . \quad . \quad . \quad . \qquad (7.13)$$

where F is the repetition frequency.

If F is 100 Hz say, then $P_2/P_1 = 83 \times 10^{-6} \times 100 \times 100$

$$= 0.83\%$$

i.e. the total average power consumption is less than 1 % of the ordinary class A amplifiers at the above duty cycle. In a multi stage system as in the present case, this saving of power dissipation leads to a great deal of design flexibility of individual stages as the peak voltage swings may now be increased to match the original power dissipation levels thus tremendously increasing the much required effective dynamic range of the system.

The same approach can be taken for the design of the power amplifier required for insonifying the test object. The only major difference here is that the required power levels are considerably higher than the individual channel power amplifiers. In this case only one unit is required. The emphasis therefore would not be mainly on the saving of power, but rather on achieving the maximum voltage swing capabilities within the permissible power dissipation levels of the active devices

involved. This is based on the fact that the maximum current and voltage capabilities of active devices are hardly achieved in practice due to the power dissipation limits. Therefore if this approach is taken, the size and the cost of the unit could also be made much lower compared to an ordinary wideband power amplifier due to the possibility of optimization.

7.9.1.1 An ideal timing scheme

Fig. 7.13 shows an ideal general timing scheme to optimise the duty cycle operation for the present type of application.

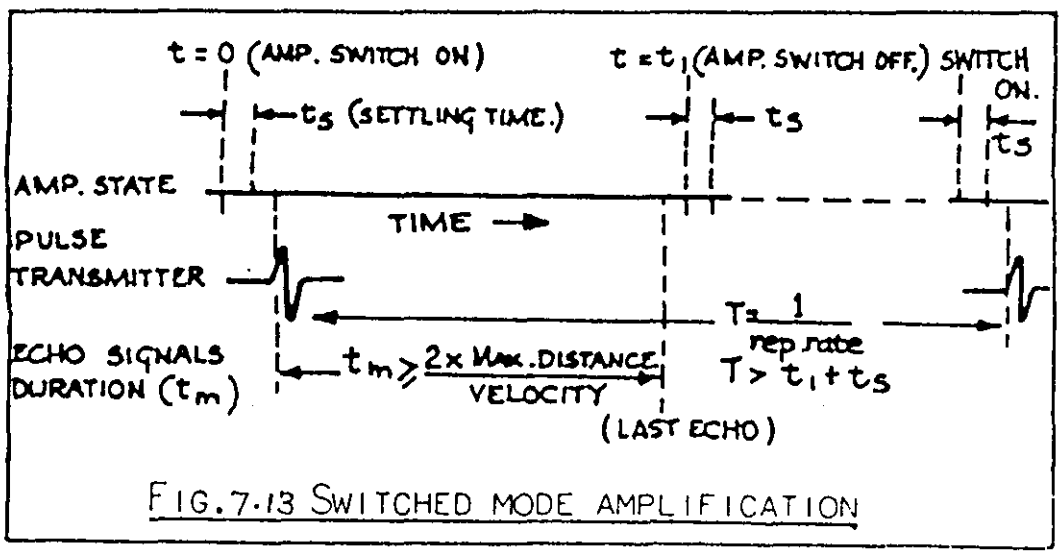

FIG. 7.13 SWITCHED MODE AMPLIFICATION

The amplifiers are switched on in parallel and allowed to settle just before the start of the ultrasonic pulse transmitter and switched off just after the arrival of the farthest echo after a time t_{max} determined by the maximum object distance in the test object medium and the process is repeated after a time T, which is the period of the repetition frequency, such that

$$t_{max} > \frac{2 \times \text{max. object distance}}{\text{velocity of sound}} \quad \cdots \quad (7.14)$$

and $T = 1 / \text{repetition rate}$, and $T > t_1 + t_s$

where t_s is the settling time and t_1 is as marked on Fig. 7.13.

Although such a scheme is conceptually simple, achieving the prescribed end result is extremely difficult. The key to success depends on how closely the switching, settling and switching off times could be approached to the ideal case and also on the suppression of strong and unwanted transients. This could probably be the reason why such amplifiers have not evolved so far for general use. Consequently a great deal of work has been done in realizing this concept and this has lead to very good results. After many trials, an amplifier stage satisfactorily operating according to the above scheme was designed, built and tested for this particular purpose and the details will be presented in chapter 11.

It should be mentioned here that the present scheme is fundamentally different from the concept of gated amplification where there is no question of establishing quiescent conditions, or to the switched amplifiers such as class D, which are only dealing with binary pulses. To the author's knowledge, there is no such amplifier developed so far which combines the properties of a particular class of amplifiers with a power gating facility , to be used in applications involving non-continuous repeated signal amplification. These amplifiers are here named as G^* (G star) amplifiers.

7.10 Considerations of size, cost etc.

It was found after a survey, that the cost of the system would be unacceptable if the amplifiers for the present application were to be bought. For example the cost of a power amplifier as the one used for insonifying the test object is in the range of £3000/=. Although lower power levels are acceptable for the channel power amplifiers, the price to be paid would still be several hundreds of pounds per amplifier and is not acceptable considering the limited resources available for the whole project. Apart from this the size would be also large as one cannot expect to find amplifiers 'tailor-made' for a particular purpose.

Hence it was neccessary to design and build a set of 30 wideband power amplifiers for the present purpose. After many attempts, a set of amplifiers operating in class A as described in chapter 11 was designed for the feasibility study. This elaborate design efforts finally made it possible to reduce the cost of the amplifiers down to about £20/= per channel. In fact the development of G* amplifiers was followed after this work as an attempt to overcome the limitations of class A as described above. Unfortunately after establishing the applicability of G*, , there were no funds or time available to complete a set of such amplifiers to replace the original ones and to adopt the new operational scheme.

7.11 CONCLUSIONS

For the purpose of feasibility study, the following parameters concerning signal amplification have been so far derived.

1. *Numerical gain* = *200*
2. *Bandwidth* = *15 MHz*
3. *Input impedance* ~ *75 ohm*
4. *Output impedance* ~ *75 ohm*
5. *Output signal swing* = *30 V p.p.*
6. *Insonifying pulse amplitude*
    1. *Transceiver mode* — *10 to 100 V p.p. (adjustable)*
    2. *Separate transducer of similar dimensions* — *50 to 200 V p.p. (adjustable)*

The following recommendations are also made for the design of a final system.

1. *Incorporation of variable gain control*
   Numerical gain setting range ~ *10 to 2000*

2. *Incorporation of Time Varying Gain,*
   TVG function synthesized as in Fig. 7.7
   Gain compensation range = *16 : 1*

3. *Higher output voltage swing* ~ *100 V p.p. and up*

4. *Incorporation of* G^* *(G star) amplifiers*

The following points are also highly emphasized.

1. *The need of wide bandwidth of array elements to minimize phase distortion as much as possible.*

2. *Good identical behaviour of the transducer array elements to avoid amplitude and differential phase distortion problems.*

3. *Use of insonifying energy control rather than gain control where ever applicable in examining very weak targets.*

--- // ---

- CHAPTER 8 -

RE-TRANSMISSION AND VISUALIZATION

Amplified echo signals are to be transmitted via an acoustic focusing system into a transparent medium where the acoustic images are made visible by an appropriate optical technique, using strokoscopic illumination. This chapter mainly examines the theoretical aspects of visualization and methods of optimizing performance followed by the derivation of parameters concerning the sonoptical geometry of the proposed new system.

8.1 INTRODUCTION

The original DUVD concept has been demonstrated by Hanstead using two distinctly different visualization techniques namely

1. Photoelastic technique
2. Schlieren technique

The first method relies upon the well known optical phenomenon in which the plane of polarization of plane polarized light is rotated when passing through a solid transparent medium containing regions of mechanical stress,[14] caused by travelling acoustic waves. The latter relies upon the refractive index changes, again caused by mechanical stress and related density change associated with the acoustic waves, in transparent media, usually a liquid.[16,17] In either case, properly synchronized stroboscopic illumination with sufficiently short flash duration and adequate intensity is required to map the acoustic images at the instant of best focus.[10]

Although the use of a solid visualizing medium is an attractive proposition in the development of the instrument, there are two main

objections to the use of the photoelastic technique in the present application. Firstly, the sensitivity is low. According to initial measurements using a glass medium, the sensitivity of the photoelastic technique was estimated to be about 50 dB below that of the schlieren technique. Secondly, selection of a suitable visualizing medium is restricted to a few materials like glass or quartz, all of which have high sound velocities leading to a geometrical design of unacceptable dimensions. This latter restriction arises from the fact that sufficient stress levels cannot be created by displacement-limited acoustic waves in other commonly used photoelastic media due to their low Young's moduli. For these reasons the photoelastic technique of visualization was abandoned.

The main problem with the schlieren technique is the need of high precision optical construction and alignments which makes it unattractive on the shop floor. Consequently, a great deal of work has been done in successfully developing a suitable schlieren visualization system as part of an integral sonoptical assembly.

At a very early stage of the feasibility study the need of a good stroboscope was strongly felt in order to prevent loss of image quality as a result of using commercial stroboscopes available at the time. Also they are so bulky that the design of a compact system seemed impossible. Hence a great deal of work has been done to overcome the above difficulties which lead to the design of a high performance, subminiature stroboscope using a super bright light emitting diode.[30] It highly improved the performance and the compactness of the whole system and the details will be presented in chapter 9. To the author's knowledge, there were no such stroboscopes available at the time.

8.2 PRINCIPLE OF SCHLIEREN VISUALIZATION

In order to identify the methods of optimizing the performance, the schlieren technique is examined here. Previous assessment of sensitivity and the effective dynamic range of the proposed system showed that the basic limitation is presented by the high threshold voltage, (V_{th}),

required. The high threshold requirement is mainly attributed to:

1. The threshold sensitivity of the medium
2. Transmission efficiency of the sonoptics

Fig. 8.1 shows a schematic diagram of a schlieren visualization system.

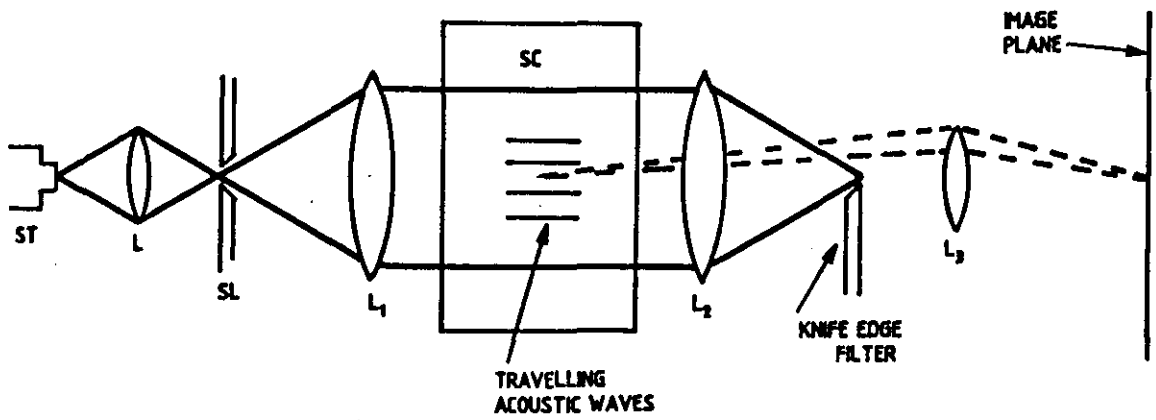

FIG. 8. 1. SCHEMATIC DIAGRAM OF A SCHLIEREN VISUALIZATION SYSTEM.

The principle of the schlieren technique may be explained in two ways. The first approach is by using geometrical optics, and secondly and more appropriately, by physical optics using light diffraction phenomena.[12,16]

In Fig. 8.1, ST is a stroboscopic source of light, L is a condenser lens which focuses as much light as possible on to a narrow rectangular slit SL, which is placed at the focus of a collimating lens L_1. The parallel beam of light is allowed to pass through a schlieren cell SC, where the acoustic images are formed, in this case by re-transmitted echo signals through the acoustic focusing system.

In the absence of any optical disturbance in the schlieren cell, the parallel beam is focused on to a knife edge in the position just to cut off the resultant image of the slit source. When the acoustic image is

formed in the schlieren medium, it modulates the refractive index of the medium accordingly which results in a certain proportion of light being deflected past the knife edge stop. The angle of deviation and hence the amount of light passed is proportional to the refractive index gradient in a direction perpendicular to the optical axis and the axis of the knife edge, effectively mapping the acoustic image. The deflected light is captured by lens L_3 to form an optical image of the disturbance in the image plane which can be a screen or a video camera tube face. The images may also be viewed directly with the naked eye in which case lens L_3 is not needed.

According to the above geometrical optics description, if the image of the slit is just obstructed by the stop then the smallest deflection should be visible, and by reducing the width of the slit, infinite sensitivity against a dark background should be achieved. However, this does not happen in practice as the sensitivity is limited by diffraction. This is evident from the presence of luminous borders on the circumference of the schlieren lens and opaque objects. Therefore under conditions of high sensitivity, as required in the present application, the geometrical optics description is no longer valid and a better understanding may be gained with a physical optics approach considering the wave nature of light. Here, the refractive index changes are considered to have caused phase retardations of the wavefront in the region of non-homogeneity rather than assuming angular deflection of rays as in the geometrical optics description.

The disturbed wavefront can be regarded as a phase object with transmittance $f(\eta)$, such that[31]

$$f(\eta) = \exp^{j\phi(\eta)} \quad . \quad . \quad . \quad . \qquad (8.1)$$

The phase retardation $\phi(\eta)$ along the direction of the optical axis would be

$$\phi(\eta) = k.\Delta n.L \quad . \quad . \quad . \quad . \qquad (8.2)$$

where Δn = refractive index modulation

L = interaction path length

k = wave number

Such a phase object is not visible to the human eye because the eye or any other sensor responds only to the intensity $|f(\eta)|^2$ which in this case is unity. The second schlieren lens L_2 has the Fourier transform property (FTP) which transforms the phase object $f(\eta)$ at the focal plane giving a corresponding pattern function $F(U)$ such that

$$F(U) = \text{Const.} \int_{-A}^{A} f(\eta) \exp^{jk\eta U/f} \, d\eta \quad . \quad . \quad . \qquad (8.3)$$

where f is the focal length of the schlieren lens.

Now some form of spatial filtering is required to remove the free field diffraction components of the phase object which in this case is provided by the knife edge, whose transmittance $H(U)$, can be written as

$$H(U) = \frac{1}{2}\left[1 + \text{sgn}(U)\right] \quad . \quad . \quad . \quad . \qquad (8.4)$$

The pattern function just behind the filter is the product $F(U) \times H(U)$ and by taking the inverse Fourier transform, which in this case is performed by the lens L_3 gives the corresponding image $G(V)$ in the image plane which is the optical conjugate of the phase object, such that[12]

$$G(V) = \text{Const.} \int_{\text{Aperture}} F(U) \exp^{jkUV/f} \, dU \quad . \quad . \quad . \qquad (8.5)$$

This process of image formation is schematically shown in Fig. 8.3 and 8.4.

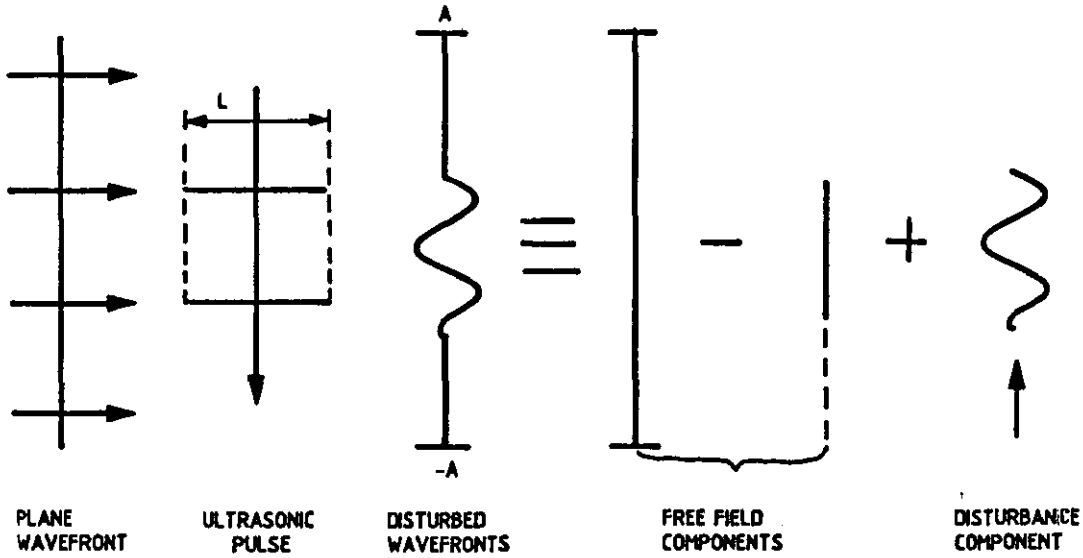

FIG. 8. 2. WAVEFRONT DISTURBANCE BY ULTRASONIC WAVE INTERACTION AND THE OPTICAL COMPONENTS OF THE DISTURBED FIELD

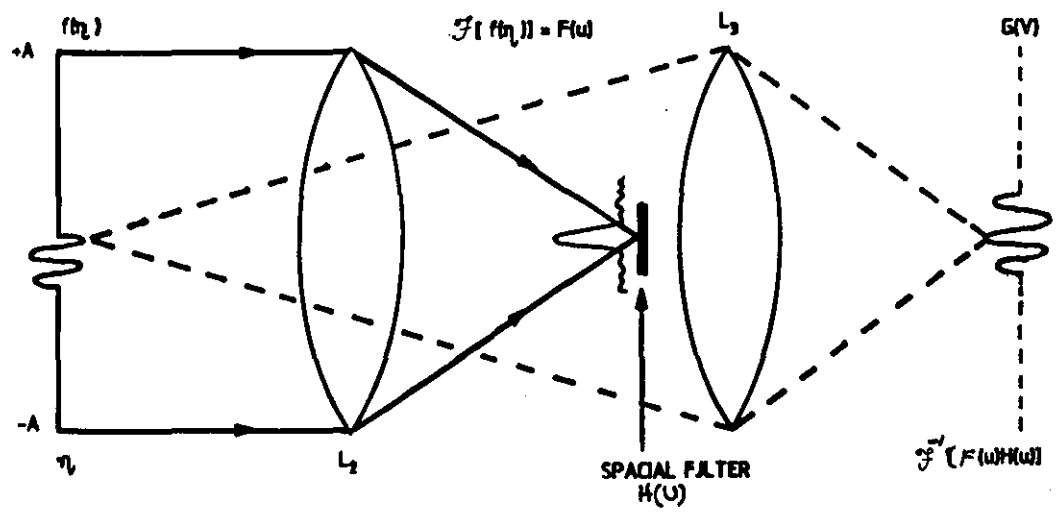

FIG. 8. 3. SCHLIEREN IMAGE FORMATION.

The relationship between image intensity distribution with the phase retardation may be understood more readily with a graphical vector representation than by an analytical approach[16], as shown in Fig. 8.4.

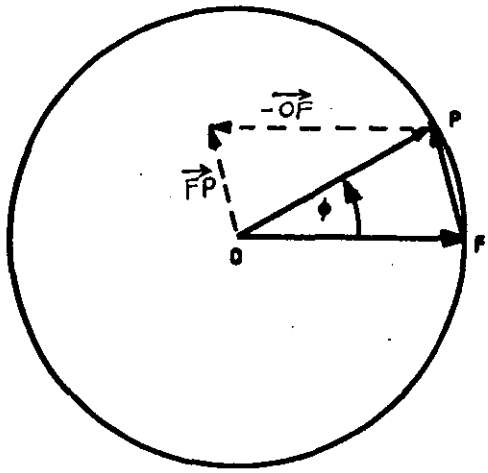

FIG. 8. 4. VECTORAL REPRESENTATION OF A PHASE OBJECT AND ITS DARK FIELD IMAGES.

If $\overrightarrow{OP}$ represents a point on the phase object and ϕ is the phase angle with respect to the free field vector $\overrightarrow{OF}$, then the image is identical to the object in the absence of a stop. Assuming the free field component is now removed by the stop, the resultant image will be the vector $\overrightarrow{FP}$. Hence it follows that for different phase retardations ϕ, not only the phase of the image varies but also its amplitude and therefore the brightness. The amplitude first increases with ϕ and reaches a maximum of twice the free field when $\phi = \pi$ and falls to zero when $\phi = 2\pi$. It is also seen that the image brightness depends only on the degree of phase retardation as given by equation 8.2 for a given free field brightness.

8.2.1 Effect of knife edge filter position

The free field diffraction pattern at the plane of the stop is the Fourier transform of the slit source. If the width of the slit is 2A and f is the focal length of the schlieren lens, then

$$F(U) = \frac{A \sin(kAU/f)}{(kAU/f)} \quad . \quad . \quad . \quad . \qquad (8.6)$$

The width of the central band in which about 90% of the light energy is concentrated is therefore $f\lambda / A$, where λ is the wavelength of the

light used. When the optical wave front is disturbed by an ultrasonic wave whose wave length is Λ , it can be considered as occupying only a very small spatial width compared to the aperture and hence its Fourier transform produces a spread out diffraction pattern function at the plane of the stop. Consequently the width of the stop required to filter the free field component does not significantly reduce the brightness of the image, even if the stop is adjusted to filter the central and the first few lateral maxima (about 3) as would be required to produce a satisfactory dark background.

However, in practice there is another important implication with regard to positioning the knife edge. This arises from the fact that the schlieren field does not uniformly darken as the cut-off is gradually increased and much of the diffracted light goes towards the edges of the field. This means that the threshold sensitivity of the schlieren is not uniform over the entire field, which is undesirable in the present application, and therefore a satisfactory solution has to be found.

The free field brightness of the image field when the knife edge stop covers all the light between $-\infty$ and the first diffraction minimum with reference to equation 8.7 can be written as[12]

$$[G(V)]^2 = \left[\text{Const.} \int_{-\infty}^{\infty} \left(\frac{\sin\alpha}{\alpha}\right) \exp j k\alpha V/f \, d\alpha \right]^2 \quad . \quad . \quad (8.7)$$

$$\alpha = k a \, U/f$$

This expression has been plotted by Speak and Walters[32] as shown in Fig. 8.6 for different positions of the knife edge with respect to the free field diffraction pattern as shown in Fig. 8.5, below.[12]

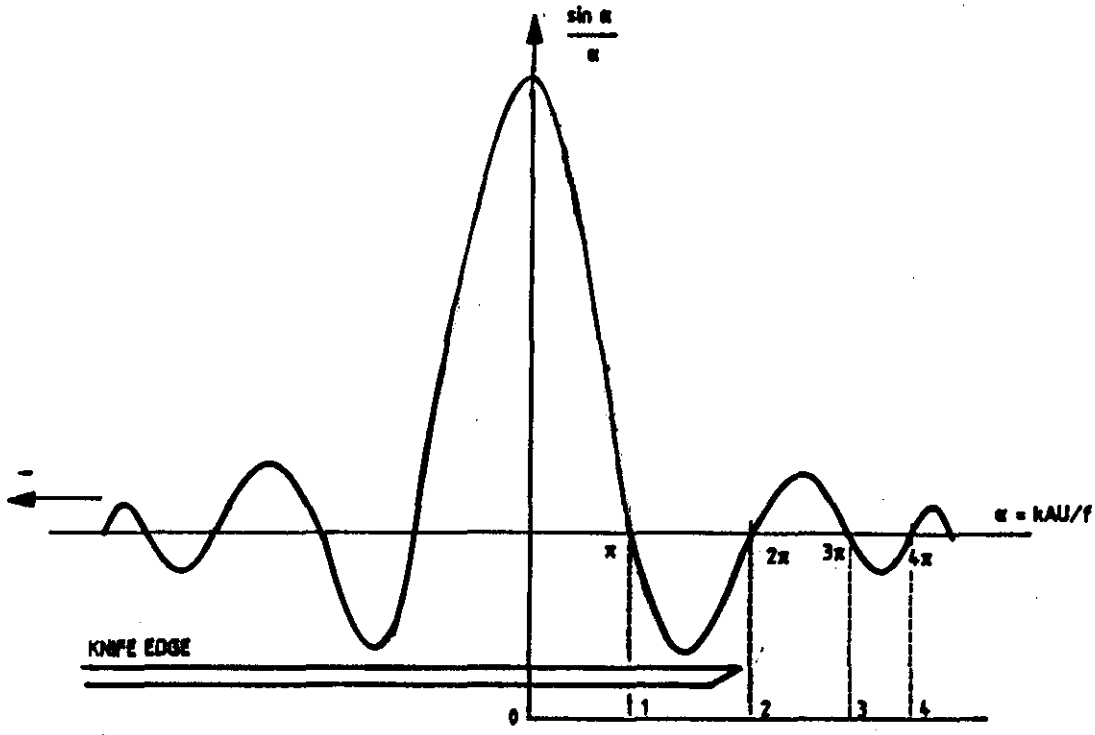

FIG. 8. 5. POSITIONING THE KNIFE EDGE IN THE FREE FIELD.

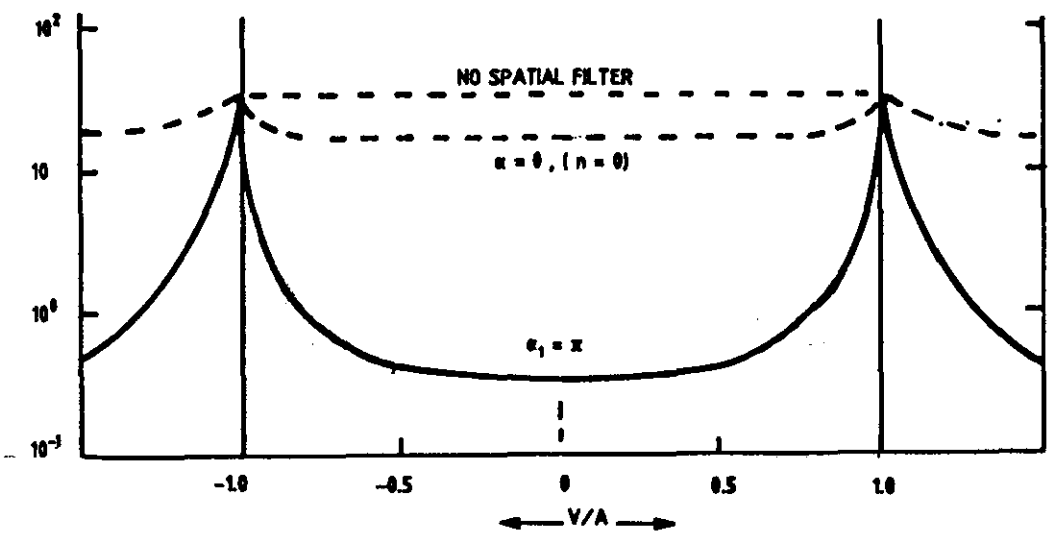

FIG. 8. 6. VARIATION OF THE BACKGROUND ILLUMINATION OF THE IMAGE FIELD (after Speak and Walters).

Hayman calculated the position of the knife edge required to achieve a background brightness of the order of 10^{-3} times that of the free field. The requirement was to place the knife edge up to about 4 diffraction minima. However, his calculations were based on the central

field illumination only, which is not adequate in the present application requiring a large field of view. As can be seen from the above plots that adjusting the knife edge to cut off more diffraction orders to achieve a lower background brightness results in an increasingly non-uniform field. As such, the threshold sensitivity will also vary accordingly. Therefore one solution to this problem is to illuminate a larger schlieren aperture than required but to use only the central region where the non-uniformity is not too great. Also a compromise between the desired level of background brightness and field uniformity with respect to the degree of cutoff would be needed.

An interesting indirect improvement was later made in the design of the optical assembly when using a video camera. In the present application the video camara is generally looking at a high contrast scene with a low average brightness. Consequently, the ALC (Automatic Luminence Control) circuits of the camera respond to the scene with the highest gain levels giving video picture noise and image blur. This situation was turned to the advantage by allowing some of the unwanted edge diffracted light to fall on to some areas of the camera tube which is well separated from the required image area of the tube face. This restored the average brightness of the scene to the required level by proper adjustment giving a very significant improvement in the TV image quality. Also the possibility exists to provide some degree of compensation by the design of a suitable ALC circuit responding preferentially to the background brightness, at least near the borders.

8.2.2 Schlieren aperture required

When one considers only the central region of a schlieren field, the aperture is not a limiting factor as far as the sensitivity is concerned as this is primarily limited by an irreducible amount of background brightness. In such cases a compact aperture schlieren system is as good as a larger one. However, according to the previous discussion, an aperture somewhat larger than required to accommodate the acoustic field would be necessary to overcome non-uniformity problems. There again a compromise has to be made between the aperture size and acceptable field

performance, as the larger the aperture, the greater the other complications such as illumination, aberations, size and cost etc. In the present application, the actual schlieren aperture required will be:

$$A = v_m \times t_{max} \quad . \quad . \quad . \quad . \quad . \quad (8.8)$$

where v_m is the velocity of sound in the schlieren medium, and t_{max} is the maximum pulse echo duration corresponding to the required object distance. Here t_{max} is equal to 83μs and the v_m of the medium selected was 0.59 mm/μs giving an aperture of about 4.9 cm. Hence if a preliminary estimation of about 0.75 for v/A according to Fig. 8.6 is used, the required aperture to give a reasonable central field uniformity would be 4.9 / 0.75 = 6.5 cm.

8.2.3 Slit width

From a theoretical point of view, slit width within reasonable limits is not expected to have a significant effect on the sensitivity of visualization apart from its use in setting a desired average brightness, most appropriate for the particular set of operating conditions. Slit widths in the range of approximately 0.1 mm to 0.5 mm was found to be satisfactory in the present case.

Attempts have been made to use a strip stop in the stop plane in place of the knife edge with the aim to utilize light energy from either side of the stop, but it did not give the desired end results. Instead, two separate, closely spaced images were formed, rather than a super-imposed single image, apparently degrading the hard earned image resolution. Close examination reveals that this is an effect of the finite slit width. The finite size of the slit causes the image diffraction patterns on either side passing a strip stop to be spatially separated and hence the images also. The implication is that, strip stops or graticule stops may not be very suitable in the case of forming high resolution schlieren images.

8.2.4 Optical aberration

Effect of chromatic aberration is often noticeable in schlieren systems using lenses and therefore the use of achromatic doublets are preferable. Also the diffracted free field light gives rise to bright coloured borders and some image blur may also be noticed. In such situations the sensitivity of the schlieren may have to be deliberately lowered and therefore the use of monochromatic stroboscopic illumination has to be considered. The problem is that such sources are not readily available. Concave mirrors may be used which eliminate chromatic aberration, but the need to have much larger focal lengths and dimensions of the optical assembly to control spherical aberration makes it unattractive in the present application. However, a suitable mirror schlieren system was also initially designed as presented in Appendix 1, but the development of the new LED stroboscope system in the mean time eliminated the problem of chromatic aberration altogether and promoted the use of a compact lens schlieren system.

8.2.5 Optical scatter

Hanstead and Hayman showed that one of the basic obstacles against achieving high sensitivity is the presence of an irreducible amount of background illumination, mainly caused by optical scatter. This was noticed in the present work also and the situation is even more aggravated when using it in an industrial environment due to additional scattering particles being deposited on the optical surfaces and also due to optical glare of the indoor lighting. Hence it was necessary to design a compact sealed schlieren system with external adjustment facilities and more details are presented in chapter 12.

8.2.6 Schlieren medium

A suitable schlieren medium was chosen by considering the following areas.

1. Sensitivity

2. Velocity of sound
3. Acoustic impedance
4. Attenuation
5. Dynamic range

The absolute sensitivity of a given medium is one of the prime considerations in the present application, but in practice a compromise has to be made between various other factors involved. For example, a high absolute sensitivity but low acoustic impedance may not give the expected improvement due to acoustic mismach losses. On the other hand higher acoustic impedance requires the product of sound velocity and the density to be high, but a high sound velocity will oppose a compact sonoptical design.

Hayman defined a theoretical visualization figure of merit, M , for a given liquid by the formula[*]

$$M = 4\,(\rho\,\partial n/\partial\rho)^2 / \rho c^3 \quad . \quad . \quad . \quad . \qquad (8.9)$$

where ρ = density of the medium
n = refractive index
c = velocity of sound

The term $(\rho\frac{\partial n}{\partial \rho})$ is also known as the elasto-optic coefficient. Based on experimental observations, Hayman derived an empirical formula for elasto-optic coefficient as

$$\rho\,(\frac{\partial n}{\partial \rho}) = 1.29\ n - 1.4 \quad . \quad . \quad . \quad . \qquad (8.10)$$

Using this relationship, he compared a large number of liquids for their theoretical figures of merit as given in table 8.1.

		Refractive index n	Density ρ $10^{3}\,kg.m^{-3}$	Sound velocity c $Km.s^{-1}$	Elasto-optic Coefficient $p\partial n/\partial p$	Figure-of-merit M $10^{-15}\,\frac{s^3}{Kg^{-1}}$	Acoustic Impedance $Z = \rho c$ $10^{6}\,Kg.m^{-2}.s^{-1}$	Attenuation coefficient $\alpha_s = \alpha/f^2$ $dB.m^{-1}\,MHz^{-2}$	Boiling point ^{o}C
1. Water	H_2O	1.33	1.00	1.48	0.322 (a	128	1.48	0.22	100
2. Carbon tetrachloride	CCl_4	1.46	1.59	0.94	0.511 (b	790	1.49	4.7	77
3. Bromoform	$CHBr_3$	1.60	2.90	0.92(b	0.655 (b	760	2.67	2.0	151
4. Chloroform	$CHCl_3$	1.45	1.50	0.99	0.470 (a	610	1.49	3.5	61
5. Di-iodomethane	CH_2I_2	1.74	3.33	0.96(b	0.863 (b	1010	3.20	2.2 (b	182
6. Iodomethane	CH_3I	1.53	2.28	0.84	0.57 (e	980	1.92	2.9	42
7. Methanol	CH_4O	1.33	0.79	1.12	0.329 (a	390	0.89	0.37	65
8. Carbon disulphide	CS_2	1.63	1.26	1.14(b	0.713 (a	1090	1.44	50.0 (b	47
9. Trichlorethene	C_2HCl_3	1.48	1.46	1.03(b	0.486 (b	590	1.50	1.7 (b	87
10. Iodo-ethane	C_2H_5I	1.51	1.94	0.88	0.55 (e	960	1.71	0.35	72
11. Ethanol	C_2H_6O	1.36	0.79	1.16	0.351 (b	400	0.92	0.45	78
12. 1,3-dibromopropane	$C_3H_6Br_2$	1.52	1.98	1.09(d	0.56 (e	490	2.16	0.70(d	167
13. Acetone	C_3H_6O	1.36	0.79	1.19	0.371 (b	410	0.94	0.47	56
14. 1-iodopropane	C_3H_7I	1.51	1.75	0.93(d	0.55 (e	860	1.63	0.47(d	102
15. 1-propanol	C_3H_8O	1.39	0.80	1.22	0.402 (c	440	0.98	0.55	97
16. Glycerol	$C_3H_8O_3$	1.47	1.26	1.86	0.50 (e	125	2.34		290
17. Ethyl acetate	$C_4H_8O_2$	1.37	0.93	1.17	0.361 (b	350	1.09	0.45	77
18. 1-iodo butane	C_4H_9I	1.50	1.62	0.97(d	0.54 (e	790	1.57	0.50(d	130
19. 1-butanol	$C_4H_{10}O$	1.40	0.81	1.26	0.419 (b	430	1.02	0.67	118
20. 2-butanol	$C_4H_{10}O$	1.40	0.81	1.19(b	0.385 (b	430	0.96	1.2 (b	100
21. Diethyl ether	$C_4H_{10}O$	1.35	0.71	0.96	0.349 (a	610	0.69	1.2	34
22. 1,2-dibromobenzene	C_6H_4Br	1.62	1.98	1.12(d	0.69 (e	680	2.22	1.3 (d	225
23. Bromobenzene	C_6H_5Br	1.56	1.50	1.15(b	0.598 (b	630	1.73	1.3 (b	156
24. Chlorobenzene	C_6H_5Cl	1.53	1.11	1.29	0.578 (b	560	1.43	1.1	132
25. Iodo-benzene	C_6H_5I	1.62	1.83	1.13(d	0.69 (e	720	2.07	1.6 (d	188
26. Nitrobenzene	$C_6H_5NO_2$	1.56	1.20	1.48	0.612 (b	380	1.78	0.69	211
27. Benzene	C_6H_6	1.50	0.88	1.32	0.522 (a	540	1.16	7.3	80
28. Anilene	C_6H_7N	1.59	1.02	1.66	0.654 (b	360	1.69	0.43(b	184
29. Phenyl hydrazine	$C_6H_8N_2$	1.60	1.10	1.74	0.682 (b	320	1.91	1.50(b	243
30. Paraldehyde	$C_6H_{12}O_3$	1.40	0.99	1.20(f	0.41 (e	390	1.19		128
31. Hexane	C_6H_{14}	1.37	0.66	1.09(b	0.416	810	0.72	0.52(b	69
32. Toluene	C_7H_8	1.50	0.87	1.32	0.54 (e	550	1.48	0.69	111
33. 2-amino toluene	C_7H_9N	1.57	1.00	1.60(b	0.625 (b	380	1.60	0.74	200
34. 1-iodo heptane	$C_7H_{15}I$	1.49	1.38	1.07(d	0.52 (e	640	1.48	0.70(d	204
35. O-xylene	C_8H_{10}	1.51	0.88	1.35	0.582 (c	620	1.17	0.45	144
36. Quinoline	C_9H_7N	1.63	1.10	1.58(b	0.698 (b	450	1.74	1.2 (b	238
37. Cinnamaldehyde	C_9H_8O	1.62	1.05	1.56(b	0.712 (b	510	1.64	6.0 (b	253
38. 1-bromonaphthalene	$C_{10}H_7Br$	1.66	1.48	1.36(b	0.730 (b	570	2.01	1.5 (b	281
39. 1-chloronaphthalene	$C_{10}H_7Cl$	1.63	1.19	1.46(b	0.703 (b	530	1.74	1.1 (b	258
40. Tricresyl phosphate	$C_{21}H_{21}PO_4$	1.56	1.20	1.50(b	0.596 (b	350	1.80	12.0 (b	410
41. Phosphorous tribromide	PBr_3	1.69	2.85	0.93(b	0.798 (b	1110	2.65	4.3 (b	173
42. Olive oil		1.46	0.91	1.44	0.48 (e	350		12.0	
43. Turpentine		1.47	0.87	1.24	0.50 (e	600	1.07		

Table 8.1 ACOUSTO-OPTICAL DATA FOR VARIOUS LIQUIDS - (After Hayman)

It can be seen that some of the liquids having the highest sensitivities presented in the above table are also toxic. Apart from this, since the use of a particular schlieren medium is very much dependent on the requirements as a whole, rather than the sensitivity alone, it was necessary to compare some of the usable media on an experimental basis. A considerable number of liquids from the above table as well as others were tested. From this excercise it was possible to choose a particular liquid by the brand name FC 75,[33] which gave a satisfactory compromise between the required properties, as given below.

Material	-	FC 75 (a fluorinated organic liquid. Non-toxic according to published data)
Refractive index		$\simeq$ 1.28 at 20 °C
Density		= 1.76 gm/ml at 20 °C
Sound velocity		= 0.59 mm/μs at 20 °C
Attenuation coeff. at 2 MHz.		=
Boiling point		= 102 °C

The elasto-acoustic coefficient and the theoretical figure of merit is calculated using equations 8.9 and 8.10 respectively, to give

$$\rho\left(\frac{\partial n}{\partial \rho}\right) = 1.29 \times 1.28 - 1.4 = 0.251$$

and $$M = 4\,(0.251)^2 / 1.76 \times (0.59) \times 10 = 697$$

Hence it can be seen from the above that FC 75 is not likely to be the most sensitive liquid compared to those presented in table 8.1, but it gives a combination of properties better suited for the present purpose, particularly with respect to its low sound velocity promoting the design of a compact schlieren system, yet with much higher sensitivity than water and less attenuation.

The other important consideration is the dynamic range of the medium used.[34] Fig. 8.7 shows some of the response curves plotted by Hayman[12] for some different liquids. These curves are used here for estimating the dynamic response only as the actual values are clearly subjective.

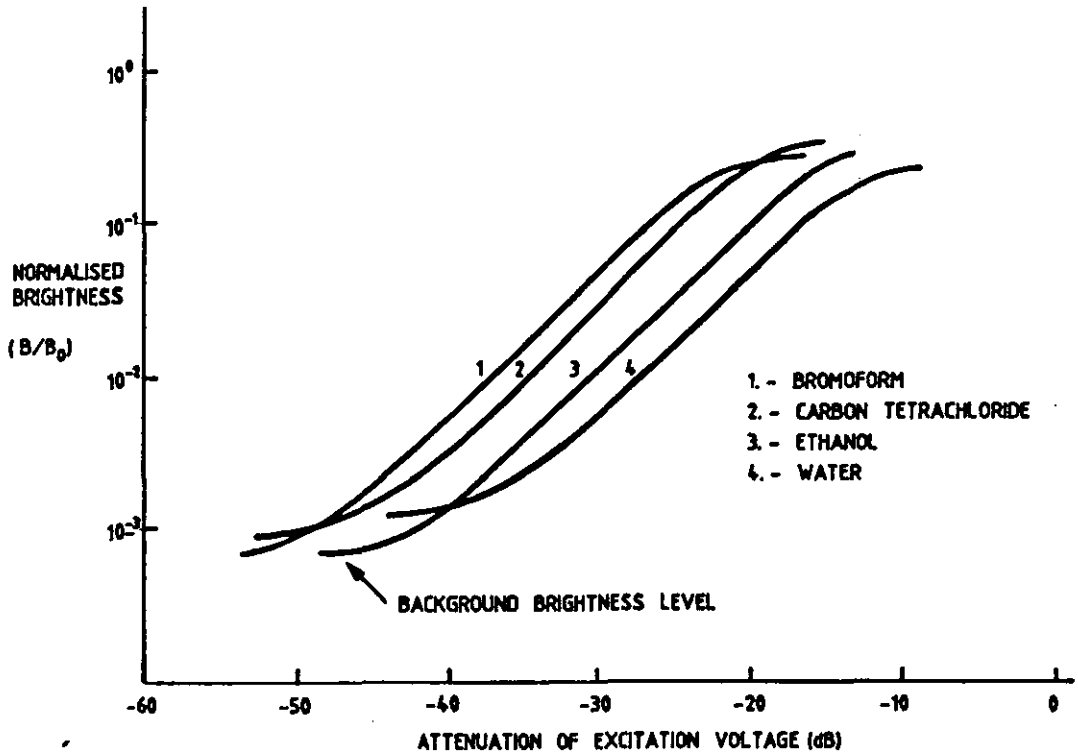

FIG. 8. 7. SCHLIEREN RESPONSE CURVES OBTAINED FOR VARIOUS LIQUIDS. (After Hayman, 1977)

These curves suggest that an overall dynamic range of about 28 dB can be expected irrespective of the medium used. Since this range is considerably larger than that of a conventional TV monitor system, the schlieren technique may be used advantageously as a useful alternative method of presenting echo data.

8.3 RE-TRANSMISSION

Having chosen an appropriate schlieren visualizing medium, it is now necessary to estimate the parameters of the sonoptics for re-transmission. The geometrical configuration chosen according to Chapter 4 consists of a curved array and cylindrical lens as shown in Fig. 8.8.

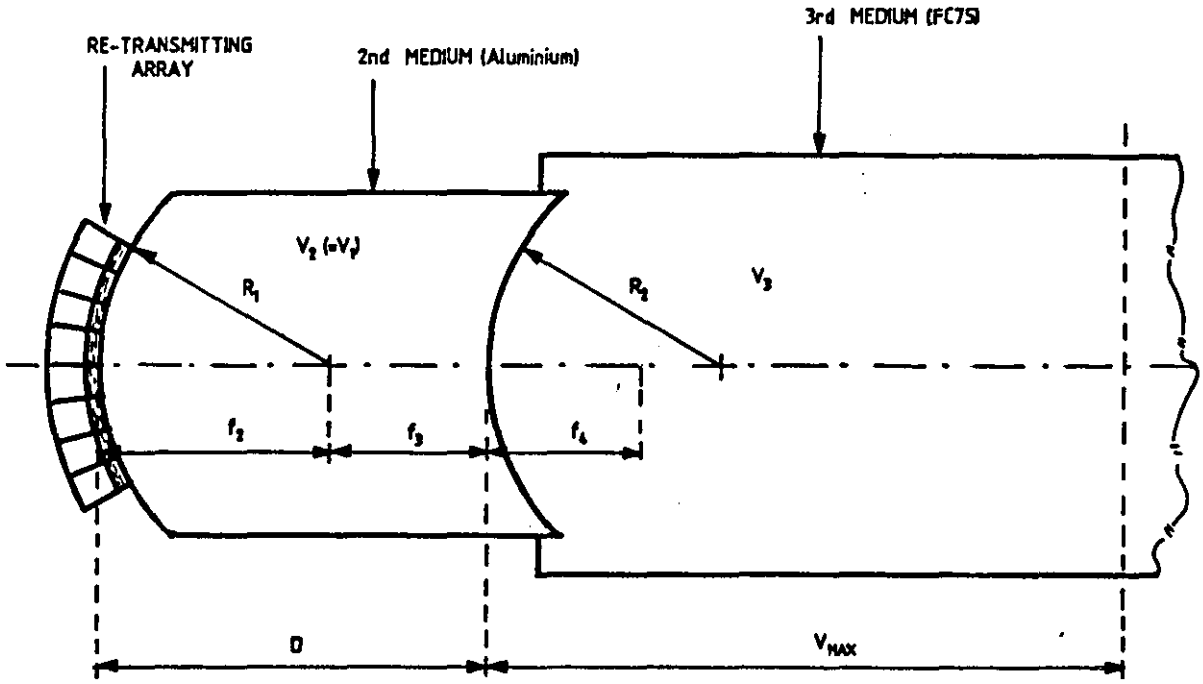

FIG. 8. 8. RE-TRANSMITTER SONOPTICS OF THE PROPOSED NEW SYSTEM.

The necessary lens calculations are basically carried out in the same way as for the DUVD with the appropriate modifications for the new geometry. With reference to design equations given in the table 4.1, the maximum object distance U_{max} is

$$U_{Max} = \left(1 + \frac{1}{\sqrt{2}} \frac{V_1}{V_3}\right) f_1$$

Here $V_1 = 6.3$ mm / μs

$V_3 = 0.59$ mm / μs

and U_{max} required = 250 mm

$$\therefore f_1 = \frac{250}{1 + \frac{1}{\sqrt{2}} \left(\frac{6.3}{0.59}\right)} \simeq 29 \text{ mm}$$

But in the present case $f_1 = f_2 = R_1 = 29$ mm, where R_1 is the radius of curvature of the curved array as well as that of the first cylindrical lens surface due to the new sonoptics. The first focal length of the second interface f_3 would be

$$f_3 = f_1 \sqrt{2} \; V_3 / V_2 \simeq 3.8 \text{ mm}$$

Similarly the second focal length of the second interface f_4 would be

$$f_4 = \sqrt{2}\, f_1 \simeq 41 \text{ mm}$$

and the radius of curvature of the second interface R_2 is

$$R_2 = 2\,(V_3/V_2 - 1)\, f_1 \simeq 37 \text{ mm}$$

The distance between the two lens interfaces D will be

$$D = f_2 + f_3 \simeq 33 \text{ mm}$$

The problem with the above set of values is that f_3 being only 3.8 mm is unacceptably small. Consequently, the aberrations will be high as the corresponding F number is very small. However, it is possible to increase the nominal value of U_{max} leading to a better set of specifications without sacrificing anything important. There is no need for a corresponding increase of the schlieren aperture at all as the required range of target information is the same, although the length of the medium will be extended by a couple of centimeters. This is not something significant with regard to the compactness.

After a number of iterative calculations a suitable value for U_{max} is chosen to be 430 mm. This resulted in the following set of specifications, calculated as before.

$f_1 = f_2 = R_1 \simeq 50$ mm , $f_3 \simeq 7$ mm , $f_4 \simeq 71$ mm

$R_2 \simeq 64$ mm , $D = 57$ mm , $V_{max} \simeq 8$ cm.

Since V_{max} is 8 cm, the length of the schlieren tank required may be chosen to be about 10 cm. The thickness of the lens is chosen as 40 mm, this being sufficient to avoid complications due to edge diffracted waves excessively reflected from the walls of the lens. The width of the lens is calculated to give a sufficient aperture to accommodate the 6 cm sector of the re-transmitting array with some allowance again to avoid edge diffracted waves causing reflection problems. An arc length of 8.5 cm was chosen giving a corresponding width of the lens to be

$$W = 2 \times 50 \sin (85 \times 85 / 2 \times 50) \simeq 75 \text{ mm}$$

This completes the basic specifications necessary for the construction of the cylindrical lens required and also the curvature of the re-transmitting array. The combination was experimentally tested with few other different designs and found to be quite satisfactory for the purpose.

8.4 CONCLUSIONS

The main conclusions of this chapter concerning the technique of visualization are the following :

1. *The photoelastic technique is not suitable for the present purpose*

2. *Nothing is lost in the way of sensitivity by designing a compact schlieren system. However, additional allowance for the schlieren aperture must be made to reduce field non-uniformity.*

3. *The possibility of achieving better stroboscopic illumination than that obtained with the conventional stroboscopes must be thoroughly investigated. Also the use of monochromatic illumination is much preferable.*

4. *Use of knife edge cut-off to be preferred over strip stops or graticule stops as these tend to form somewhat extended images noticeable in the case of high resolution schlieren images.*

5. *Although even ordinary lenses can produce schlieren images the use of high quality lenses must be considerd in the present design to achieve higher sensitivity by reducing aberrations and glare.*

6. *Optical scatter must be kept to a minimum by choosing high quality optical components, ensuring cleanliness of the schlieren tank and the medium and also providing adequate shield against dust and ambient light.*

The following sonoptical design specifications have been derived :

1. *The schlieren aperture required (medium being FC 75)* = *4.8 cm*

2. *The aperture of the lens to give an acceptable central field uniformity* = *6.5 cm*

3. *First radius of curvature of the aluminium lens (R_1)* = *50 mm*

4. *Second radius of curvature of the aluminium lens (R_2)* = *64 mm*

5. *Distance between the two surfaces (D)* = *57 mm*

6. *Width of the lens (W)* = *75 mm*

7. *Thickness of the lens (t)* = *40 mm*

8. *Length of the schlieren tank (l)* = *10 cm*

These dimensions are as marked in FIG. 8.9.

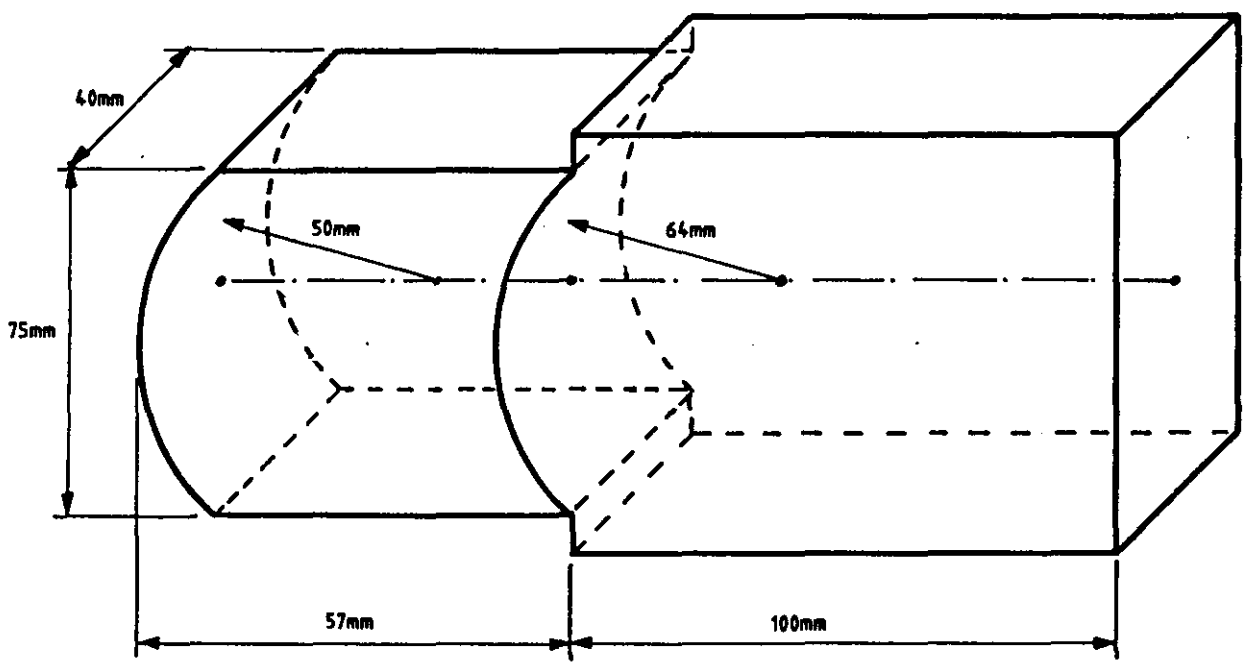

FIG. 8.9 APPROPRIATE DIMENSIONS OF THE SONOPTICAL GEOMETRY.

- CHAPTER 9 -

DEVELOPMENT OF A NEW STROBOSCOPE

It was emphasized in the previous chapter that good stroboscopic illumination was essential for the present application. This chapter deals with the requirements in quantitative terms and the situation with regard to the commercially available stroboscopes, finally leading to the development of a new, high performance, sub-miniature stroboscope based on a super bright Light Emitting Diode (L.E.D).

9.1 INTRODUCTION

An essential element for visualizing the path of ultrasound in a transparent medium by schlieren or photoelastic visualization techniques is a good quality stroboscope. The conventional stroboscope which relies on some form of a gas discharge to generate light pulses, suffers from a series of problems such as too long a flash duration, jitter, large size and crooked shape of the source resulting in non-uniform illumination, change of flash energy and duration with the repetition rate, inconsistency and ageing. Apart from these limitations, other drawbacks of commercial stroboscopes are bulkiness and high cost.

Providing an accurate time window of short enough duration is an important requirement to preserve the quality of the acoustic images formed. The extent to which the above drawbacks affect the images will now be examined. Particular reference will be made to the General Radio Strobotac stroboscope[35] which was available in the Department at the time. The price of this instrument was in the range of £1000/-.

9.1.1 Flash duration

Fig. 9.1 shows a typical plot of light intensity versus flash duration

for a conventional stroboscope such as the one mentioned above.[35]

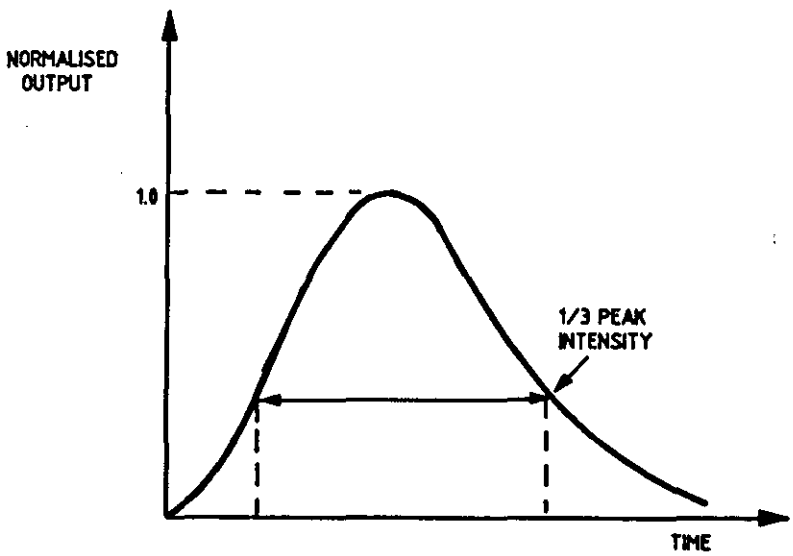

FIG. 9. 1. OUTPUT LIGHT INTENSITY vs. TIME (GR 1538 A handbook)

REPETITION FREQUENCY (Hz) (APPROX)	FLASH DURATION (MICROSECONDS)
2 - 12	3.0
11 - 70	1.2
67 - 417	0.8
400 - 2500	0.5

TABLE. 9. 1. FLASH DURATION FOR 1/3 PEAK INTENSITY.

It is clear from the above that the flash duration is far too long to be able to resolve one ultrasonic wavelength in the axial direction at 2 MHz in the schlieren field. If the size of the acoustic image I is one wavelength, then the size of the optical image I' would be

$$I' = v / f + v t \quad . \quad . \quad . \quad . \quad (9.1)$$

where v = velocity of sound,
f = frequency of ultrasound,
t = flash duration,

therefore the effect of the finite flash duration is to stretch the size of the image and hence decrease the resolution.

9.1.2 Jitter

Jitter can arise in the case of conventional stroboscopes from the time uncertainty of the random gas discharge process, which cannot be easily

controlled. The result is the spatial flicker leading to degradation of optical resolution and hence image quality. If ± J is the time jitter present and t is the flash duration, then the size of the optical image I'' as would be recorded on a photographic film over a considerable number of exposures will be

$$I'' = v / f + v t + 2 J v \quad . \quad . \quad (9.2)$$

The effect of jitter and flash duration are shown in Fig 9.2

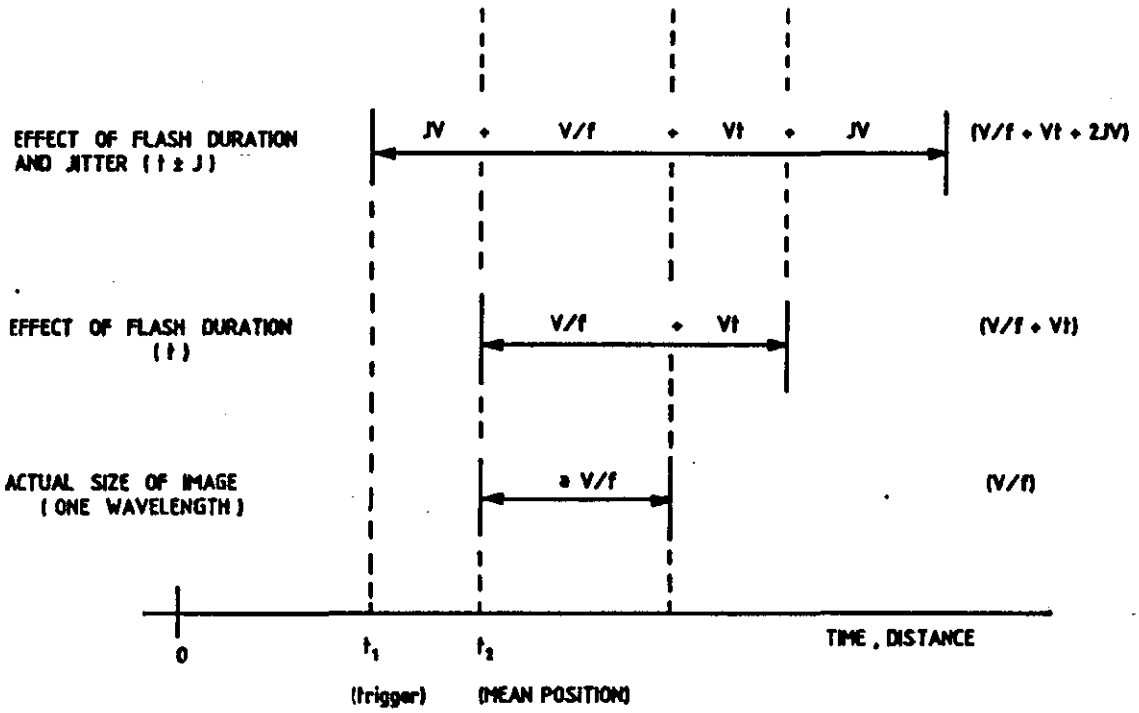

FIG. 9. 2. EFFECT OF FLASH DURATION AND JITTER ON THE IMAGE RESOLUTION.

The percentage change in image size would be $\left(\frac{I'' - I}{I} \right) \times 100$

$$\frac{I'' - I}{I} = f \times (t + 2J) \times 100 \quad . \quad . \quad . \quad (9.3)$$

Substituting typical values observed

$$\frac{I'' - I}{I} = 2 \times 10^{6} \times (0.8 + 2 \times 0.5) \times 10^{-6}$$

$$= \underline{360\ \%}$$

This is totally unacceptable as the acoustic image resolution is degraded by a factor of 3.6 or more. (It is useful to compare the schlieren image of a short acoustic pulse at 2 MHz obtained with such a stroboscope and that developed by the author Fig.9.7). The above percentage change is also directly dependent on the frequency.

9.1.3 Possible improvements to the conventional stroboscope

Looking at the construction of a discharge tube e.g. the one in the General Radio strobotac and the trigger circuits, one can identify a series of trigger electrodes assembled in the discharge tube to initiate the discharge process. Supposing a secondary timing circuit is designed to operate in synchronism with the trigger circuit in a way as to remove the excitation grid potential a short time after it is being applied, the discharge cannot occur unless it has already started. In this way out-of-time flashes can be effectively removed reducing the jitter but at the expense of average intensity and the apparent reduction in the repetition frequency as a statistical function of the duration allowed. Further, by deliberate reduction of flash energy, that is by manipulating the discharge circuits some improvements in the flash duration may also be achieved. However, these are rather involved and therefore other possible alternatives are also to be examined.

Another spark source giving shorter pulses has been used by Hanstead and others,[34] but apart from the low light output and the emission of harmful UV light, it is not attractive in the present application due to many operational problems and large size. The other problem with the discharge devices in general, is that the emitted light is non-monochromatic. This leads to significant chromatic aberration when a lens schlieren system is used. The use of a pulsed laser is technically feasible, but it is not a satisfactory solution due to the hazards involved and also due to the size and the cost.

9.2 THE DEVELOPMENT OF A NEW STROBOSCOPE USING A LIGHT EMITTING DIODE

In the case of a gas discharge tube stroboscope, the long flash duration

and jitter are caused by the time uncertainties involved with the discharge process itself. There is uncertainty with regard to the start of the discharge after the trigger pulse is applied and once the discharge is started, there is no effective means of control or stop at a desired point. Thus the advantages of high stability electronic timing and synchronization possible with electronic circuits cannot be fully utilized with this type of stroboscope.

If a light source could be accurately controlled by a trigger signal whose duration is 10 ns, say, and if the jitter in the the trigger signal is about 1 ns, then the percentage image elongation as registered by the light source according to equation 9.3 would be

$$\frac{I'' - I}{I} \times 100 = 2\times10^{6} (10 \times 10^{-9} + 1 \times 10^{-9}) \times 100$$

$$\simeq 2\%$$

This is a satisfactory figure for the present application but as mentioned above such performance cannot be achieved with gas discharge stroboscope tubes. Hence it is necessary to have the light emitting process directly under the control of the electronic triggering and timing circuits, which can perform to even better specification if carefully designed.

9.2.1 The concept of L.E.D. stroboscope

It seems at this stage that both control and timing could be accurately achieved if a Light Emitting Diode (L.E.D.) is used as a source of stroboscobic light. This is because the current can be controlled by the forward voltage applied to the diode according to the Eber's Mole diode equation[37]

$$I = I_{o} (\exp^{\frac{qV}{KT}} - 1) \quad . \quad . \quad . \qquad (9.4)$$

where I_o = reverse saturation current

q = electronic charge

v = forward voltage applied

K = Boltzman's constant

T = absolute temperature

while the apparent brightness of the light emitted under normal conditions is directly proportional to the current density through the junction according to the equation[38]

$$B = \frac{3940\ \eta_{ext}\ L\ J}{\lambda} \cdot \frac{A_J}{A_S} \text{ (Nits)} \quad . \quad . \quad . \quad (9.5)$$

where η_{ext} = external quantum efficiency

L = the luminuous efficiency of the eye

J = the junction current density

A_J / A_s = ratio of the junction area to observed emitting surface

λ = the emission wavelength in μm.

Hence the possibility exsists to control the light flash duration and its shape by electronic means down to the limits of circuit performance.

However, the fundamental problem with a L.E.D. in this application seems to be the very limited light output normally obtainable with the specified forward currents. To the author's knowledge, there was no manufacturer's literature concerning such short pulses yet requiring high light output, nor other satisfactory attempts that could be directly related to the requirements of the proposed system. Therefore the feasibility of developing a LED stroboscope to satisfy the illumination requirements of the present system was examined.

According to equation 9.5, the optical output should linearly increase with the current, but this does not appear to be happening in the case of DC as can be seen from a typical LED characteristics curve.[39] Fig.9.3.

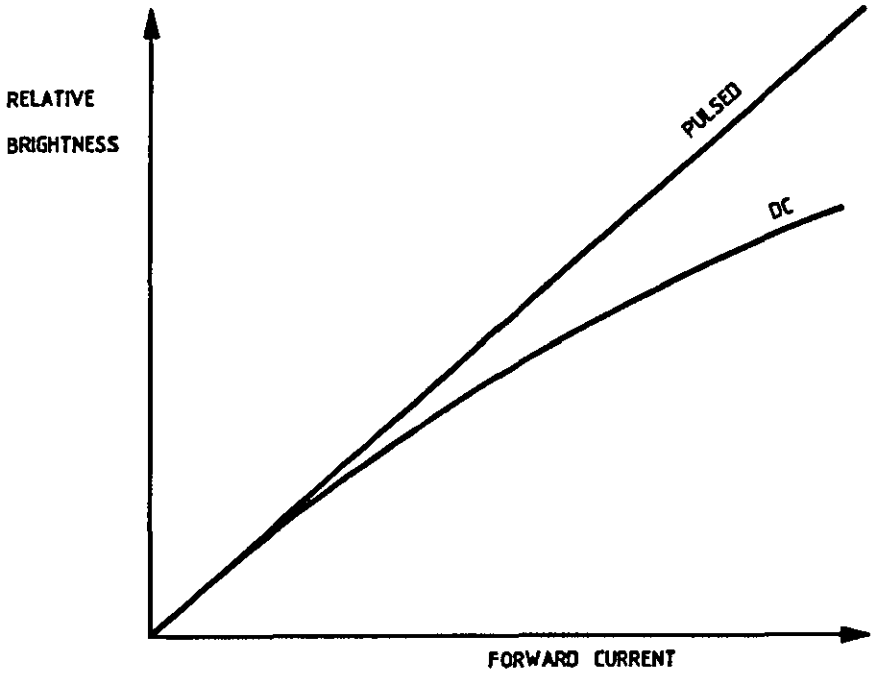

FIG. 9. 3. COMRARISON OF DC AND PULSED OPERATION OF LED.

It is interesting to note that in the case of pulsed operation, the linearity is seen at least over the range of measurements presented, while the DC curve tends to flatten out quickly indicating diminishing returns in brightness with increase in forward current. Unfortunately, the manufacturer's data do not cover pulse operation except in a very limited sense for pulsed currents up to about 300 mA and durations in the range of ms which are far removed from the requirements of the present application. Therefore, a series of experiments was carried out to examine the limits of operation of LEDs in the pulsed mode.

A large number of radiometric measurements was taken with respect to pulse width, repetition rate and the current passed through a Stanley H-500 high brightness LED.[39] Using these data, graphs were plotted such as the one showed in Fig. 9.4, to assess the maximum safe current. It was found that very high current could be passed through the diode under the required conditions and even at 20 A , which was the limit of the drive circuit used, there was no indication of optical saturation or any danger to the device.

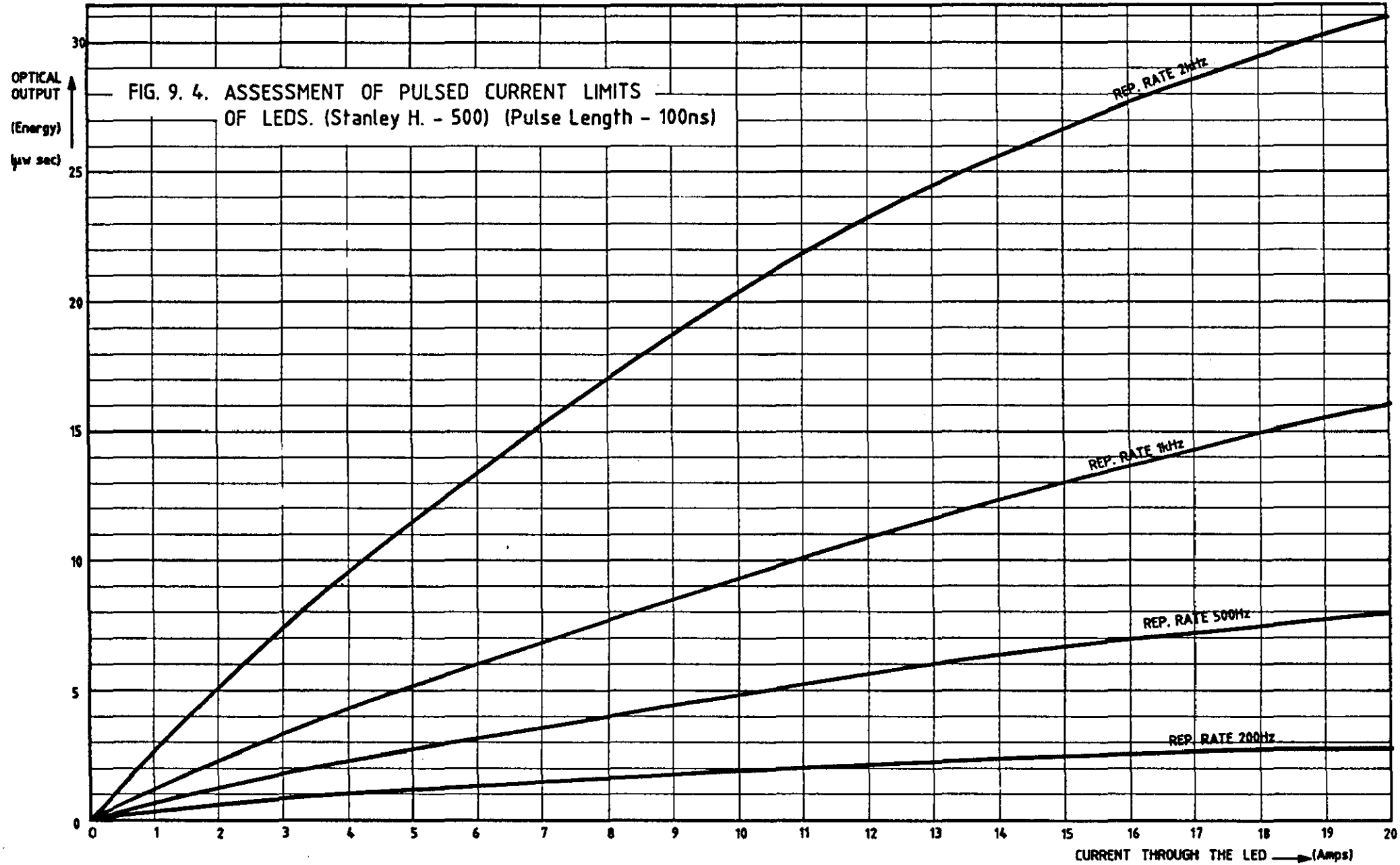
FIG. 9. 4. ASSESSMENT OF PULSED CURRENT LIMITS OF LEDS. (Stanley H. - 500) (Pulse Length - 100ns)
OPTICAL OUTPUT (Energy) (μw sec)
REP. RATE 2kHz
REP. RATE 1kHz
REP. RATE 500Hz
REP. RATE 200Hz
0
5
10
15
20
25
30
0 1 2 3 4 5 6 7 8 9 10 11 12 13 14 15 16 17 18 19 20
CURRENT THROUGH THE LED (Amps)

From these experiments it was found that the discrepancy between the DC and the pulsed characteristics is caused by a temperature rise effect at the diode junction and provided that the current pulses do not raise the junction temperature excessively, the peak optical output increases linearly with the increase in current, at least up to a several tens of Amp. Even at such heavy currents no optical saturation was observed and the optical output is proportional to the duty cycle. Under these conditions the brightness was more than adequate for the purpose, being able to register the image field well, even with a single pulse. An added advantage, not possible with electrical discharge stroboscope is that there are three parameters now available for controlling the brightness, namely, the peak current, pulse duration, and the repetition rate. Hence the average brightness could be maintained reasonably constant over a wide range of operating conditions.

9.2.2 Choice of a suitable LED

The efficient performance of an LED in the present application depends on a group of factors as follows.

1. Luminosity
2. Emissive surface area
3. Thermal mass of the substrate and the heat dissipation of the device
4. Electrical characteristics such as
   (a) Bulk resistance of the substrate, leads and the contacts
   (b) Junction capacitance and the diffusion capacitance
   (c) Dynamic resistance
   (c) Lead inductance
5. Spatial distribution of emission
6. Peak wavelength and spectral distribution
7. External surface condition

Apart from a wide variety of LEDs available, the above factors do vary considerably even within the same type of device. For example, two high brightness LED of the same type may have a luminous intensity

variation between 300 mcd to 500 mcd[39] representing a percentage change as high as 33%. Although the spatial distribution of some LEDs can be quite narrow, which is a real advantage over the discharge stroboscope, the LEDs are not always free from manufacturing defects such as small mis-orientation of the optical axis, dark spots ect., giving alignment problems. On the other hand out of the electrical characteristics mentioned above, junction capacitance, diffusion capacitance and the dynamic resistance are all nonlinear quantities[40] and depend on the bias conditions. Hence high frequency equivalent circuit analysis under heavy current conditions is rather involved. The following approximate representation as in Fig. 9.5 may be considered to examine some of the features.

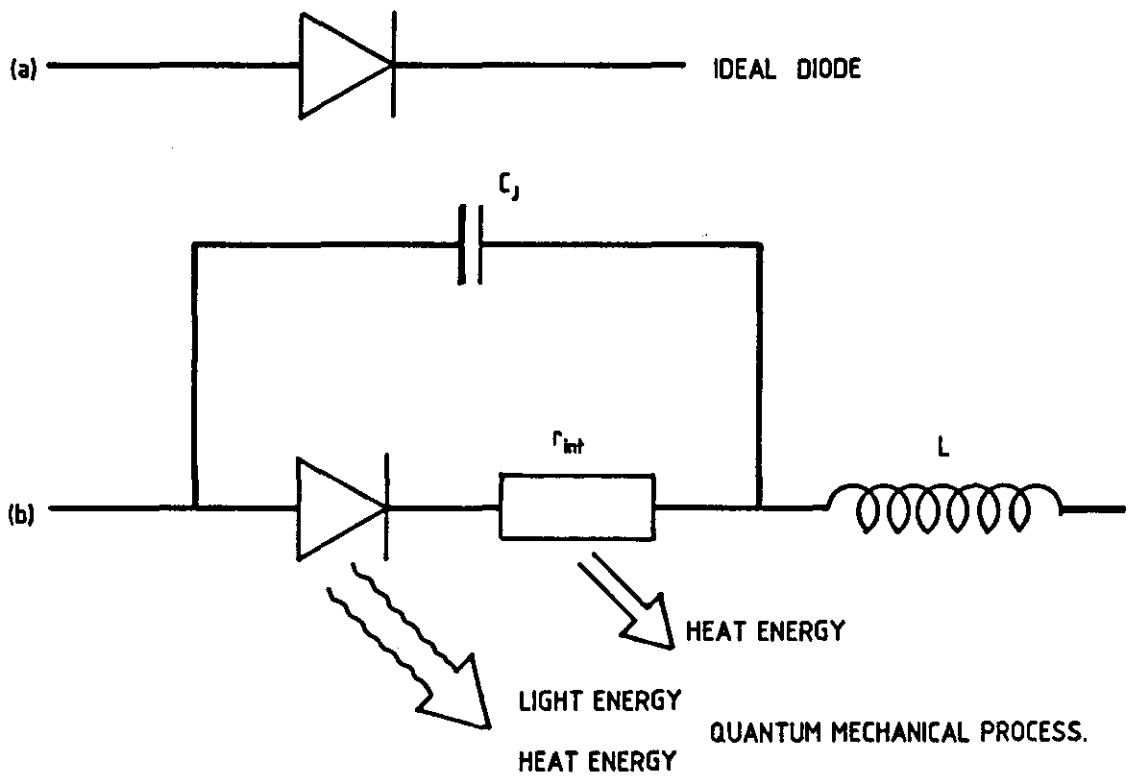

FIG. 9. 5. REPRESENTATION OF A LED AT HIGH FREQUENCY.

C_J preferentially bypasses high frequency components, while L presents higher impedance. Furthermore, L and C_J can resonate at high frequency causing difficulties of extracting charge from the diode junction. On the other hand, the higher the r_{int} the higher the drive required causing higher internal dissipation. As discussed above, this is the main cause

of lowering the luminuous conversion efficiency of the LED. All these mean that for optimum performance, LEDs have to be chosen by screening measurements and trials. Although initially a Stanley H-500 high brightness LED was chosen for the experiments, the final stroboscope was designed later with a much brighter Stanley H-2000 LED which became available only afterwards. It is expected that even brighter LEDs will become available in the near future.

9.2.3 Stroboscopic driver design considerations

A closed form approximation for the transient response of a high radiance double-hetrojunction LED in terms of 10 to 90 percent rise time may be written as in standard text[41]

$$t_{10-90} = \left(\frac{2C_J}{\beta i} + \tau \right) \ln 9 \qquad . \quad . \quad . \quad (9.6)$$

where
- β = q / 2 K T
- q = electronic charge
- i = current step for driving the LED
- K = Boltzman constant
- τ = minority carrier life time

Although the junction capacitance C_J is voltage dependent due to the distributed nature of the stored charge, the rise time according to equation 9.5 may still be improved by current peaking if necessary. This can be done by passing current in excess of the desired level for a short time and also applying a negative bias at the end of the pulse period for a short time to sweep out the injected carriers. In addition the application of a small forward bias on the LED would also be useful in reducing the activation delay.

As estimated before, the current pulses required in the present application were in the order of 20 A, the duration in the range of 10 ns and a maximum repetition frequency of about 2 kHz. Generating such

current pulses with very short duration presents major difficulties in the circuit and layout design. Since the low level trigger pulses can be readily obtained from the conventional pulse generators, the efforts were concentrated mostly on the design of a suitable driver. The heavy current pulses mean that the circuit inductance and the resistance of critical components and wiring, however small, become a major concern, while the shortness of the pulses of the order of 10 ns means that the overall bandwidth must be in excess of 100 MHz. Furthermore, adequate protection against sharp spikes and instabilities leading to spontaneous destruction of the devices must be taken care of. After many trials the stroboscope driver circuit as shown in Fig. 9.6 was initially designed.

Basic operation of the circuit is briefly described as follows. T_1 and T_2 form a complimentary emitter follower stage designed to give an output impedance of the order of 3 ohms which drives a VN 10 KM MosFET in the pulsed mode. The amplified pulse is developed across the primary of a phase inverting pulse transformer (1 : 1, bifilar winding on a Feralex 'P' grade, MM 623 ring core) with a resistance in parallel, of the order of 22 ohm. The secondary winding is referenced to ground and also shunted by a suitable resistance to lower the impedance further to drive a set of 4 VN 88 AF mosfets in parallel which operates the LED connected between a higher voltage supply of the order of 50 V and the common drain. The input impedance of the driver is dominantly resistive and is in the order of 50 ohm.

This configuration was successfully used throughout to the final design. The main differences have been in the choice of components, incorporation of an indicator circuit, slightly different biasing arrangements and the layout (Figs. 9.6 - 9.8). All these circuits performed extremely well as can be seen from the typical test results. (fig. 9.7). Care has been exercised to protect the circuits adequately, since any accidental damage would result in painstaking repair work. Fig.9.7 also shows the assembly of the first prototype on a bread board and Fig 9.9 shows the final subminiature but more powerful version for the imaging system compacted into a lens cap.

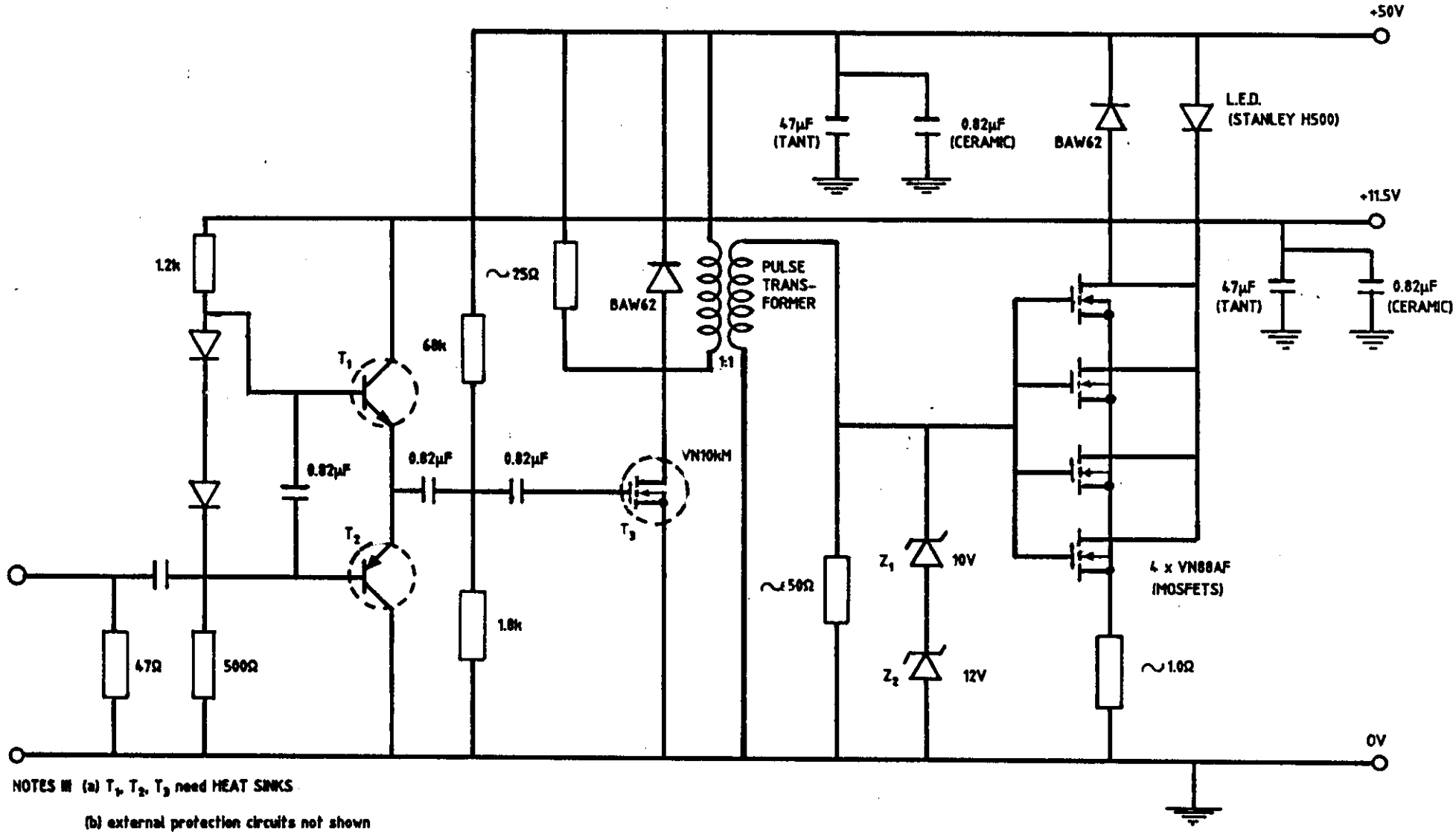

NOTES : (a) T_1, T_2, T_3 need HEAT SINKS

(b) external protection circuits not shown

FIG. 9. 6. L.E.D. STROBOSCOPE DRIVER CIRCUIT.

Designed by: G.P.P. GUNARATHNE.

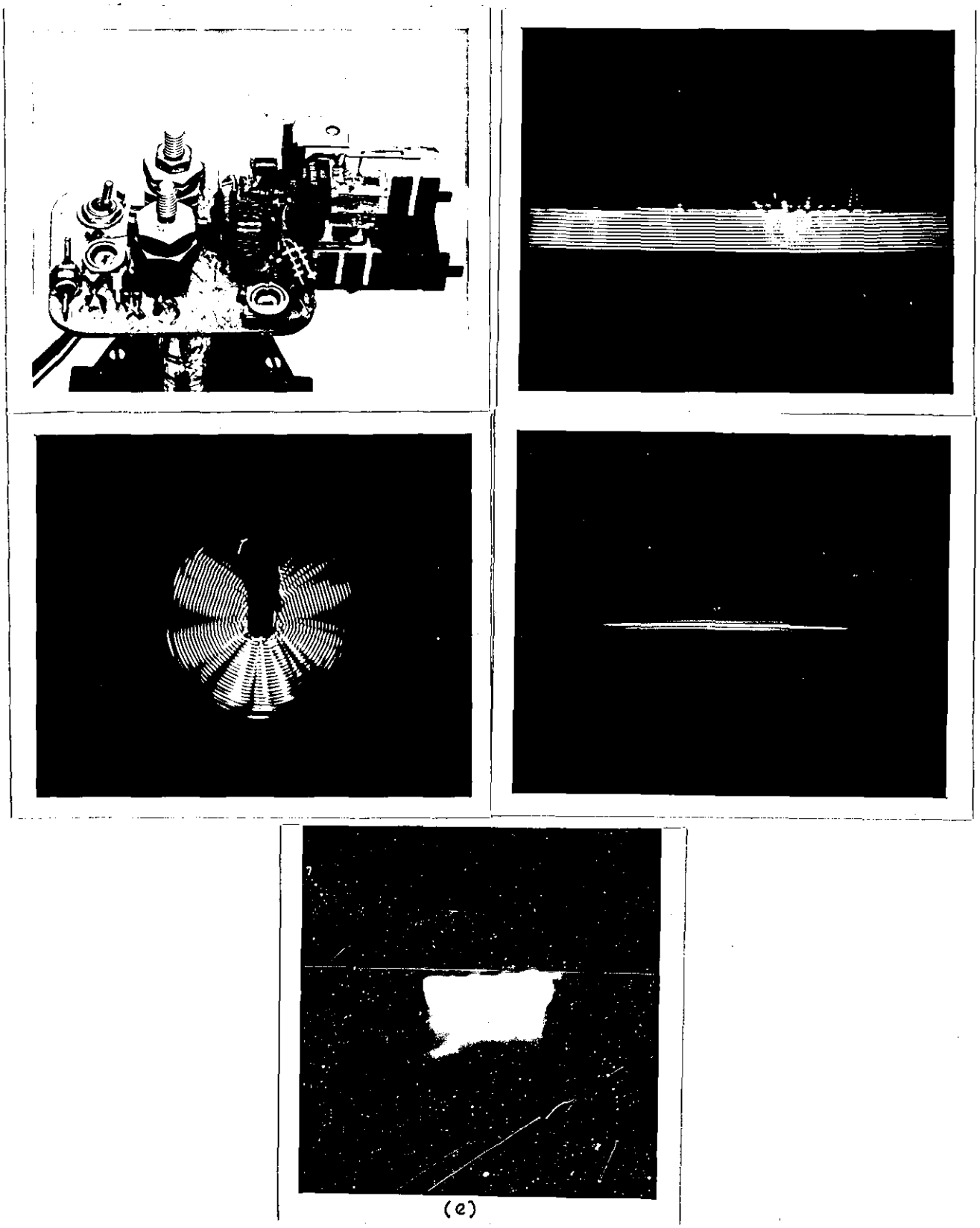

Fig. 9.7 THE FIRST ASSEMBLY AND TYPICAL TEST RESULTS.

(a) The first prototype LED stroboscope on a bread board

(b) A schlieren image of a long train of pulses

(c) Cylindrical field of a small transducer driven at 2MHz

(d) A pulse approximately one wavelength long

(e) The above pulse as seen with the conventional Strobotac

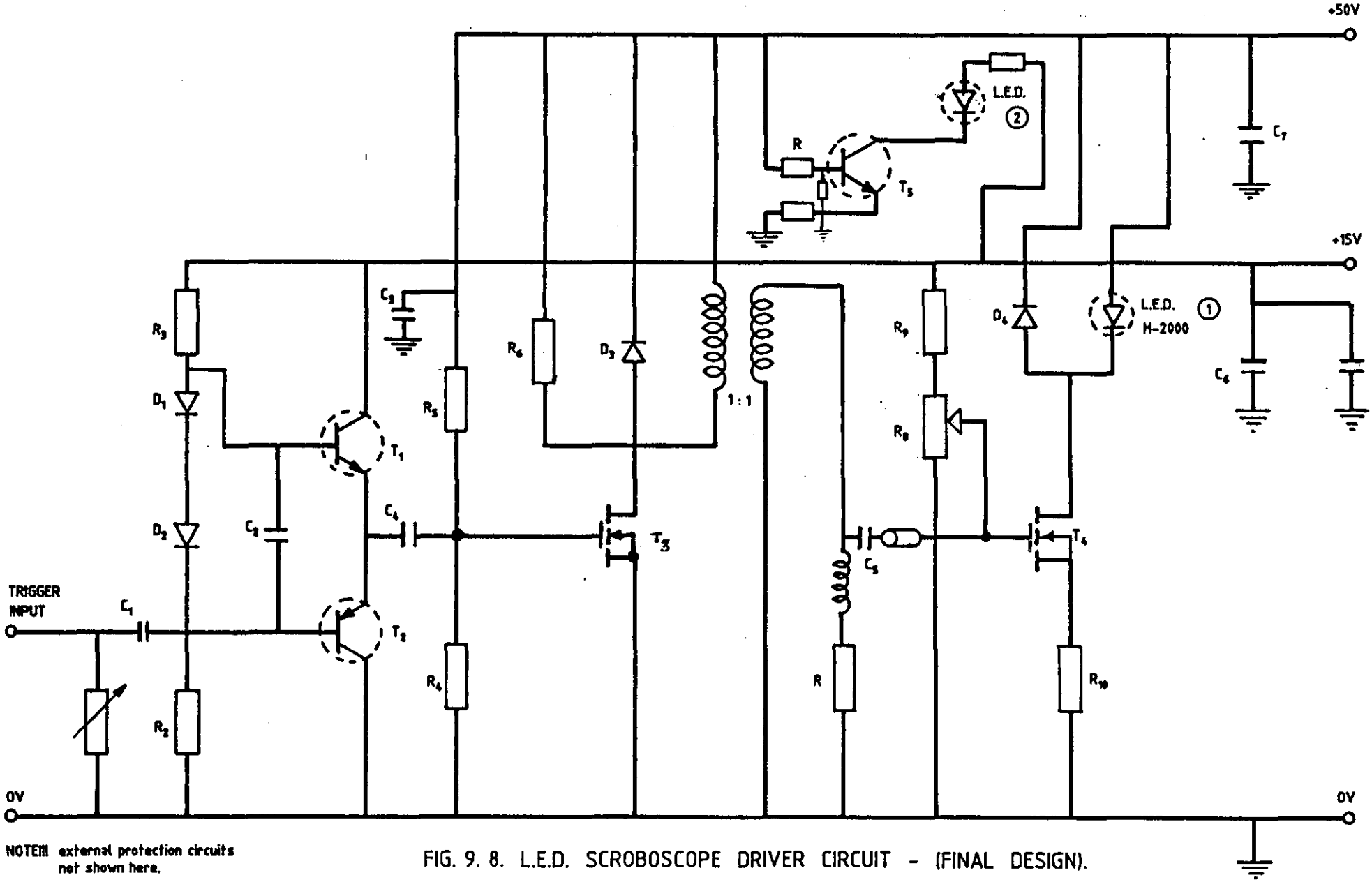

NOTE!!! external protection circuits not shown here.

FIG. 9. 8. L.E.D. SCROBOSCOPE DRIVER CIRCUIT - (FINAL DESIGN).

By: G.P.P. GUNARATHNE.

L I S T O F C O M P O N E N T S

transistors

1.	T_1	=	BFW 16 A	npn Bipolar
2.	T_2	=	2N 5583	pnp Bipolar
3.	T_3	=	VN 88 AF	Mosfet
4.	T_4	=	IRF 120	Power Mosfet
5.	T_5	=	ZTX 302	npn Bipolar

Capacitors

1.	C_1	=	2 μF	Ceramic monolythic	50 V
2.	C_2	=	2 μF	"	"
3.	C_3	=	1 μF	"	"
4.	C_4	=	2 μF	"	"
5.	C_5	=	2 μF	"	"
8.	C_6	=	47 μF	Tantalum	63 V
9.	C_7	=	47 μF	"	"

Resistors

1.	R_1	=	220 ohm ,	1 / 4 W	trimpot
2.	R_2	=	1 K // 100 ohm	"	metal film
3.	R_3	=	1.2 K	"	"
4.	R_4	=	1.8 K	"	"
5.	R_5	=	68 K	"	"
6.	R_6	=	~22 ohm	"	"
7.	R_7	=	1 K	"	trimpot
8.	R_8	=	~0.9 ohm	"	metal film
9.	R_9	=	10 K	"	carbon
10.	R_{10}	=	1 K	"	"
11	R_{11}	=	2.2 K	"	"

Signal Diodes

1. BAW 62
2. ''
3. ''
4. ''

Light Emitting Diodes

1. Stroboscopic source - Stanley Hi-Super bright H-2000 LED
2. Dual supply indicator - Stanley ESBR 2201 (not critical)

Pulse transformer

1. Core - MM 623 Feralex 'P' grade ferrite ring core
2. Winding - gauge 22 enameled copper wire, 23 turns, 1:1 bifiler

Fig. 9.9 THE LED STROBOSCOPE ASSEMBLED IN A LENS CAP READY TO BE LOCKED IN TO THE OPTICAL ASSEMBLY.

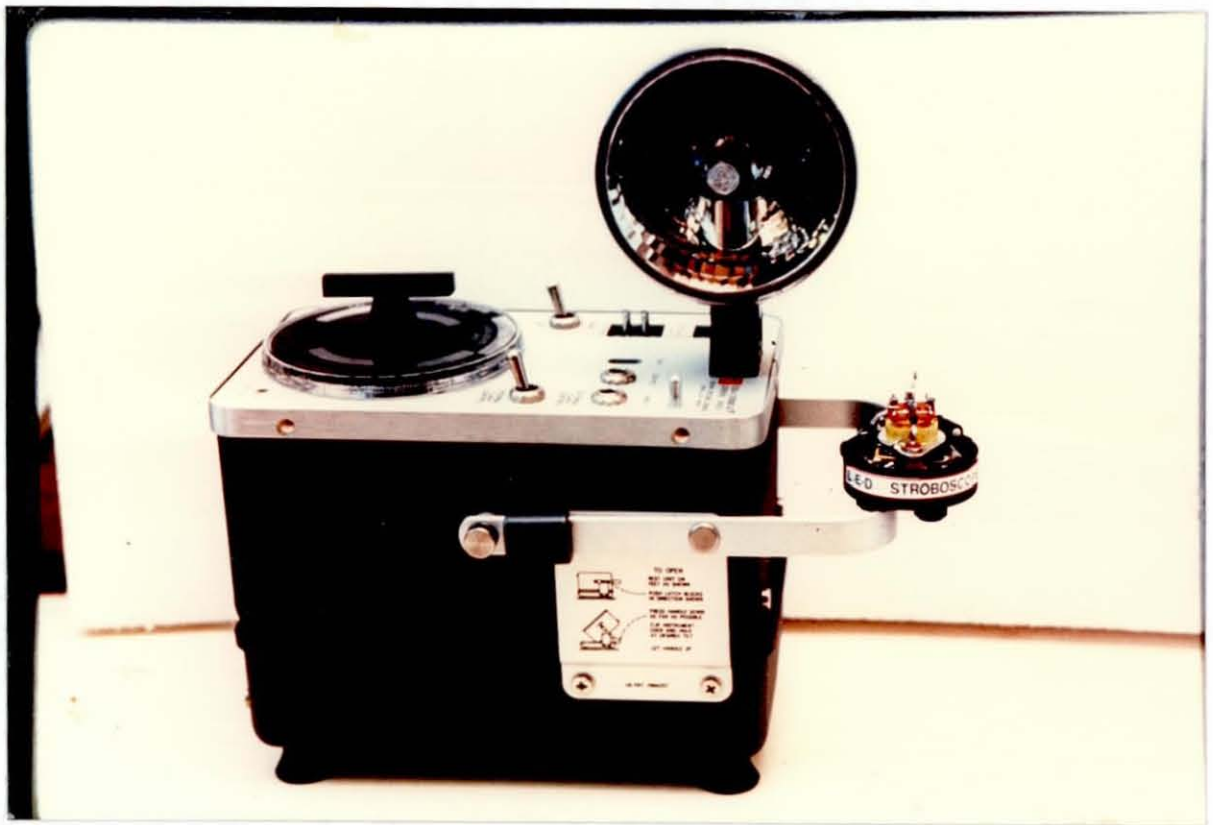

Fig.9.10 THE LED STROBOSCOPE ON THE HANDLE OF THE STROBOTAC

After the successful development of this LED stroboscope, it was published in Ultrasonics, July 1983. See appendix 3.

9.3 *CONCLUSIONS*

The conventional gas discharge stroboscopes are not suitable for the present application. A new stroboscope has been successfully developed based on a Super bright Light Emitting Diode driven with very short, very high current pulses. Its light output is more than adequate for the purpose, being able to show up the schlieren images well, even with a single pulse. The advantages compared to ordinary stroboscopes can be summarized as follows.

(1). Extremely short flash duration, independent of repetition rate; 10 ns or even shorter pulses are possible as assessed by the current pulses, compared to 30 to 50 ns of a spark discharge stroboscope or 0.5 to 3 μs of a commercial gas discharge stroboscope whose flash duration varies with the repetition rate in the above range.

(2). Completely free from jitter

(3). Nearly monochromatic emission

(4). *Well defined shape of source and spacial emission giving uniform illumination over the entire field of interest*

(5). *Pulse width and pulse energy can be accurately controlled*

(6). *Long working life*

(7). *Small physical size*

(8). *Very low cost*

-- // --

- CHAPTER 10 -

DESIGN AND CONSTRUCTION OF TRANSDUCER ARRAYS

The importance of high quality transducers in the present application was mentioned in Chapter 7. However, it was apparent that commercially available transducer arrays and backings fall far short of the requirements. As such, new techniques have been developed for the construction of high quality transducer arrays using a new type of backing made of dental alloy epoxy mixture under closely controlled conditions. Analysis of the factors involved and the details of the process are presented in this chapter.

10.1 INTRODUCTION

Variability of the properties of ultrasonic transducers is one of the main problems often encountered in practice. (Fig. 10.1)[7]. In the case of a flaw detector, transducers having rather different characteristics can still serve the same purpose, while in the case of a conventional switched array B-scanner, the uniformity of the elements is somewhat important, although not critical. However, in the present case the situation is very different as the whole process of image re-construction depends on the accuracy of the amplitude and phase information of the echo signals forming images by direct interference of acoustic waves. As mentioned earlier, this depends largely on the performance of the transducer arrays.

When the transducers are physically small, the failure rate and the variability are even greater. Therefore, it is not difficult to appreciate the nature of the task to make two transducer arrays, each consisting of 30 tiny elements with sufficiently identical properties. It is worth mentioning at this stage that not even the original DUVD has such requirements as there are no arrays involved.

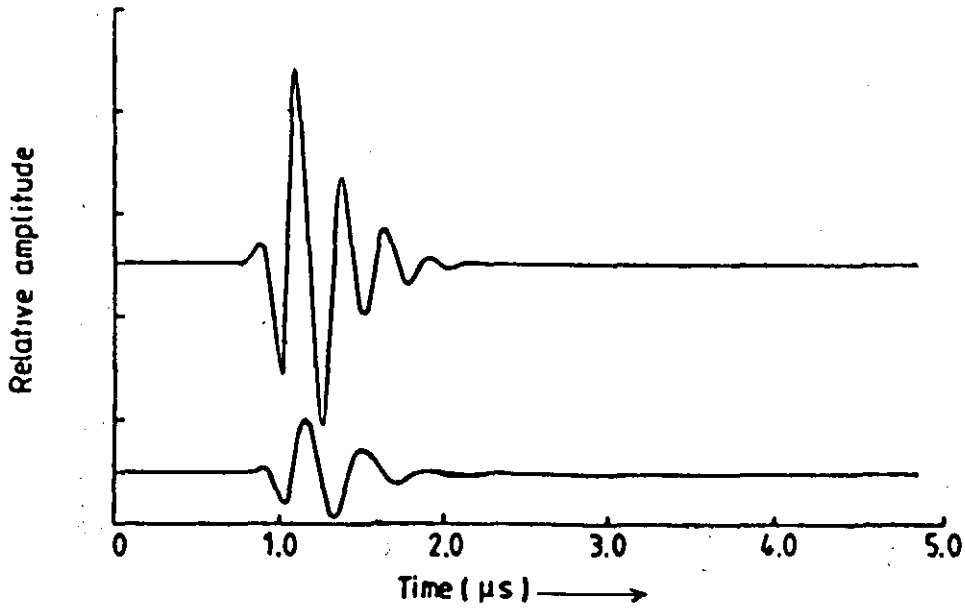

Fig. 10.1 VARIABILITY OF ULTRASONIC TRANSDUCERS - Response of two nominally identical commercial transducer probes, (Silk, 1984)

10.2 EARLY CONSTRUCTION PROCESS

Early attempts were made with transducer crystals backed by tungsten araldite slugs purchased from the manufacturers. These crystals were bonded with epoxy to the backings in the usual way and then the array elements were cut to size. After many time consuming trials it became evident that the required performance cannot be achieved in this way, mainly due to the poor quality standards of the raw materials. For example, the acoustic impedance of the slugs earlier purchased for making the arrays varied between 17×10^6 Nsm^{-3} and 5×10^6 Nsm^{-3}. The attenuation figures in the pulse echo mode at 2 MHz for a particular slug for example varied in excess of 23 dB just from one end to the other over a length of only 15 to 20 mm indicating severe local variations. On the other hand, crystals even of the same batch were different too, causing great deal of problems when replacing any defective elements or making new arrays.

10.3 INVESTIGATIONS OF BASIC PROBLEMS and IDENTIFICATION OF PARAMETERS

In respect of the above, one has to exercise tight control over the materials, composition and the process adopted. Screening tests had to be developed to chose the right materials. The materials used include :

1. Piezoelectric material
2. Backing materials
3. Bonding materials
4. Additives
5. Surface protection materials

10.3.1 Piezoelectric material

After several trials, it was found that PZT 5H was better suited for the purpose. Further experiments showed that some crystals, even if they are of the same kind and batch, were more difficult to damp than others. Because it was so important to obtain a bandwidth as wide as possible, initial damping and bandwidth tests were carried out on transducer crystals to select the most suitable ones. It was also observed through many trials that a high degree of initial poling favours not only the sensitivity but leaves more room for achieving wider bandwidth. Therefore the selected crystals were re-poled to the maximum possible limits. Another observation was that in the process of damping a transducer mechanically, a reflection free interface can not be achieved even if the impedance of the backing material was made equal to that of the ceramic with an extremely thin bond line. Apart from these, some other factors influencing performance and uniformity among the crystals of the same kind were identified, such as

1. The state of adherence between the substrate and the electrode
2. Thickness and uniformity of electrode layer
3. External surface texture

The efficiency can be severely impaired by poor adherence of the electrode layer. This situation was clearly demonstrated in some cases where the transducers did not give wideband response with good backings and bondings to which other crystals responded very well. Upon examination, it was found that the state of adherence of the silver electrode layers was very poor and in some cases they just peeled off after sticking on a piece of cellotape and then removing it. (Fig. 10.1). Small scale re-silvering and poling gave better results.

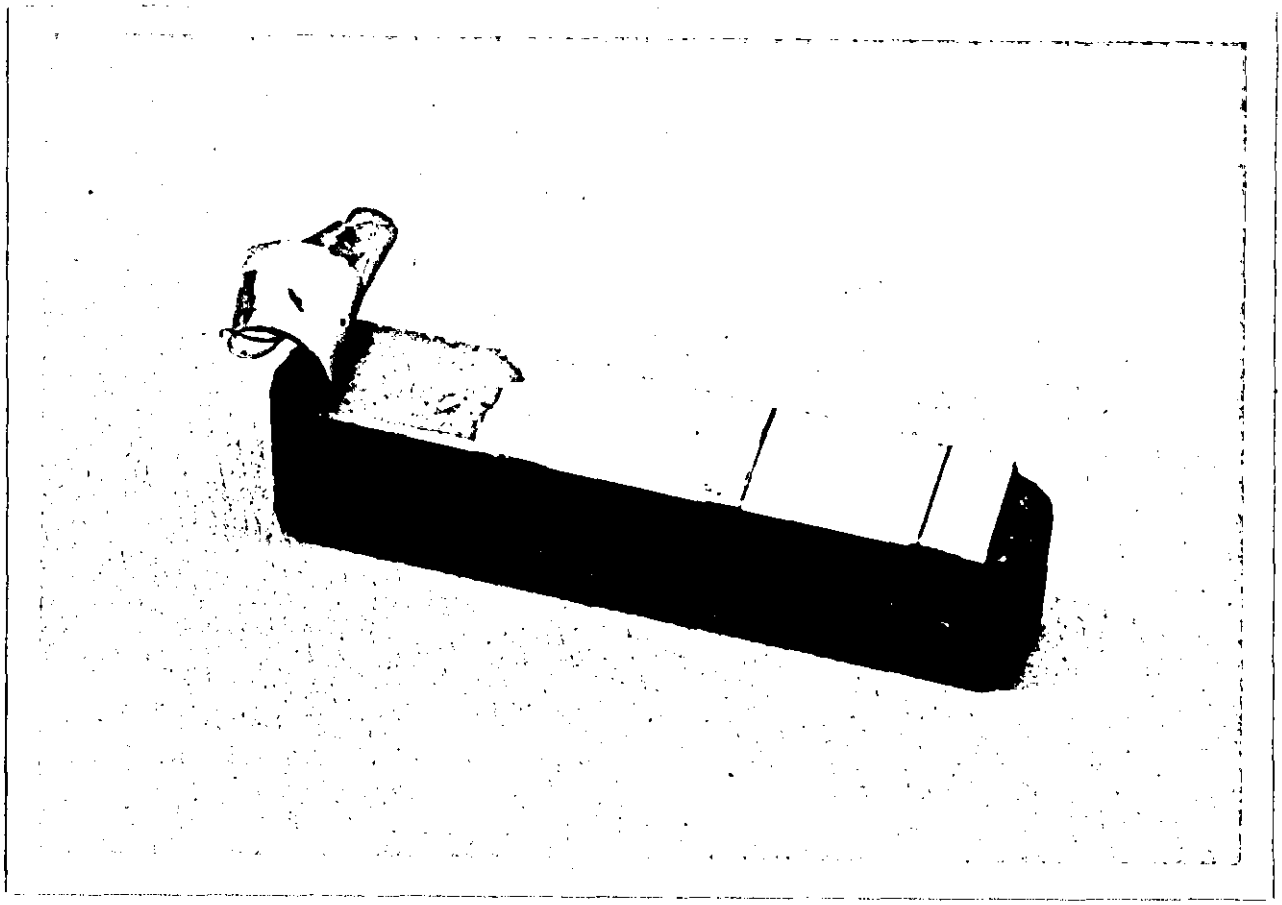

Fig. 10.2 A TRANSDUCER WITH A POORLY ADHERED ELECTRODE LAYER

Another important aspect found was the surface texture of a given crystal. This affects the bond between the transducer and the backing material both in terms of adherence and effectiveness and hence the performance. When a crystal having dissimilar surface textures on each side is cut into two halves and the opposite faces were bonded to the same backing material under identical conditions, different responses were given, indicating the influence of the surface texture. Generally both short spatial roughness and long spatial waviness variations were seen on different crystals. (Figs. 10.3 a and 10.3 b). They differed so much at one stage that the surfaces had to be specially prepared and characterized further by surface texture measurements.

At the same time excessive thickness and the lack of uniformity of the silver layers often presented problems. After constant appealing to the manufacturer, this aspect was sufficiently improved for the purpose.

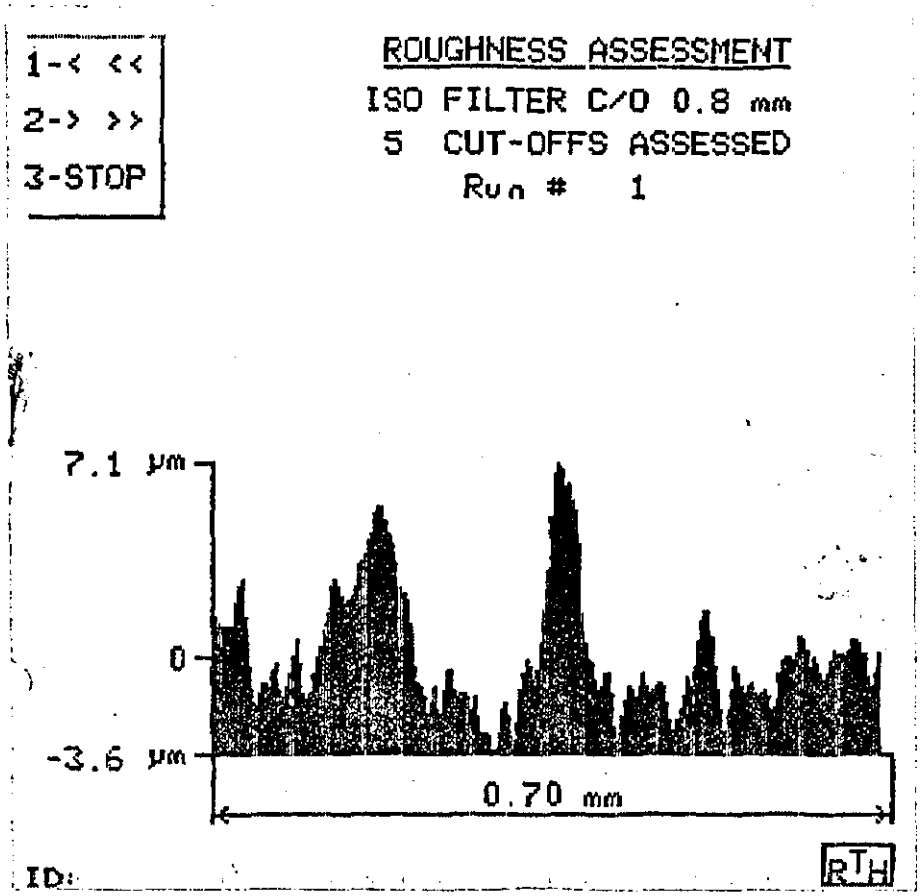

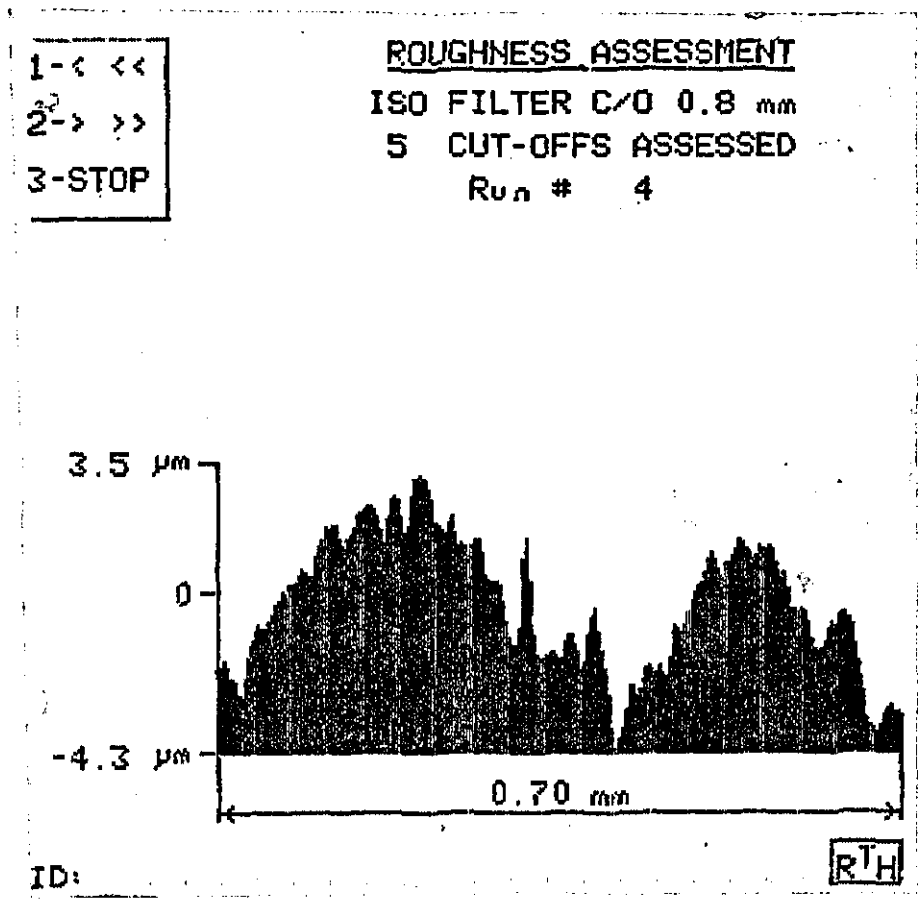

Fig. 10.3 SURFACE TEXTURE DIFFERENCES IN SOME TRANSDUCER CRYSTALS

10.3.2 Backing material

An ideal backing material may have the following properties.

1. Specific acoustic impedance close to that of the transducer material
2. A high attenuation coefficient
3. Freedom from back scatter

These properties, specially (1) and (2) are hard to achieve simultaneously.

According to classical theory the specific acoustic impedance of a medium is given by

$$Z = \rho c \qquad . \quad . \quad . \quad . \qquad (10.1)$$

where ρ is the density of the medium and c is the velocity of sound.

When a travelling wave meets a medium of different acoustic impedance, not all the energy is transmitted, such that

$$\frac{\text{Transmitted Energy}}{\text{Incident Energy}} = \frac{4Z_1 Z_2}{(Z_1 + Z_2)} \qquad (10.2)$$

where Z_1 = specific acoustic impedance of first medium
and Z_2 = specific acoustic impedance of second medium

Therefore it follows theoretically that if the acoustic impedance of the backing material is made to be equal to that of the crystal, and the two surfaces are kept in intimate contact, the damping on the transducer will be at its maximum value and all the incident energy will be transmitted. However, this condition is not practically achieved as mentioned before as there is an intermediate electrode layer and a coupling layer of either oil, an adhesive or a cold weld etc., of finite thickness separating the transducer and the backing medium. In this

situation, however thin these layers are, the process of acoustic energy transmission is a lot more complicated than that given in equation 10.2. Classical theory and the basic transducer model presented in Chapter 7, Fig. 7.9, fail to give an insight into this behaviour and many other factors outlined previously. Therefore it is worth examining the situation with more appropriate transducer models such as Mason's equivalent circuit model[42] and Krimholt , Leedom and Matthaei[43] (KLM), equivalent circuit model to identify the influence of various parameters concerning the construction of arrays.

10.3.3 Transducer modelling - Mason's equivalent circuit

The Mason's model relies mainly on the use of transmission line analogy to acoustic wave propagation and represents all the three ports namely front and back acoustic ports and the electrical port of the transducer. Fig. 10.4(b) shows the Mason's equivalent circuit for a thin transducer in one dimension. In this model, the mechanical and electrical properties of the transducer are represented by separate branches linked by an ideal transformer having a turns ratio 1 : N, where $N = C_o h_{33}$, C_o = static capacitance, h_{33} = piezoelectric deformation coefficient. The impedances Z_1 , Z_2 and Z_3 include cyclic terms governed by the thickness of the piezoelectric disc and represent the effects of the reflection of ultrasonic energy at the boundaries of the disc.

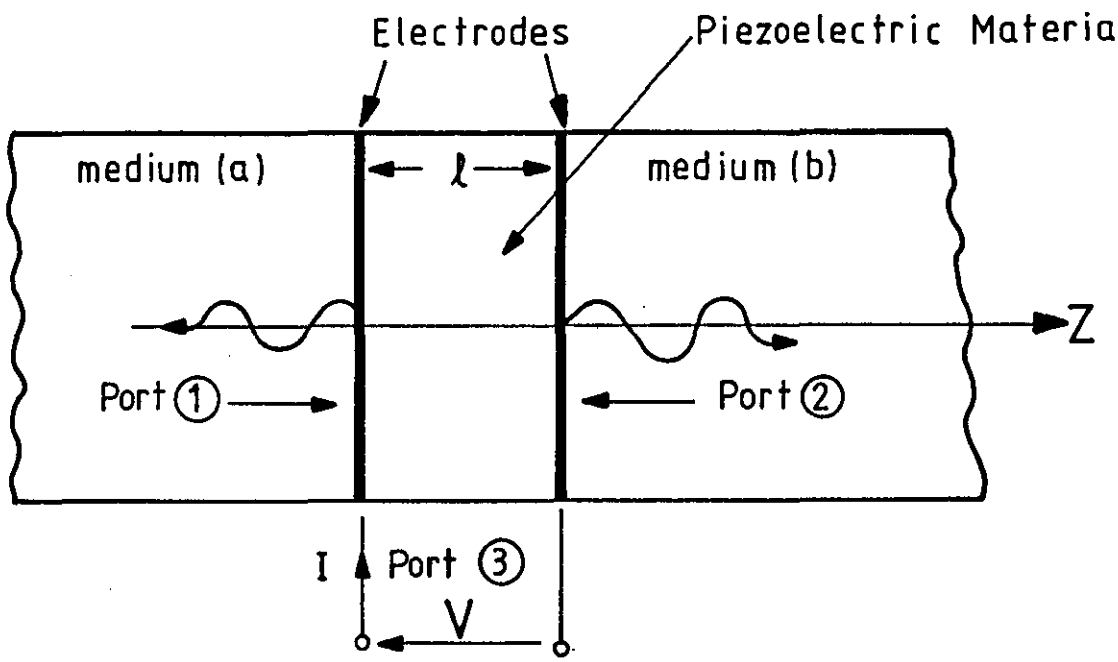

FIG.10.4(A) TRANSDUCER GEOMETRY SHOWING THE THREE PORTS

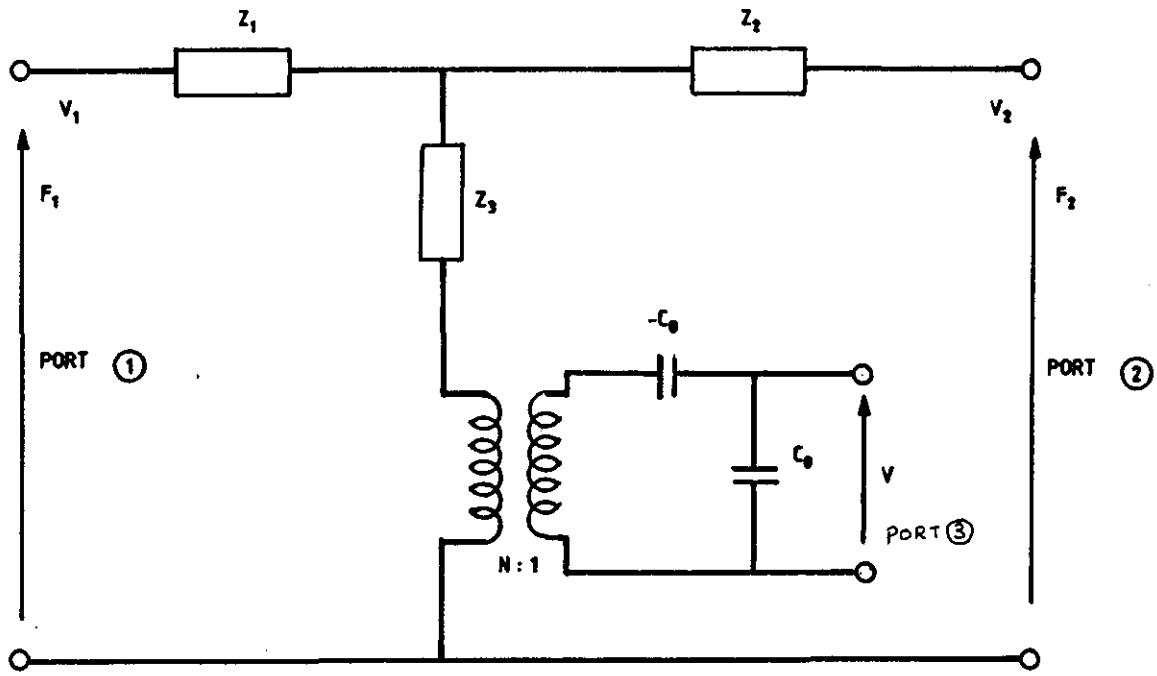

FIG. 10. 4(b). MASON'S EQUIVALENT CIRCUIT (ELECTRIC FIELD PARALLEL WITH PARTICLE VELOCITY).

With this model, there is provision for incorporation of the additional layers such as electrode layer, bond line and face plates etc. by appropriate electrical counterparts so that better approximation to the real operation could be made. For a layer of material having finite thickness t, the impedance Z_{in} is given as in standard text[7] and with reference to Fig. 10.5.

$$Z_{in} = Z_l \left[\frac{Z_B + Z_l \tanh(\phi t_l)}{Z_l + Z_B \tanh(\phi t_l)} \right] \quad . \quad . \quad . \quad (10.3)$$

$$\phi = \alpha + j2\pi f/c \quad . \quad . \quad . \quad (10.4)$$

where Z_B = acoustic impedance of backing medium

Z_l = impedance of the layer material (e.g. a bond layer)

α = attenuation coefficient

f = centre frequency

c = velocity of sound

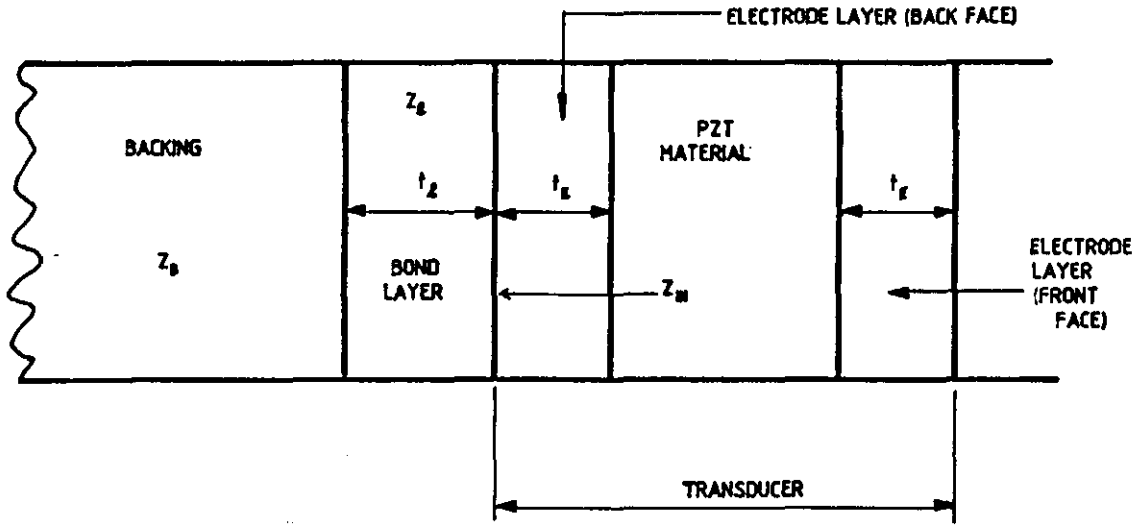

FIG. 10. 5. ACOUSTIC IMPEDENCE PRESENTED BY LAYERS OF FINITE THICKNESS.

It is also shown that the characteristic impedance of an attenuating medium is no longer $\rho \times c$, but is given by[7]

$$Z = Z_o\left[1/(1+r^2) - jr/(1+r^2)\right] \quad . \quad . \quad . \quad (10.5)$$

$$r = \alpha C/ 2\pi f \quad . \quad . \quad . \quad (10.6)$$

where Z_o is the impedance of an equivalent non-attenuating medium.

This could be followed successively through to any number of layers. It is now not difficult to see the dependence of acoustic transmission on parameters such as finite thickness, attenuation and acoustic impedance, bond layers and electrode layers which the classical theory fails to represent. It could also be seen that in the case of making arrays any local variations of the above parameters are far more significant and could easily cause non-identical behaviour.

One of the problems with Mason's model is that it is rather difficult to interpret the effects in the reverse order. That is to say what would be the implication of modifying the electrical model in terms of constructional features. In this respect the transducer model developed

by Krimholtz, Leedom and Matthaei, (KLM model) as shown in Fig. 10.6 is more flexible to be used in interactive transducer design. Here the piezoelectric element is represented as a lossless acoustic transmission line of length L coupled at its mid point to a lumped network, representing the electrical properties of the disc. Any other layers can be added to these acoustic outlets as acoustic transmission lines by their acoustic impedance and the thickness as a function of phase. Mechanical and electrical branches are again linked by an ideal transformer of turns ratio 1 : N[7]

where $$N = \left[k_T (\pi/2\pi f_o C_o Z_o) \; \text{Sinc} \; (f/2f_o) \right]^{-1}$$

and the reactance of C_o, X_E is given by

$$X_E = k_T^2 \; \text{Sinc} \; (f/f_o)/2\pi f C_o$$

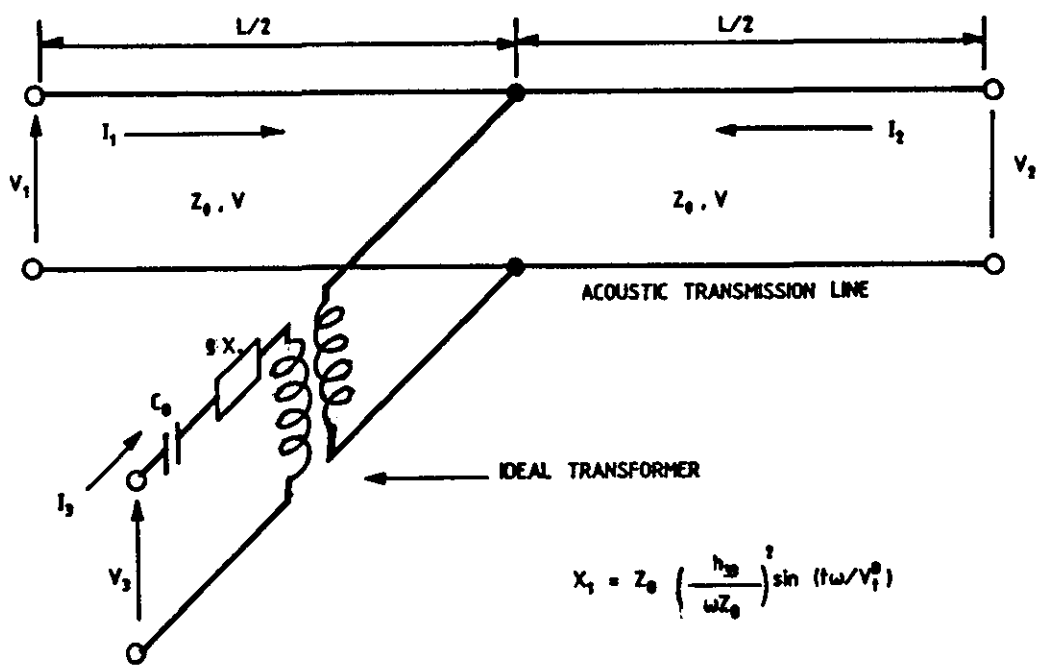

FIG. 10. 6. KLM TRANSDUCER CIRCUIT MODEL.

For optimum bandwidth, the Q values of the mechanical and electrical branches are matched. The mechanical Q value Q_m is

$$Q_m \simeq \frac{\pi}{2} \left(\frac{Z_p}{Z_B + Z_F} \right) \quad . \quad . \quad . \quad (10.7)$$

where Z_p is the impedance of the ceramic material, Z_F and Z_B are the equivalent impedance seen by the transducer at the front and the back ports respectively. Electrical Q value is given by

$$Q_e = \frac{\pi}{4k_T^2} \left(\frac{Z_B + Z_F}{Z_p} \right) \quad . \quad . \quad . \quad (10.8)$$

Equating Q_e and Q_m for optimum bandwidth gives

$$Z_B + Z_F \simeq \sqrt{2} \; Z_p \, k_T \quad . \quad . \quad . \quad (10.9)$$

Substituting typical values for Z and k_T as 28 and 0.68 respectively,

$$Z_B + Z_F \simeq 27 \times 10^6 \; N s m^{-3}$$

This means that in the present case, the object medium being steel with an impedance of about 46×10^6 Nsm^{-3}, bandwidth and efficiency cannot be optimized without some impedance transformation at the front end e.g. using matching layers. However, for the feasibility study this may be omitted due to the large amount of work involved. For the time being if aluminium is used as the test object medium, whose impedance is only about 17×10^6 Nsm^{-3}, bandwidth optimization according to equation 10.9 can still be done without any matching layers and therefore the system performance could be evaluated without loss of generality. This is the case for the re-transmitting array any way, as it is to be directly coupled to the aluminium lens.

Hence if the impedance at the front face is assumed to be about 14×10^6 Nsm^{-3}, (taking into account, the drop from the nominal value of aluminium due to protective layers and bond layers, cf. equation 10.3), then the required back face impedance according to equation 10.9 would be about 13×10^6 Nsm^{-3}. Again considering the effect of bond layers, the required impedance of the backing itself in this case would be about 16×10^6 Nsm^{-3}. This agrees with experiments where the optimum bandwidths were obtained with backings whose acoustic impedance was not equal to that of the ceramic, but considerably less in the range of 14 to 20×10^6 Nsm^{-3}.

Apart from the impedance one other important consideration has been the attenuation of the backing medium. Impedance, attenuation and the path length required are clearly related. Normally the higher the impedance, the lower the attenuation and therefore the longer the length of the medium required to prevent significant reflections back to the transducers. However, in the case of making arrays with conductive backings, this presents a crucial problem due to increased inter-element capacitive cross-coupling as will be shown below. See Fig. 10.7.

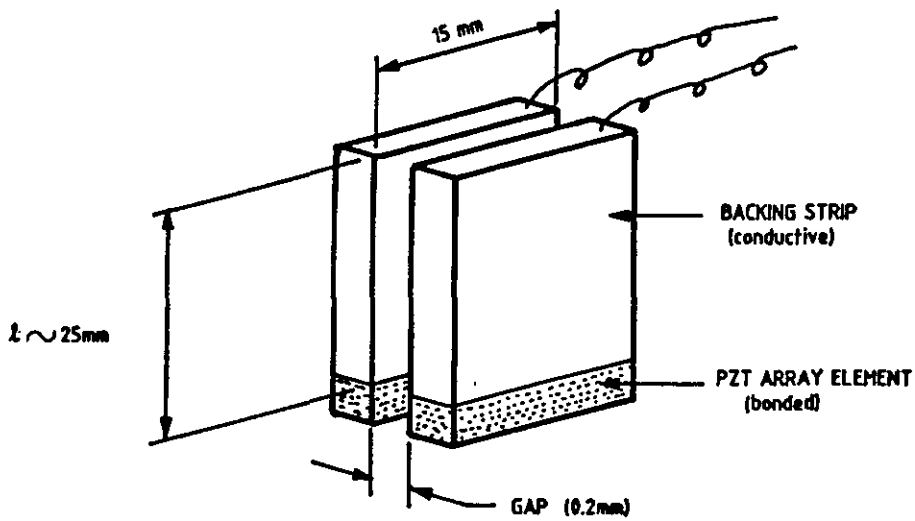

FIG. 10.7. CAPACITIVE CROSS-COUPLING OF TRANSDUCER ELEMENTS

The capacitance formed between two backing strips as in Fig. 10.7 can be written as[44]

$$C = A \varepsilon / d \qquad . \quad . \quad . \quad . \qquad (10.10)$$

where A is the surface area of the backing, d is the element spacing and ε is the permittivity of air ($= 8.85 \times 10^{-12}$ F m^{-1}). Substituting typical values, gap width = 0.2 mm, backing length = 25 mm, the value of the capacitance C would be

$$\therefore \quad C = 15 \times 25 \times 8.85 \times 10^{-12} / 0.2$$

$$\simeq 20 \text{ PF}$$

Therefore, at 2 MHz, the reactance of the cross-coupling capacitance would be

$$X_C = 1/2\pi f_o C = 1/2\pi \ 2 \times 10^6 \times 20 \times 10^{-12}$$

$$\simeq 4000\ \Omega$$

Assuming the transducer impedance is approximately 500 Ohm resistive at the centre frequency, two consecutive elements may be represented as in Fig. 10.8.

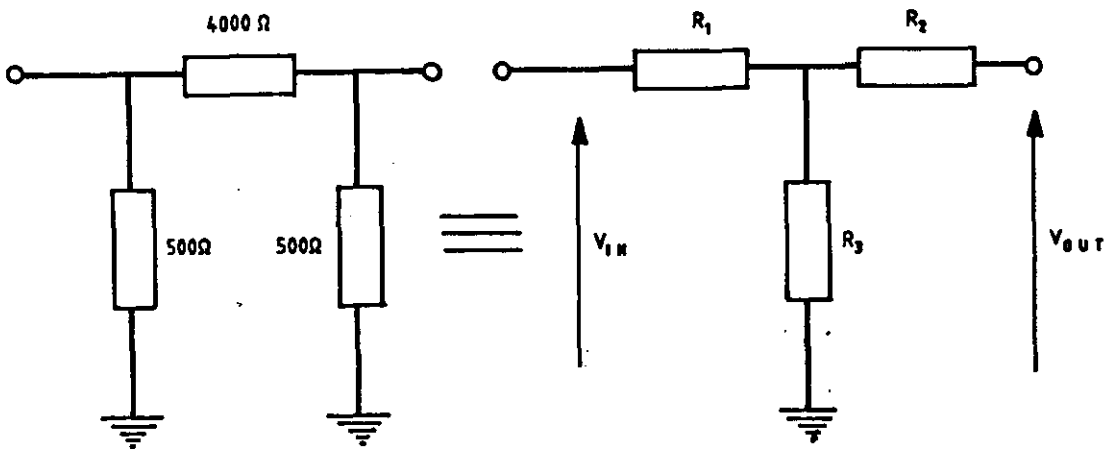

FIG. 10.8. AN EQUIVALENT CIRCUIT REPRESENTATION OF INTER-ELEMENT CAPACITIVE CROSS-COUPLING.

If a voltage V_{in} is induced in element 1, the voltage transmitted to element 2 via cross-coupling would be

$$V_{out} = R_3 / (R_1 + R_3) \ V_{in}$$

$$= K_c \ V_{in}$$

where $K = R_3 / (R_1 + R_3)$ may be treated as the cross-coupling factor. By star delta transformation,

$$R_1 = R_2 = 4000 \times 500 / 5000 = 400 \text{ Ohm}$$

and R_3 = 500 x 500 / 5000 = 50 Ohm

$\therefore$ K = (50 / 550) 100 $\simeq$ 10 %

Although the actual figure will be somewhat less than this in the present application, the influence of inter-element capacitive cross-coupling can be quite serious if lower width/gap ratios are to be implemented and/or at high frequencies.

Earlier trials were made with tungsten loaded araldite, but the attenuation at the required impedance was rather low for the purpose and therefore various attempts were made with materials to achieve better attenuation vs impedance figures. From this exercise, a better compromise was found with a fine grain dental alloy mixed with epoxy in appropriate proportions and made under closely controlled conditions and the details will be presented later in the chapter.

Further attempts were made to develop non-conductive backings using aluminium oxide powder with the aim of avoiding capacitive cross-coupling all together. One of the problems with the aluminium oxide backings were some backscatter and reflection from non-homogeneous sites as a result of using fairly coarse grain powder which was already available at the time.

10.3.4 Adhesion and bond line effects

One of the most serious problems faced in the construction of the array was due to the variability of the properties of bond line between the transducer and the backing and also the protection layers at the front face. Some preliminary experiments were carried out using carefully prepared glass samples bonded by various adhesives and mixtures of adhesives and suspensions to study the nature of variability of bonds under controlled conditions. (Fig. 10.9).

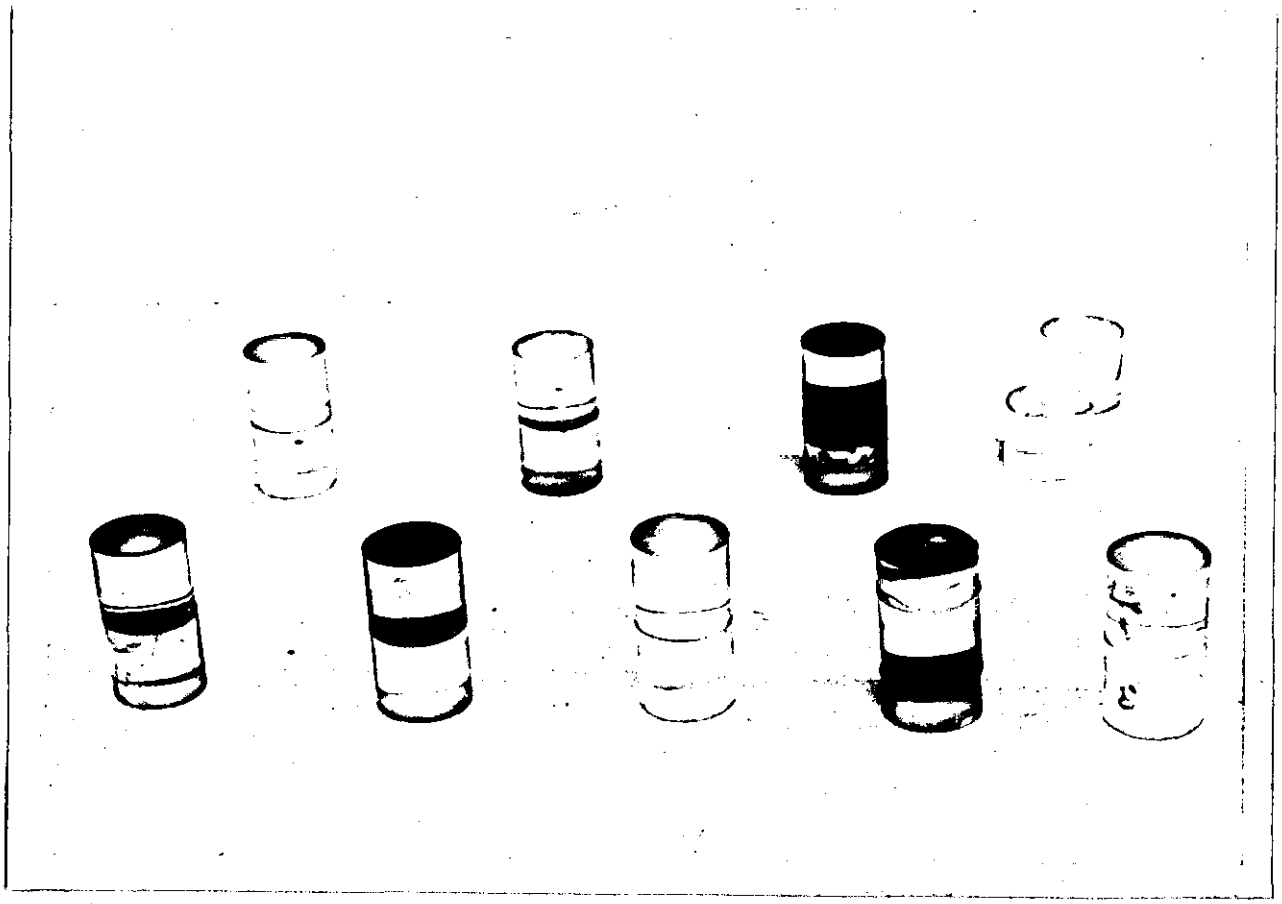

Fig. 10.9 EXAMINING BOND EFFECTIVENESS USING GLASS SPECIMENS

One of the observations was that not even a near reflection free interface was formed in any occasion. The minimum reflection observed did not fall anything below 15 to 20 % of the incident amplitude and also the variabilities between the samples were very significant. Because the samples were glass, it was possible to observe how easy to form patchy bonds and also how to avoid them. There was evidence that the structural strength of the bond also played a significant role in acoustic transmission through the interface. Additives with the aim to increase the impedance of the bond material did not always go according to the expectations. Although the impedance was raised in this way, the consequant loss of structural strength and increase in bond line thickness at higher proportions of the additives counteracted a possible improvement in performance. Factors of importance are

1. Bond line thickness and its uniformity over the required area
2. Structural strength of the bond
3. Acoustic impedance of the bond material

4. Attenuation coefficient - α
5. Acoustic wavelength - λ

Classical approach again does not give any insight into these but examination of equations 10.3 and 10.4, reveals the important features of a bond line. As $\tanh(i\phi t_l) \longrightarrow \phi t_l$, for small bond thicknesses t_l, eq. 10.3 can be re-written as

$$Z_{in} \simeq \frac{Z_l (Z_B + Z_l \phi t_l)}{Z_l + Z_B \phi t_l} \quad . \quad . \quad . \quad . \quad (10.11)$$

where Z_{in} is the impedance seen by the probe at the back face.

If $Z_l \ll Z_B$

$$Z_{in} \simeq Z_B \Big/ \left[1 + (Z_B / Z_l)\phi t_l\right] \quad . \quad . \quad . \quad . \quad (10.12)$$

i.e. for Z_{in} to be equal to Z_B, $(Z_B / Z_l)\,\phi t_l$ must be small. For the present case (Z_B / Z_l) is about 5.5 and if about 20 % reduction in apparent backing impedance Z_{in} is permitted as before, then from 10.12

$$|\phi t| \simeq 0.25/5.5 \sim 0.045$$

But $$\phi = \alpha + \frac{i2\pi f}{C}$$

For the epoxy mixture used the attenuation coefficient α is in the range of 1.2 nepers mm^{-1} and $(2\pi f / c) \simeq 5$ mm at 2 MHz. Substituting the appropriate values for $|\phi t_l|$

$$t_l \simeq 0.045 / (1.2^2 + 5^2)^{1/2} = 8.7 \times 10^{-3} \text{ mm}$$

This is an unfavourable situation as the bond line thickness has to be maintained below a few microns, and even at the above value of 8.7 μm, the apparent reduction in effective backing impedance is 20 %. Now turning to the surface texture measurements, Fig.10.3, the importance

of careful surface preparation before bonding is self evident. The local variations in the transducer crystal alone is sufficient to cause enough problems.

It must be mentioned at this stage that in the manufacture of probes, such local variations are of a much less serious nature as far as the uniformity of two probes are concerned due to the averaging effect over a comparatively large surface area. But the situation becomes more and more prominent when the size of the transducers is small, comparable to the type of spatial surface variations of the crystal leading to increased non-uniformity in the case of arrays.

On the same reasoning, not only the transducer but the surface texture of the backing is just as important and the experiments showed that this is even more difficult to control.

Fortunately, techniques were developed later to improve the surface texture of the backings leaving only short term spatial roughness within limits and little long term spatial waviness. The effect of local variations on a small transducer can be treated as increasing the average bond line thickness. Now if representative values obtained from surface texture measurements are substituted to give an average bond line thickness of about 20 μm, then the effective impedance as seen by the transducer for the same backing in the present case would be about 36 % less than that of the backing itself, which is totally unsatisfactory. i.e. for a change of bond line thickness of only 11 μm, the effective backing impedance was varied by about 16 %. This type of change is typical but if great care is not taken, the situation could be far worse.

Although the absolute impedance values are different, some idea of what reduction in backing impedance alone means in terms of performance can be gained by comparing theoretically expected pulse shapes of two transducers as seen in Fig. 10.10, after Silk[7] (1984). The difference of impedance between the backing from 1st to 2nd in Fig. 10.10 is only about 12 % and the bond line thickness is assumed to be zero.

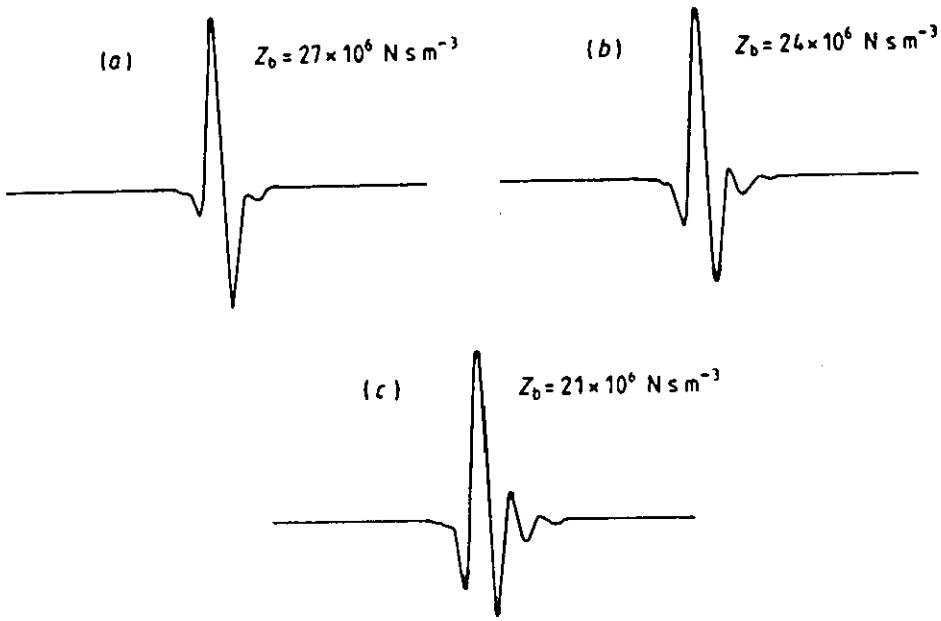

Fig. 10.10 VARIABILITY OF PULSE SHAPE AS A FUNCTION OF ACOUSTIC IMPEDANCE OF THE BACKING, ASSUMING ZERO BOND LINE THICKNESS. (Silk,1984)

Apart from the apparent reduction of the backing impedance, the finite bond line thickness seems to have far more consequences particularly if wideband performance is required as in the present case. It was observed in experiments that when the mechanical damping was gradually increased, the corresponding improvement in the bandwith was not symmetrical about the centre frequency. The low frequency response is readily enhanced while the high frequency side was relatively much poorer (Fig. 10.15 a through d). This can also be understood in terms of bond line properties. Returning to eq. 10.4, where $\phi = \alpha + i 2\pi f / c$, it is seen that the bond line thickness limit is a function of frequency because the attenuation in polymer materials like araldite is proportional to frequency. Hence the effective damping impedance will fall with frequency leading to high frequency energy being trapped within the PZT material. This explains the experimental observations where mechanical damping gave little improvement towards the high frequency end of the transducers. Therefore on the same argument it must also be mentioned that whatever the layers involved in the front end must be extremely thin and well coupled to the test object to irradiate or receive short pulses. It also seems to be an advantage to force the transducers to operate somewhat below the nominal resonance frequency to achieve better phase performance because in effect

mechanical damping preferentially improves the low frequency spectrum of the transducer.

10.4 THE CONSTRUCTION PROCESS

The fundamental areas of critical importance that need to be handled in the construction process are

1. Transducer material
2. Backing material
3. Bond line

The transducer material selected was PZT 5H and after screening tests and re-poling as mentioned previously, the thickness of the silver electrodes was further reduced as far as possible by careful scraping and polishing. The surface to be bonded was carefully treated with degreasing agents and the surface texture measurements were repeated They were then stored in acetone to prevent oxidation and contamination of surface until ready to be used.

10.4.1 The development of high quality transducer backings

As mentioned before, the earlier transducers were made with tungsten araldite slugs purchased from manufacturers. These slugs were cylindrical in shape and therefore the surface required for bonding was prepared initially by milling along the length. However, it was later found that the impedance of the slugs varied severly from one end to the other. Experiments suggested that this is mainly caused by the method of compacting the powder. Usually these slugs are made by compacting the tungsten araldite powder mixture by applying pressure from one side of the charge in a cylindrical mould. Due to the frictional forces mainly set up at the interface between the charge and the wall of the mould, the powder is not compressed uniformly leading to the type of changes observed along the slug. To avoid this problem, a steel mould was designed such that pressure could be applied along a rectangular surface having dimensions slightly larger than that of the transducer

to be bonded. Any impedance variation down the slug in this case is largely irrelevant and may well be used to an advantage to achieve higher attenuation for a given backing length, without affecting the impedance presented to the transducer. In fact this was deliberately done at a later stage.

Many trials were made with different materials to achieve suitable attenuation vs impedance characteristics for a length of the medium not exeeding the limits discussed previously. As mentioned before, dental amalgam showed a better compromise for the purpose but it was soon evident that whatever the material used, achieving the required properties and the uniformity are largely dominated by the process adopted. The earlier backings made with the dental amalgam still showed very high non uniformity.

By adding more powder and applying differential pressure to the sections where there is low impedance, it was found possible to restore uniformity along a plane just below the top surface which can be accessed by milling. However, the problem was to know exactly how much mixture should be added, when and to what extent the differential pressure should be applied and also what changes in temperature and curing time etc. are to be made. To overcome these problems, a technique of monitoring the properties of the backing while it is being made inside the mould was developed, as trial and error construction proved expensive, time consuming and giving little success. To the author's knowledge, such monitoring and adjustment techniques are not carried out in the industrial manufacture of transducer backings.

In order to monitor the properties, the mould was re-designed to accommodate a set of 6 small closely identical transducers on either side of the mould forming three pairs facing each other (Fig.10.11). These transducers were coupled to control and monitoring circuits so as to send and receive ultrasonic pulses in the reflection and through transmission mode separately.

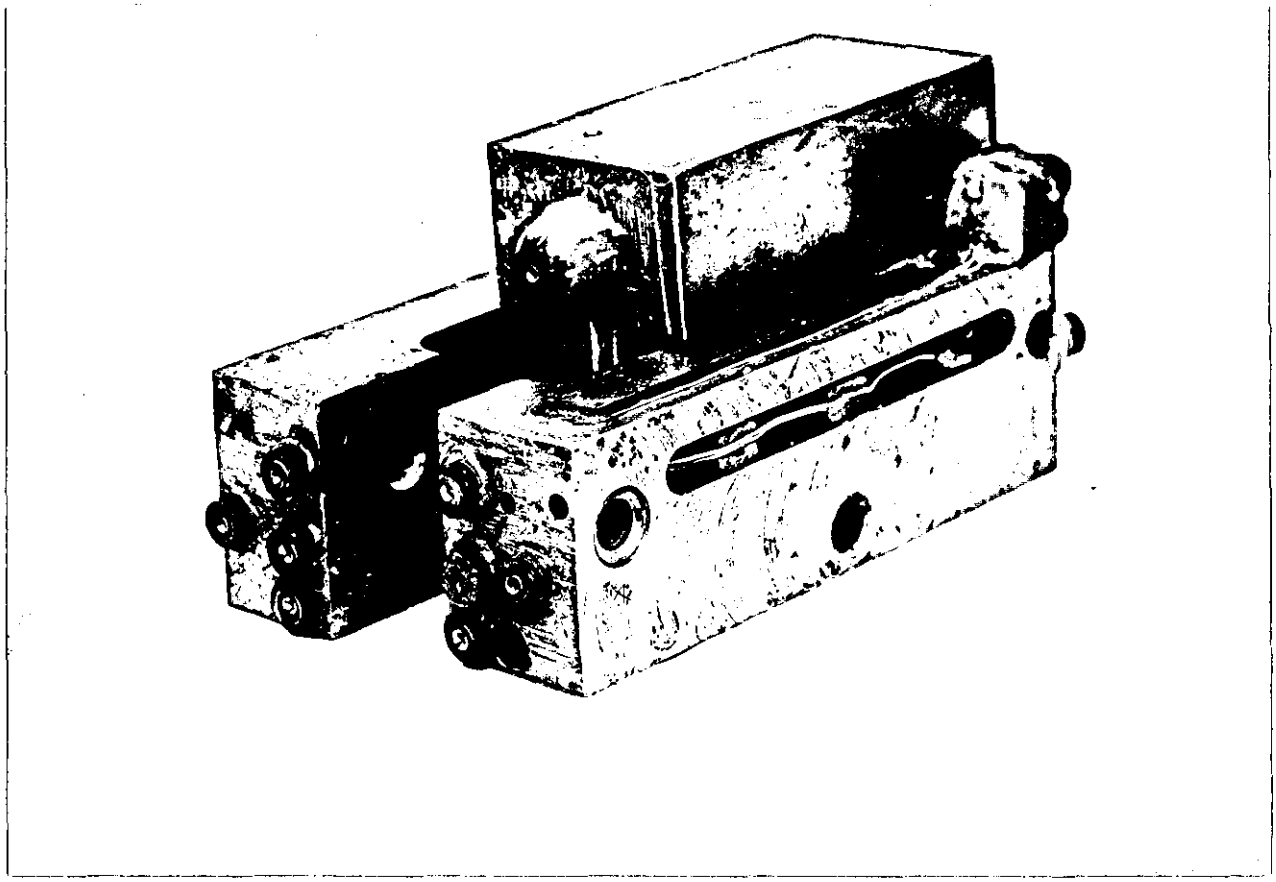

Fig. 10.11 MOULD FOR MAKING HIGH QUALITY TRANSDUCER BACKINGS

When the mixture is placed in the mould and pressure is initially applied, the transducers were activated to send pulses across the charge at different places along its width. The acoustic impedances at those places could be measured in this way by considering the reflected amplitudes at the steel/backing interface, while the attenuation figures were obtained by examining the transmitted signal amplitudes received by the opposite set of transducers. It so happened that the attenuation measurements were far more informative and accurate than the impedance measurements and also monitoring attenuation only was sufficient to make any necessary adjustments to achieve uniformity, the required impedance and other properties of the backing before the completion of the curing process. The mould is made in three parts, each fitted with internal heaters. The temperature of the mould is sensed by a thermistor fixed inside and was used to regulate the temperature of the mould fairly accurately by a proportional temperature controller designed to supply the required heater current at the temperature set on the dial. See Figs. 10.12.

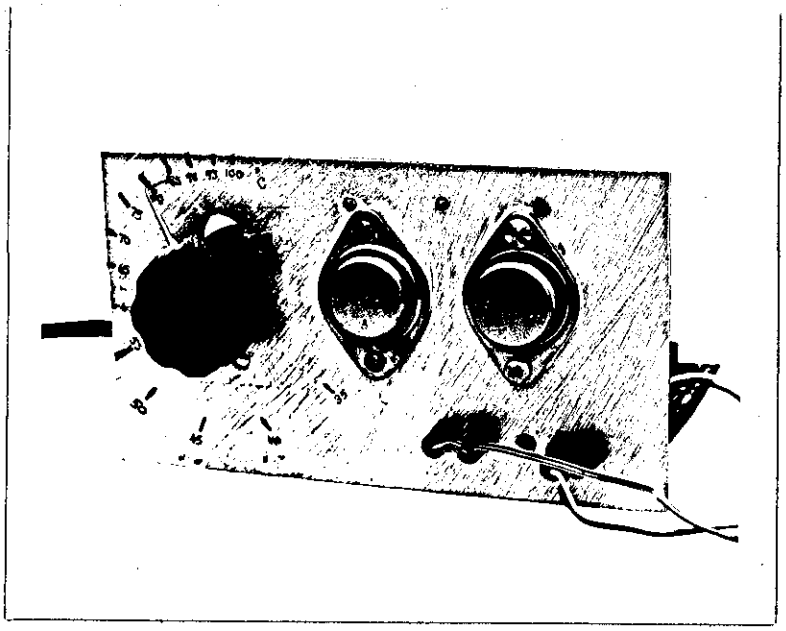

Fig. 10.12 THERMOSTAT CONSTRUCTION

Unlike the case of tungsten araldite, the dental alloy/epoxy mixture has three variable constituents, namely the metallic powder mixture, mercury and epoxy so that better control over the required properties may be achieved. A typical amalgam slug made for this purpose has the following approximate composition.

Fine grain dental alloy	=	80 gms
Mercury	=	40 gms
Slow setting epoxy	$\simeq$	7 gms

These components are thoroughly mixed and sieved with a 500 microns sieve and packed into the mould. The process conditions were as follows.

Curing temperature	=	85 °C $\pm$ 0.5 °C
Pressure	$\simeq$	350 psi
Curing time	$\simeq$	2 to 3 hours
Relaxation time	$\simeq$	30 hours

Fig. 10.13 and 10.14 show the set ups for monitoring the properties and making these backings according to this new approach.

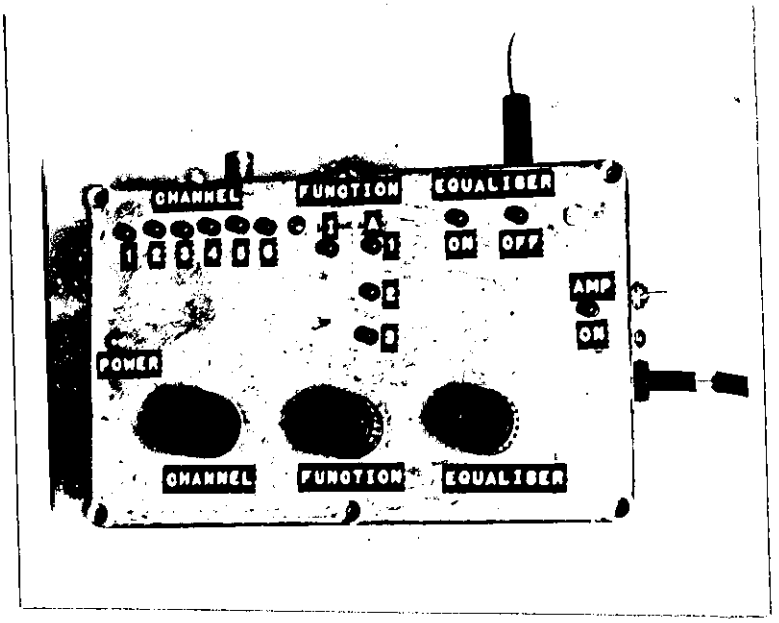

Fig. 10.13 THE EQUIPMENT MADE FOR CONTROLLING AND MONITORING THE ACOUSTIC PROPERTIES OF THE BACKINGS.

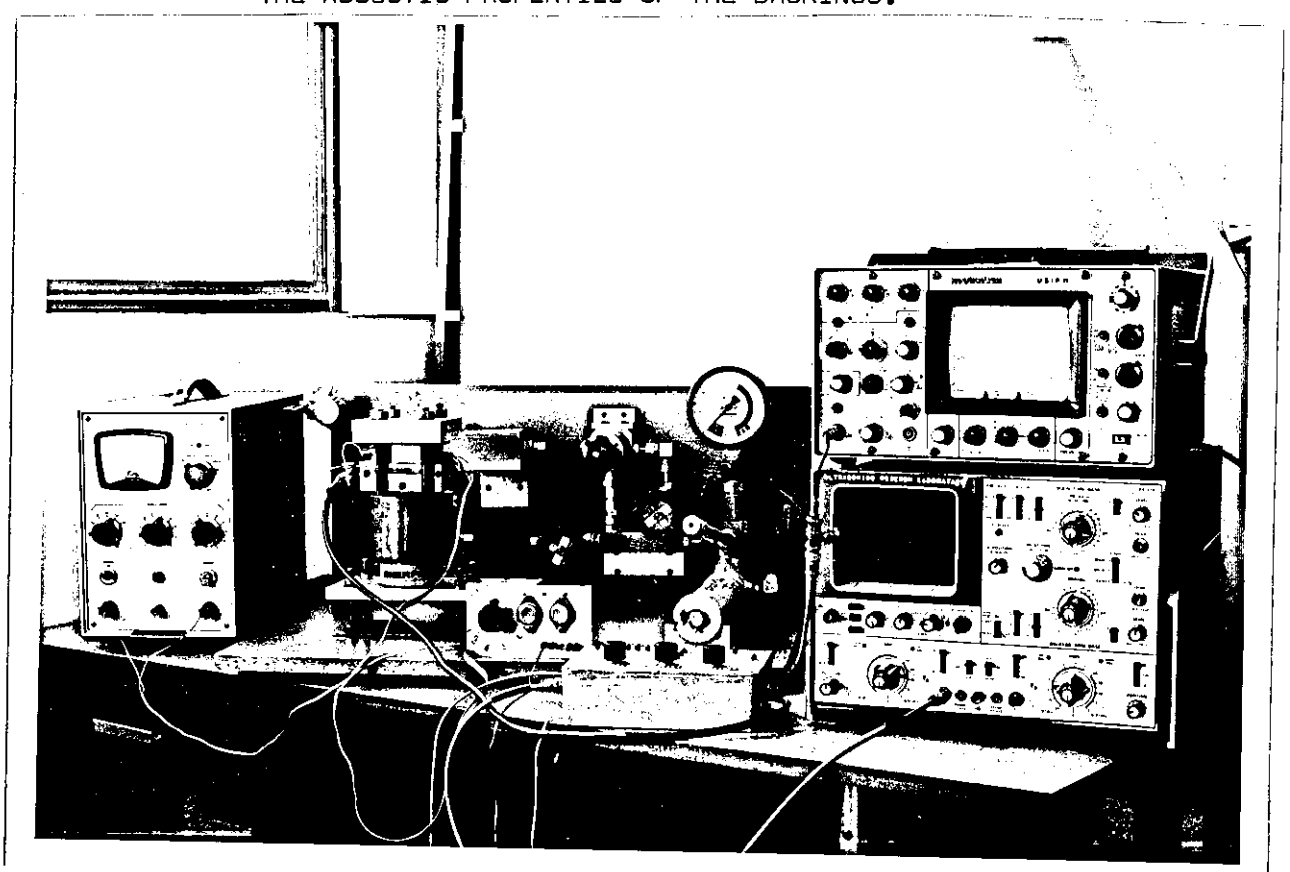

Fig. 10.14 THE NEW APPROACH OF MAKING HIGH QUALITY TRANSDUCER BACKINGS

As there is provision to make adjustments to correct non-uniformities when detected by the ultrasonic monitoring system, the backings made in this way gave much superior uniformity and performance. In the case of an amalgam backing mercury plays an important dual role, i.e. as a sensitve ingredient to control the acoustic properties as well as in structural bonding of the slug. The addition of slow setting epoxy in this case is mainly to modify the attenuation characteristics. Therefore there is a great deal of flexibility in achieving the required overall properties compared to the conventional tungsten araldite backings.

However, one of the most difficult problems with the dental amalgam is that it hardens too quickly leaving very little time to prepare the mixture correctly and to transfer in to the mould to start the process. Also it was noticed that the components of the dental powder were not the most favourable with respect to the required end results although it was good enough for the purpose. It is worth mentioning at this stage that as mercury amalgamates with a large number of metals and alloys, there is the possibility to make even better backings with other alloy materials having more favourable acoustic properties and slower amalgamation rate than dental amalgam.

10.4.2 Bonding material and bond layers

As mentioned before, this was the most critical subject to be dealt with. Experiments carried out with glass samples suggest that addition of small amount of fine grain high density metallic powder to epoxy gives some improvements in the acoustic properties of the bond line. These improvements are to be expected according to eq. 10.11 which in effect means a relaxation of bond line thickness due to a possible increase in the acoustic impedance. However, on the contrary, when tungsten powder is added in larger proportions, the performance gradually dropped in spite of the increase in acoustic impedance of the bond material. This could well be due to the inability to achieve small layer thickness as a result of an increase in viscosity of the epoxy mixture. Also these bonds tended to be very patchy. Hence it is not possible to improve the

performance of a transducer meaningfully in this way.

However, an interesting method was developed to achieve higher bond line impedance without leading to higher layer thickness as follows. Firstly, the surfaces were prepared until the roughness of the mating surfaces were comparable with the size of the particles being added. Then tungsten powder (average particle size of approximately 0.5 microns) was lightly added taking care not to add too much to cause any significant increase in viscosity. This mixture was warmed to about 55 °C in partial vacuum for about 20 minutes. The crystal and the backing were also maintained at this temperature throughout. Then the epoxy mixture was applied to both the surfaces and brought into contact under moderate pressure. After this the backing was massaged with the crystal under pressure until at one point it was caught by the backing.

Since the surface roughness is comparable to the particle size, the hills and the voids of the mating surfaces offer greater resistance to the movement of the particles when the massaging is done. Therefore, a certain amount of filtering or separation of tungsten particles from epoxy within the bond layer can be expected, causing the tungsten particles to be deposited in the voids which would have otherwise been filled mostly with low density epoxy. The result is therefore, an increase in the effective impedance of the bond layer without increasing the layer thickness and hence the performance.

The sandwich is then allowed to cure at a fairly elevated temperature of about 70 °C and under pressure for about 6 hours and then allowed to cool down to the room temperature, but without releasing the external pressure. After the transducer is cooled, the pressure is released and the resulting transducer is left to relax for a period not less than 12 hours before being used in the next stage of construction. The reason for this period of relaxation is that the amalgam slug changes its properties significantly in re-heating operations and takes a considerable length of time to settle down.

Casting a backing on a crystal has also been tried as an alternative

approach, but it never gave good results anywhere near to that obtained by separately bonding the crystal to the backing as described above. This was mainly due to the uncontrollability and the patchiness of the bond layer formed and therefore the idea of casting was abandond.

On top of the backing a thick layer of tungsten loaded epoxy was added. The transducer was then cut right through including the backing with a high speed diamond impregnated saw, to form the required dimensions of the array element as obtained in Chapter 5. The crystals used were originally made with a small bevel along one edge (about 0.5 mm margin) so that very fine electrodes could be soldered to the front face of each element without leaving any protrusions above the plane of the crystal. Soldering was necessary for reliable operation and to prevent failures. However, the area available for soldering was very small (0.5 x 1 mm approx.) and also had to be completed within a time no more than a second making it a very strenuous task. Solder itself had to be first prepared by dissolving silver to near saturation so that the thin silver layer on the element is not dissolved away within the time of soldering. According to the author's experience, conductive epoxy and silver paints are not suitable for making connections to the array elements as they lower the reliability of the probe array. Furthermore, if used as bonding adhesives they often degrade the efficiency and the performance significantly.

After making the arrays, the elements were individually tested for performance. The earlier arrays made by conventional techniques showed a great deal of variability, low bandwidth and high failure rate. Figs. 10.15(a) to 10.15(d) show the gradual improvements achieved by developing this new process of transducer construction presented in this chapter.

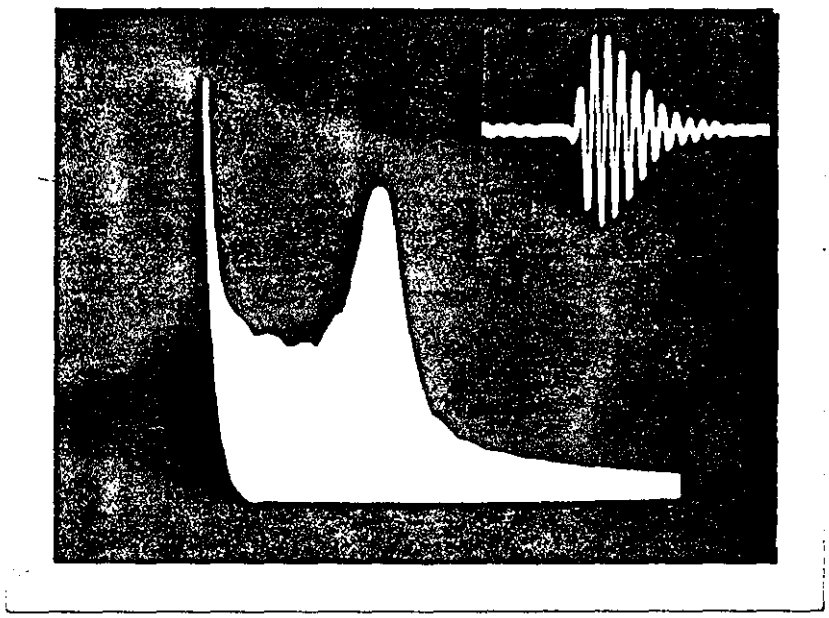

(a) UNBACKED TRANSDUCER ELEMENT (2 MHz)

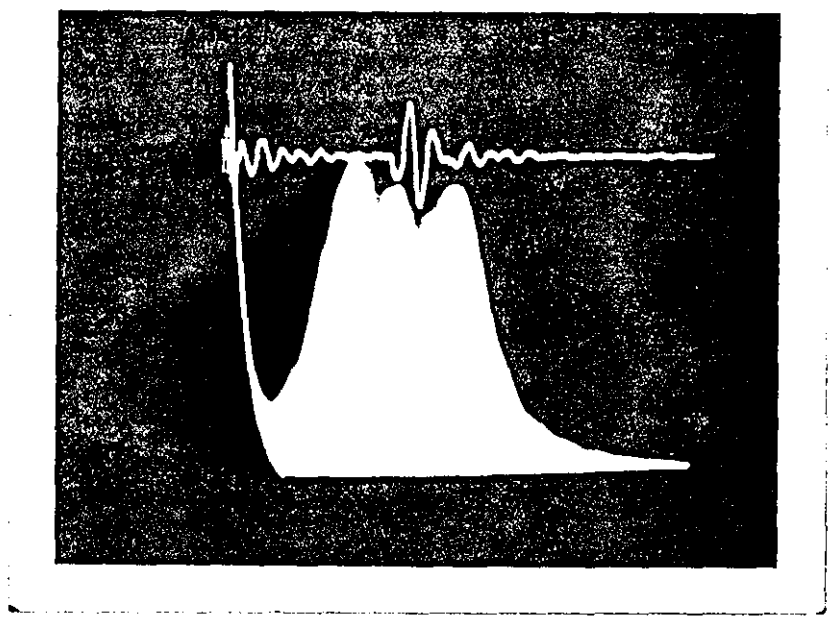

(b) ARRAY ELEMENT BACKED BY TUNGSTEN ARALDITE (conventional approach)

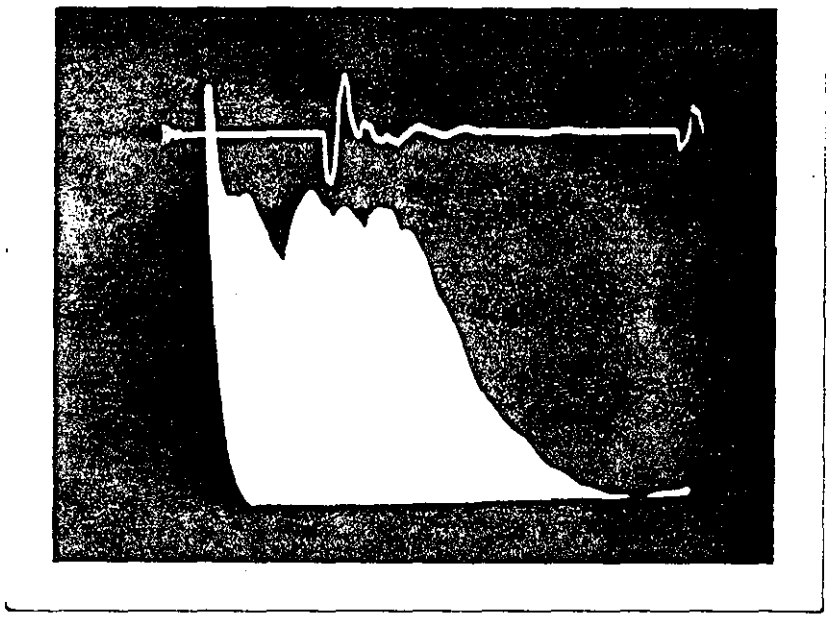

(c) NEW APPROACH - AMALGAM BACKING (conventional bonding)

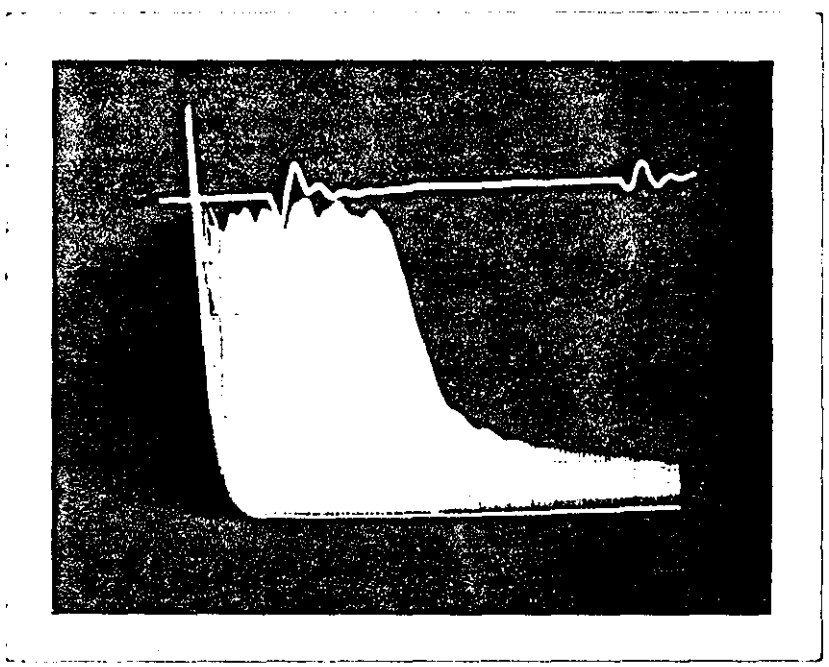

(d) NEW APPROACH - AMALGAM BACKING (bonding as described above)

Fig. 10.15 BRIEF COMPARISION OF TRANSDUCER PULSE PERFORMANCE
(conventional technique vs new technique)

In the case of the receiving array, a protective surface layer is necessary. Thin sapphire plates may be used for this purpose, but as it was not possible to obtain them in time, a thin aluminium shim was bonded in a similar fashion as described above to go ahead with the feasibility study. This was not necessary for the re-transmitter array. However the problem with the re-transmitting array was to make and maintain the curvature accurately as even a slight error dramatically degraded the performance. The earlier re-transmitting arrays showed unacceptable changes in curvature with ambient temperature variations. This was later eliminated by applying a bond material along a sector on the upper part of the assembly which provided just the right amount of expansion to counteract the changes. Figs. 10.16(a) and 10.16(b) show a straight receiving array of 30 elements and a curved re-transmitting array with 15 elements constructed by this process.

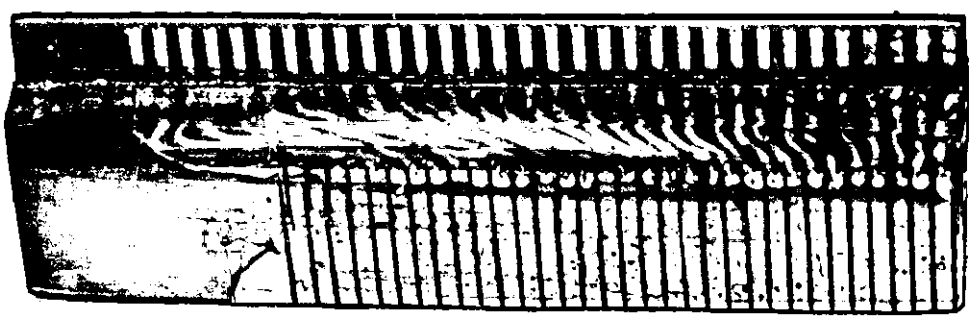

1

(a). A HIGH QUALITY 2 MHz RECEIVING ARRAY OF 30 ELEMENTS

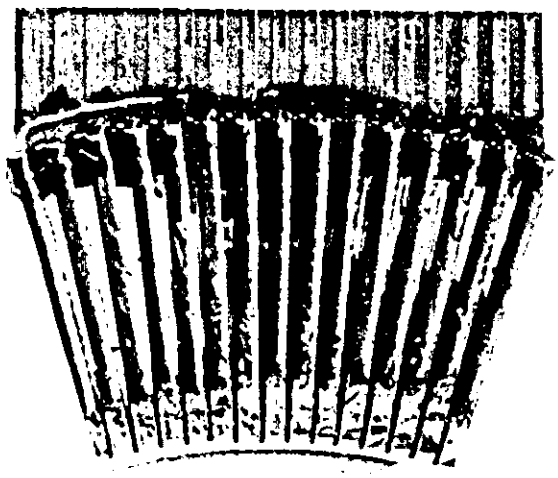

(b). A HIGH QUALITY 2 MHz, 15 ELEMENT RE-TRANSMITTING ARRAY

Fig. 10.16 HIGH PERFORMANCE TRANSDUCER ARRAYS DEVELOPED ACCORDING TO THE NEW TECHNIQUES, WITH STANDARD EDGE CONNECTOR PLUG IN ASSEMBLY

It is worth mentioning here that, although the techniques adopted were only briefly described, all the stages of making these arrays to the required specifications were extremely involved and time consuming. Until an array is finally completed, tested and proved to be operating satisfactorily, catastrophe could occur all the way to the end particularly due to the constraints set by the tight specifications and the uniformity required. However, the improvement in performance achieved by the development of these new techniques was overwhelming. Some idea may be gained by comparing a set of images of the same object produced by the system with the new and the earlier arrays as shown in Fig. 13.3. This in effect justifies the theoretical estimation of array parameters carried out earlier for the present purpose and the construction techniques developed to achieve the expected end results.

10.5 CONCLUSIONS

The problems concerning the performance and construction of transducers with particular emphasis on arrays were analyzed using equivalent circuit models. It was found that in the case of a backed transducer, the properties of the bond and the bond line thickness between the transducer and the backing have critical influence on the performance of the transducer. Variations of the bond line properties has been identified as the main cause of variability between transducer elements in an array. The practical difficulties involved and the ways of improving the bond line properties have been discussed.

It was also noticed that in the case of arrays, the length of the backing medium that can be used is more restricted than for ordinary transducers due to inter-element capacitive cross-coupling. Hence the impedance vs. attenuation characteristics of the backings are of a more concern in the construction of wideband transducer arrays. In this respect, it is found that better compromise can be achieved by using materials other than conventional tungsten loaded araldite backings. One such material found was the dental alloy amalgam mixed with slow setting epoxy in appropriate proportions and made under closely controlled process conditions. Non-conductive backings have also been developed using aluminium oxide powder. If the right particle size is used, these backings have potential use particularly in high frequency arrays and/or at low width to gap ratio of the elements.

It was also found that whatever the material used in the construction of backings, closely controlled process conditions are essential to achieve the desired properties and uniformity. For this purpose, special techniques for monitoring the properties of the backings while they are being made was successfully developed.

The far superior performance of the arrays developed according to this new approach is demonstrated and the results justify the analytical and constructional techniques adopted.

- CHAPTER 11 -

DESIGN AND CONSTRUCTION OF ELECTRONIC CIRCUITS

This chapter briefly presents the essential design and construction details of wideband amplifiers, power supply and several other electronic circuits including indicator, control and protection. Most of these components were first built for the purpose of feasibility study followed by further development towards the construction of a working prototype.

11.1 INTRODUCTION

Apart from the difficulties already faced in the design and construction of various parts of the system as described in the previous chapters, the design and successful operation of the electronic circuits to the required specifications were also very involved. Breaking into high frequency oscillations and thermal problems were more than usual when the power amplifiers were assembled in the system. Hence to avoid building the basic functional elements of the system over and over again and to ensure fail safe operation, various protective measures had to be taken. However, much of these complications could be avoided in the design of a final system when the problems involved have been studied through the assembly of the first prototype.

11.2 Design and construction of amplifiers

Several amplifier designs have been tried since achieving the required specifications were difficult due to many constraints. Not even the physical size of the amplifiers could be ignored in this case as the assembly of 30 amplifiers can become unacceptably bulky. Furthermore, if care is not taken, it may even introduce significant differential phase errors as a result of excessive differences in connecting cable lengths. For example, each one meter difference in cable length between

two channels leads to about 3.6 degrees phase difference between the two. On the other hand, having a considerable power dissipation, the amplifiers cannot be packed too closely due to difficulty of heat extraction. Besides high frequency interference problems may also lead to instabilities.

Considering the time, money and various other constraints, the configuration as shown in Fig. 11.1 was designed and built. This design requires only a small number of readily available components which helped to keep the cost below £20 per channel. Although some relaxation in specifications with respect to terminal impedances had to be made, these amplifiers were acceptable to proceed with the feasibility study. The idea at the time was to change over to G^* amplifiers in the final stage of the system design.

Fig. 11.2(a) shows the p.c.b. version of these amplifiers while Fig. 11.2(b) shows a thick film version, but using standard components, developed with the aim to achieve a greater number of channels within a given space. Thick film circuits were more difficult to develop in this case due to high frequency layout and heat dissipation problems. However, after developing the thick film version, there were not enough funds to produce a complete set of amplifiers due to a rise in the thick film component price. Therefore the p.c.b. version was adopted.

Having completed the construction of the above amplifiers, 15 of them were assembled in a main frame and the feasibility of the proposed system was demonstrated for the first time using a laboratary bench type set up. The results of this study will be presented in the next chapter together with the results obtained from the first working prototype to compare the vast improvements made by the development of the new array technology, improved optics and the overall design of the system. Apart from establishing the conceptual validity of the system, this feasibility study was particularly useful in identifying the areas of improvements required in the design of the first imaging system.

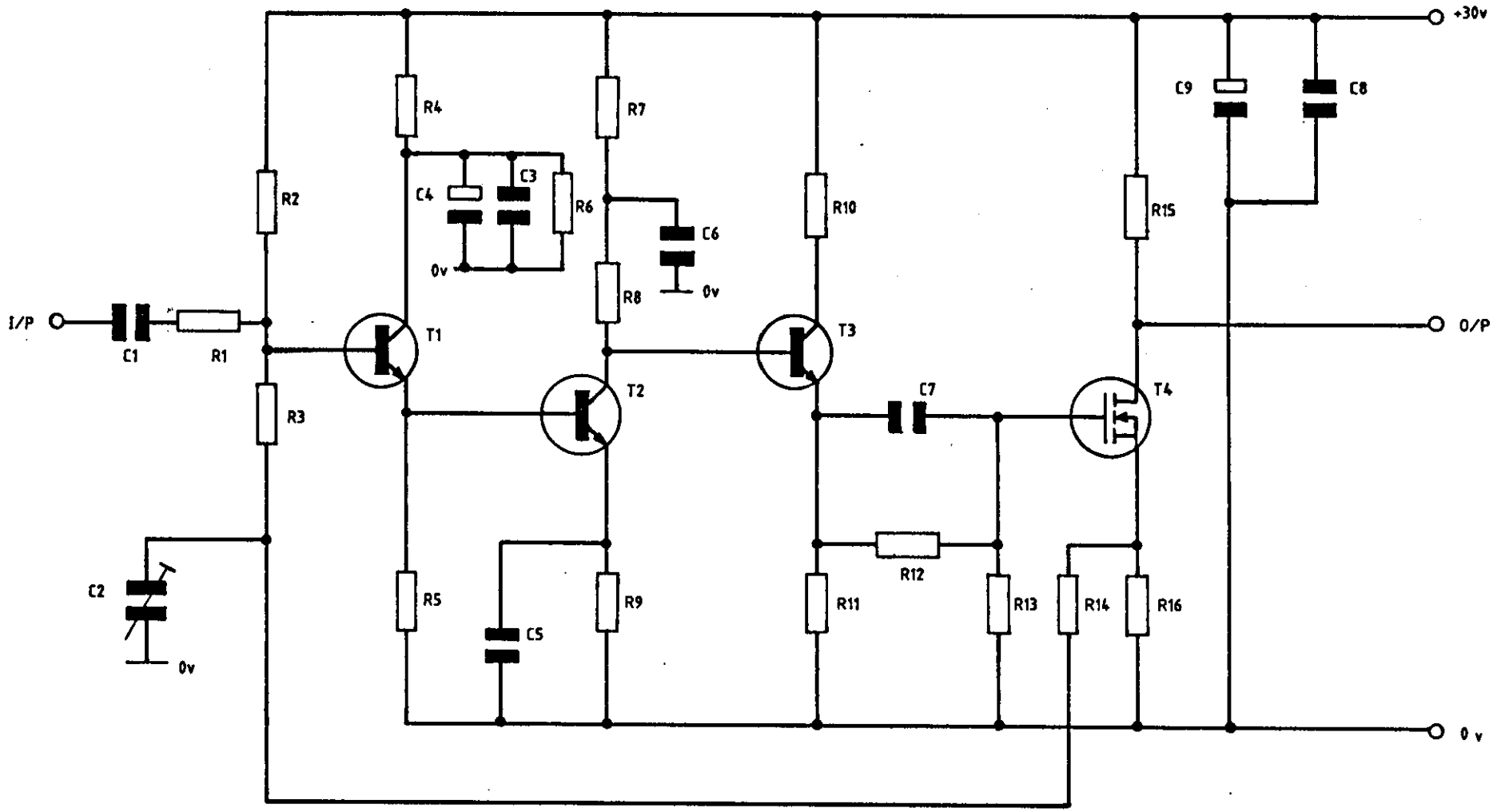

FIG.11.1 CHANNEL AMPLIFIER CIRCUIT DIAGRAM..

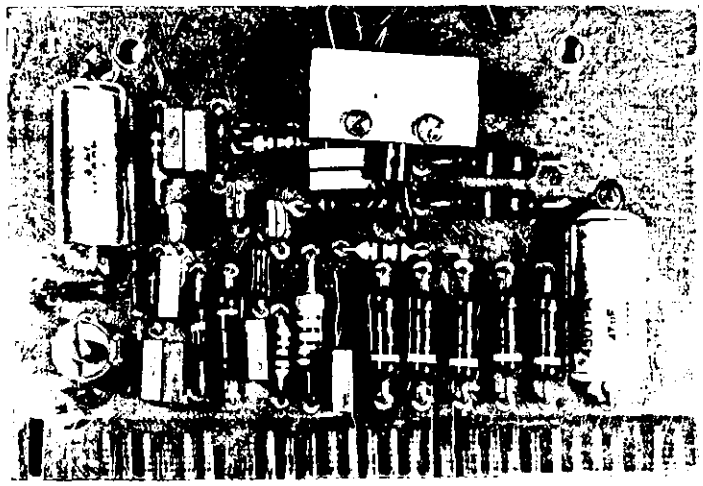

1

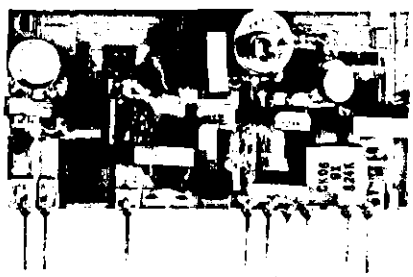

2

Fig. 11.2 CONSTRUCTION OF CHANNEL AMPLIFIERS. - (1) Standard p.c.b. version. (2) A thick film version

COMPONENTS LIST

Resistors

R_1	=	180	0.025 W
R_2	=	270 k	"
R_3	=	4.7 k	"
R_4	=	1 k	0.5 W
R_5	=	680	0.025 W
R_6	=	1 k	"
R_7	=	100	"
R_8	=	2.7 k	"
R_9	=	22	"
R_{10}	=	330	0.5 W
R_{11}	=	130	"
R_{12}	=	68 k	0.025 W
R_{13}	=	270 k	"

Capacitors

C_1	=	2 F	50 V	ceramic
C_2	=	2 - 10 pF		trimmer
C_3	=	1 F	50 V	ceramic
C_4	=	47 F	35 V	tantalum
C_5	=	2 F	50 V	ceramic
C_6	=	1 F	50 V	ceramic
C_7	=	2 F	50 V	ceramic
C_8	=	1 F	50 V	ceramic
C_9	=	47 F	35 V	tantalum

Transistors

T_1	=	ZTX 320

R_{14}	=	1.8 k	0·025 w	T_2 =	ZTX 320
R_{15}	=	94	~3 W	T_3 =	ZTX 314
R_{16}	=	8.2	1 W	T_4 =	VN 10 KM (V-MOS FET)

One of the problems with the above amplifier being a small unit, the thermal conduction from the power stage to the rest of the circuit was rather excessive. Also due to overall feedback and wide bandwidth the tendency to oscillate was fairly high. Also it was not possible to separate the receiving probe array from the amplifiers over a considerable length due to capacitive loading and the attenuation of the received signals degrading the sensitivity and the bandwidth performance. Furthermore, the need to increase the output voltage swing to enhance the effective dynamic range as predicted in Chapter 7 was evident. Therefore in order to overcome these difficulties a new design was made where the amplifiers were separated into three miniature stages and used in cascade. Also local negative feed back was adopted in the designs rather than overall feedback. This approach also helped to interchange different designs more easily to asses their suitability. The three separate modules were :

1. Pre-amplifier module
2. Inter stage amplifier module
3. Power amplifier module

11.2.1 Pre-amplifier module

The use of the preamplifiers in this case was mainly to match the transducers to the cables and to provide sufficient gain to compensate for the attenuation losses in the cables over a considerable distance. A useful facility that had been incorporated was transceiver mode of operation so that the receiving probe array could be used as the transmitter as well. A problem with the transceiver mode amplifiers in general is the dead zone, for example 5 μs is typical in commercial amplifiers. An advancement in the new design is that a dead zone of typically less than 0.5 μs was achieved with an input protection

up to 1 kV insonifying pulses and a bandwidth in excess of 60 MHz.

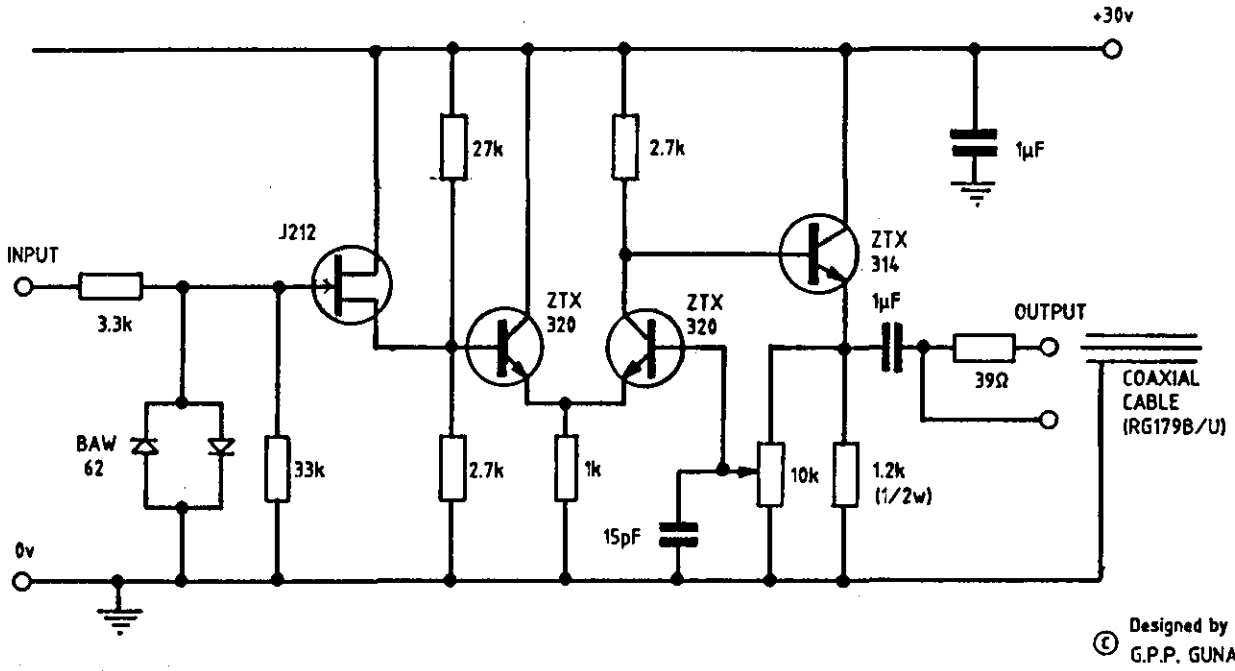

Fig.11. 3. ARRAY HEAD AMPLIFIER CIRCUIT DIAGRAM

The primary specifications and ratings are as follows.

1.	Gain	=	8.5 dB
2.	Input impedance	=	37 k // 3 pF
3.	Output impedance	=	10 Ω or 50 Ω , (selectable)
4.	Bandwidth	=	over 60 MHz at 3dB
5.	Input protection	=	upto 1 kV
6.	Dead zone (Tx/Rx)	=	0.15 - 0.5 µs (typical), 1.25 µs (max.)
7.	Maximum undistorted output	=	~ 2 V
8.	Supply voltage	=	+ 30 V
9.	Supply current	=	25 mA
10.	Operating temperature	=	75 °C (max.)

When all the channels were assembled as shown in Fig. 11.4, it was small enough to be clipped on to the operators lower arm. These amplifiers were also provided with channel select, impedance trimming and switch selectable transceiver mode facilities in the final assembly.

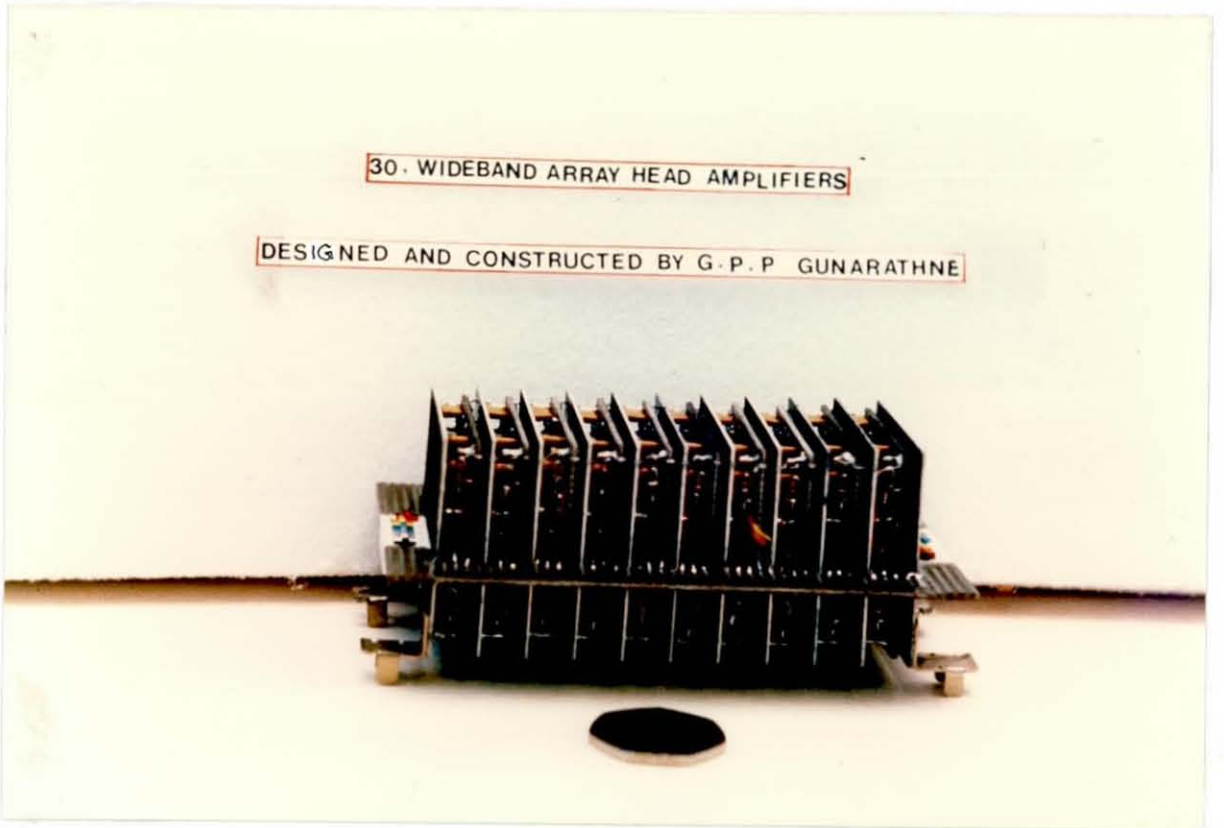

Fig. 11.4 THE ASSEMBLY OF 30 MINIATURE WIDEBAND ARRAY HEAD AMPLIFIERS

Although the above amplifiers were rated upto 75 °C, the assembly was fitted with overheat sensors to protect against any accidental damage. With these amplifiers, a cable length of upto 50 m (RG179B/U) can be used giving freedom for remote operation. Fig. 11.5 shows the modified arrangement for transceiver operation.

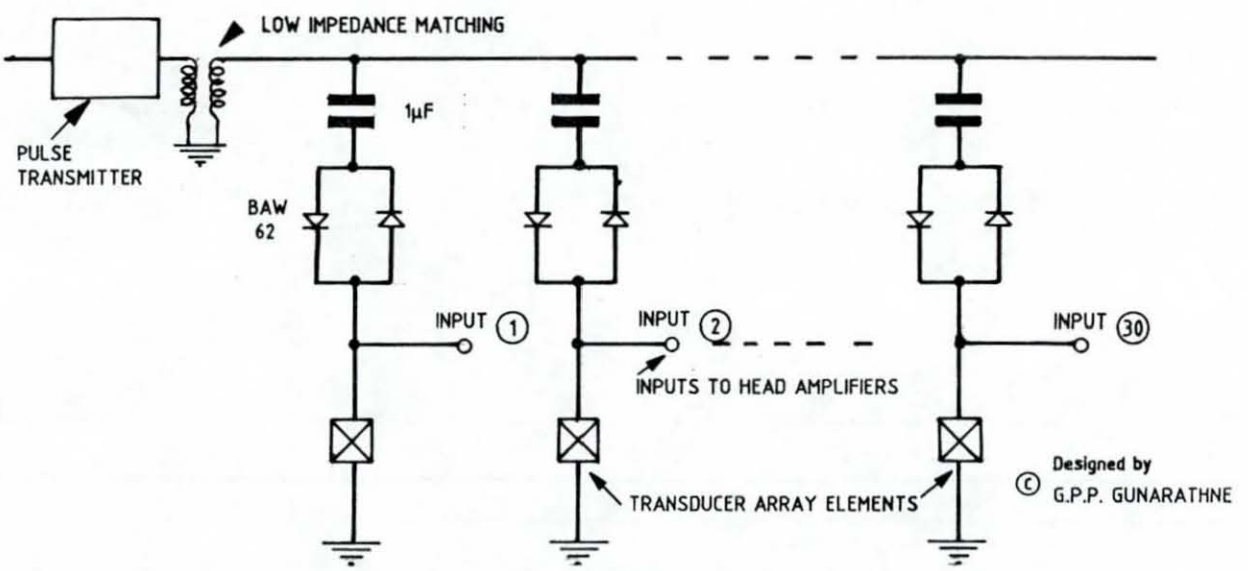

Fig.11. 5. CONFIGURATION FOR PARALLEL TRANSCEIVER MODE OF OPERATION

11.2.2 Inter-stage amplifier

The purpose of this stage is to provide sufficient gain and low output impedance required to drive a V-MOS power stage at high frequency and over a wide bandwidth. Also it is convenient to introduce in here variable gain as discussed in chapter 7 and also other facilities such as signal gating and modulation which will be useful in later experimentation.

However, for the feasibility study, variable gain facilities were not introduced due to the additional amount of work. The inter-stage amplifier circuit diagram and a thick film adaptation of this design are shown in Fig. 11.6 and 11.7.1 respectively. The p.c.b. version was better in terms of the high frequency response, but needed a little more space. In both these versions the circuit layout design was rather critical due to the high frequency wideband requirements as well as size and thermal dissipation aspects.

The primary specifications and the ratings of the above amplifier are as follows.

1.	Gain	=	24 dB
2.	Bandwidth	=	over 50 MHz
3.	Input impedance	=	50 Ohm
4.	Output impedance	=	10 Ohm
5.	Maximum undistorted output	=	16 V p.p.
6.	Supply voltage	=	40 V
7.	Supply current	=	50 mA
8.	Operating temperature	=	75 °C (max.)
9.	Dimensions (thick film)	=	1" x 2"

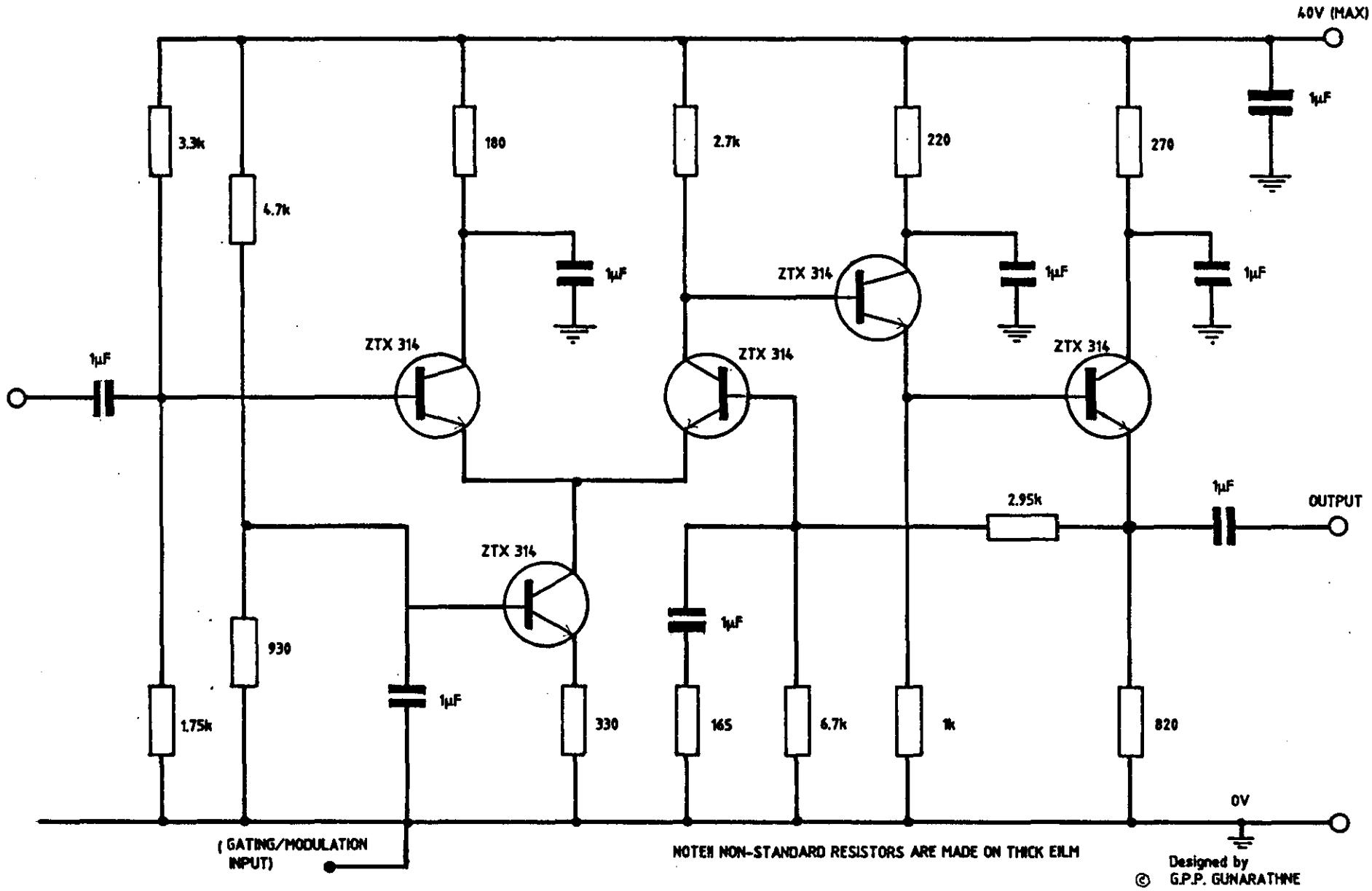

FIG.11.6 WIDEBAND INTER-STAGE (DRIVER) AMPLIFIER

11.2.3 Power stage

Array elements have to be driven at a low impedance of the order of 75 Ohm. Being a class A output stage, most of the power is dissipated in here with low efficiency and heat extraction problems when all the 30 channels are assembled. Therefore it is an ideal place to introduce G^* amplification (chapter 7). The G^* may be implemented in different ways and in combination with other circuits where duty cycle operation is applicable to save power and cost. As the active elements are now operating in a power switched mode, (not simply signal gating), the devices can withstand much higher currents during the ON period and therefore the output requirements can be satisfied with a fewer number of stages, making the design cheaper but far more efficient. Therefore G^* has the greatest potential in low duty cycle applications such as in most ultrasonic instrumentation and sonar. Fig.11.8 shows the circuit diagram of a G^* configuration designed for the present purpose.

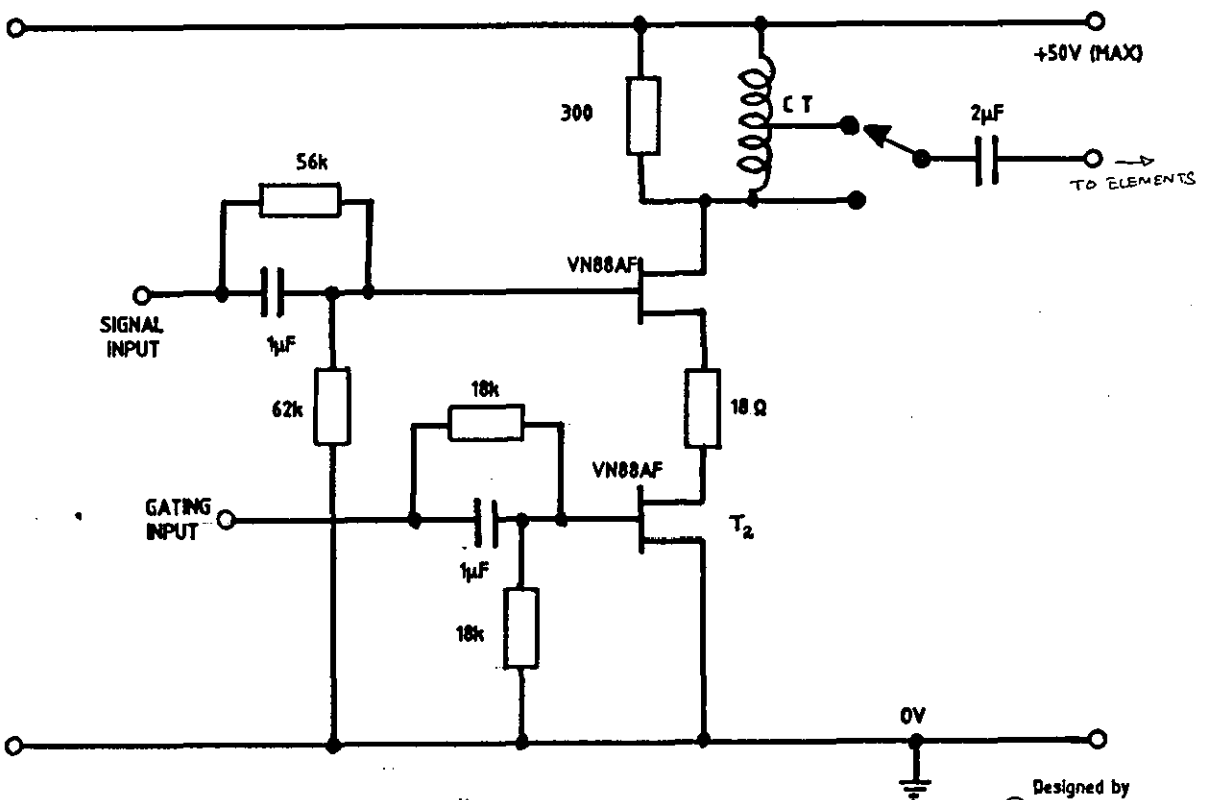

FIG.11. 8 A G^* POWER AMPLIFIER STAGE

In the above circuit, TR is an auto transformer of bifilar construction using a high frequency ferrite ring core (Ferelex "P" grade) with the winding shunted by 300 Ohm to give an output impedance of 75 Ohm, required to damp the transducer elements correctly as discussed in Chapter 7. The biasing and coupling to the driver is established by the capacitve/resistive network at the input of the V-MOS power FET, T_1. Power switching is accomplished by the V-MOS FET T_2 in the lower chain which is driven with the appropriate sequence as shown in Fig. 7.13.

When T_2 is fully switched on, it can be replaced by r_{DS} (on) presenting a total source resistance of the order of 20 Ohm to T_1 and the output stage first responds in a way similar to a pulse amplifier. Timing is arranged according to Fig.7.13 such that when the drain voltage returns to Vss, the echo signals are received by the amplifier. During the 83 μs signal period, this G^* stage behaves as a class A amplifier, except for its ability to handle much higher power levels compared to an ordinary continuously driven amplifier.

When the stage is switched off, another pulse is produced due to the free-wheeling action of the transformer. Since these pulses are coherent in all the channels, they have the effect of producing a straight line schlieren image at the beginning and the end of the field. These are by no means a problem in this case as they can either be arranged to fall outside the field of the image or deliberately allowed in the field of view as ultrasonic markers, indicating the top and the bottom of the test object. In the latter case, the switching speed of T_2 is adjusted such that there is only a little spectral energy around 2 MHz so that the resulting markers are not excessively bright. Fig. 11.7 (2) shows a thick film version of this amplifier.

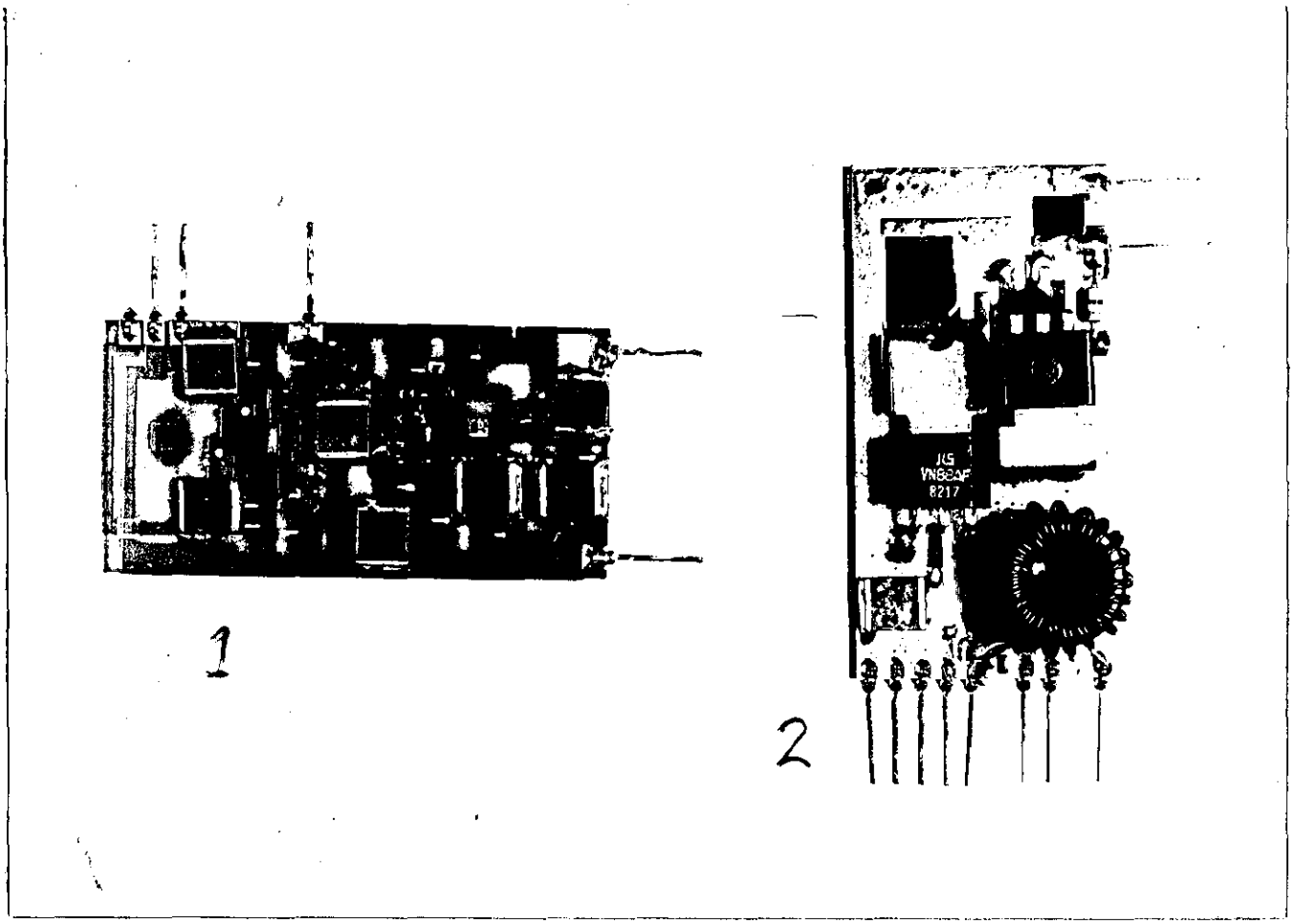

Fig. 11.7 THICK FILM IMPLEMENTATIONS. (1) INTER-STAGE (Driver)
(2) A G* AMPLIFIER STAGE

The specification of this stage are as follows

1.	Gain	=	17.5 dB
2.	Bandwidth (source impedance 10 Ohm)	=	26 MHz at 3 dB
3.	Input impedance	=	62 k // 50 pF
4.	Output impedance	=	75 Ohm or 300 Ohm selectable
5.	Max. undistorted output	=	45 V pp
6.	Max. rep. rate	=	2 kHZ at 30% duty cycle
7.	Supply voltage	=	50 V d.c.
8.	Operating temperature	=	75 °C Max.
9.	Dimensions	=	1" x 2" x 0.5" , (on thick film)

The modifications to the basic imaging system if the above three stage amplifiers are to be used are shown in Fig. 11.9.

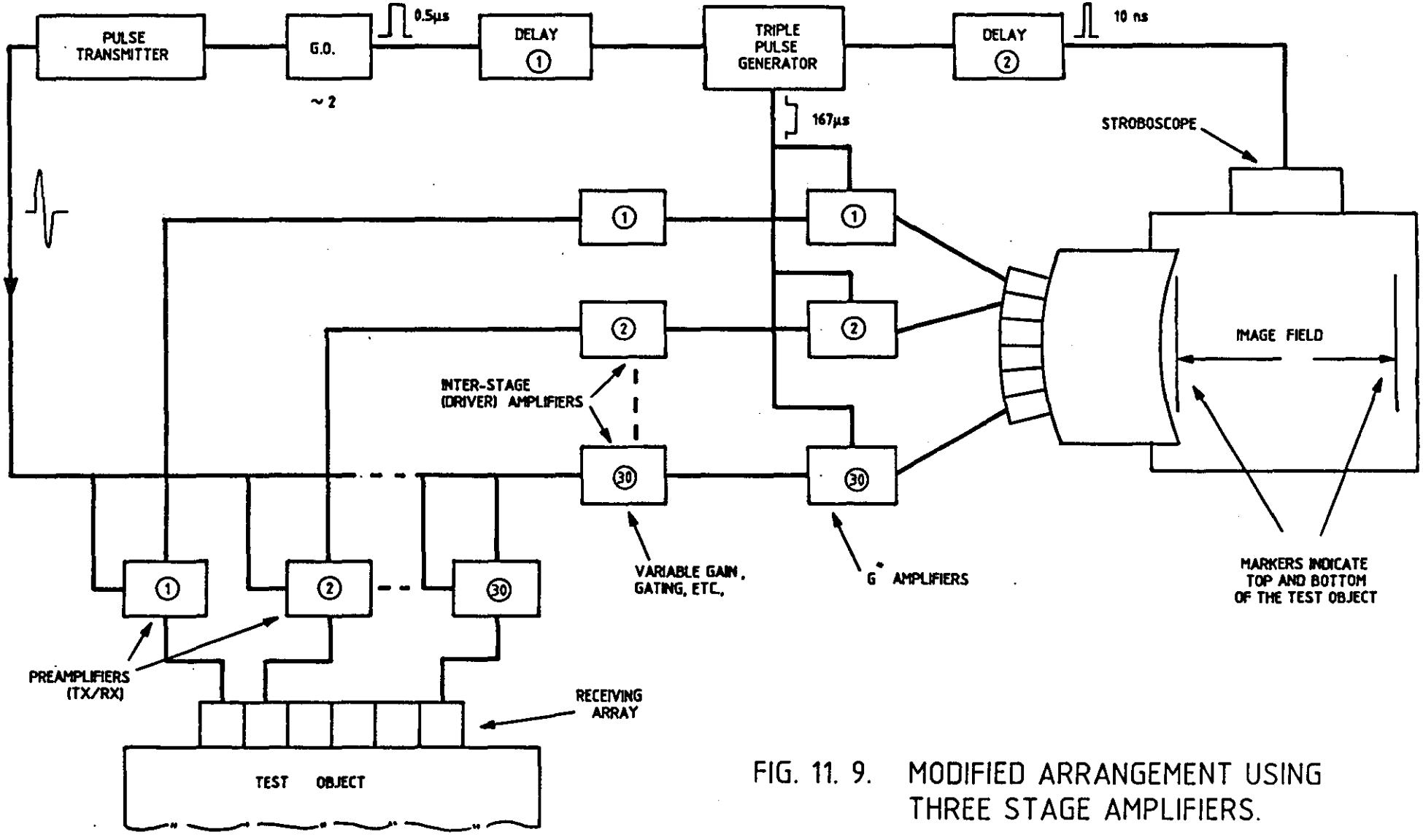

FIG. 11. 9. MODIFIED ARRANGEMENT USING THREE STAGE AMPLIFIERS.

However, after the completion of the design of the above three stage amplifiers, there were not enough funds to make a complete set of 30 units except the set of pre-amplifiers. Therefore the system had to be designed with pre-amplifiers and the earlier set of class A amplifiers made for the feasibility study. However, provisions were made in the design of the system to accommodate the new amplifiers, if sufficient funds were received before the completion of the project.

11.3 POWER SUPPLY DESIGN

The main requirements of the power supply were as follows

1. 30 V , 8 A
2. 50 V , 500 mA
3. 11.5 V , 100 mA
4. 15 V , 1 A
5. 5 V , 0.75 A

In addition to good regulation, the supply impedance at high frequencies had to be kept low, particularly on the 30 V and 50 V supply lines. Hence, apart from satisfying the nominal power requirements, the general layout was also an important consideration.

After a market survey it was found that purchasing power supplies to meet the requirements cannot be done mainly on the grounds of cost. Hence a tailor-made design was called for. First the possibility of designing a switched mode power supply was examined with the aim to reduce the size and achieve higher efficiency. However, it became clear that the cost and the amount of work involved in designing a suitable switched mode power supply would be considerably more than building a conventional power supply unit. Also the residual high frequency interference in the case of a switched mode power supply could lead to undesirable effects in the present application. Hence a conventional power supply was designed. A small ready made Harwell power supply unit was already available at the time which was also modified to supply a few boards to reduce the demands on the main power supply unit.

Although not needed in the design of a final system, many protection circuits had to be incorporated to avoid catastrophic failures during the assembly of the first prototype system. The design is such that in the event of a failure such as an accidental short circuit or overheat etc., the power supply is automatically switched off and indicate the fault on a panel of LEDs. Fig. 11.10 shows the basic supply arrangement and Fig. 11.11 shows a schematic circuit diagram of the main power supply unit.

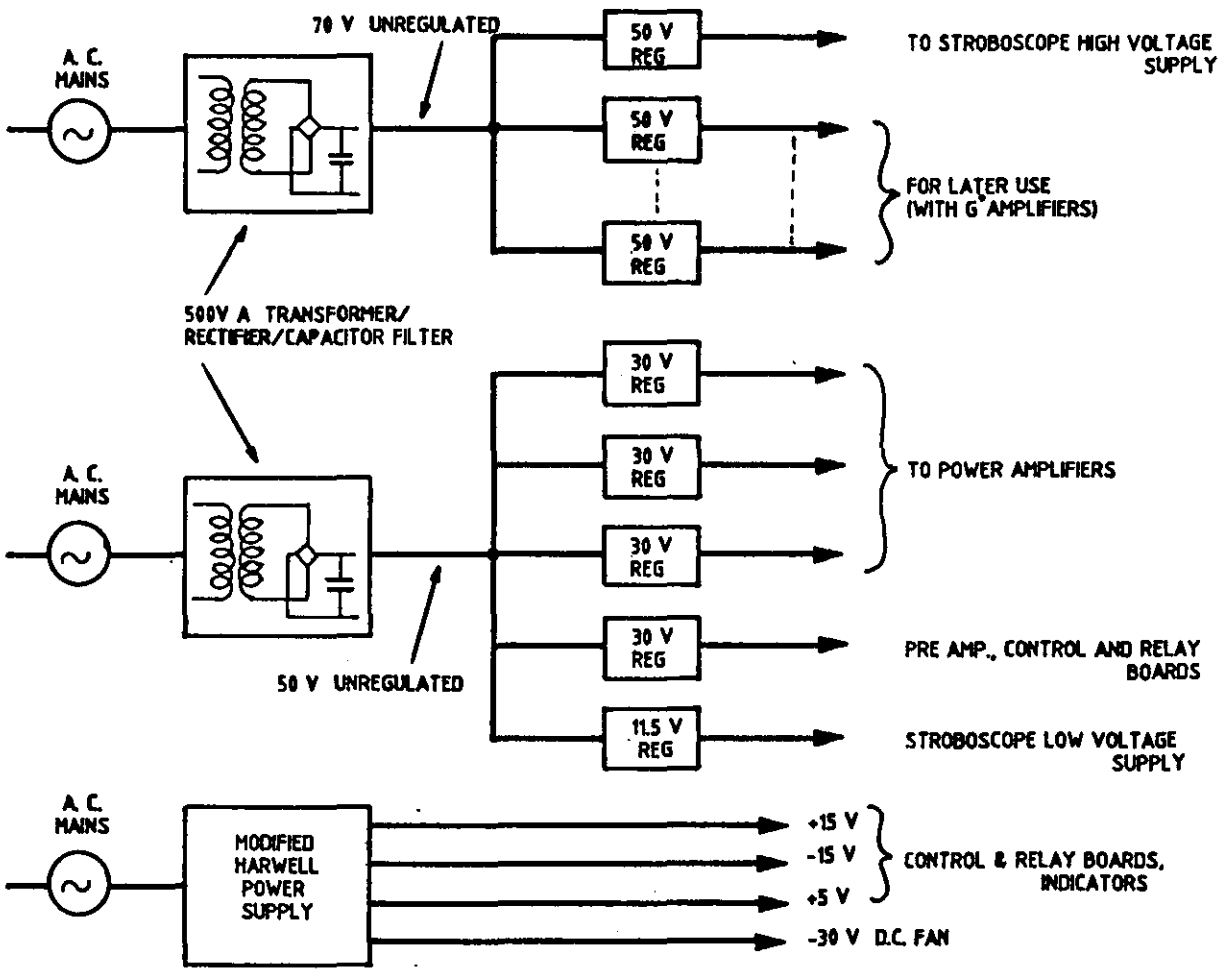

FIG. 11. 10. SUPPLIES TO VARIOUS PARTS OF THE SYSTEM

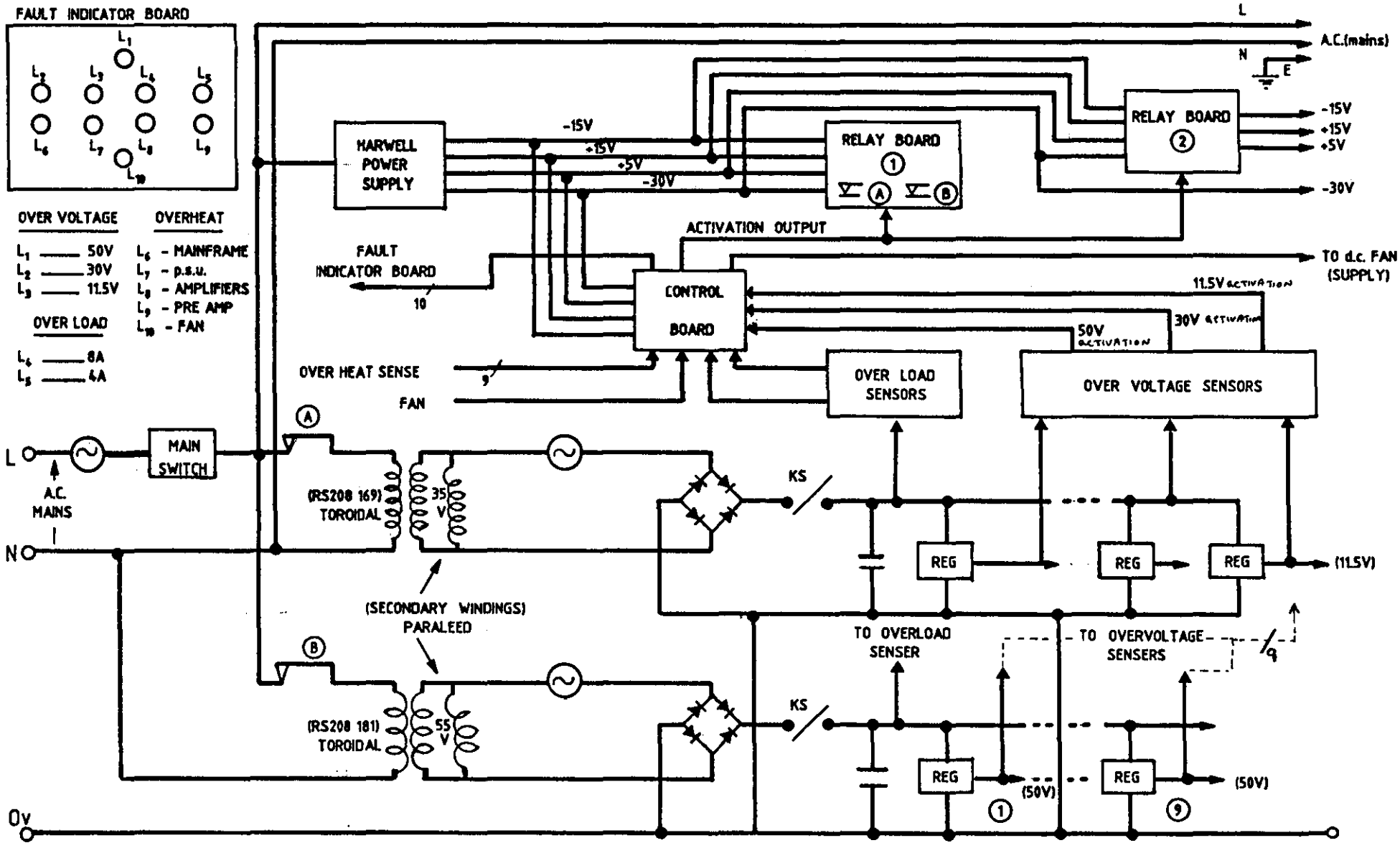

FIG. 11.11 MAIN POWER SUPPLY UNIT

Fig.11.12 shows the front panel layout of the power supply.

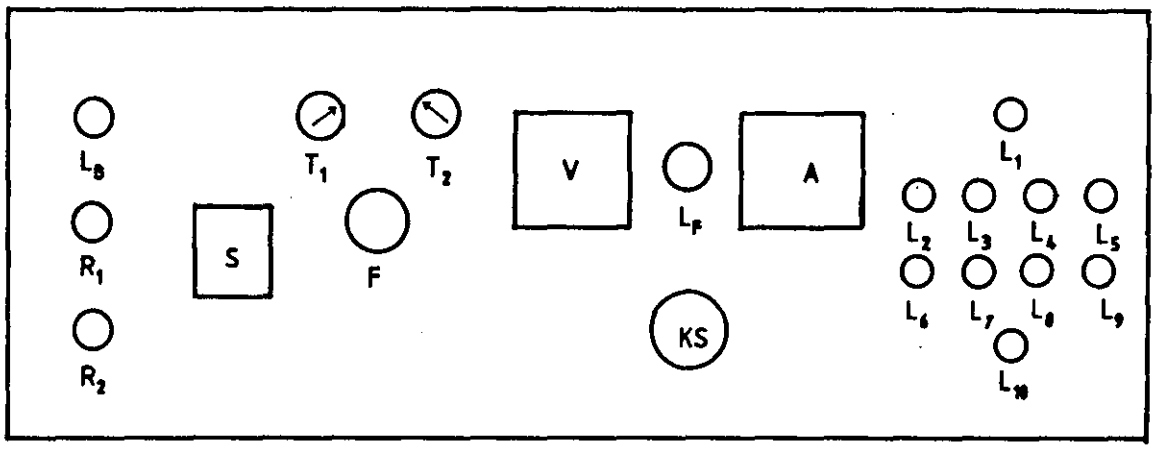

The main functions of the front panel components are as follows.

Component	Description	Function
S	Mains switch	Switches on the supply including the Harwell module
KS	Key switch	d.c. ON/OFF to the main frame
F	Main fuse	Isolate a.c. mains
R_2	Re-set button	Re-sets relay (2)
R_1	Re-set button	Re-sets relay (1) and (2) (re-sets the main power supply)
L_B	Bi-colour L.E.D.	red - fault exist green - fault cleared
L_F	Flashing L.E.D.	Visual alarm
T_1 , T_2	Potentiometers	Over-load trip set for the two main supply lines
V	Volt meter	indicate the input voltage to 30 V regulators
A	Ammeter	indicate the total current drawn from the 30 V supply lines
L_1 - L_{10}	L.E.D. (LATCH) indicators	indicate faulty conditions in the system as described before

11.4 OTHER CIRCUITS DESIGNED FOR THE SYSTEM

11.4.1 Frequency control and counter circuits

Trimming the frequency of operation was found to be useful during the feasibility study to achieve optimum results. The sinusoidal pulse was generated by a voltage controlled oscillator (Harwell 95/01582/6). Voltage sweep necessary for this module was obtained using a linear high stability potentiometer connected between + 5 V and earth. The operational frequency was monitored on an 8 digit LED display using a frequency counter built into the system. The design of this frequency counter and the frequency control arrangement are shown in Fig. 11.12.

11.4.2 Stroboscope protection

Many pulse generators produce a stream of spurious pulses just after switching on or switching off from the mains. Such pulses are not normally visible on a CRT due to their shortness of existence, but long enough to damage the stroboscope almost instantly. This was also the case with the pulse generator used in the system (Lyons PG 71). Therefore some protection had to be provided. This was achieved by delaying the supplies to the stroboscope through a relay network giving sufficient time for the transients to die down (Fig. 11.13).

Although the input is grounded within a short time, this protection alone is not always adequate to prevent damage in the event of a mains failure. This is to be improved at a later stage, preferably by designing a tailor-made pulse generator for the present purpose.

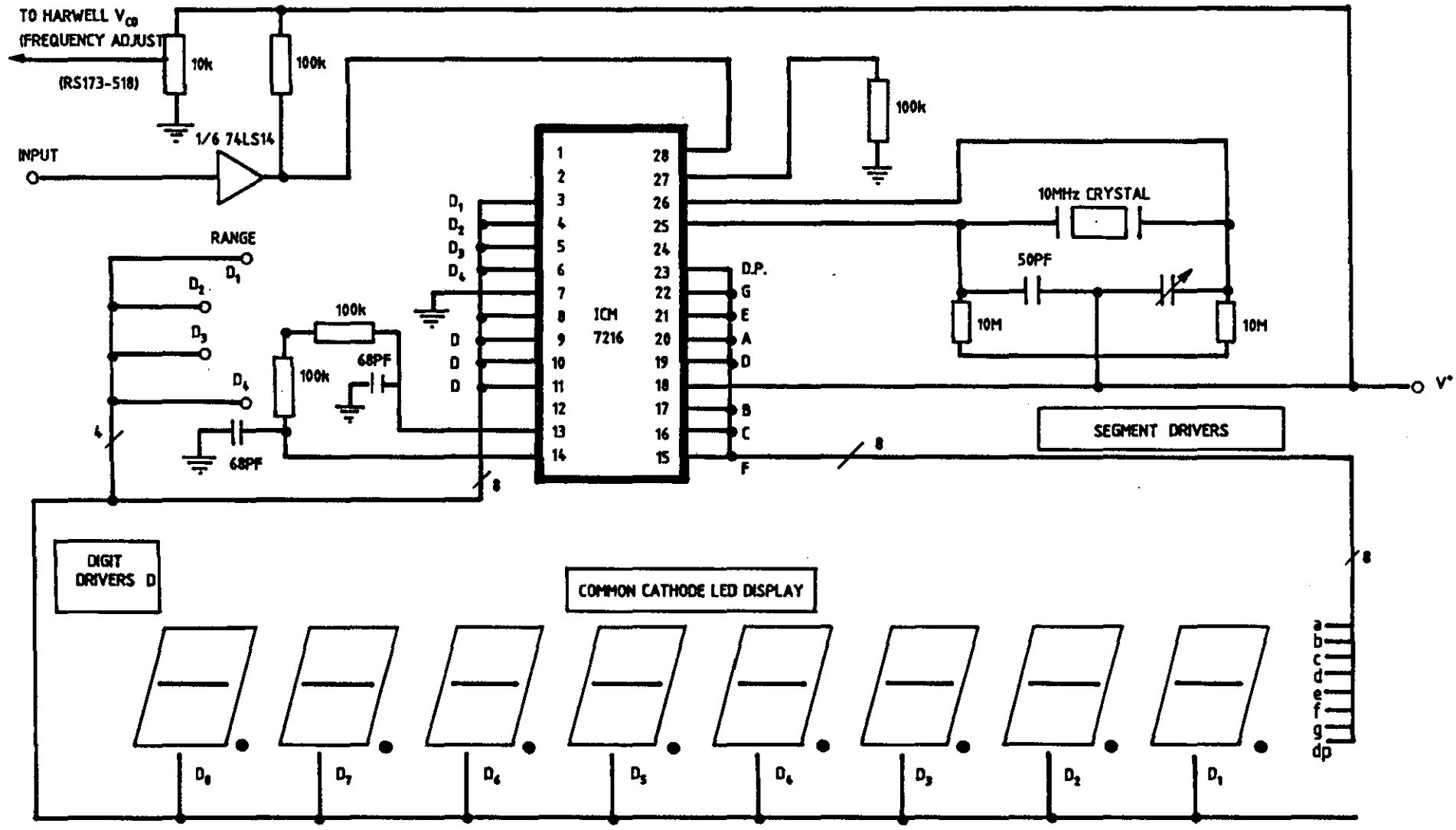

FIG. 11.12 FREQUENCY CONTROL AND COUNTER CIRCUIT.

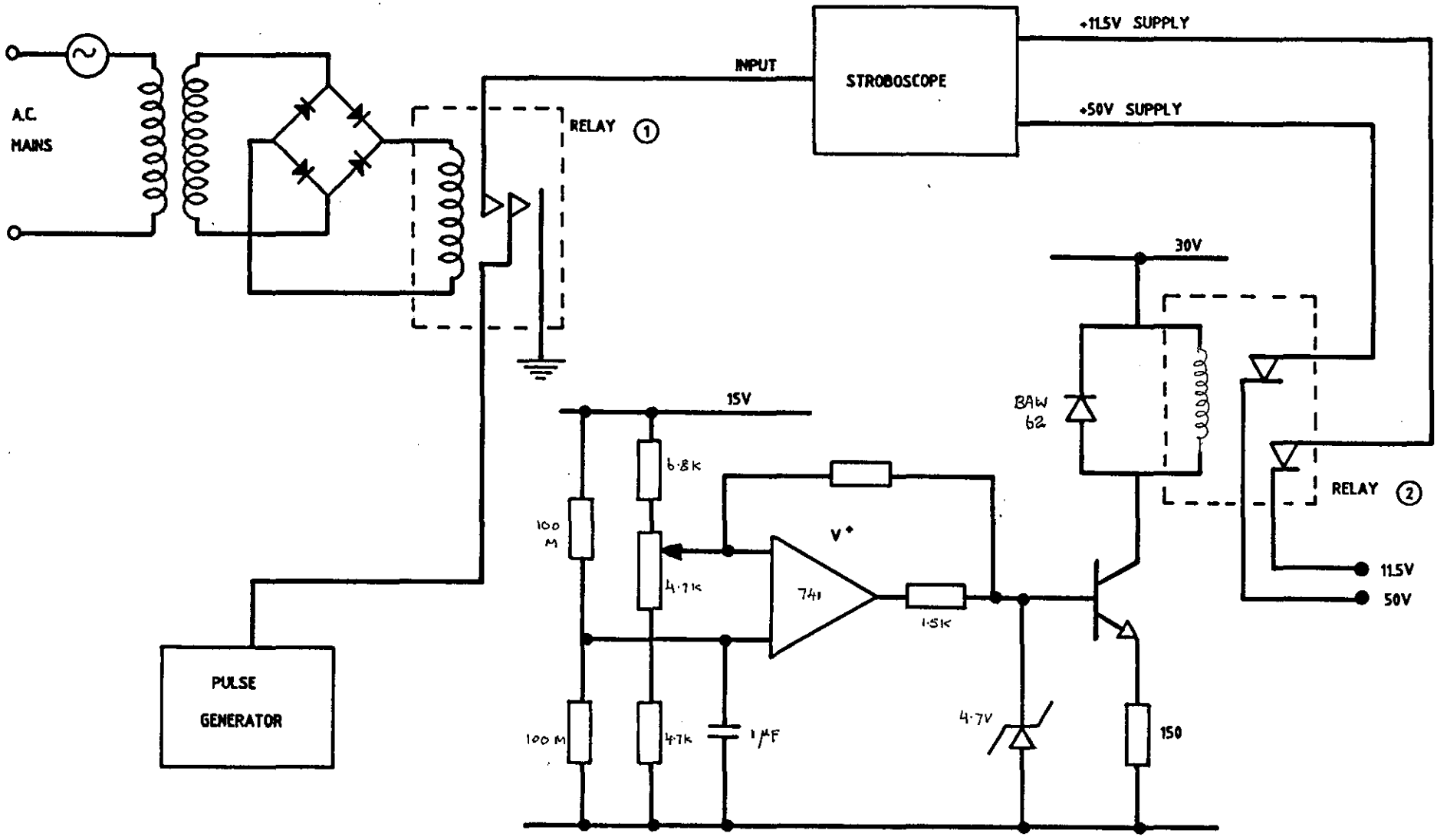

FIG. 11.13 STROBOSCOPE PROTECTION CIRCUITS

11.5 CONCLUSIONS

Electronic and electrical circuits necessary for the feasibility study and the assembly of the first working prototype, including amplifiers, power supply, control and protection, frequency monitoring and control etc. have been successfully designed. A future system can be considerably compacted and made more efficient by adopting the G category of amplifiers whose performance and suitability in this application was established. These amplifiers may also be useful in other low duty cycle applications, particularly in battery operated systems. The thick film adaptation of the three stage amplifiers with the optional transceiver operation facilities, as discussed, offer even greater flexibility and better performance.*

Extra care must be taken in the assembly of high frequency wideband and pulse circuits due to the possibility of high frequency instabilities and heat dissipation problems.

--- // ---

- CHAPTER 12 -

THE ASSEMBLED NEW IMAGING SYSTEM

This chapter deals with the general assembly of the first working prototype imaging system to be used as a practical instrument in the industrial environment. Ergonomical aspects have also been considered as far as possible in the overall design of the system.

12.1 INTRODUCTION

Apart from the work that has already gone into the development of various building blocks of the system, the influence of the non-ideal conditions of an actual testing environment, such as vibrations, ambient light, electrical noise etc. must be avoided as far as possible by appropriate design techniques. Due to the limitations of time and resources not all the requirements could be met at this stage except the most essential areas as outlined below.

12.2 ASSEMBLY OF THE SCHLIEREN OPTICAL SYSTEM

This is one of the most crucial areas of the present system because schlieren instruments normally require precision mounting and adjustments. This also means that they are vulnerable to vibrations. Hence kinematic mounting and rugged construction were essential.

Optical disturbances such as dust accumulation on optical elements, stray light from the environment or unwanted internal reflections are the common difficulties faced in the design of a high sensitivity schlieren system. Nagy described a technique by which the background illumination of schlieren systems could be considerably reduced. Here a close circuit TV system is used with a camera consisting of an image orthicon video tube which is operated in the form of a locking amplifier. However, the relatively low sensitivity of the image

orthicon compared to the newly developed camera tubes and the additional complexity of the circuits involved, do not make this technique attractive for the present application. Hence light tight construction was also essential.

On the other hand, the schlieren tank itself needs to be sealed while taking care of any expansion of the liquid due to the changes in ambient temperature. This was achieved by an integral design consisting of a schlieren tank built on the aluminium lens to which the re-transmitter array was bonded as shown in Fig. 12.1. The schlieren tank is filled with FC 75 and sealed with a layer of RTV rubber cast on the liquid surface without trapping any air. The design is such that the expansion of the liquid is taken care of by the deformation of this seal without rupture within a temperature range of 10 - 35 °C.

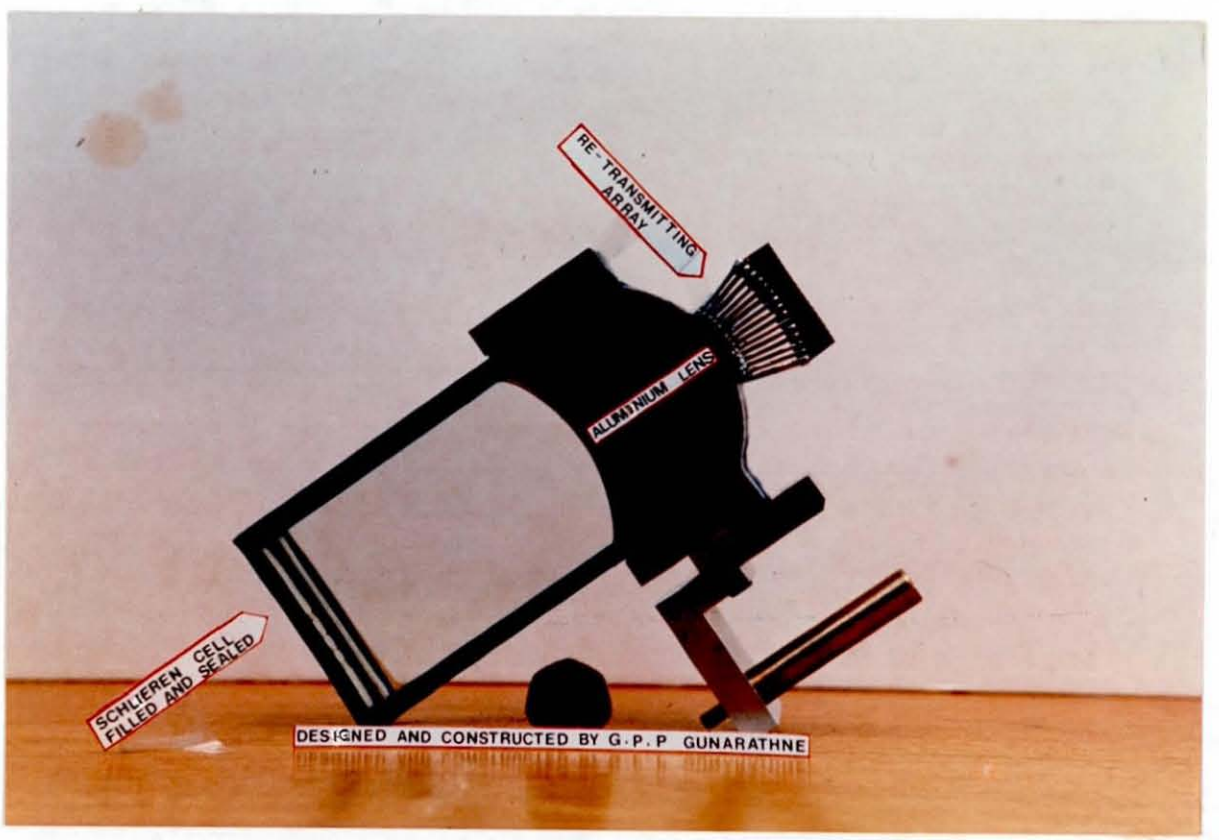

Fig. 12.1 THE SCHLIEREN CELL FILLED AND SEALED.
(50 p coin to compare the size)

The schlieren system itself was made very compact by the choice of a pair of wide aperture high quality camera lenses (focal length 80mm, aperture 1.2). The lenses were kinematically mounted on high precision optical railings to achieve precision adjustments and vibration immunity. All the necessary precision adjustment facilities were provided. In order to display the schlieren images on a closed circuit TV system, a small video camera (RCA TC 2014/UX) was fitted. If direct viewing is required, this camera can be easily removed and replaced afterwards without having to go through any elaborate adjustments again. The assembly of this compact schlieren system is shown in Fig. 12.2.

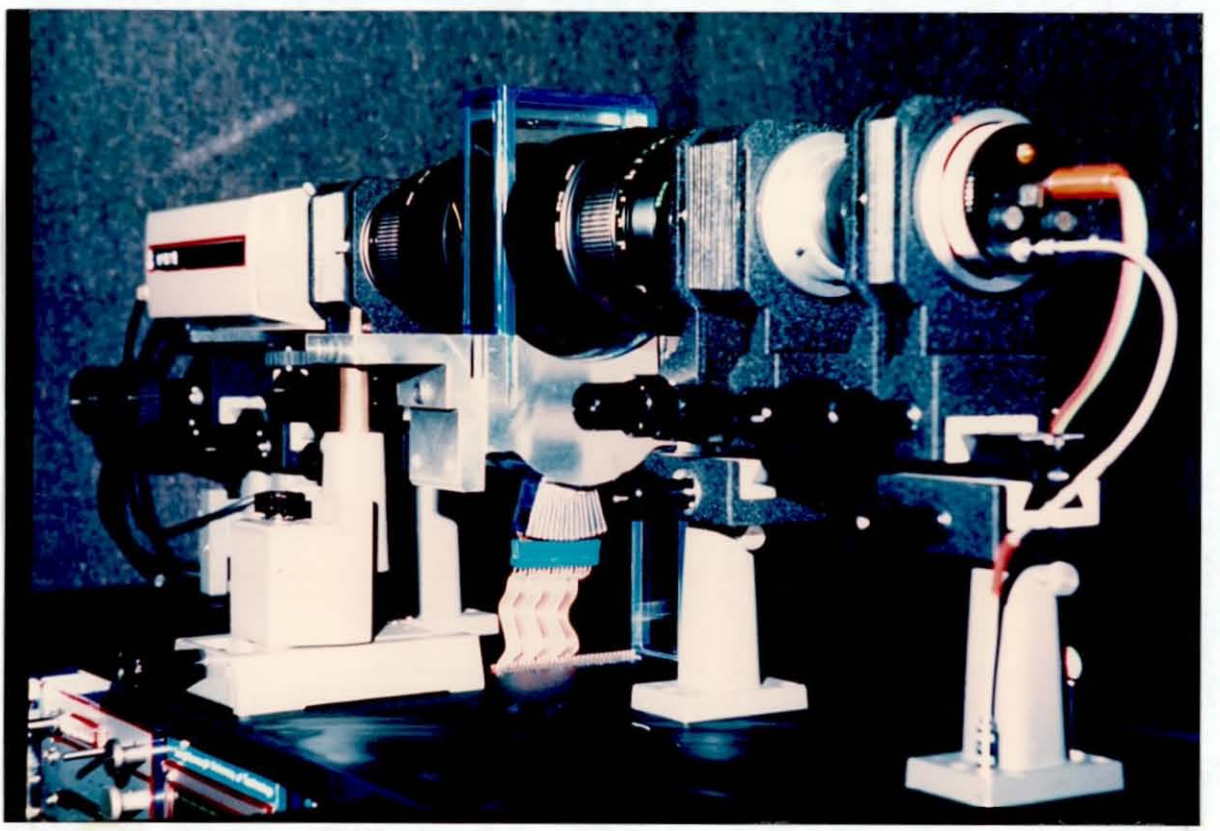

Fig. 12.2 THE ASSEMBLY OF THE SCHLIEREN OPTICAL SYSTEM

On the extreme right of the above photograph is the L.E.D. stroboscope mounted inside a lens cap. The slit controlling the light input and the knife edge filter on the other side of the second lens are all inside light-tight bellows. The design is such that no appreciable amount of ambient light gets into the optical assembly and hence the system can be

operated in full day-light without the need of any dark environment.

12.3 THE MAIN FRAME

The main frame is fitted with a dual pulse generator (Lyons PG 71) and all the necessary modules for generating a gated pulse of required duration and frequency, attenuator to control the output transmitter energy, frequency control and display, an A-scan display CRT, a 5" video monitor, power and signal sockets, the 30 channel power amplifiers, interfaces for external video equipments to record and display test results. The front view of the assembly is shown in Fig. 12.3.

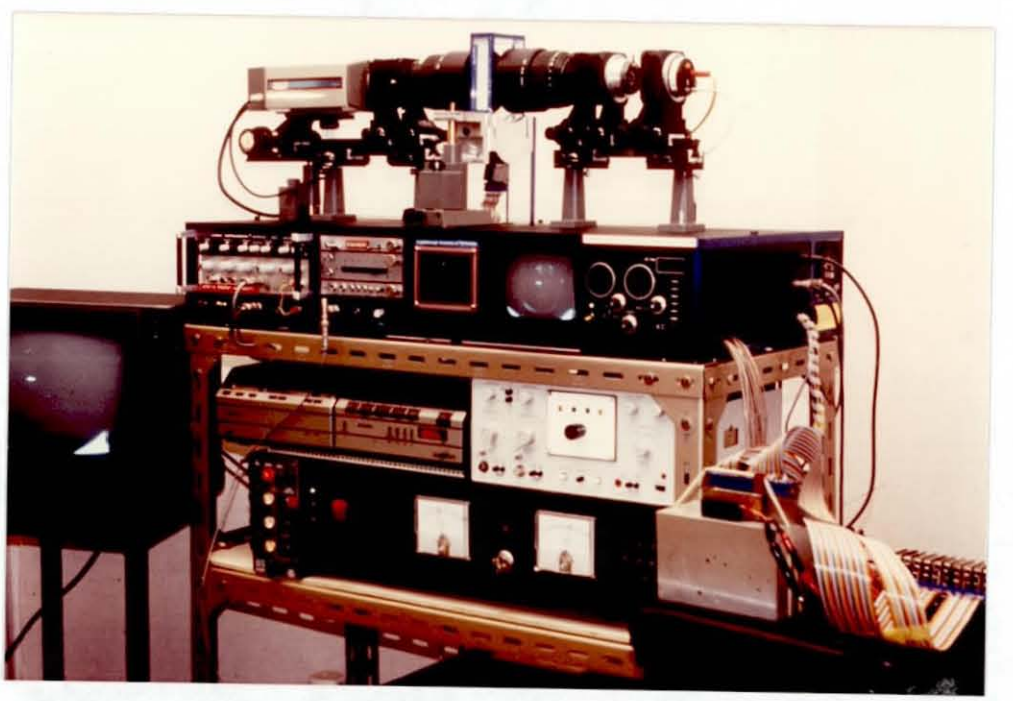

Fig. 12.3 FRONT VIEW OF THE NEW IMAGING SYSTEM

The power amplifiers are assembled in the back of the system and forced ventilation is provided by an extractor fan sucking air into the housing beneath each amplifier compartment. The rate of air flow is automatically adjusted to the inside temperature by a feedback control

network. This helps to prevent excessive reduction of output signal amplitudes as a result of thermal shut down properties of the V-MOS transistors. The assembly of the amplifiers is shown in Fig. 12.4.

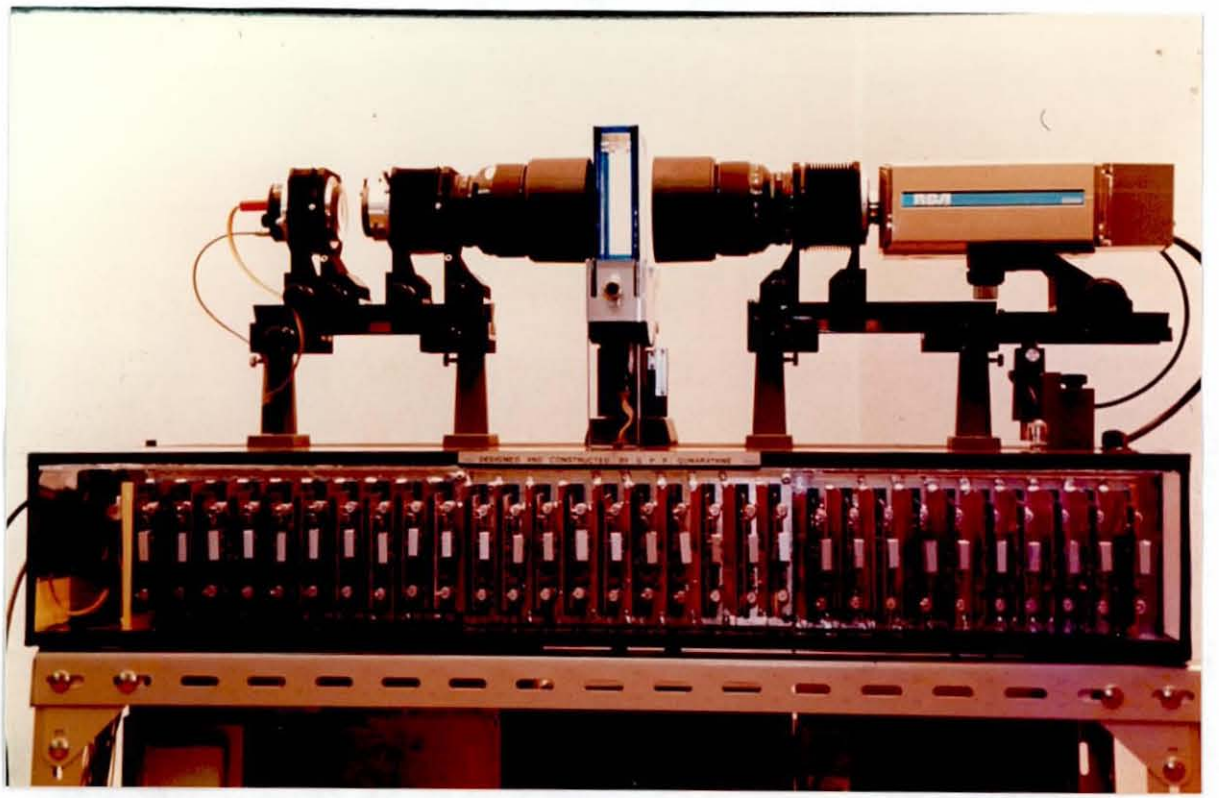

Fig. 12.4 REAR VIEW OF THE SYSTEM

12.4 *CONCLUSIONS*

Implementation of the new technique to suit the requirements and conditions of industrial testing environment has been a prime consideration. A key area of development which made it possible to utilize the full potential of this new technique outside the laboratory was the design and construction of a compact schlieren system incorporating a powerful L.E.D. stroboscope and a sealed compact schlieren cell. This assembly is insensitive to typical vibrations of all kinds experienced on a shop floor giving perfectly steady images. Furthermore, it can be operated in full daylight without the need of any dark environment. The general assembly of the whole system is such that

it can be conveniently operated with controls and displays ergonomically arranged to aid the operator. The overall dimensions of the first prototype assembly are 1 m x 0.5 m x 0.5 m. With further advances in the electronics already described and other constructional techniques, any future model can be comparable in size to that of a conventional flaw detector of the early type.

--- // ---

- CHAPTER 13 -

RESULTS AND CONCLUSIONS

This chapter presents the details of the operational procedure of the new imaging system followed by the results achieved. Its unique features and the areas of special applications are outlined. Prospective future development together with final conclusions are also presented.

13.1 INTRODUCTION

As mentioned in the previous chapter, care has been taken in the development of this new imaging system to promote its use effectively as a practical inspection instrument in the industrial environment. This was only possible as the result of developing all the different areas involved as separate building blocks giving due considerations to technical and ergonomical[45] aspects. Operation and manipulation of the system is therefore straightforward and the operational procedures with respect to the first prototype system are outlined below.

Performance of this new imaging system as presented later in this chapter reveals its unique capabilities in spite of the fact that it was the very first working prototype operating with only half the number of channels assembled.

13.2 OPERATIONAL PROCEDURES

Fig. 13.1 shows the system block diagram and Fig.A.2.1 shows a schematic diagram of the assembly except the schlieren optics. When testing, the receiving probe array is coupled to the test object with a liquid couplant such as oil or jelly. The initial settings to be ensured before switching on the system with reference to Figs. 13.1 and A.2.1 are given in Appendix 2.

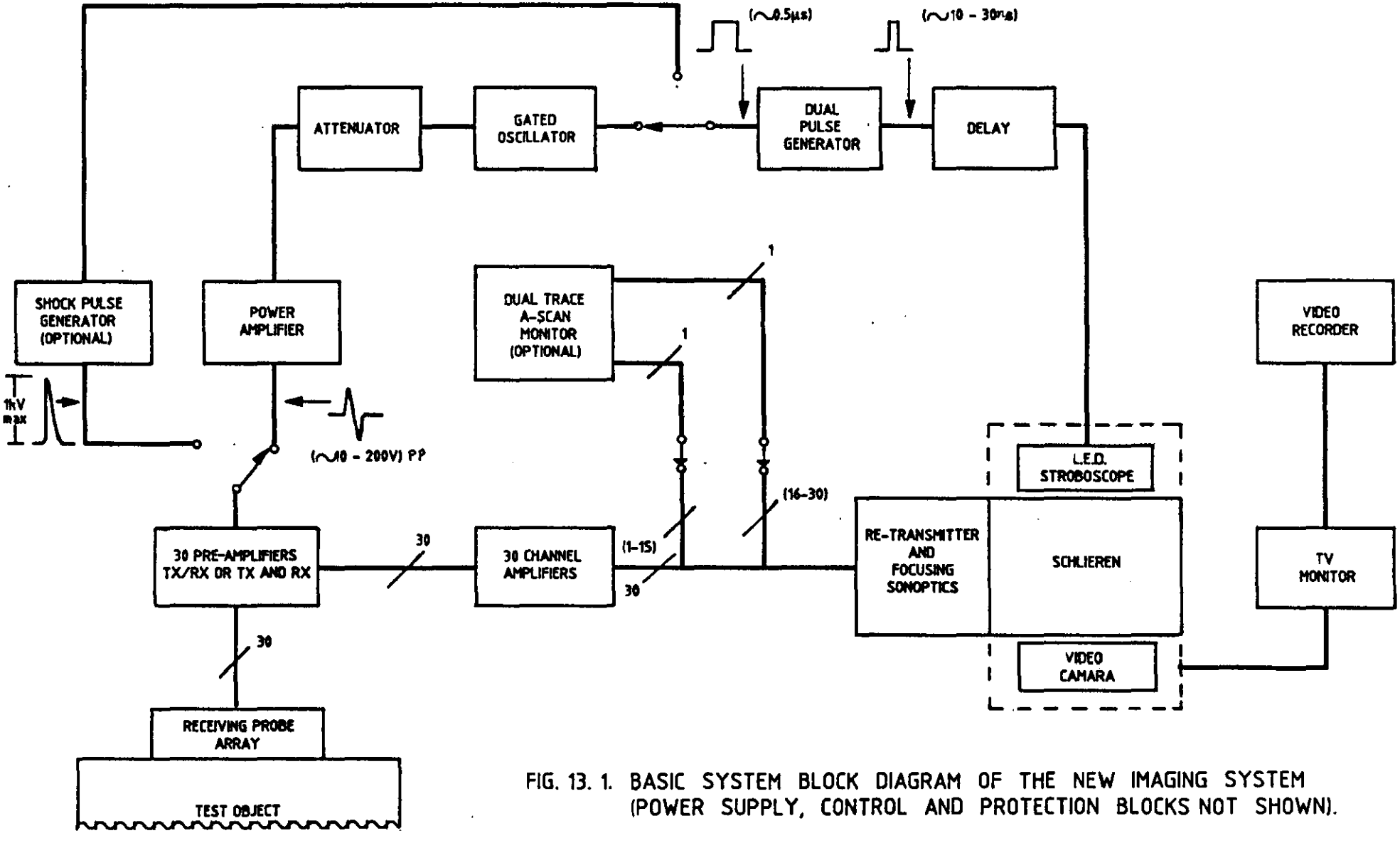

FIG. 13. 1. BASIC SYSTEM BLOCK DIAGRAM OF THE NEW IMAGING SYSTEM (POWER SUPPLY, CONTROL AND PROTECTION BLOCKS NOT SHOWN).

Either separate transmitter / receiver or transceiver mode of operation may be selected with the appropriate D.I.L. switches fixed on the array head amplifier module. It is also possible to use shock-excitation if required, instead of the gated sinusoidal excitation. However, as discussed in chapter 6, the gated sinusoidal excitation gave far better results and flexibility of operation. In this case the only change required is to use the oscillator gate trigger pulse to synchronize the shock-excitation device directly, which is to be connected to the system in place of the power amplifier.

The test object is insonified with a short pulse of ultrasound and the delay of the stroboscope is set appropriately such that, the images are optically 'frozen' in time at the instant of best focus. The required delay t_D in the present case would be :

$$t \simeq 2 \times 250 / 6 + 57 / 6 \simeq 90\ \mu s$$

An A-scan display of signals derived from the elements of the array is provided for quick monitoring of targets and the state of the coupling between the test object and the receiver probe array. The corresponding images are seen next to it in real time on the TV monitor.

13.3 RESULTS

Some results obtained during the feasibility study and with the first working prototype are presented below. These demonstrate :

(a) The conceptual validity and the unique capabilities of the new imaging system.
(b) The remarkable improvements achieved since the first demonstration of the feasibility.

13.3.1 Verification of linearity, isochronicity and magnification

Fig 13.3(a) shows an aluminium test block with a set of holes drilled at an angle of 45° to the test surface. The aperture of the probe used is

only sufficient to illuminate about four holes as shown in the diagram. Fig. 13.3(b) is the corresponding image formed. (Since the aperture used is small, the two holes at the centre are preferentially illuminated giving much brighter schlieren images compared to the outer ones. Therefore these two holes are seen apparently smeared since the dynamic range of the video monitor system is not sufficient to accommodate this range of brightness.)

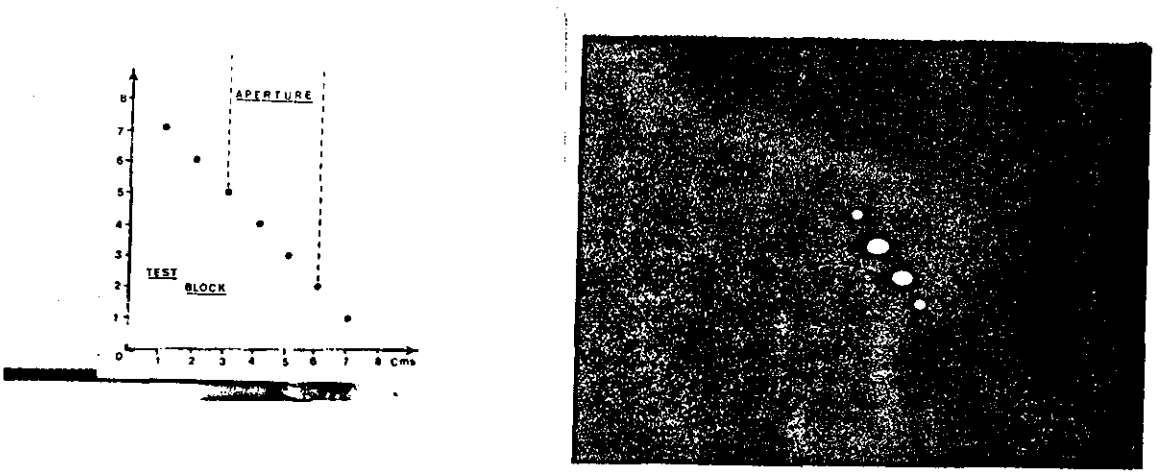

(a) TEST BLOCK (b) IMAGE OF FOUR HOLES

FIG. 13.1

The straightness and the correct relative positions of the image are clearly seen which demonstrates the linearity aspect of the system. Isochronicity is also obvious since a number of image positions can be seen at the same time.

The axial and lateral magnifications M_L and M_A according to equation 3.11 are related by

$$M_A/M_L = 2^{\frac{1}{2}} \quad . \quad . \quad . \quad . \quad (3.11)$$

Since the angle of the line joining the holes in the test object is 45°, and if α is the corresponding angle of the image to the horizontal axis, then it can be shown that

$$M_A/M_L = \tan \alpha \quad . \quad . \quad . \quad . \quad (13.1)$$

At the instant of best focus, the angle of the image as in Fig. 13.1 (b) is approximately 55° . Since $\tan 55^{\circ} = 1.4128 \simeq \sqrt{2}$, the relationship between the two magnifications derived using paraxial ray optics is verified.

The inequality of the two principal magnifications in general do not cause any problem as far as the numerical values remain constant. However, the magnifications may be equalized if necessary by adopting cylindrical viewing lenses or by altering the horizontal or the vertical magnifications of the video monitoring system.

13.3.2 Accuracy, resolution, sensitivity and field of view

Accuracy

An example of the spatial accuracy of the images formed can be seen from Fig.13.2. Fig.13.2(a) is an aluminium test block containing drilled holes. Fig. 13.2(b) is an image of the three holes at the centre of the block marked 1, 2 and 3 which are about 6 cm below the test surface. The holes 1 and 2 are marginally closer than 2 and 3, by about 2 mm. This is clearly revealed in the image.

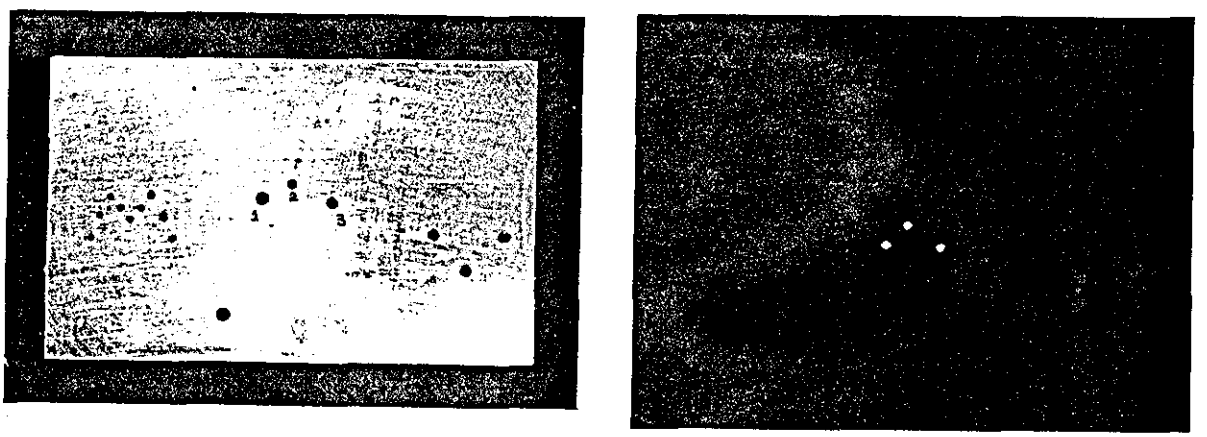

(a) TEST BLOCK (b) IMAGE OF THREE HOLES

FIG. 13.2

Lateral resolution

The lateral resolution was experimentally assessed by imaging a series of drilled holes with different spacings at different depths and was found to comply with the theoretical expectations. For example the lateral resolution obtained with an aperture of only 3 cm around a depth of 6 cm from the test surface was about 2 wavelengths. The ability to give lateral resolution close to theoretical limits is the result of the full aperture contributing to image resolution.

Axial resolution

The axial resolution is around a wavelength in the object medium. Results showed that these achievements were mainly due to introducing the high quality transducer arrays and the L.E.D. stroboscope, developed after the initial feasibility study. This is clearly evident, for example, when comparing the images of the three holes in Fig 13.2(b) with that obtained during the initial feasibility study (Fig. 13.3). It can be seen that both the resolution and the spatial accuracy of the images have been greatly improved.

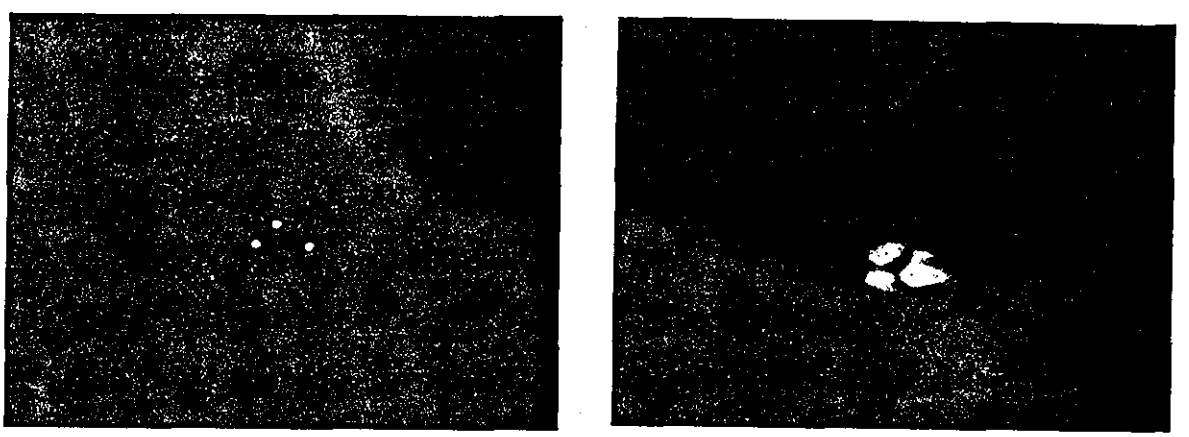

RESULTS WITH THE PROTOTYPE SYSTEM RESULTS DURING FEASIBILITY STUDY

FIG. 13.3 COMPARISON OF THE RESULTS ACHIEVED WITH THE FIRST PROTOTYPE SYSTEM AND THAT OBTAINED DURING THE FEASIBILITY STUDY.

Temporal resolution

The temporal resolution on the other hand has reached the highest limits possible in ultrasonic imaging. This is another unique feature of the new system being capable of producing a complete image of the whole object field with a single pulse, practically within its time of flight. The repetition frequency in the first prototype could be varied up to 1 kHz or even more, depending on the requirements. The light output from the L.E.D. stroboscope is well adequate to register the whole image field even with a single flash, which is particularly useful in high speed photography. During experiments concerning real time aspects, it was also possible to image some moving targets with this system, although the conditions were far removed from what it had been designed for. Demonstration of its unique real time capabilities have been recorded on Video and already presented at some seminars and at international conferences.[46,47,48]

Sensitivity

The sensitivity of the system is also very high, for example, the three holes shown in Fig.13.2 are imaged with an insonifying pulse of the order of 50 V pp only, while the present circuits allow at least 20 times as much. Another example is that it was possible to image a drilled hole of the size of about 1.5 mm diameter at a depth of 25 cm from the test surface. As mentioned above, all these results are obtained with only 15 channels and when all the 30 channels are in operation, even better results can be expected.

Field of view

The axial field (depth range) accommodated by the system is very large. As mentioned previously, the first prototype accommodates at least 25 cm deep object field in steel for any one setting of the schlieren aperture while the sonoptics has a maximum target depth range of 40 cm. Furthermore, its lateral field of view is also large as is evident from the following.

Fig. 13.4(a) shows a test block containing some drilled holes where the first hole at the top is only 3 cm below the test surface. As can be seen, the receiving probe array is not directly above any of these targets. Fig.13.4(b) shows the corresponding image which demonstrates the ability of the system to examine a large lateral field of view.

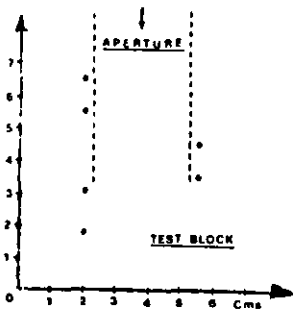

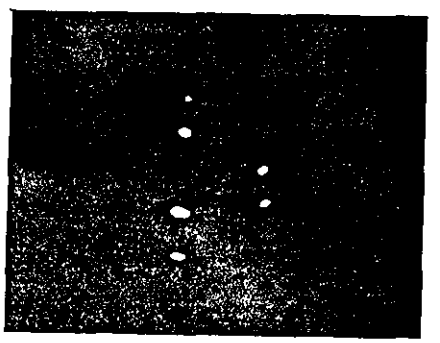

TEST BLOCK IMAGE OF HOLES

FIG. 13.4

Vertically orientated defects

The large lateral field of view together with the ability of the system to image targets which are one beneath the other are favourable features in the examination of vertically orientated defects - an area which is fraught with difficulties in practice. Again, this become possible due to the very nature of the present technique of image re-construction where all the channels are operating in parallel. Here the targets which are not seen by a few elements are still exposed to the others.

Fig. 13.5 shows a steel T-weld which contains some natural weld defects. Fig.13.5(a) and (b) show the shapes, sizes and the orientation of two cracks found inside this T-weld. (Fig. 13.5 b appears to be rather smeared as it was re-photographed during a video demonstration while Fig.13.5 a is a direct polaroid photograph from the main frame video monitor during a testing session, hence of better quality.) However,

the C-shaped crack in Fig.13.5(b) is an interesting one as it further demonstrates the ability of the system to display vertically orientated as well as shadowed targets.

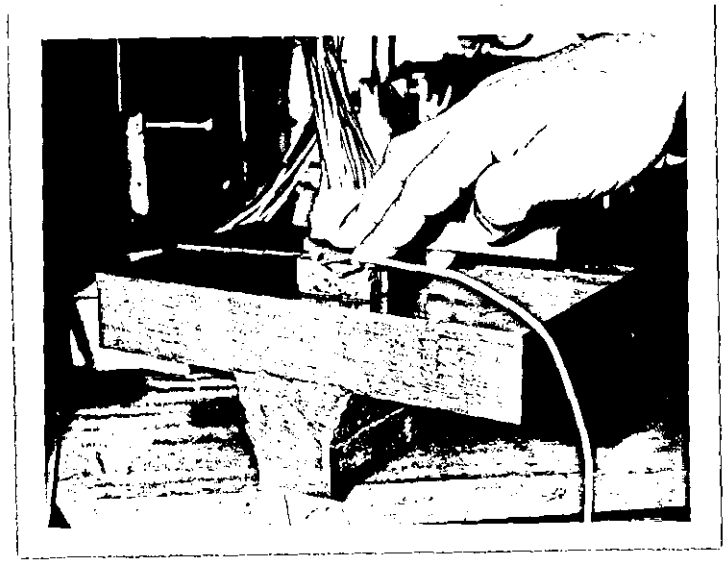

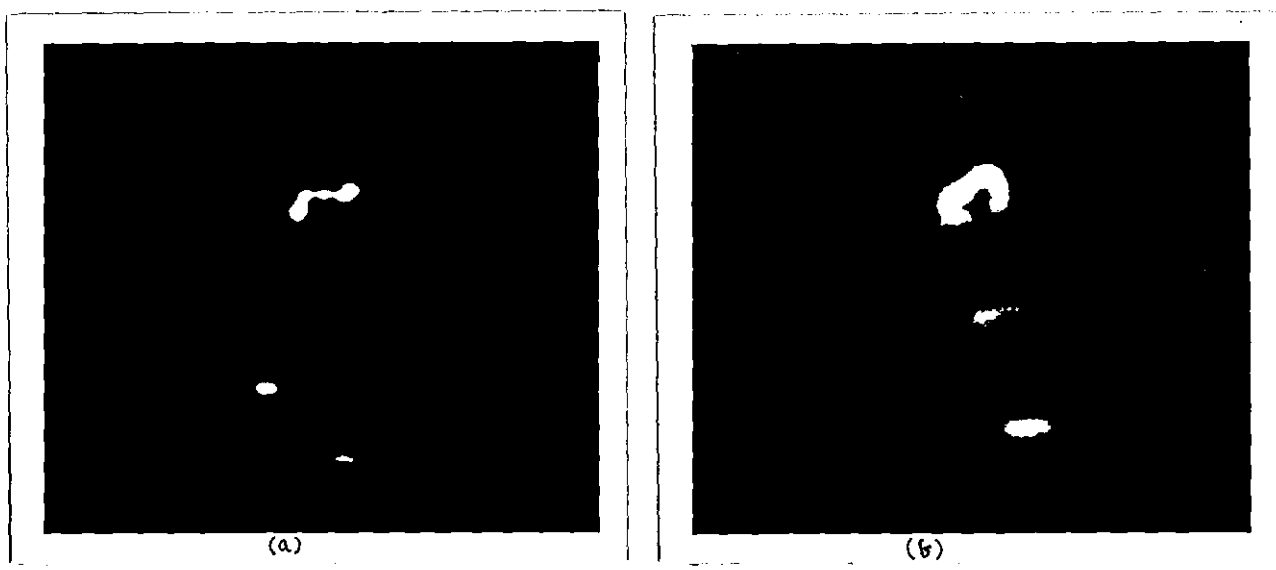

Fig. 13.5 CRACKS FOUND IN A T-WELD

Further results have been recorded on video tape demonstrating the unique real-time and single pulse imaging capabilities, lateral resolution, repeatability, off-axis imaging and testing of a cast iron machine bed which contained a number of natural defects.

13.4 FINAL CONCLUSIONS

It is seen that the present day imaging systems in general are moving more and more towards the use of digital computers and sophisticated signal processing techniques. Although such systems have many attractive features, there can be inherent drawbacks too, such as low speed inadequate image quality these being the result of involved lengthy processing and other limitations arising from the particular technique used.

In this respect the new imaging system presents obvious advantages mainly due to its fundamental simplicity which requires just analogue and optical image processing. The sonoptical schlieren arrangement does all the image re-construction in place of the digital computers and the like with remarkable speed and accuracy. The technique offers an unusual combination of useful features such as extremely high speed, high resolution, large field of view, and compactness as given above. Its temporal resolution is such that a single pulse produces a complete image of the whole object field, practically within its time of flight, hence the ultimate limit of speed possible in ultrasonic imaging has been reached. Furthermore, the new technique possesses the ideal characteristics of the DUVD namely linearity and isochronicity. These benefits taken together with its relatively low cost, makes this system unique in the field of ultrasonic imaging.

The introduction of transducer arrays and electronic amplification in to the concept of DUVD have been the key factors in the development of the new system. This eliminated the low sensitivity of the DUVD technique while the design of the new sonoptics enabled the system to give focused B-scan type images. Another feature is that unlike in the case of DUVD, where the images are always inverted, the use of arrays made it possible to form the images in the correct relative order.

Various areas have also been developed in the course of this work which included wide aperture compact sealed schlieren system, miniature L.E.D.

stroboscope, wideband miniature transducer head amplifiers, wideband power amplifiers, a new category of amplifiers named G featuring high efficiency and low power consumption, high quality transducer arrays and transducer backings.*

Special applications

Apart from its use as a general inspection tool in NDT, the new system could also find application in a variety of special areas, utilizing its unique capabilities. For example, as a result of introducing transducer arrays, the system sonoptics can be designed to take into account non-planar test surfaces as well. This possibility could be particularly useful in testing non-planar, but uniform geometrical objects such as pipes or axles. Also this adaptability to non-planar surfaces together with its unique real-time performance may be utilized in another interesting area, not explored so far in NDT imaging, is fatigue testing. A typical example would be: real time monitoring of fatigue cracks developing in critical components or part of a system in service. The remote operation is also possible as the receiving probe array could be separated over a large distance when using the head amplifier module. This could be particularly useful in situation where the access is restricted or in applications such as underwater structural testing.

Medical applications

Another special area out side NDT which needs to be examined in depth is the fields of medical applications. The factors that great promote its use in this direction are the excellent real time imaging capabilities, high resolution and sensitivity. Furthermore, proper coupling is not difficult to achieve compared to NDT work.

However, in medical applications the object medium, being biological tissues, possesses widely different and unfavourable characteristics compared to most NDT materials. For example, the attenuation in tissue is comparatively high while the medium itself is non-homogeneous

and the impedance contrast between the targets of interest could be very low. The sound velocity is also very low and therefore, for a given operational frequency, much smaller element spacings and gap widths are needed. Furthermore, unlike in NDT, the insonifying energy cannot be increased beyond specified dosages due to the hazards involved. This means that as the echo signals are generally much weaker than in NDT, the sensitivity and the gain bandwidth product must be raised sufficiently in order to achieve useful results. Although this could be well within reach, the main problem appears to be the construction of arrays to the required specifications as this would largely determine the quality of the images and the artefacts formed.

In principle, the use of this technique in medical applications would be attractive. However, the whole subject must be studied in depth as simply forming images may not be sufficient to justify development; the quality of imaging must be at least comparable or better than that produced by the exsisting systems.

Areas needing further development

One of the problems that need to be solved is to establish a method of ensuring good coupling between the receiver probe array and the test object. Although achieving good coupling is a common problem with all ultrasonic contact testing equipment, the errors that could be introduced by inadequate or non-uniform coupling in the present case are more significant. This is mainly because the present system relies totally on amplitude and phase information of echo data. One possibility to improve coupling is to allow a certain amount of flexibility or relative movement between the elements of the receiving array. It may also be possible to translate such relative displacement into appropriate changes in delay between the channels by electronic means so that the effect of changes in surface profiles within limits are automatically compensated. The possibility of using PVDF transducers must also be considered although this would require much higher gain to compensate for the loss of sensitivity.

As mentioned before, the present system was developed with some important limits such as phase tolerance, gain-bandwidth product assigned on the basis of what can be practically achieved so that the full potential of the technique in practice may be revealed. It is therefore now important to carry out system optimization. This would involve further theoretical and experimental work concerning parameters such as maximum allowable phase tolerance, gain-bandwidth product, reduction of transmission losses, for example by using matching layers wherever applicable. Obviously any possible relaxation of such parameters would ease the constructional work and expand the range of application. Such studies could also indicate the possibility of amalgamating standard techniques such as dynamic compression, a degree of electronic focusing or phase angle alterations which would be quite useful in practice.

Another area that may be worth studying is the use of shear waves for insonification and reception of echo data as this could improve image resolution and even enhance the detectability of axially orientated defects. The incorporation of Time Varying Gain (TVG), remote sensitivity control, improving the effective dynamic range and the use of G^* type amplifiers as emphasized in previous discussions are some other areas that would promote the immediate usefulness of this new system. The assembly can be further compacted and it is likely that a future model could be designed with the size comparable to that of a conventional flaw detector of the early type.

Finally with the results achieved, it may be concluded that the new imaging system developed in this project would find wide acceptance as a practical inspection tool, in the field of ultrasonic imaging.

--- // ---

APPENDICES

- A P P E N D I X - 1 -

MIRROR SCHLIEREN DESIGN CONSIDERATIONS

The advantages and disadvantages of using mirrors compared to lenses in the present application are given below.

Advantages

1. No chromatic aberration
2. Larger field of view possible
3. Lower background illumination
4. Lower cost

Disadvantages

1. Spherical aberration
2. Substantial increase in the dimensions of the system
3. Astigmatism
4. Mounting and alignment difficulties

In the case of mirrors, the overall dimensions of the arrangement is largely determined by the separation of the mirrors required. Front face aluminised concave mirrors with focal length 100 cm and diameter 15 cm were chosen for the present purpose. If the angle of obliquity of parallel light beam is arranged to be about 4°, then the combination gives a usable circular field of view of about 10 cm.

Obviously the schlieren mirrors have to be kinematically located to achieve the required precision and accuracy of adjustment. Hence an experimental kinematic mirror mount with four degrees of freedom (two translational and two rotational) as shown in Fig.A.1.1(a) and (b) was designed. However, the development of the L.E.D. stroboscope in the mean time promoted the use of a lens schlieren system. Therefore the mirror schlieren arrangement was not further developed.

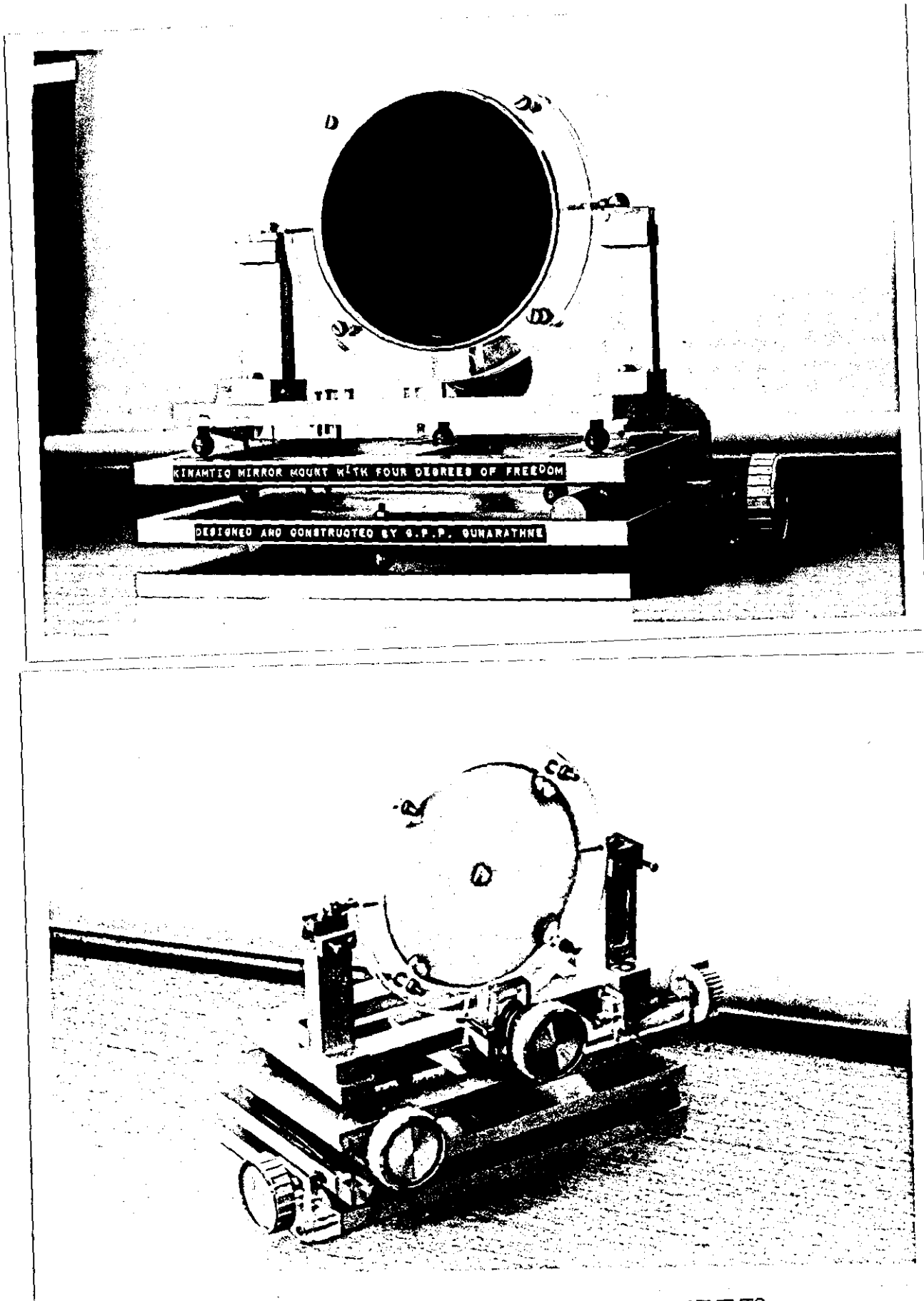

FIG. A.1 KINEMATIC MOUNTING OF MIRRORS WITH ADJUSTMENTS

- A P P E N D I X - 2 -

The initial settings that have to be ensured before switching on the first prototype with reference to Figs. 13.1 and A.2.1 are given below.

Initial settings

Description	*Setting*
Stroboscope trigger pulse duration	*10 to 30 ns*
Trigger pulse amplitude	*5 to 10 V*
Oscillator gating pulse duration	*0.5 s approx.*
Gate pulse amplitude	*1 V max.*
Repetition frequency (depends on application)	*¾ 1 kHz*
Delay between the trigger and the gating pulse	*95 s approx.*

Head amplifier module

D.I.L miniature power switches, 1 - 10, (as on the module)	*ON*
D.I.L miniature switches, 14 - 20 (impedance trimming)	*OFF*
D.I.L switch 12 (Tx / Rx) selector	*ON for Tx/Rx*
D.I.L switches 11 and 13 (Tx/Rx and two additional insonifying probes on either side of the receiving array - Composite probe)	*(ON for the composite)*

Miscelleneous

Insonifying energy control (input attenuation)	*-20 dB*
Frequency of operation	*1.8 MHz*
Dual trace A-scan monitor (channels selected)	*1 and 30*
Main frame video monitor	*set to video*
Power supply key switch (KS)	*OFF*

Either separate transmitter / receiver or transceiver mode of operation may be selected with the appropriate D.I.L. switches fixed on the array

head amplifier module. It is also possible to use shock-excitation if required, instead of the gated sinusoidal excitation. However, as discussed in Chapter 6, the gated sinusoidal excitation gave far better results and flexibility of operation. In this case the only change required is to use the oscillator gate trigger pulse to synchronize the shock-excitation device directly, which is to be connected to the system in place of the power amplifier.

GENERAL LAYOUT OF COMPONENTS AND CONTROLS. (REF. FIG. 13.2)

1. *Repetition rate controls (coarse and fine)*
2. *Delay control 1*
3. *Gate pulse width and amplitude controls (coarse and fine)*
4. *Delay control 2*
5. *Stroboscope trigger pulse width controls (coarse and fine)*
6. *Stroboscope trigger pulse amplitude control*
7. *Gate pulse out*
8. *Stroboscope trigger pulse out*
9. *Main frame oscillator frequency control*
10. *Frequency counter (8 digit) L.E.D. display*
11. *Frequency counter sampling gate width and d.p. selector*
12. *Gated sinusoidal pulse output socket*
13. *Internal/external power amplifier selector*
14. *External (excitation) pulse input*
15. *RF/Video selector*
16. *Main frame TV/Video monitor power switch*
17. *Power supply status indicator*
18. *Power supply reset 1*
19. *Power supply reset 2*
20. *Main switch*
21. *30 V line overload trip set*
22. *50 V line trip level set*
23. *Main fuse*
24. *Key switch*
25. *Visual alarm*
26. *External power amplifier input*
27. *External power amplifier output*

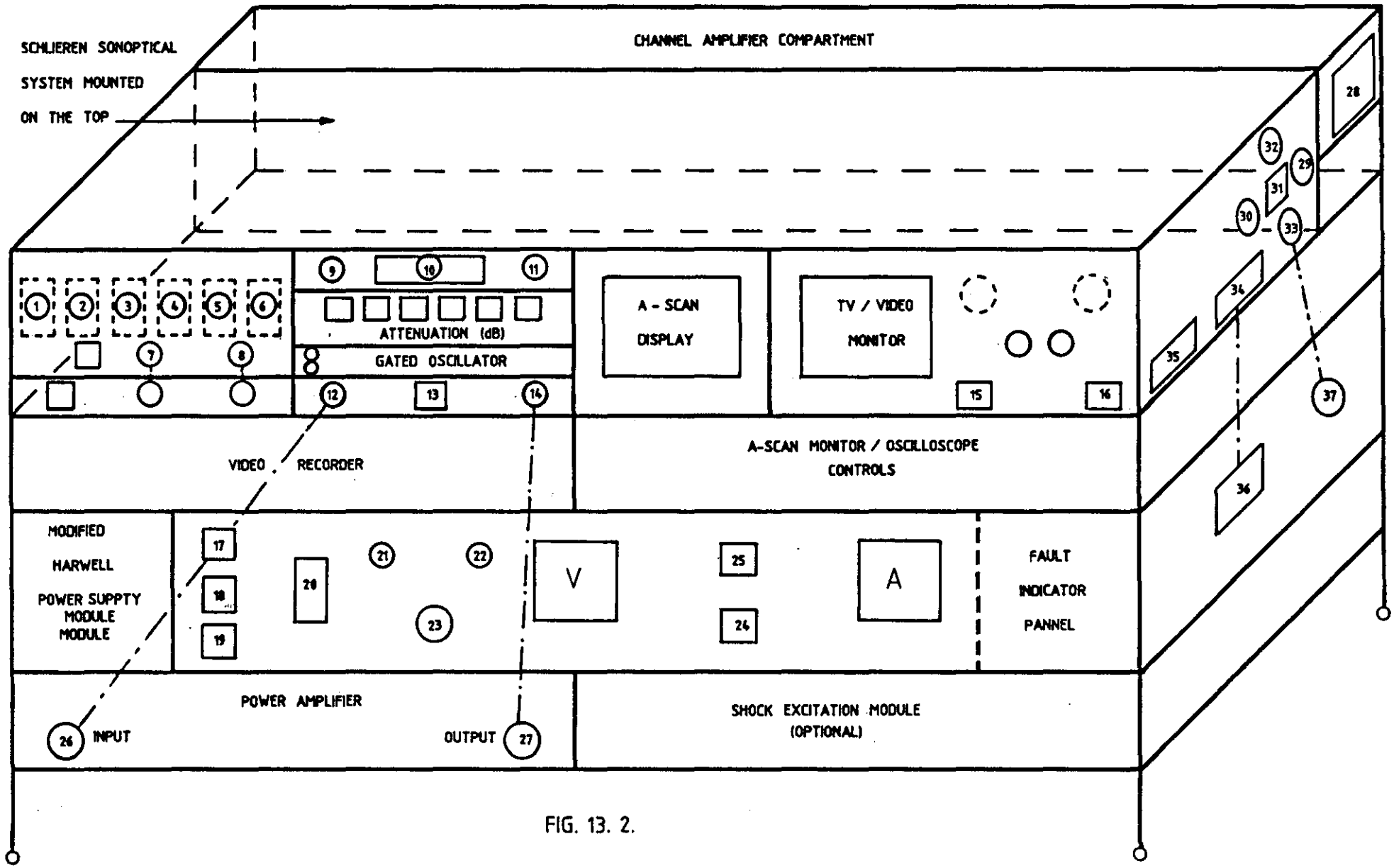
SCHLIEREN SONOPTICAL
SYSTEM MOUNTED
ON THE TOP
CHANNEL AMPLIFIER COMPARTMENT
ATTENUATION (dB)
GATED OSCILLATOR
A - SCAN
DISPLAY
TV / VIDEO
MONITOR
VIDEO RECORDER
A-SCAN MONITOR / OSCILLOSCOPE
CONTROLS
MODIFIED
HARWELL
POWER SUPPTY
MODULE
MODULE
V
A
FAULT
INDICATOR
PANNEL
POWER AMPLIFIER
INPUT
OUTPUT
SHOCK EXCITATION MODULE
(OPTIONAL)

FIG. 13. 2.

28. *Extractor fan (forced ventilation to channel amplifier compartment)*
29. *Video input to an external monitor (if used)*
30. *Video input from an external monitor (if used)*
31. *External and internal monitor selector*
32. *RF input (optional)*
33 *and 37. a.c mains link from power supply to main frame*
34 *and 36. d.c power link from power supply to main frame*
35. *Cables out to the head amplifier/receiving probe array*

- APPENDIX-3 -

LIST OF PUBLICATIONS

The following publications have already been made.

1. *A new stroboscope for schlieren and photoelastic visualisation of ultrasound : G.P.P. Gunarathne and J. Szilard, Ultrasonics July, 1983, pp. 188 - 190, and Ultrasonics International 83 conference Procedings, pp. 74 - 78, Butterworth and Co (Publishers) Ltd.*

2. *A real time high frame rate ultrasonic imaging system : G.P.P. Gunarathne and J. Szilard, Ultrasonics International 85 Conference Proceedings, July 1985, pp. 98 - 104 (oral presentation by the author followed by a video demonstration).*

3. *A new ultrasonic imaging system. - G.P.P. Gunarathne and J. Szilard Ultrasonics symposium, Oct. 1985, San Fransisco, USA. (oral presentation by the uthor).*

4. *A real time ultrasonic imaging system. - (invited paper) G.P.P. Gunarathne and J. Szilard, Colloquim on "Developments in tomography for NDT and medical applications". 11 March 86, The Institution of Electrical Engineers, London, Digest No: 1986/34. (Oral presentation and a video demonstration by the author).*

Research note

A new stroboscope for schlieren and photoelastic visualization of ultrasound

G.P.P. GUNARATHNE and J. SZILARD

Conventional stroboscopes, when used for visualizing the path of ultrasound in a transparent medium, suffer from many problems including too long a flash duration, jitter and inconsistency. To overcome these limitations a new stroboscope has been developed which is based on a light emitting diode driven with very short, very high current pulses.

KEYWORDS: ultrasonics, visualization, stroboscopes, light emitting diodes

Introduction

An essential element for visualizing the path of ultrasound in a transparent medium by schlieren or photoelastic visualization techniques is a good quality stroboscope. The conventional stroboscope, which relies upon some form of a gas discharge to generate light pulses, suffers from too long a flash duration, inconsistency, change of flash energy with repetition rate, jitter and aging. Apart from these limitations, other drawbacks of commercial stroboscopes are bulkiness, and high cost.

As an attempt to overcome these limitations a new stroboscope has been developed using super-bright light emitting diodes. The average output power of LEDs is too small for them to be used effectively as stroboscopic light sources, but if the flash duration is short enough and the duty cycle is such that the average power dissipation is within the specified limits, the peak currents can exceed the rated average current by a factor of 10^3 or more. Under these conditions, the light output obtained is well adequate for most schlieren applications. The flash duration can be as short as 10 ns and free from jitter. This enables resolution far superior to that possible with gas discharge or spark light sources. A further advantage is the monochromatic light, which helps to reduce the cost of optics in the schlieren system. The far superior performance of the LED stroboscope makes it a natural choice for ultrasonic visualization purposes and many other applications.

Pulse operation of LEDs

The light emitted by a LED is the result of a process of recombination of carriers taking place at the forward biased diode junction in the presence of injected minority carriers. The apparent brightness B is given by the formula[1]

$$B = \frac{3940\,\eta_{ext} LJ}{\lambda} \frac{A_j}{A_s} \text{ cd m}^{-2} \text{ (Nits)}$$

where η_{ext} is the external quantum efficiency, L the luminous efficiency of the eye, J the junction current density A cm^{-2}, A_j/A_s the ratio of the junction area to observed emitting surface, and λ the emission wavelength in μm.

According to the above formula, the optical output would increase linearly with the current. However, as the junction temperature increases due to the current, efficiency decreases, resulting in diminishing returns of the output light power with current. Hence, in the case of normal dc operation, the maximum light output obtainable from a given LED is primarily limited by the thermal dissipation of the device. Therefore under steady state conditions the optical output also depends on the thermal resistance between the diode junction and the environment, and also on the ambient temperature.

Figures 1 and 2 show a simple equivalent circuit and

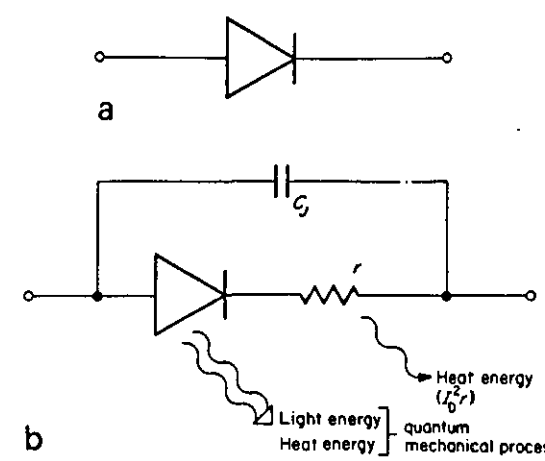

Fig. 1 a – Ideal diode; b – equivalent circuit of practical diode

The authors are in the Department of Electronic and Electrical Engineering, University of Technology, Loughborough, Leicestershire, UK. Paper received 30 March 1983.

0041-624X/83/040188-03/$03.00

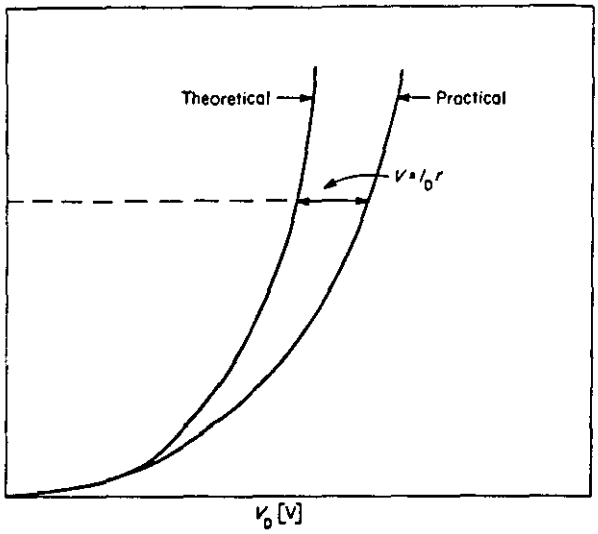

2 General current-voltage characteristics of a diode

ent - voltage characteristic for a light emitting diode. 3 shows the relationship between the relative intensity mission against the current through the diode in the tinuous and pulse modes up to about 50 mA for a sP LED. Since heat dissipation within the LED is a ıary limiting factor, it is clear from Figs 1 and 2 that diode forward resistance is an important consideration. refore, in order to obtain a better optical output:

LED with a low internal resistance may be selected, ıe LED may be operated in a low temperature nvironment.

er ordinary practical conditions, only the first remedy propriate. Certain LEDs now available in the market remarkably high efficiency. Stanley Hi-Super Bright s are some examples. They offer a continuous light ut[2] of typically 500 mcd at 20 mA compared to about d from an ordinary LED at the same current. For this n and for their good linearity over an extended current , red LEDs of this kind have been used for the first type stroboscope made, which gave a very satisfactory rmance.

re 3 reveals two further important characteristics of a . Firstly, in the pulse operation, the LED is far more ent than in the continuous mode and secondly, it is ı more linear over an extended range of currents.

it is observed in experiments that if the average power ıation is well below the permissible limit, the apparent al saturation in the case of the dc operation is removed at highly elevated currents. These features are of great rtance as far as the design of a stroboscope is concerned enormous current pulses can be passed through the e if the flash duration is short enough and the duty is such that the average power dissipation is within ecified limits. This results in very bright light flashes elevated conversion efficiency. By way of comparison,) which is rated for a maximum forward steady ıt of 50 mA at 25°C could take 100 ns pulses of ıt as high as 20 A or even more at a duty cycle of 0.2% (2 kHz repetiton). If the pulse width or the tion rate is reduced, the current may be further ısed to compensate to some extent for the drop in ge brightness.

Our Stanley Hi-Super Bright LED gave an output energy per flash of 0.03 μJ when driven by 100 ns, 19 A pulses. It is observed that the ultrasonic field was clearly visible when illuminated by a single flash of a pulse mentioned above.

LED driving circuit

Switching times of LEDs can be as short as a few nanoseconds if the driving circuit is designed carefully. For stroboscopic applications the maximum pulse current capabilities of the circuit is a primary limitation. Attention must also be paid to avoid excessive distortion of short pulses and the circuit must be stabilized against various interferences due to high current pulses and transients generated, etc.

The assembled device is shown in Fig. 4. Approximate dimensions are 7.6 x 5.1 x 2.5 cm. It is capable of switching pulses up to about 20 A. The circuit consists of only four active elements in three stages and this indicates the low cost involved. Total power consumption is less than 1 W. A low impedance pulse generator typically of the order of 50 Ω triggers the device.

The above stroboscope is successfully used in ultrasonic schlieren systems. This is illustrated in Fig. 5 showing two examples of clear and stable images that could be easily obtained with a simple schlieren system using this stroboscope. Because of the nearly monochromatic light of the LED, it is relatively easy to produce high contrast schlieren images even with ordinary non-achromatic lenses rather than mirrors.

Conclusions

A new stroboscope has been successfully built based on a LED driven with very short, very high current pulses. The advantages compared to ordinary stroboscopes can be summarized as follows.

(1) Extremely short flash duration, independent of repetition rate; 10 ns or even shorter pulses are possible as assessed by the current pulses; compared to 30 to 50 ns of a spark discharge stroboscope[3] or 0.5 to 3 μs of a commercial gas discharge tube stroboscope[4] whose flash duration varies with the repetition rate in the above range.

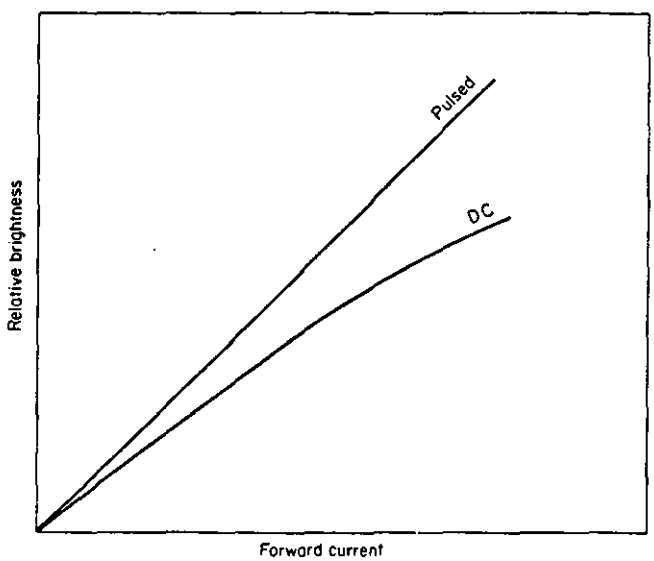

Fig. 3 Comparison of pulse and dc operation of a GaAsP LED

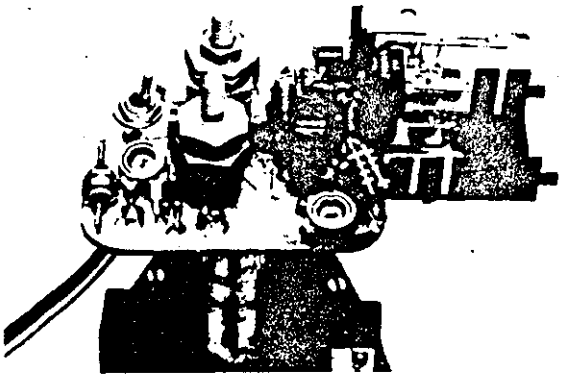

Fig. 4 Stroboscope on a breadboard

(2) Completely free from jitter.

(3) Nearly monochromatic emission.

(4) Pulse width and pulse energy can be accurately controlled.

(5) Long working life.

(6) Small physical size.

(7) Very low cost.

If still more light is needed, an array of LEDs may be used.

A further publication is planned to cover more detailed aspects of the stroboscope.

Acknowledgement

This work was a part of a project sponsored by Risley Nuclear Power Development Laboratories, United Kingdom Atomic Energy Authority. The authors gratefully acknowledge their indebtedness for this support.

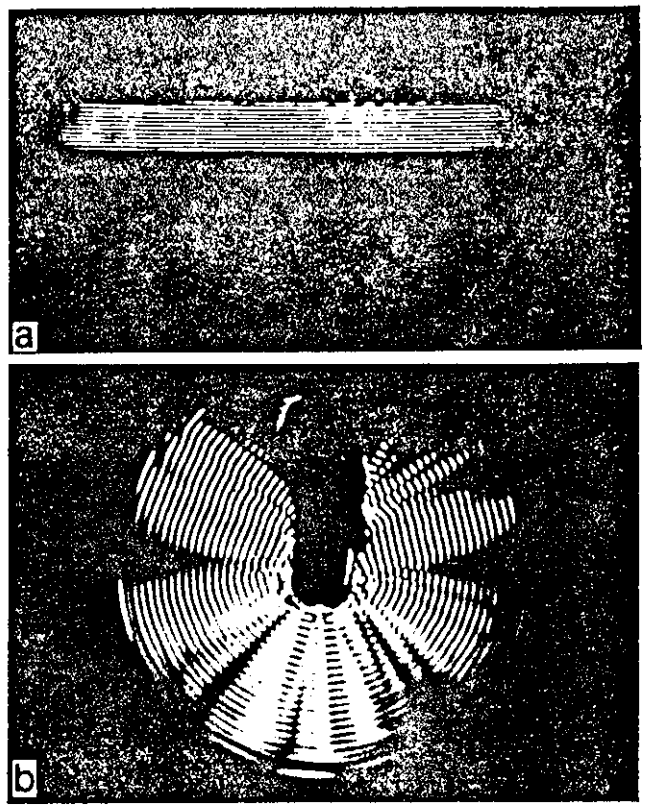

Fig. 5 a — A gated burst of ultrasonic waves emitted from a large 2 MHz transducer; b — cylindrical field of a small 2 MHz transducer driven by a long train of sine waves

References

1 Turner, L.W. Electronic Engineers Reference Book, 4th Ed., Newnes-Butterworths, London (1976)

2 Stanley, Hi-Super Bright LEDs, H-500, H-300 data sheets, Lohuis Lamps Ltd., LEE Building, Parkfield Road, Coleshill, Birmingham

3 Wyatt, R.C. *J. Phys. E.* 7, (1974) 437

4 Handbook of Strobotac (GR 1538-A), Gen. Rad. Inc. 1979, Concord Massachusetts, June 1979

A REAL TIME HIGH FRAME RATE ULTRASONIC IMAGING SYSTEM

G.P.P. GUNARATNE AND J. SZILARD

Department of Electrical and Electronic Engineering, Loughborough University of Technology, Loughborough, Leicestershire, LE11 3TU, England

Many problems are found in present day ultrasonic imaging systems such as low speed, high cost, large size etc. A new system has been developed to overcome many of these limitations by extending the principle of Hanstead's Direct Ultrasonic Visualisation of Defects[1] [DUVD] system. The inherently low sensitivity of the DUVD is eliminated by intorducing electronic amplification using transducer arrays while preserving its ideal features by adopting a new sonoptical design. The first experimental model has a nominal depth range of up to 40 cm in steel and takes only 0.15 ms to produce a high resolution focused B-scan type image of the whole object field.

1 INTRODUCTION

The inherent potential of ultrasonic imaging in non destructive testing and medical applications leaves plenty of room for further development. The new system described here offers many advantages such as high speed, good resolution, large field of view, compactness, ease of operation and low cost etc.

The basic principle is an extension of Hanstead's Direct Ultrasonic Visualisation of Defects[1] [DUVD] system. The main problem with the DUVD is its low sensitivity. Further work on this technique has also been reported by Hayman[2] in 1977 and by Bar-Cohen et.al.[3] in 1978. Even so, at its best, the object field is only a few cms in width, length and depth. Therefore in spite of its attractive features and simplicity, the DUVD has not been implemented in practice.

Developing further the basic concept of the DUVD by introducing electronic amplification between a set of receiver and re-transmitter arrays, the problem of low sensitivity is eliminated, while preserving the ideal characteristics of the concept, namely the linearity and isochronicity. Another feature of the system is that it is showing a slice of the DUVD display and presenting it as a very high resolution B-scan type image.

A number of areas have been developed during the course of this work, some of which are also briefly outlined. These include a high performance wide aperture compact schlieren system, a new miniature L.E.D. stroboscope, wide band rf amplifiers, miniature wideband transducer head amplifiers, high quality transducer arrays and backings etc.

2 DESCRIPTION OF THE NEW SYSTEM

2.1 THE BASIC CONCEPT OF DUVD

DUVD essentially consists of a pair of acoustic lenses, [Fig.1] designed in such a way as to produce a 3D image with two other special properties called linearity and isochronicity, as mentioned above. The term linearity here refers to its ability to maintain a constant object-to-image spatial relationship, while isochronicity means that when the object is insonified with a short pulse, all the echoes from

different targets (defects), irrespective of their distances, arrive simultaneously at their respective image points, thus giving the system its ability to display the whole image at once. The ultrasonic image is made visible either by the photoelastic technique or by the schlieren technique using a stroboscopic flash of light.

3 THE NEW CONCEPT

The new concept[4] is aimed at maintaining the ideal characteristics of the DUVD, namely the linearity and isochronicity, while eliminating the problem of low sensitivity. This is done by designing a new sonoptical geometry and introducing electronic amplification between a set of receiver and re-transmitter arrays. The concept may be summarized as follows.

(1) SIGNAL INTERCEPTION

(2) AMPLIFICATION

(3) RE-TRANSMISSION

It is apparent that the new technique is a great deal more involved than the DUVD, due to the requirements to be met in each of the above areas. The basic parameters investigated are listed below.

3.1 SIGNAL INTERCEPTION

(1) No. OF CHANNELS
(2) TRANSDUCER ELEMENT SPACING
(3) ELEMENT WIDTH TO GAP RATIO
(4) PHYSICAL SIZE, SHAPE, AND THE TRANSDUCER MATERIAL
(5) CENTRE FREQUENCY etc.

The first two parameters were estimated by a preliminary computer simulation using the model shown in Fig.(2). The aim here was to obtain an idea of the sharpness of the images and the extent of artefacts that may be formed in a given image space as a function of the number of channels and element spacing. The mathematical model used is

$$P_{(xy)} = \sum_{i=1}^{N} \frac{e^{-j(kr_i + \phi_i)}}{r_i} \qquad (1)$$

Where $P_{(x\,y)}$ is the pressure distribution at point (x,y) in the image space, r_i is the distance from the i^{th} element of the array and k is the wave number. For the first prototype a centre frequency of 2 MHz was chosen with element spacing of 0.7λ, and thirty channels, although the feasibility study was carried out with only fifteen. The results were excellent as can be seen from Figs.8 and 9.

3.2 AMPLIFICATION

With short pulses the received signals contain a broad band of frequencies. Raising the power of these signals to a level sufficient for visualisation without distortions and differential phase errors between channels need careful attention. In this respect various areas have been investigated as listed below, from which the amplifier design specifications were formulated.

(1) TYPICAL AND WORST CASE INPUT SIGNAL LEVELS
(2) OUTPUT SIGNAL LEVELS
(3) PHASE DISTORTION AND BANDWIDTH CONSIDERATIONS
(4) DYNAMIC RANGE

(5) INPUT AND OUTPUT IMPEDANCES
(6) DAMPING CHARACTERISTICS
(7) NOISE LEVEL
(8) POWER CONSUMPTION
(9) SIZE
(10) COST, etc.

A set of wideband rf power amplifiers operating in class A was designed for early experiments. Although these are still in use, a new category of amplifiers here named as G giving higher efficiency and dynamic range has been developed and tested for this particular purpose. It operates in switched mode but retains the ideal characteristics of class A during the pulse period when the signal transmission takes place. A set of 30 miniature wide band array head amplifiers Fig.3 were also developed which matches the transducers to the cables up to a usable length of 50 metres. Thus remote operation is also possible. These amplifiers have a 1 kV surge protection at the front end with short dead zone enabling them to be used in transceiver mode of operation as well. The amplifier assembly can be clipped to the operators lower arm for easy operation.

3.3 RE-TRANSMISSION

In addition to the basic parameters investigated under [3.1], the sonoptical geometry had to be determined. After examining a few possibilities a final geometry consisting of a curved array and a cylindrical lens was designed in place of the two lens arrangement of the DUVD. This curved array replaces one of the two lenses in the DUVD set up, thus simplifying it further and enhancing the sensitivity even more.

3.3.1 VISUALISATION

The schlieren technique was adopted using a sensitive liquid as the visualising medium. One of the most significant improvement has been the development of a new L.E.D. stroboscope[5] which greatly improved the performance and compactness of the whole system. It is capable of outputting light far in excess of what is required for the purpose. Even a single pulse shows the whole image field. This stroboscope is assembled inside a lens cap as shown in Fig.4.

4 CONSTRUCTION OF ARRAYS

This is an area of great importance in achieving good results close to theoretical limits. For example the axial resolution is directly dependent on the pulse width and consequently the wide band performance of the array elements is paramount. It is well known that nominally identical transducers very often differ widely in performance. The situation is even more acute when the transducers are physically small as lateral modes of vibrations become more significant. One can therefore envisage the difficulties of making two 30 element arrays with sufficiently identical characteristics between the individual elements.

After investigating the bisic requirements, a considerable amount of work has been done in developing high quality arrays. This includes a new approach in the development of high quality transducer backings. Both conductive and non-conductive backings were developed. The non-conductive backings are specially meant for the use in higher frequency arrays to achieve low electrical cross coupling. This work is intended to be published later.

5 THE ASSEMBLY AS A WHOLE

Figs.5 and 6 show the assembly of the first experimental prototype. Fig.7 shows the system block diagram. A high performance, wide aperture, compact schlieren setup is designed and kinematically mounted such that it is insensitive to typical vibrations of all kinds experienced on a shop floor, hence the images are perfectly steady. Furthermore, this particular setup can be used in full daylight without the

need of any dark environment. Overall dimensions of the whole assembly are 1 m by 0.5 m by 0.5 m. With further advances in electronics and construction techniques any future model may be comparable in size to that of a conventional flaw detector of the early type.

5.1 OPERATION

When testing, the array is coupled with oil to the test object. Either separate transmitter/receiver or transceiver mode may be selected. The test object is insonified with a short pulse of ultrasound and the delay of the stroboscope firing circuit is set appropriately. An A-scan display of signals is provided for quick detection of targets in the test object. The corresponding images are seen next to it in real time on the TV monitor. These images can be recorded on a VTR if necessary. The image field may also be seen with the naked eye directly from the schlieren without the CCTV.

6 RESULTS

Two examples of images produced by the first system at an early stage of development are shown in Figs 8 and 9. Fig.[8] shows images of three holes drilled in an aluminium test block and Fig.9 shows an image of an actual crack found in a T-weld. Note that in Fig.8 the holes marked 1 and 2 are closer than 2 and 3 by about 3 mm and the vertical offset of 1 and 3 about 2 mm which are clearly shown in the image. The longitudinal resolution is very close to a wavelength; this being the result of the development of wideband high quality arrays and amplifiers.

7 DISCUSSION AND CONCLUSIONS

From what is seen in the market today and during the past few years it is apparent that the present day imaging in general is moving more and more towards the use of digital computers and sophisticated signal processing techniques. Although they have many attractive features, there can be inherent drawbacks such as low speed and inadequate image quality, these being the result of involved lengthy processing, loss of information and other limitations arising from the particular technique used.

In this respect the new imaging system presents obvious advantages mainly due to its fundamental simplicity which requires only analogue processing. The sonoptical schlieren arrangement does all the image re-construction, in place of digital computers and the like at a fraction of the cost and with remarkable accuracy and minimum time. Even in its present form with only 15 elements operating, its resolution is high, typically in the order of a wavelength in the longitudinal direction and about 1.5 wavelengths laterally at a depth of around 6 cm in the test block. Its sensitivity is also high, for example the three holes shown in Fig.8 are imaged with an insonifying pulse of around 50 V p.p. only while the present circuits allow 20 times as much. It operates in real time, i.e. a complete image is formed by a single pulse, thus in a section of steel 400 mm deep an image is formed in about 0.15 ms and the frame rate can be as high as 1kHz or more. This is just the time of flight of the pulse. Compare this with minutes or hours taken by other existing systems. Furthermore the interpretation of results are straightforward and less operator-dependent. These benefits, taken together with its remarkably low cost, make the system unique in the field of ultrasonic imaging.

All these features are ideal for medical applications as well and this possibility is intended to be explored in depth, as the work done so far is concerned with NDT only. Further work has also been planned on system optimization and coupling to non-uniform surfaces.

REFERENCES

(1) P.D. Hanstead : Three-dimensional imaging of ultrasound : Direct Ultrasonic Visualisation of Defects, Nature, 239, 273-274, 1972

(2) A.J. Hayman : Schlieren Visualisation of Ultrasonic images. Ph.D. thesis, City University, London, 1977.

(3) Y. Bar-Cohen, B. Ben-Joseph and E. Harnik : Compact sensitive instrument for direct visualisation of defects. Rev. Sci. Instruments, 49, 1709 - 1911, 1978

(4) Patent application No 8510802 filed 29th April 1985

(5) G.P.P. Gunarathne, J. Szilard : A new stroboscope for schlieren and photoelastic visualisation of ultrasound, Ultrasonics, July 1983, 188 - 190

ACKNOWLEDGEMENT

This work was supported by the United Kingdom Atomic Energy Authority and was performed at Loughborough University of Technology. The authors wish to thank Dr. P. Highmore, project supervisor at the Risley Nuclear power development Laboratories for his continuous support and encouragement. Thanks are also due to the technical staff of the department of electrical and electronic engineering, Loughborough University of Technology and also to the others who gave their whole hearted support during the course of this work.

FIGURES

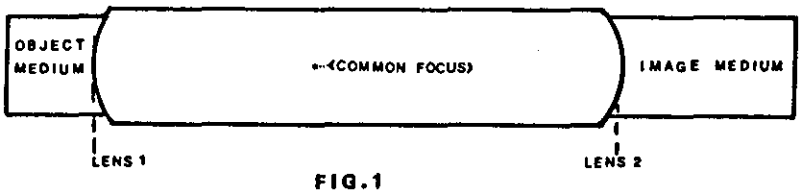

FIG.1

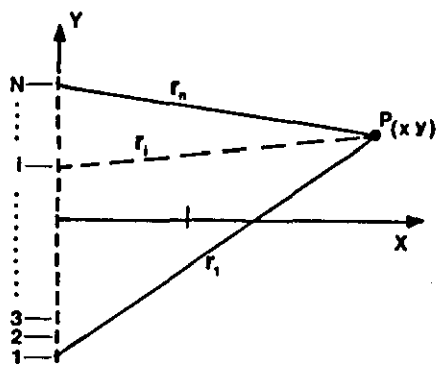

$$P(xy) = \sum_{i=1}^{N} \frac{e^{-j(kr_i + \phi_i)}}{r_i}$$

FIG.2

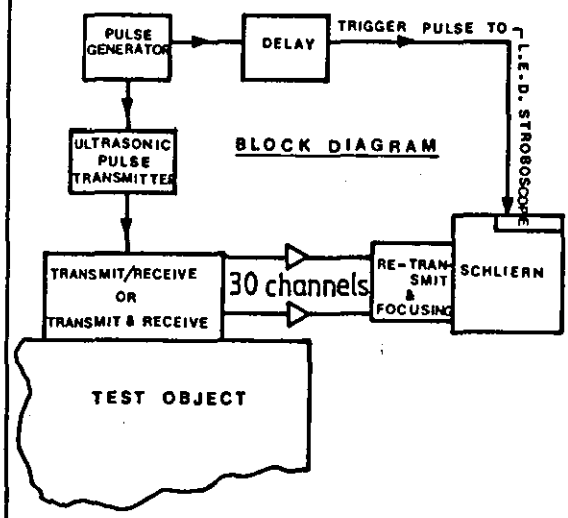

FIG.7

80 WIDEBAND ARRAY HEAD AMPLIFIERS

DESIGNED AND CONSTRUCTED BY G.P.P. GUNARATHNE

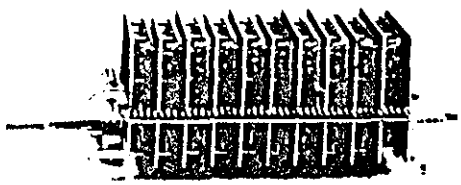

FIG·3

L.E.D STROBOSCOPE

DESIGNED AND CONSTRUCTED BY G.P.P. GUNARATHNE

FIG·4

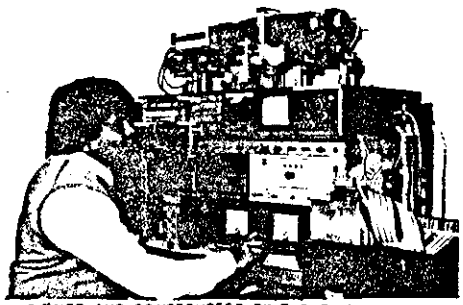

DESIGNED AND CONSTRUCTED BY G.P.P. GUNARATHNE.

FIG·5 - FRONT VIEW

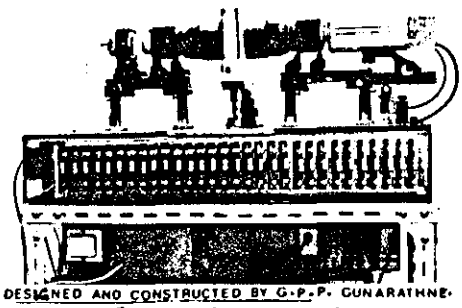

DESIGNED AND CONSTRUCTED BY G.P.P. GUNARATHNE.

FIG·6 - BACK VIEW

FIG·8(a) - A TEST BLOCK

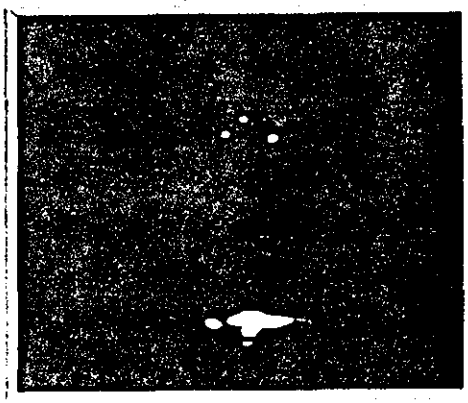

FIG 8 (b)

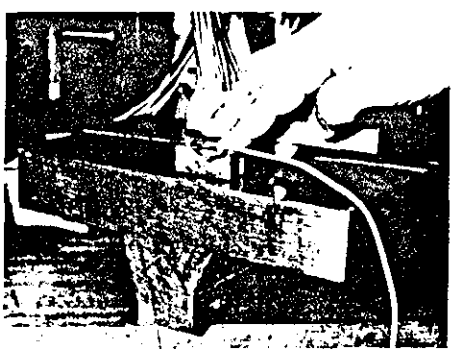

FIG·9(a) - A T-WELD

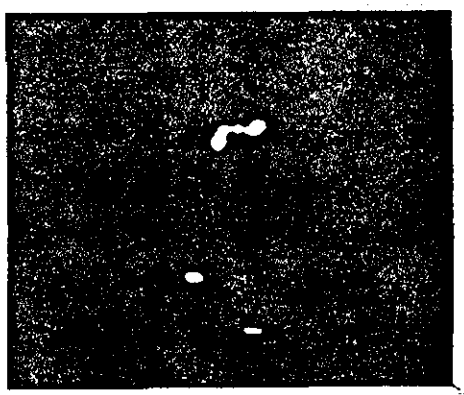

FIG 9 (b)

A NEW ULTRASONIC IMAGING SYSTEM

G.P.P. GUNARATHNE AND J. SZILARD

UNIVERSITY OF TECHNOLOGY
LOUGHBOROUGH, LEICS. LE 11 3TU, U.K
ENGLAND

ABSTRACT

A REAL TIME ULTRASONIC IMAGING SYSTEM FEATURING GOOD RESOLUTION, HIGH SENSITIVITY, LOW COST ETC, HAS BEEN DEVELOPED. IN TESTING, THE TEST OBJECT IS INSONIFIED WITH A SHORT PULSE OF ULTRASOUND AND THE ECHO SIGNALS ARE RECEIVED WITH AN ARRAY OF TRANSDUCERS. THESE SIGNALS ARE AMPLIFIED IN PARALLEL CHANNELS AND ARE RE-TRANSMITTED INTO A TRANSPARENT MEDIUM USING A SPECIAL ARRANGEMENT OF A SECOND TRANSDUCER ARRAY AND AN ACOUSTIC FOCUSING SYSTEM. THIS IN TURN PRODUCES A FULL ACOUSTIC IMAGE OF THE TEST OBJECT FIELD AND IS MADE VISIBLE BY SYNCHRONISED STROBOSCOPIC ILLUMINATION. THE FIRST EXPERIMENTAL PROTOTYPE HAS A NOMINAL DEPTH RANGE OF UP TO 40 CM IN STEEL AND TAKES ONLY 0.15 MS TO PRODUCE A HIGH RESOLUTION FOCUSED B-SCAN TYPE IMAGE OF THE WHOLE OBJECT FIELD.

1. INTRODUCTION

MANY PROBLEMS ARE OFTEN SEEN IN ULTRASONIC IMAGING SYSTEMS SUCH AS LOW SPEED, INADEQUATE RESOLUTION, LARGE PHYSICAL SIZE, HIGH COST ETC. THE NEW SYSTEM DESCRIBED HERE IS CAPABLE OF OVERCOMING MANY OF THESE LIMITATIONS AND IS BASED ON A NEW DEVELOPMENT ALONG THE LINES OF HANSTEAD'S DIRECT ULTRASONIC VISUALISATION OF DEFECTS[1] [DUVD] PRINCIPLE.

ALTHOUGH DUVD HAS VERY REMARKABLE FEATURES, THE FUNDAMANTAL PROBLEM IS ITS LOW SENSITIVITY. THIS IS MAINLY SO AS THE SYSTEM IS 'PASSIVE', IN THAT IT ONLY UTILIZES THE INSONIFYING ENERGY FOR ACOUSTIC IMAGE FORMATION AND HEAVY ENERGY LOSSES ARE INVOLVED. FURTHER WORK ON THIS TECHNIQUE HAS ALSO BEEN REPORTED BY HAYMANN[2] IN 1977 AND BY BAR-COHEN ET.AL.[3] IN 1978. EVEN SO, AT ITS BEST, THE SENSITIVITY OF THE DUVD FALLS FAR SHORT OF THAT REQUIRED FOR PRACTICAL IMPLEMENTATION. THE OTHER DRAWBACKS ARE THE DIFFICULTIES IN COUPLING AND MANIPULATION.

INTRODUCING ELECTRONIC AMPLIFICATION BETWEEN A SET OF RECEIVER AND RE-TRANSMITTER ARRAYS, THE BASIC CONCEPT OF DUVD IS CHANGED FROM 'PASSIVE' TO 'ACTIVE', SOLVING THE PROBLEM OF LOW SENSITIVITY, WHILE THE IDEAL CHARACTERISTICS ARE PRESERVED BY DESIGNING A NEW SONOPTICAL GEOMETRY. IN THIS WAY THE PROBLEM OF MANIPULATION IS ALSO SOLVED AS THE PROBE ARRAY IS NOW SEPERATED FROM THE REST OF THE SYSTEM.

A NUMBER OF AREAS HAVE BEEN DEVELOPED DURING THE COURSE OF THIS WORK, WHICH ARE ALSO BRIEFLY OUTLINED. THESE INCLUDE A HIGH PERFORMANCE WIDE APERTURE COMPACT SCHLIEREN SYSTEM, A NEW MINIATURE L.E.D. STROBOSCOPE,[4] WIDEBAND RF AMPLIFIERS, HIGH QUALITY TRANSDUCER ARRAYS AND BACKINGS ETC.

THIS PAPER ALSO PRESENTS SUPPLEMENTARY TEST RESULTS TO THE PREVIOUS PUBLICATION AT THE ULTRASONICS INTERNATIONAL 85 CONFERENCE[5] HELD IN JULY 1985, LONDON.

2. BASIC CONCEPT OF DUVD

HANSTEAD'S DUVD SYSTEM ESSENTIALLY CONSISTS OF A SPECIAL ARRANGEMENT OF A PAIR OF ACOUSTIC LENSES AS SHOWN IN FIG. 1.

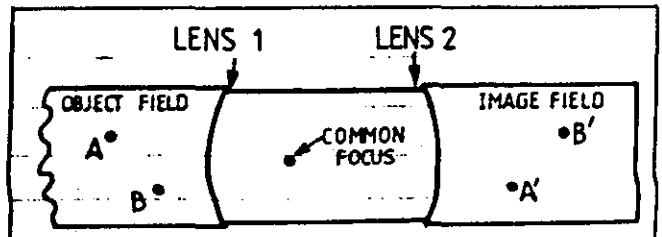

FIG. 1 TWO-LENS DUVD ARRANGEMENT.

APART OF BEING CAPABLE OF PRODUCING 3D ACOUSTIC IMAGES, DUVD HAS TWO OTHER SPECIAL PROPERTIES CALLED 'LINEARITY' AND 'ISOCHRONICITY'. THE TERM LINEARITY HERE REFERS TO ITS ABILITY TO MAINTAIN A CONSTANT OBJECT-TO-IMAGE SPATIAL RELATIONSHIP, WHILE ISOCHRONICITY MEANS THAT WHEN THE TEST OBJECT IS INSONIFIED WITH A SHORT PULSE, ALL THE ECHOES FROM DIFFERENT TARGETS [DEFECTS], IRRESPECTIVE OF THEIR DISTANCES, ARRIVE SIMULTANEOUSLY AT THEIR RESPECTIVE IMAGE POINTS, THUS GIVING THE SYSTEM ITS ABILITY TO DISPLAY THE WHOLE IMAGE AT ONCE. THE ULTRASONIC IMAGE IS MADE VISIBLE IN A SUITABLE TRANSPARENT MEDIUM EITHER BY PHOTOELASTIC TECHNIQUE OR SCHLIEREN TECHNIQUE OF VISUALISATION USING STROBOSCOPIC FLASH OF LIGHT.

3. THE NEW CONCEPT

THE MAIN FEATURES OF THE NEW CONCEPT[6] CAN BE SEEN FROM FIG. 2, WHICH ARE ALSO SUMMARIZED BELOW.

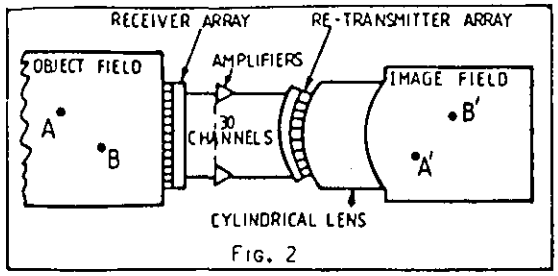

FIG. 2

(1) ECHO SIGNAL RECEPTION BY MEANS OF A LINEAR ARRAY OF TRANSDUCERS.
(2) AMPLIFICATION OF RECEIVED SIGNALS IN PARALLEL CHANNELS.
(3) RE-TRANSMISSION OF AMPLIFIED ECHO SIGNALS INTO AN OPTICALLY TRANSPARENT MEDIUM USING A SECOND ARRAY OF TRANSDUCERS, FORMING A PART OF AN ACOUSTIC FOCUSING SYSTEM.

EACH OF THESE AREAS HAD TO BE EXAMINED IN DETAIL IN ORDER TO IDENTIFY THE DESIGN PARAMETERS OF THE SYSTEM AS OUTLINED BELOW.

3.1 SIGNAL RECEPTION

(1) NO. OF CHANNELS
(2) TRANSDUCER ELEMENT SPACING
(3) ELEMENT WIDTH-TO-GAP RATIO
(4) PHYSICAL SIZE, SHAPE AND TRANSDUCER MATERIAL
(5) CENTRE FREQUENCY ETC.

THE FIRST TWO PARAMETERS WERE ESTIMATED BY A PRELIMINARY COMPUTER SIMULATION USING THE MODEL AS SHOWN IN FIG. 3 BELOW.

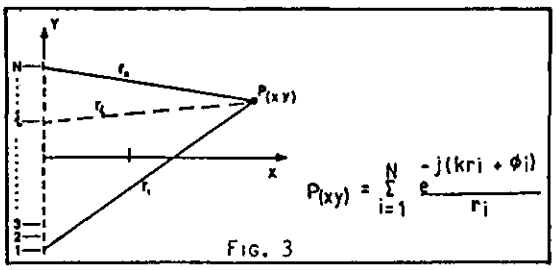

FIG. 3

WHERE, P IS THE ACOUSTIC PRESSURE AT POINT [x,y],
r_i IS THE DISTANCE FROM THE i_{th} ELEMENT,
ϕ_i IS THE RELATIVE PHASE W.R.T. 1^{st} ELEMENT,
AND K IS THE WAVE NUMBER.

AIM HERE WAS TO OBTAIN AN IDEA OF THE SHARPNESS OF THE IMAGES AND THE EXTENT OF ARTIFACTS THAT MAY BE FORMED IN A GIVEN IMAGE SPACE AS A FUNCTION OF THE NUMBER OF CHANNELS AND ELEMENT SPACING. FOR THE FIRST PROTOTYPE, A CENTRE FREQUENCY OF 2 MHz WAS CHOSEN WITH ELEMENT SPACING OF 0.7 , AND THIRTY CHANNELS, ALTHOUGH THE FEASIBILITY STUDY WAS CARRIED OUT WITH ONLY FIFTEEN. EVEN SO, THE RESULTS ARE VERY REMARKABLE AS CAN BE SEEN FROM TYPICAL TEST RESULTS PRESENTED. [PAGE 3]

3.2 SIGNAL AMPLIFICATION

POWER OF THE RECEIVED SIGNALS HAS TO BE RAISED TO A LEVEL SUFFICIENT FOR THE PARTICULAR ACOUSTO-OPTIC TECHNIQUE OF VISUALISATION USED. IN ORDER TO ACHIEVE GOOD RESOLUTION AND IMAGE QUALITY, THE RECEIVED AND RE-TRANSMITTED PULSES MUST BE AS SHORT AS POSSIBLE REQUIRING FAITHFUL AMPLIFICATION OVER A BROAD BAND OF FREQUENCIES. THESE TOGETHER WITH THE ELECTRICAL DAMPING REQUIREMENTS OF THE TRANSDUCERS TO ACHIEVE WIDEBAND RESPONSE PLACES HEAVY DEMANDS ON THE AMPLIFIERES. IN THIS RESPECT, VARIOUS AREAS HAVE BEEN INVESTIGATED, AS LISTED, FROM WHICH THE AMPLIFIER DESIGN SPECIFICATIONS WERE FORMULATED.

(1) TYPICAL AND WORST CASE INPUT SIGNAL LEVELS
(2) OUTPUT SIGNAL LEVELS
(3) PHASE DISTORTION AND BANDWIDTH CONSIDERATIONS
(4) DYNAMIC RANGE
(5) INPUT AND OUTPUT IMPEDANCES
(6) DAMPING CHARACTERISTICS
(7) POWER CONSUMPTION
(8) SIZE
(10) COST ETC.

A SET OF WIDEBAND RF POWER AMPLIFIERS OPERATING IN CLASS A WAS DESIGNED FOR EARLY EXPERIMENTS. ALTHOUGH THESE ARE STILL IN USE, A NEW CATEGORY OF AMPLIFIERS HERE NAMED AS G* GIVING HIGHER EFFICIENCY AND DYNAMIC RANGE HAS BEEN DEVELOPED AND TESTED FOR THIS PARTICULAR PURPOSE. IT OPERATES IN SWITCHED MODE BUT RETAINS THE IDEAL CHARACTERISTICS OF CLASS A DURING THE PERIOD WHEN THE SIGNAL AMPLIFICATION TAKES PLACE. THIS CONCEPT IS ILLUSTRATED IN FIG. 4.

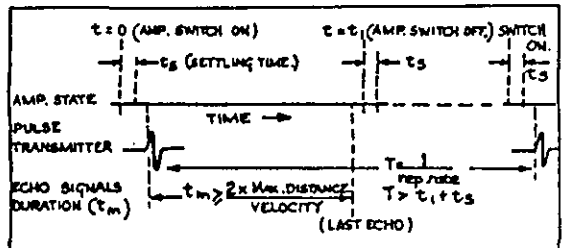

FIG. 4 SWITCHED MODE AMPLIFICATION

A SET OF 30 MINIATURE WIDEBAND ARRAY HEAD AMPLIFIERS WERE ALSO DEVELOPED WHICH MATCHES THE TRANSDUCERS TO THE CABLES UP TO A USABLE LENGTH OF 50 METRES. FIG. 5, [PAGE 4]. THUS REMOTE OPERATION IS POSSIBLE. THESE AMPLIFIERS HAVE A 1 kV SURGE PROTECTION AT THE FRONT END WITH SHORT DEAD ZONE ENABLING THEM TO BE USED IN THE TRANSCEIVER MODE OF OPERATION AS WELL. THIS AMPLIFIER ASSEMBLY IS SMALL ENOUGH TO BE CLIPPED TO THE OPERATORS LOWER ARM.

3.3 RE-TRANSMISSION AND VISUALISATION

A SONOPTICAL GEOMETRY CONSISTING OF A CURVED ARRAY AND A CYLINDRICAL LENS WAS DESIGNED TO RE-TRANSMIT THE AMPLIFIED SIGNALS INTO THE VISUALISING MEDIUM. THIS ARRANGEMENT IS CAPABLE OF PRODUCING FOCUSED B-SCAN TYPE ACOUSTIC IMAGES OF THE TEST OBJECT FIELD.

IN ORDER TO VISUALISE THE ACOUSTIC IMAGES, THE SCHLIEREN TECHNIQUE WAS ADOPTED. A SEALED COMPACT SCHLIEREN SYSTEM WAS DESIGNED AND KINEMATICALLY MOUNTED SUCH THAT IT IS INSENSITIVE TO VIBRATIONS EXPERIENCED IN USE, GIVING PERFECTLY STEADY IMAGES. THIS PARTICULAR SETUP CAN BE OPERATED IN FULL

DAYLIGHT WITHOUT THE NEED OF ANY DARK ENVIRONMENT.

ONE OF THE MOST SIGNIFICANT IMPROVEMENTS HAS BEEN THE DEVELOPMENT OF A NEW L.E.D. STROBOSCOPE WHICH GREATLY IMPROVED THE PERFORMANCE AND THE COMPACTNESS OF THE WHOLE SYSTEM. IT IS CAPABLE OF OUTPUTTING LIGHT FAR IN EXCESS OF WHAT IS REQUIRED FOR THE PURPOSE. EVEN A SINGLE PULSE SHOWS THE WHOLE IMAGE FIELD. THIS STROBOSCOPE IS ASSEMBLED INSIDE A LENS CAP AS SHOWN IN FIG. 6, [PAGE 4].

4. CONSTRUCTION OF ARRAYS

THIS IS A VITAL AREA IN ACHIEVING GOOD RESULTS. THE INDIVIDUAL ELEMENTS OF THE ARRAY MUST HAVE,

(1) WIDEBAND PERFORMANCE
(2) GOOD SENSITIVITY
(3) MINIMAL CROSS-COUPLING
(4) SUFFICIENTLY IDENTICAL BEHAVIOUR

THIS IS DIFFICULT TO ACHIEVE, ESPECIALLY WHEN THE TRANSDUCERS ARE PHYSICALLY SMALL AS THE LATERAL MODES OF VIBRATIONS BECOME MORE SIGNIFICANT. A CONSIDERABLE AMOUNT OF WORK HAS BEEN DONE IN ACHIEVING THESE OBJECTIVES. IN THIS RESPECT, A NEW APPROACH HAS BEEN TAKEN TO DEVELOP BOTH CONDUCTIVE AND NON-CONDUCTIVE HIGH QUALITY TRANSDUCER BACKINGS

5. THE ASSEMBLY AS A WHOLE

FIG. 7 ON PAGE 4, SHOWS THE FIRST EXPERIMENTAL PROTOTYPE. OVERALL DIMENSIONS OF THE WHOLE ASSEMBLY ARE 1 M BY 0.5 M BY 0.5M. WITH FURTHER ADVANCES IN ELECTRONICS USED AND CONSTRUCTION TECHNIQUES, ANY FUTURE MODEL MAY BE COMPARABLE IN SIZE TO THAT OF A CONVENTIONAL FLAW DETECTOR OF THE EARLY TYPE. FIG. 9 BELOW SHOWS THE SYSTEM BLOCK DIAGRAM.

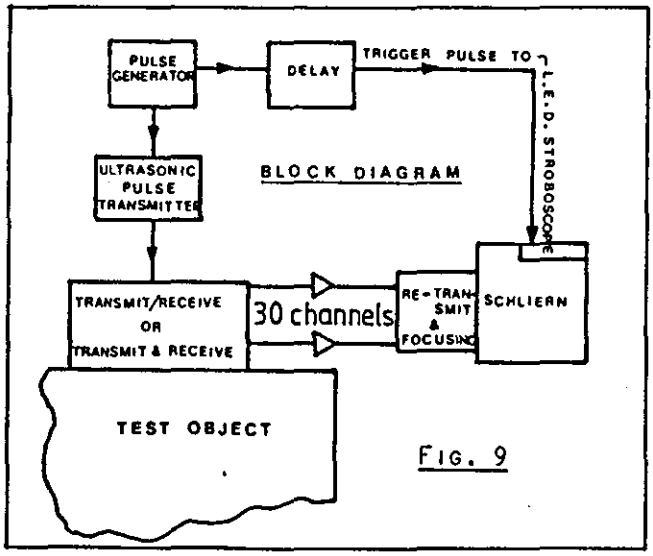

FIG. 9

WHEN TESTING THE RECEIVING ARRAY IS COUPLED WITH OIL TO THE TEST OBJECT. EITHER SEPERATE TRANSMITTER RECEIVER OR TRANSCEIVER MODE MAY BE SELECTED. THE TEST OBJECT IS INSONIFIED WITH A SHORT PULSE OF ULTRASOUND AND THE DELAY OF THE STROBOSCOPE TRIGGERING CIRCUIT IS SET APPROPRIATELY. AN A-SCAN DISPLAY OF SIGNALS IS PROVIDED FOR QUICK MONITORING OF TARGETS. THE CORRESPONDING IMAGES ARE SEEN NEXT

6. RESULTS

FIGS. 10 TO 13 SHOW SOME TYPICAL TEST RESULTS OBTAINED WITH THE FIRST PROTOTYPE, OPERATING WITH ONLY 15 CHANNELS.

FIG. 10 IS AN IMAGE OF A LINE OF HOLES DRILLED AT AN ANGLE IN AN ALUMINIUM TEST BLOCK. THIS IMAGE DEMONSTRATES THE LINEARITY AND ISOCHRONICITY ASPECTS OF THE SYSTEM.

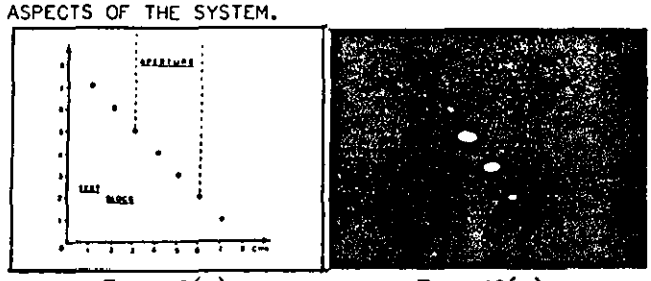

FIG. 10(A) FIG. 10(B)

FIGS. 11(A) & 11(B) SHOWS THE ABILITY OF THE SYSTEM TO EXAMINE A LARGE FIELD OF VIEW. NOTE THAT THE RECEIVING ARRAY IS NOT DIRECTLY ABOVE ANY OF THE DRILLED HOLES. THIS IS A FAVOURABLE FEATURE WHEN EXAMINING VERTICALLY ORIENTED DEFECTS.

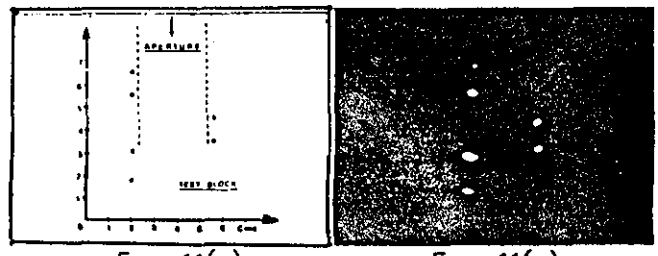

FIG. 11(A) FIG. 11(B)

FIG. 12(A) SHOWS THREE HOLES DRILLED IN A TEST BLOCK. NOTE THAT THE HOLES MARKED 1 AND 2 ARE CLOSER THAN 2 AND 3 BY ABOUT 3 MM AND THE VERTICAL OFFSET OF 1 AND 3 ABOUT 2 MM WHICH ARE CLEARLY SEEN FROM THE IMAGE. THIS GIVES AN IDEA OF THE ACCURACY ACHIEVED WITH THIS SYSTEM.

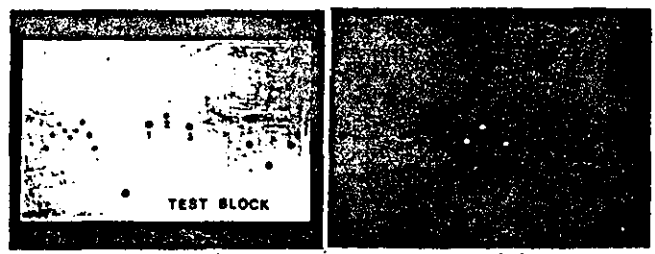

FIG. 12(A) FIG. 12(B)

FIG. 13(A) & (B) BELOW SHOW TWO IMAGES OF CRACKS FOUND IN A T-WELD CONTAINING NATURAL DEFECTS.

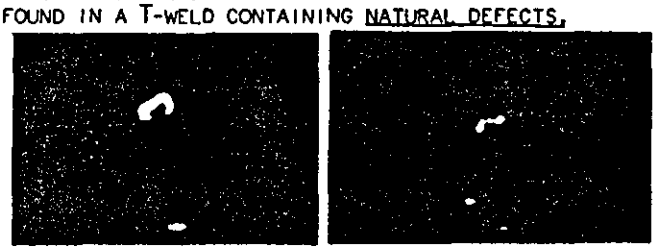

THE SENSITIVITY OF THE SYSTEM IS HIGH. FOR EXAMPLE THE THREE HOLES SHOWN IN FIG. 13(A) ARE IMAGED WITH AN INSONIFYING PULSE OF AROUND 50 V ONLY, WHILE THE PRESENT CIRCUITS ALLOW 20 TIMES HIGHER VOLTAGES.

EVEN IN ITS PRESENT FORM WITH ONLY FIFTEEN CHANNELS OPERATING, ITS RESOLUTION IS ALSO HIGH, TYPICALLY IN THE ORDER OF A WAVELENGTH IN THE LONGITUDANAL DIRECTION AND ABOUT 1.5 TO 2 WAVELENGTHS LATERALLY AT A DEPTH OF AROUND 5 TO 6 CM IN THE TEST BLOCK.

IT OPERATES IN REAL TIME, I.E. A COMPLETE IMAGE IS FORMED BY A SINGLE PULSE, WITHIN A PERIOD REQUIRING JUST THE TIME OF FLIGHT OF THE PULSE IN THE TEST OBJECT AND IN THE SONOPTICAL ARRANGEMENT OF THE SYSTEM. THUS IN A SECTION OF STEEL 400 MM DEEP, AN IMAGE IS FORMED IN ABOUT 0.15 MS. THE FRAME RATE MAY BE RAISED AS HIGH AS 1 KHZ OR MORE.

SINCE THE SYSTEM OPERATES IN REAL TIME AND WITH THE IMAGES OF ACOUSTIC DISCONTINUITIES WHOSE SHAPES AND POSITIONS ARE KNOWN, EG. DRILLED HOLES, THE REPEATABILITY ASPECT OF THE SYSTEM COULD EASILY BE SEEN. FURTHERMORE, THE INTERPRETATION OF RESULTS ARE STRAIGHTFORWARD AND LESS OPERATOR DEPENDENT.

7. DISCUSSIONS AND CONCLUSIONS

IT IS SEEN THAT THE PRESENT-DAY IMAGING SYSTEMS IN GENERAL ARE MOVING MORE TOWARDS THE USE OF DIGITAL COMPUTERS AND SOPHISTICATED SIGNAL PROCESSING TECHNIQUES. ALTHOUGH SUCH SYSTEMS HAVE MANY ATTRACTIVE FEATURES, THERE CAN BE INHERENT DRAWBACKS SUCH AS LOW SPEED, INADEQUATE IMAGE QUALITY ETC., THESE BEING THE RESULT OF INVOLVED LENGTHY PROCESSING AND OTHER LIMITATIONS ARISING FROM THE PARTICULAR TECHNIQUE USED.

IN THIS RESPECT THE NEW IMAGING SYSTEM PRESENTS OBVIOUS ADVANTAGES MAINLY DUE TO ITS FUNDAMENTAL SIMPLICITY WHICH REQUIRES JUST ANALOGUE PROCESSING. THE TECHNIQUE OFFERES AN UNUSUAL COMBINATION OF USEFUL FEATURES IN IMAGING APPLICATIONS AS GIVEN ABOVE. THESE BENEFITS TAKEN TOGETHER WITH ITS REMARKABLY LOW COST, MAKE THIS SYSTEM UNIQUE IN THE FIELD OF ULTRASONIC IMAGING.

ALL THESE FEATURES ARE IDEAL FOR MEDICAL APPLICATIONS AS WELL AND THIS POSSIBILITY IS INTENDED TO BE EXPLORED IN DEPTH AS THE WORK DONE SO FAR IS CONCERNED WITH NDT ONLY. FURTHER WORK HAS ALSO BEEN PLANNED ON SYSTEM OPTIMISATION AND COUPLING TO NON UNIFORM SURFACES.

REFERENCES

(1) P.D. HANSTEAD : THREE DIMENSIONAL IMAGING OF ULTRASOUND : DIRECT ULTRASONIC VISUALISATION OF DEFECTS, NATURE, 239, 273 - 274, 1972.

(2) A.J. HAYMAN : SCHLIEREN VISUALISATION OF ULTRASONIC IMAGES. PH.D. THESIS, CITY UNIVERSITY, LONDON, 1977.

(3) Y. BAR-COHEN, B. BEN-JOSEPH AND E. HARNIK : COMPACT SENSITIVE INSTRUMENT FOR DIRECT VISUALISATION OF DEFECTS. REV. SCI. INSTRUMENTS, 49, 1709 - 1911, 1978.

(4) G.P.P. GUNARATHNE, J. SZILARD : A NEW STROBOSCOPE FOR SCHLIEREN AND PHOTOELASTIC VISUALISATION OF ULTRASOUND, ULTRASONICS, JULY 1983, 188 - 190

(5) G.P.P. GUNARATHNE, J. SZILARD : A REAL TIME HIGH FRAME RATE ULTRASONIC IMAGING SYSTEM : ULTRASONICS INTERNATIONAL 85 CONFERENCE PROCEEDINGS, JULY 1985.

(6) PATENT APPLICATION NO. 8510802 FILED 29-4-1985

ACKNOWLEDGEMENT

THIS WORK WAS SUPPORTED BY THE UNITED KINGDOM ATOMIC ENERGY AUTHORITY AND WAS PERFORMED AT LOUGHBOROUGH UNIVERSITY OF TECHNOLOGY. THE AUTHORS WISH TO THANK DR. P. HIGHMORE, PROJECT SUPERVISOR AT THE RISLEY NUCLEAR POWER DEVELOPMENT LABORATARIES FOR HIS CONTINUOUS SUPPORT AND ENCOURAGEMENT. THANKS ARE ALSO DUE TO THE TECHNICAL STAFF OF THE DEPARTMENT OF ELECTRONIC ENGINEERING, LOUGHBOROUGH UNIVERSITY OF TECHNOLOGY AND ALSO TO THE OTHERS WHO GAVE THEIR WHOLE HEARTED SUPPORT DURING THE COURSE OF THIS WORK.

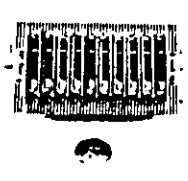

FIG.5

[L E D STROBOSCOPE]

DESIGNED AND CONSTRUCTED BY G. P. P. GUNARATHNE

FIG.6

THE NEW IMAGING SYSTEM —(1st EXPERIMENTAL MODEL)

FIG.7

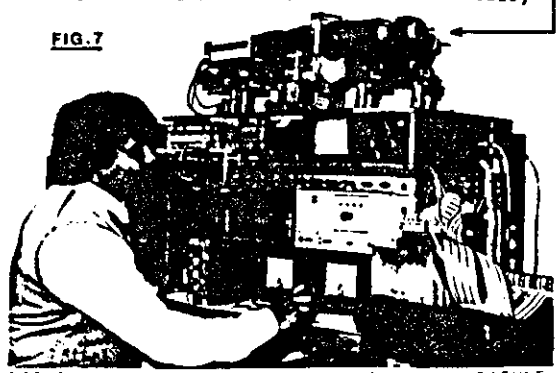

DESIGNED AND CONSTRUCTED BY G.P.P. GUNARATHNE

A REAL TIME ULTRASONIC IMAGING SYSTEM

G.P.P. GUNARATHNE AND J. SZILARD

A new real time ultrasonic imaging system featuring high resolution, good sensitivity, low cost etc. has been developed. The new system is based on the principle of Hanstead's Direct Ultrasonic Visualisation of defects[1] [DUVD] technique. The inherently low sensitivity of the DUVD is eliminated by introducing electronic amplification using transducer arrays while preserving its ideal properties by adopting a new sonoptical design. The first experimental model has a nominal depth range of up to 40 cm in steel and takes only 0.15 ms to produce a high resolution focused B-scan image of the whole object field.

Introduction

Hanstead's DUVD system[1] is one which is capable of producing 3D images of targets in a test object medium with two other special properties called 'linearity' and 'isochronicity'. 'Linearity' here refers to its ability to maintain a constant object-to-image spatial relationship, while isochronicity means that when the test object is insonified, all the echoes from different targets [defects], irrespective of their distances, arrive simultaneously at their respective image points. The design of the system is such that ultrasonic images are formed in a transparent medium, made visible by photoelastic technique or by schlieren technique using stroboscopic flash of light. See Fig. 1.

The main problem with the DUVD is its low sensitivity. This is because the system is 'passive', in that it only utilizes the insonifying energy for acoustic image formation and heavy energy losses are involved. Further work has also been reported by Hayman[2] in 1977 and by Bar-Cohen et all.[3] in 1978. Even so, the sensitivity of DUVD falls far short of that required for practical implementation

The new concept[4]

The main features of the new concept can be seen from Fig. 2, as follows

1. Echo signal reception by means of a linear array of transducers.
2. Amplification of received signals in parallel channels.
3. Re-transmission of amplified signals into an optically transparent medium using a second transducer array forming a part of an acoustic focusing system

Echo signal reception

The following areas have been examined.

1. Number of channels
2. Transducer element spacing
3. Element width to gap ratio
4. Length of the elements
5. Transducer material
6. Centre frequency

The first two parameters were estimated by a preliminary computer simulation using the model shown in Fig.3. The mathematical model used is

$$P_{(xy)} = \sum_{i=1}^{N} \frac{e^{-j(kr_i + \phi_i)}}{r_i} \qquad (1)$$

G.P.P. Gunarathne and J. Szilard are at the Department of Electrical and electronic engineering, Loughborough University of Technology, Loughborough, UK.

IEE DIGEST NO: 1986/34.

where $p_{(x,y)}$ is the pressure distribution at point (x,y) in the image space, r_i is the distance from the ith element, ϕ_i is the relative phase w.r.t. 1st element and k is the wave number. For the first prototype a centre frequency of 2 MHz was used. From the above simulation an element spacing of 0.7 , and thirty channels were chosen, although the feasibility study was carried out with only fifteen. Even so, the results are very remarkable as seen from Figs. 6 & 7.

Signal amplification

Power of the received signals has to be raised to a level sufficient for the particular acousto-optic technique of visualisation used. In order to achieve good resolution and image quality, the received and re-transmitted pulses must be as short as possible requiring faithful amplification over a broad band of frequencies. These together with the electrical damping requirements of the transducers to achieve wideband response places heavy demands on the amplifiers. Following areas have been examined in the design of the amplifiers.

1. Input signal levels
2. Output signal levels
3. Bandwidth considerations
4. Dynamic range
5. Noise levels
6. Input and output impedences
7. Damping characteristics
8. Power consumption
9. Size
10. cost

A set of wideband rf power amplifiers operating in class A was designed for early experiments. Although these are still in use, a new category of amplifiers here named G giving higher efficiency and dynamic range has been developed and tested for this particular purpose. It operates in switched mode but retains the ideal characteristics of class A during the period of signal amplification. This concept is illustrated in Fig. 4.

A set of 30 miniature wideband array head amplifiers were also développed which matches the transducers to the cables up to a usable length of 50 metres. These amplifiers have a 1 kV surge protection at the front end with a short dead zone enabling them to be used in the transceiver mode of operation as well.

Re-transmission and visualisation

A sonoptical geometry consisting of a curved array and a cylindrical lens was designed to re-transmit the amplified signals into the visualising medium. This arrangement is capable of producing focused B-scan type images of the object field. Schlieren technique was adopted for visualising the acoustic images.

One of the most significant improvements has been the development of a new sub-miniature L.E.D. stroboscope[5] which greatly improved the performance and the compactness of the whole system. It is capable of outputting light far in excess of what is required for the purpose. Even a single pulse shows the whole image.

Construction of arrays

This is a vital area in achieving good results. The individual elements of the arrays must have

1. Wideband performance
2. Good sensitivity
3. Adequate omni-directional response
4. Minimul cross-coupling
5. Sufficiently identical behaviour

These are difficult to achieve simaltaneously, specially when the elements are physically small and a considerable work has been done in achieving good results. In this respect, good quality transducer backings were also developed.

The operation of the system.

Fig. 5 shows the system block diagram. When testing, contact coupling is used. Either seperate transmitter receiver or transceiver mode may be selected. The test object is insonified with a short pulse and the delay of the stroboscope trigger circuit is set appropriately. The images are seen in real time on a TV monitor or may be seen directly through the schlieren system.

Some test results

Fig.s 6 and 7 show some typical test results obtained with the first prototype, operating with only 15 channels. Fig. 6(a) shows three holes drilled in a test block and 6(b) is the corrosponding image. Note that the holes marked 1 and 2 are closer than 2 and 3 by about 2 mm which is clearly seen from the image. Fig. 7(a) and (b) show the images of natural cracks found in a T-weld.

Discussions and conclusions

The new imaging system is fundamentally different to any other existing imaging techniques and offers an unusual combination of useful features such as extremely high speed, high resolution, good sensitivity, linearity, good accuracy and repeatability etc. A complete image is formed by a single pulse practically within the time of flight of the pulse. Frame rate may be as high as 1 kHz or more giving very high temporal resolution compared to other systems. These benefits taken together with its remarkably low cost, make this system unique in the field of ultrasonic imaging.

These features are ideal for medical applications as well and this possibility is intended to be explored as the work done so far is concerned with NDT only.

References

1. P.D. Hanstead : Three dimensional imaging of Ultrasound : Direct Ultrasonic Visualisation of Defects, Nature, 239, 273 - 274, 1972

2. A.J. Hayman : Schlieren visualisation of ultrasonic images. Ph.D. thesis, City University, London, 1977.

3. Y. Bar-Cohen, B. Ben-Joseph and E. Harnik : Compact sensitive instrument for Direct visualisation of defects.

4. Patent application No. 8510802 filed 29-04 1985

5. G.P.P. Gunarathne and J. Szilard : A new stroboscope for schlieren and photoelastic visualisation of ultrasound : Ultrasonics, July 1983, 188 - 190

6. G.P.P. Gunarathne and J. Szilard : A real time high frame rate ultrasonic imaging system : Ultrasonics International 85 Conference Proceedings, July 85.

7. G.P.P. Gunarathne and J. Szilard : A new ultrasonic imaging system : IEEE 85, Ultrasonics symposium, Oct. 1985, San Fransisco, USA.

Acknowledgement

This work was supported by the United Kingdom Atomic Energy Authoriy and was performed at Loughborough University of Technology. The Authors wish to thank Dr. P. Highmore, project supervisor at the Risley Nuclear Power Development Laborataries for his continuous support and encouragement. Thanks are also due to the technical staff of this department.

FIGURES

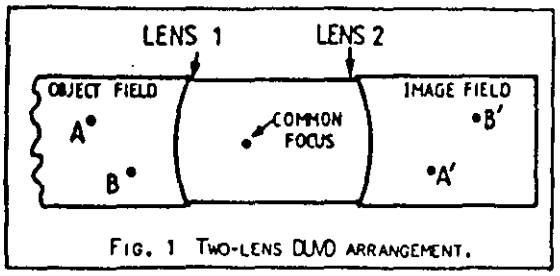

FIG. 1 TWO-LENS DUVO ARRARGEMENT.

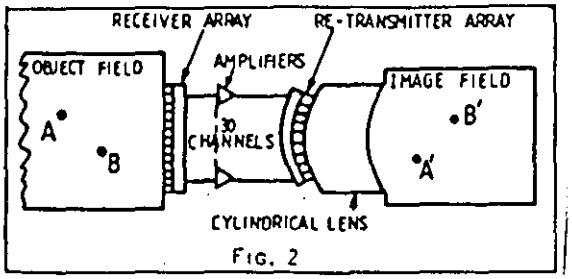

FIG. 2

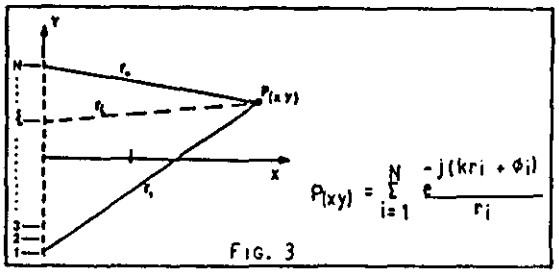

FIG. 3

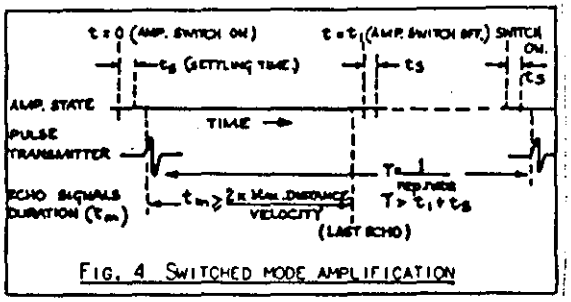

FIG. 4 SWITCHED MODE AMPLIFICATION

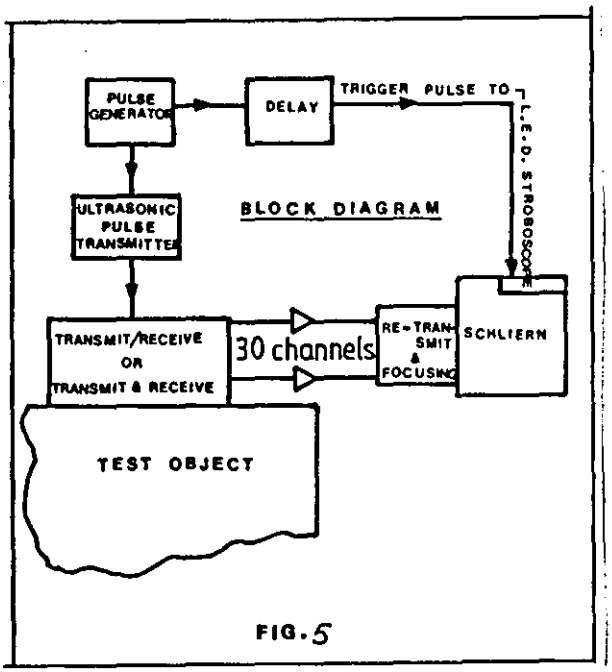

FIG. 5

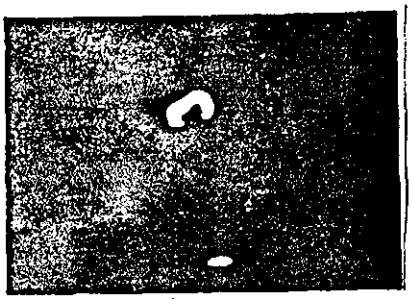

FIG 7(a)

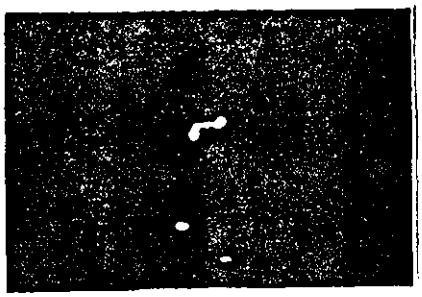

FIG 7(b)

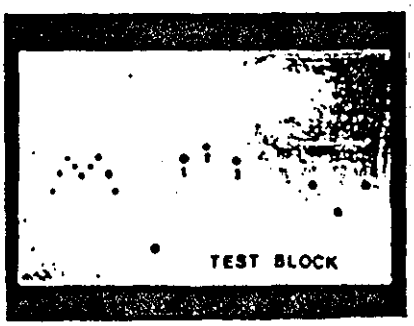

FIG 6(a)

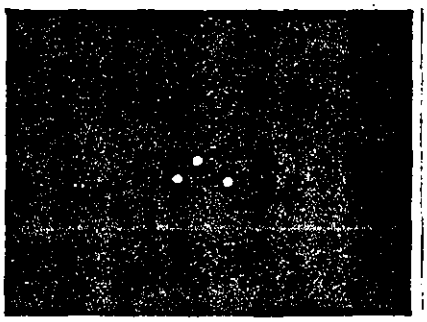

FIG. 6(b)

REFERENCES

1. Size measurement and characterization of weld defects by ultrasonic testing, Report series, part 1, 1979, Welding Institute reference 3527/4/77, Cambridge, pp 1 - 13, 49 - 51.

2. Mc Dicken, W. N. : Diagnostic Ultrasonics, (second edition) - John Wiley and sons Inc, 1981, New York, pp. 18 - 40, 154 - 167, 187 - 216.

3. Rose, J. L. and Goldberg, B. B. : Basic physics in diagnostic Ultrasonics, John Wiley and sons, New York, 1979, pp. 42 - 56, 72 - 105, 124 - 133, 255 - 261.

4. Szilard, J. : Ultrasonic Testing, Non-conventional testing techniques 1982, John Wiley and sons, New York, pp. 41 - 69, 127 - 133.

5. Greguss, P. : Ultrasonic Imaging, First edition 1980, Focal press Ltd., London, Chapter 5, pp. 96 - 98

6. Hanstead, P. D. : A new ultrasonic focusing system for materials inspection, J.Physics D : Appl. Phys., Vol. 7, 1974, pp. 226 - 241.

7. Silk, M.G. : Ultrasonic transducers for Non Destructive Testing, British Library Cataloguing in Publication data, 1984, Adam Hilger Ltd., Bristol. Chapter 3, chapter 5 pp. 81, 90 - 93, chapter 6.

8. Carl, F. et. al, : Fundamentals of Digital Ultrasonic Imaging, IEEE trans., Sonics and Ultrasonics, Vol. SU 31 No.4, July 1984. pp. 195 - 217.

9. Duck, G. M. : The Display and Processing of Digital Images from a sector scanning sonar, Ph.D. thesis, July 1980, Chapter 2, pp. 8 - 13.

10. Hildebrand, B. P. and Brenden, B. B. : An Introduction to

Acoustical Holography, plenum press, New York, 1972. Chapter 6, pp. 137 - 158, as in Ultrasonic Testing by J. Szilard.

11. Hanstead, P. D. : Direct Ultrasonic Visualization of Defects, Ph.D. thesis, 1973, City University. PP. 5 - 31, 48 - 53, 101.

12. Hayman, A. J. : Schlieren Visualization of Focused Ultrasonic images. Ph.D. thesis, 1977, City University, chapter 1, page 3, chapter 3, pp. 14 - 28, chapter 4, pp. 36 - 37, chapter 10 Appendix 1, pp. 116 - 117.

13. Hayman, A. J. and Hanstead, P.D. : Developments in Direct Ultrasonic Visualization of Defects. Ultrasonics, May 1979, pp. 105 - 112.

14. Hall, G. : Ultrasonic wave visualization as a teaching aid in Non-Destructive Testing, Ultrasonics, March 1977, pp. 57 - 69. (Vol. No. 15).

15. Hall, K. G. : Crack depth measurement in rail steel by Rayleigh waves aided by photoelastic visualization. Non Destructive Testing June, 1976, pp. 121 - 126.

16. Vasilev : Schlieren methods, Ketter Publishers Ltd., London, 1971 Chapter 3, pp. 56 - 59.

17. Greer, A. S. and Cross, B. T. : Schlieren techniques for NDT, Non Destructive Testing, June 1970, pp. 169 - 172.

18. Bar-Cohen, Y. et. al. : Compact sensitive instrument for Direct Ultrasonic Visualization of Defects. Rev. Sci. Instrum., 49(12), Dec. 1978, pp. 1709 - 1711.

19. Bar-Cohen, Y. : Schlieren Visualization of Acoustically Imaged Defects. Materials Evaluation / 41 / Jan. 1983, pp. 88 - 93.

20. Bruneel, C. et. al : Reconstruction of an acoustical image using an

'acousto-electronic lens device. Ultrasonics, Nov. 1977, pp. 263 - 264.

21. William, S. B. : Underwater Acoustic System analysis, Prentice - Hall, Inc., 1984. Chapter 6, pp. 172, 189 - 195, chapter 11, pp. 326 - 335.

22. Krautkrämer, J. , Krautkrämer, H. : Ultrasonic Testing of Materials, Third edition, 1983. Chapter 6, pp. 107 - 112.

23. Challis, R.E. and Harrison, J.E. : Transmission circuits for thick transducer transmission test systems. Ultrasonics, May 1984, pp. 103 - 109.

24. Hardy, K. : High frequency circuit design, Reston Publishing Company, Inc. 1978, Virginia. Chapter 1, pp. 1 - 23.

25. Millman, J. : Microelectronics, McGraw - Hill Book Company, 1979, New York. Chapter 13, pp. 484 - 486.

26. Carson, R. S. : High frequency amplifiers, John Wiley and sons, New York, 1982. Chapter 2, page 52,

27. Weinstein, D. G. : Polyvinylidene Fluoride Acoustic Transducers and Imaging Arrays. Ph.D. thesis, 1983. Stanford University, USA. Chapter 4, page 41.

28. Floyd, T. L. : Electronic devices, Charles E. Merrill Publishing Company, Ohio (1984). Chapter 8, pp. 274 - 304.

29. Grossner, N. R. : Transformers for electronic circuits, second edition, 1983. McGraw-hill, Inc., Chapter 8, pp.300 - 302.

30. Gunarathne, G.P.P., and Szilard, J. : A new stroboscope for schlieren and photoelastic visualization of ultrasound, Ultrasonics, July 1983, pp. 188 - 190.

31. Stark, H. : Modern electrical communications, Prentice / Hall Inc., 1979, Englewood. pp. 574 - 581.

32. Speak, G. S. and Walters, D. J. : Optical considerations and limitations of the schlieren method, Ministry of supply, Aeronautical research, Council reports and Memoranda (H.M.S.O., London,1954), as in Hayman's Ph.D. thesis.

33. Technical information - "Fluorinated" brand electronic liquids, Chemical Division, Minnesota Mining and Manufacturing Company, 1965.

34. Hanstead, P. D. : The sensitivity of schlieren systems for viewing ultrasound. Eigth World Conference on Nondestructive Testing, 1976.

35. GenRad stroboscope reference manual (GR 1538-A Strobotac Electronic Stroboscope), GenRad Ltd., Bucks. Page 24.

36. Wyatt, R. C. : An externally-triggered repetitive spark light source giving short flash duration with low time jitter., C.E.G.B. report SSD/SW/M.407 Feb. 1972, as in Hanstead's Ph.D. thesis.

37. Ryder, J. D. : Electronic fundamentals and applications, Pitman Publishing Limited, London, 1977. Chapter 1, page 27.

38. Turner, L. W. : Electronic Engineeres Reference Book, 4th Ed., Newnes-Butterworths, London (1976).

39. Stanley, Hi-Super Bright LEDs, H-500,H-300 data sheets, Lohuis Lamps Ltd., Birmingham

40. Gower, J. : Optical Communication Systems, Prentice Hall International, Inc., (1984), London. PP 213 - 228.

41. Keiser, G. : Optical fiber communication, McGraw Hill Book Company, London (1983). Chapter 4.

42. Mason, W. P. : Electromechanical transducers and wave filters, Princeton, NJ, Van No strand (1948); as in Ultrasonic transducers for Non Destructive Testing by M. G. Silk.

43. Leedom, D. A., Krimholtz, R., and Matthei, G. L. : "Equivalent circuits for transducers having arbitrary even-or-odd symmetry piezo electric Excitation", IEEE Trans. Sonics Ultrasonics, Vol. SU-18, PP. 128-141, 1971.

44. Duncan, T. : Physics, John Murray (Publishers) Ltd. London (1982) pp. 241 - 242.

45. Shackel, B. : Applied Ergonomics Handbook, 5th Ed.(1978), IPC Business Press Ltd., Surrey. Chapters 3, 4.

46. Gunarathne, G. P. P. and Szilard, J. : A real time high frame rate Ultrasonic imaging system. Ultrasonics International 85 Conference Proceedings, Butterworths, London (1985). PP. 98 - 104.

47. Gunarathne, G. P. P. and Szilard, J. : A new ultrasonic imaging system. IEEE, Ultrasonics Symposium, Oct. 1985, San Francisco.

48. Gunarathne, G. P. P. and Szilard, J. : A real time ultrasonic imaging system. Colloquim on "Developments in tomography for NDT and medical applications", March 1986. IEE, London. Digest No. 1986/34.

49. United Kingdom Atomic Energy Authority, London. : UK Patent Application (Ultrasonic flaw detection), GB 2160973A, Published 2nd Jan. 1986.

--- // ---

THE NEW REAL-TIME HIGH SPEED ULTRASONIC IMAGING SYSTEM

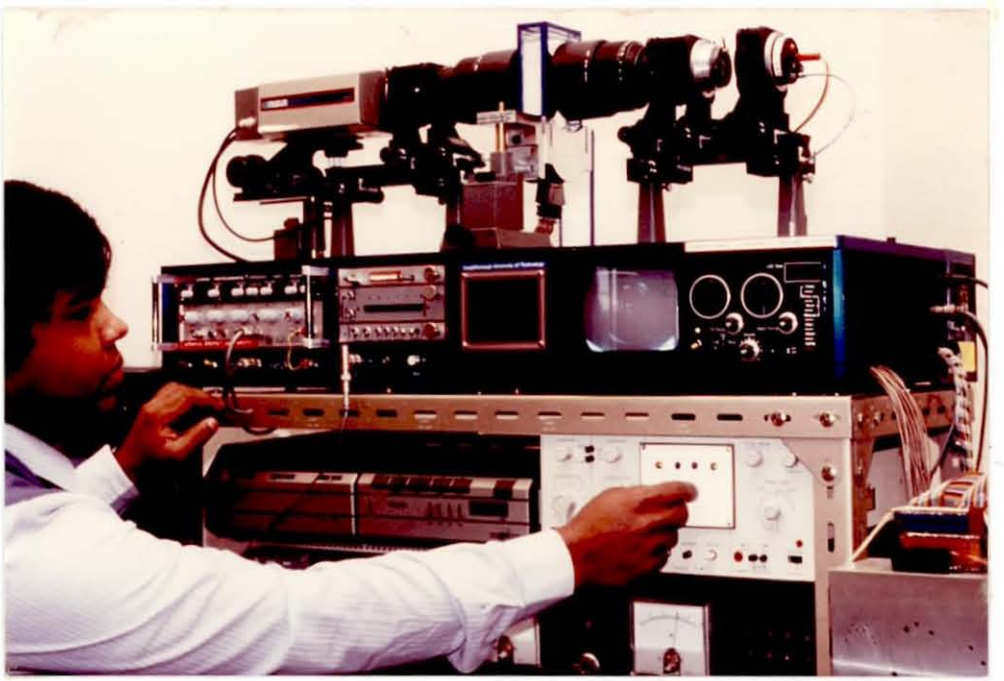

DESIGNED AND CONSTRUCTED

BY

G. P. P. GUNARATHNE.